

Universidade do Minho
Escola de Engenharia

Lívia de Souza Simões

Development of bio-based micro- and nanostructures from milk whey proteins, as a vehicle for controlled release and delivery of bioactive compounds in food matrices

Tese de Doutoramento
PhD in Chemical and Biological Engineering

Trabalho efetuado sob a orientação dos
Professor Doutor António Augusto Vicente
Doutor Óscar Leandro da Silva Ramos

July, 2019

DIREITOS DE AUTOR E CONDIÇÕES DE UTILIZAÇÃO DO TRABALHO POR TERCEIROS

Este é um trabalho académico que pode ser utilizado por terceiros desde que respeitadas as regras e boas praticas internacionalmente aceites, no que concerne aos direitos de autor e direitos conexos.

Assim, o presente trabalho pode ser utilizado nos termos previstos na licença abaixo indicada.

Caso o utilizador necessite de permissão para poder fazer um uso do trabalho em condições não previstas no licenciamento indicado, deverá contactar o autor, através do RepositóriUM da Universidade do Minho.



This thesis was financially supported by FCT under the scope of the strategic funding of UID/BIO/04469/2013 unit and COMPETE 2020 (POCI-01-0145-FEDER-006684), BioTecNorte operation (NORTE-01-0145-FEDER-000004) funded by the European Regional Development Fund under the scope of Norte2020 - Programa Operacional Regional do Norte and Conselho Nacional de Desenvolvimento Científico e Tecnológico (CNPq) - Brazil (205137/2014-8).















ACKNOWLEDGEMENTS/AGRADECIMENTOS

Foram muitas alegrias e dificuldades que ultrapassei durante esta etapa, que me fizeram ter uma nova perspectiva sobre a ciência e a vida. Mas eu nunca estava sozinha, sempre que olhava ao meu redor, tinha alguém comigo. Gostaria de agradecer a todos que de alguma forma contribuíram para a conclusão desta tese. Há muitas, espero não esquecer ninguém.

Primeiramente, gostaria de expressar a minha gratidão aos meus orientadores. Quero agradecer ao Professor Vicente pelo apoio, orientação, disponibilidade e pela confiança a mim outorgada para o desenvolvimento desta tese. Igualmente agradeço ao Óscar, pelos ensinamento e conselhos que foram fundamentais no decorrer desses quatro anos. É um privilégio poder trabalhar com vocês!

À instituição de acolhimento, Centro de Engenharia Biológica da Universidade do Minho pela disponibilização do espaço e equipamentos necessários à realização deste trabalho. Agradeço ao apoio técnico da Paula, Diana, Maura, Vitória e ao Sr. Santos pela disponibilidade.

Aos meus colegas do Laboratório de Instalações Piloto (LIP) em especial a Isa, Luiz Fasolin, Michele, Joana, Ana Cristina, Ricardo, Rui, Maria, Luís Loureiro, Raquel, Zita, Michel, Daniel, Arlete pelo bom convívio, boas discussões e alegrias compartilhadas.

Aos meus pais e irmãs que sinto imensas saudades. Agradeço pelo amor, carinho e todas as coisas importantes da vida que não são consigo expressar em palavras. Mesmo com a distância se fizeram sempre presentes.

Um agradecimento muito especial ao meu amor Pedro, que embarcou comigo nesta jornada com seu constante apoio aos meus objetivos e sonhos. Obrigada pela dedicação. Obrigada pela oportunidade de crescer e aprender com você.

STATATEMENT OF INTEGRITY

I hereby declare having conducted this academic work with integrity. I confirm that I have not used plagiarism or any form of undue use of information or falsification of results along the process leading to its elaboration.

I further declare that I have fully acknowledged the Code of Ethical Conduct of the University of Minho.

University of Minho,

Full name: Lívia de Souza Simões

Signature: _____

ABSTRACT

Development of bio-based micro- and nanostructures from milk whey proteins, as a vehicle for controlled release and delivery of bioactive compounds in food matrices

β-lactoglobulin (β-Lg) is the major protein fraction of bovine whey serum and due to its gelation capacity, it has the ability to form micro- and nanostructures and entrap bioactive compounds. This thesis aims at providing information for the development and characterization of micro- and nanostructures from β-Lg, purified from a commercial whey protein isolate, to incorporate, protect and delivery of bioactive compounds with different water solubilities. The stability of β-Lg micro- and nanostructures was assessed under various environmental conditions as well as in food simulants and throughout an *in vitro* gastrointestinal model. Homogeneous and stable β-Lg structures were formed at pH 6 with thermal treatment at 80 °C for 15 min. In this conditions, β-Lg nanostructures (with diameter sizes ≤ 100 nm) and β-Lg microstructures (with diameters size between 200-300 nm) were formed with 5 mg mL^{-1} and 15 mg mL^{-1}, respectively. Riboflavin and quercetin were used as hydrophilic and hydrophobic bioactive model compounds, respectively. The impact of environmental conditions (e.g. pH, temperature, ionic strength, and storage temperature) on stability of such structures were investigated. β-Lg structures maintaining their particle size, polydispersity index and surface charge under acidic, neutral or alkaline conditions, at thermal treatments up to 70 °C and during storage for 50 days. The release mechanism of bioactive model compounds from β-Lg structures a was assessed into two food simulants with different hydrophobicities under 4 °C and 25 °C, by fitting the Linear Superimposition Model to the experimental data. The relaxation is the main release mechanism of both bioactive model compounds. Caco-2 cell viability experiment demonstrated that riboflavin and quercetin at concentration up to 0.021 mg mL^{-1} and 0.016 mg mL^{-1}, respectively, entrapped on β-Lg micro- and nanostructures did not have any impact on cell viability. *In vitro* gastrointestinal tract model showed that the entrapment of riboflavin and quercetin into β-Lg micro- and nanostructures increased stability, bioaccessibility, and bioavailability of both bioactive model compounds, when compared with these in their free form. In conclusion, strict control of the physicochemical conditions allowed the development of β-Lg structures with the desired characteristics and capable to act as delivery systems for hydrophilic and hydrophobic compounds, until the intestine.

Keywords: Whey proteins; Bio-based structures; Protein aggregation; Delivery systems; Food simulants.

RESUMO

Desenvolvimento de micro- e nanoestruturas de base biológicas a partir das proteínas do soro do leite, como veículo de libertação controlada e entrega de compostos bioativos em matrizes alimentares

β-lactoglobulina (β-Lg) constitui a principal fração proteica do soro bovino, principal agente gelificante capaz de formar micro- e nanoestruturas e incorporar compostos bioativos. Esta tese objetivou fornecer informações sobre desenvolvimento de micro- e nanoestruturas a partir da β-Lg purificada de um isolado de proteína do soro, para incorporar compostos bioativos com diferentes solubilidades. Avaliou-se a estabilidade β-Lg micro- e nanoestruturas em diferentes condições ambientas, o perfil de libertação dos compostos bioativos em diferentes simulantes alimentar e ao longo do *in vitro* trato gastrointestinal. β-Lg estruturas homogenias e estáveis foram formadas em pH 6, aquecidas a 80 °C por 15 min. Nessas condições, a concentração inicial de 5 mg mL^{-1} β-Lg foram obtidas β-Lg nanoestruturas (diâmetro ≤ 100 nm), e com 15 mg mL^{-1} β-Lg microestrutura (diâmetros entre 200-300 nm). Riboflavina e a quercetina foram empregados como modelo de compostos hidrofílico e hidrofóbico, respectivamente. Avaliou-se a estabilidade de tais estruturas em várias condições ambientais (e.g., pH, temperatura, força iônica e temperatura de armazenamento). β-Lg micro- e nanoestruturas mantiveram tamanhos e homogeneidade em condições ácidas, neutras ou alcalinas, sob tratamentos térmicos até 70 °C e durante o armazenamento por 50 dias. O mecanismo de libertação da riboflavina e quercetina através das β-Lg micro- e nanoestruturas foi avaliado em dois simulantes alimentares a 4 °C e 25 °C, através do ajuste do modelo matemático "Linear Superimposition Model" aos dados experimentais. A relaxação demonstrou ser o principal mecanismo de libertação dos dois compostos bioativos testados. A viabilidade em células Caco-2 não foi afetada para concentrações de até 0.021 mg mL^{-1} para riboflavina de 0.016 mg mL^{-1} para quercetina, quando incorporadas nas β-Lg micro- e nanoestruturas. Estudos *in vitro* no sistema gastrointestinal demostrou que as β-Lg micro- e nanoestruturas aumentou a bioacessibilidade, estabilidade e biodisponibilidade dos compostos bioativos modelos, quando comparadas com a sua forma livre. Em conclusão, demostrou-se que o controle rigoroso das condições ambientais permite o desenvolvimento de β-Lg estruturas com capacidade de serem utilizados como sistemas de entrega de compostos bioativos com diferentes solubilidades até o intestino.

Palavras–chaves: Proteína do soro; Base biológica; Agregação proteica; Sistema de entrega; Simulante alimentar.

TABLE OF CONTENTS

LIST OF FIGURES xiii

LIST OF TABLES xvii

LIST OF GENERAL NOMENCLATURE xx

CHAPTER 1. 2

1.1. Research background and motivation 3

1.2. Research aims 5

1.3. Thesis outline 5

1.4. References 6

CHAPTER 2. 8

2.1. Food nanotechnology 9

2.2. Bio-based materials as ingredients for the encapsulating matrix 9

2.2.1. Proteins 10

2.2.2. Polysaccharides 11

2.2.3. Lipids 12

2.2.4. Different combinations of bio-based materials 13

2.3. Bioactive compounds 14

2.3.1. Vitamins 15

2.3.1.1. Riboflavin 16

2.3.2. Antioxidants 16

2.3.2.1 Quercetin 16

2.4. Development of protein structures through thermal gelation process 17

2.5. Protein structures characterization techniques 18

2.5.1. Dynamic light scattering 18

2.5.2. ζ-potential 18
2.5.3. Fourier transform infrared spectroscopy 19
2.5.4. Circular dichroism 19
2.5.5. Fluorescence spectroscopy 19
2.5.6. Fast protein liquid chromatography 20
2.5.7. Transmission electron microscopy 20
2.6. Food simulants 20
2.7. Caco-2 cell models 21
2.8. *In vitro* digestion model 21
2.9. Protein structures considerations in the food industry 23
2.10. Safety and regulatory considerations 24
2.11. References 25

CHAPTER 3. 34
3.1. Development of β-Lg structures 35
3.1.1. Feedstocks and chemicals 35
3.1.2. β-Lg purification method 35
3.1.3. Experimental design to optimize the development of β-Lg micro- and nanostructures 36
3.1.4. Development of β-Lg micro- and nanostructures 37
3.2. Characterization of β-Lg micro- and nanostructures 38
3.2.1. Particle size, polydispersity index, and surface charge 38
3.2.2. Turbidity 38
3.2.3. Fluorescence measurements 38
3.2.4. Circular dichroism 39
3.2.5. Native polyacrylamide gel electrophoresis (Native-PAGE) 40

3.2.6. Fast protein liquid chromatography 40
3.2.7. Fourier-transform infrared spectroscopy 40
3.2.8. Transmission electron microscopy 41
3.3. Association of bioactive model compounds to β-Lg micro- and nanostructures 41
3.3.1. Feedstocks and chemicals 41
3.3.2. Hydrophilic model compound – Riboflavin 41
3.3.3. Hydrophobic model compound – Quercetin 42
3.3.3.1. High performance liquid chromatography 43
3.4. Stability under various environmental conditions 43
3.4.1. pH stability 43
3.4.2. Ionic strength stability 43
3.4.3. Temperature stability 44
3.4.4. Storage temperature stability 44
3.5. *In vitro* release profile of bioactive model compounds from β-Lg micro- and nanostructures 44
3.5.1. Material 44
3.5.2. Release kinetics profile 44
3.5.3. Mathematical modelling 45
3.5.4. Statistical analysis 46
3.6. Caco-2 cells studies and gastrointestinal (GI) model and 46
3.6.1. Feedstocks and chemicals 46
3.6.2. β–Lg micro- and nanostructures effect on Caco-2 cells 47
3.6.2.1. Cell culture 47
3.6.2.2. Cytotoxicity assay 47
3.6.2.3. Caco-2 cell culture permeability 47
3.6.2.4. Cellular uptake assay 50

3.6.3. *In vitro* digestion 50
3.6.3.1. Bioactive model compounds bioavailability 52
3.6.3.2. Monitoring protein hydrolysis degree during *in vitro* digestion 53
3.7. References 54

CHAPTER 4. 59
4.1. Introduction 60
4.2. Results and discussion 62
4.2.1. β-Lg purification 62
4.2.2. Development of β-Lg micro- and nanostructure 66
4.3. Conclusions 74
4.4. References 75

CHAPTER 5. 79
5.1. Introduction 80
5.2. Results and discussion 82
5.2.1. Bioactive model compounds association 82
5.2.2. Morphology 86
5.2.3. Binding properties 87
5.2.4. β-Lg structures stability under various environmental conditions 92
5.2.5. *In vitro* release kinetics 96
5.3. Conclusions 102
5.4. References 103

CHAPTER 6. 109

6.1. Introduction 110
6.2. Results and discussion 112
6.2.1. β-Lg micro- and nanostructures effect on cell viability 112
6.2.1.1. Cell viability 112
6.2.1.2. Cell permeability 16
6.2.2. Evaluation of β-Lg micro- and nanostructures responsiveness along *in vitro* digestion process 116
6.2.3. β-Lg micro- and nanostructures hydrolysis degree during *in vitro* digestion 118
6.2.4. Native polyacrylamide gel electrophoresis (Native-PAGE) 120
6.2.5. Bioactive model compounds behaviour under gastrointestinal environmental conditions 123
6.2.6. Bioactive model compounds bioaccessibility, stability and bioavailability 126
6.3. Conclusions 130
6.4. References 130

CHAPTER 7. 135
7.1. General conclusions 136
7.2. Guidelines for the future works 137

SUPPLEMENTARY MATERIAL 139

LIST OF FIGURES

CHAPTER 1

Figure 1.1 - Schematic representation of the motivation for the work presented in this thesis ... 4

CHAPTER 2

Figure 2.1 - Schematic diagram representing the main physiological conditions present in the human digestive system. Adapted from Simões et al., (2017) 22

CHAPTER 3

Figure 3.1 - Schematic representation of development β-Lg micro- and nanostructures by gelation process. 37

Figure 3.2 - *In vitro* release system : jacketed reactors for controlling temperature A) and samples into dialysis membrane B)..... 44

Figure 3.3 - Cytotoxicity assay using Caco-2 cell seeded at a cell density of 4×10^{4} cells/well in 96-well plate. 47

Figure 3.4 - Schematic representation of Caco-2 cells seeded on polycarbonate membrane u for permeability measurements. 49

Figure 3.5 - Schematic representation of a simulated *in vitro* digestion method. (Adapted from Minekus et. al, 2014)..... 51

CHAPTER 4

Figure 4.1 - Typical particle size distribution curve (by intensity) obtained for purified and commercial unheated β-Lg, prepared at 10 mg mL^{-1} and pH 6..... 62

Figure 4.2 - Comparison between (•) purified β-Lg and (Δ) commercial β-Lg solutions. (A) Intrinsic fluorescence emission spectra at 295 nm; (B) extrinsic fluorescence emission spectra at 370 nm; (C) Far-UV CD spectra; (D) Native-PAGE. Standard deviation is represented by error bars. 65

Figure 4.3 - Values of particle size (A), polydispersity (PDI) (B), surface charge (C), normalized maximum peak of intrinsic fluorescence at 295 nm (D) and normalized maximum peak of extrinsic fluorescence intensity at 370 nm (E) of β-Lg structures formed at pH 6 after heating at 80 °C for 5, 10 and 25 min at protein concentrations of 5, 10 and 15 mg mL^{-1}. Each data point is the average of nine successive measurements and the error bars show the standard deviation. [a,b,c,d] Means labelled with the same letter do not statistically differ from each other ($p > 0.05$). 70

Figure 4.4 - Far-UV circular dichroism spectra of unheated β-Lg at 5, 10 and 15 mg mL^{-1} and heated β-Lg at 80 °C for 15 and 25 min for 5, 10 and 15 mg mL^{-1} at pH 6 (average ± standard deviation represented by error bars). 72

Figure 4.5 - TEM images of β-Lg at native state A), β-Lg microstructures B), and β-Lg nanostructures C) (scale bar = 200 nm, magnification = 50,000 x)..... 74

CHAPTER 5

Figure 5.1 - TEM images of β-Lg/riboflavin microstructures A), β-Lg/quercetin microstructures B), β-Lg/riboflavin nanostructures C), β-Lg/quercetin nanostructures D) (scale bar = 200 nm, magnification = 50.000 x). 86

Figure 5.2 - Extrinsic fluorescence emission spectra at 370 nm of microstructures: β-Lg a); β-Lg/riboflavin b); and β-Lg/quercetin c); and of nanostructures: β-Lg d); β-Lg/riboflavin e); β-Lg/quercetin f)..... 87

Figure 5.3 - Far-UV CD spectra (190-260 nm) of microstructures: β-Lg a); β-Lg/riboflavin b); and β-Lg/quercetin c); and of nanostructures: β-Lg d); β-Lg/riboflavin e); β-Lg/quercetin f). 89

Figure 5.4 - FTIR spectra of β-Lg/riboflavin micro- and nanostructures A) and β-Lg/quercetin micro- and nanostructures B), being a) β-Lg microstructures; b) β-Lg microstructures associated with respective bioactive model compound; c) free bioactive model compound; d) β-Lg nanostructures; and e) β-Lg nanostructures associated with respective bioactive model compound. 90

Figure 5.5 - Release profiles of riboflavin from β-Lg micro- A) and β-Lg nanostructures B); and quercetin from β-Lg microstructures C), added into the following food simulants: a) 50 % at 25 °C; b) 50 % at 4 °C; c) 10 % at 25°C and d) 10 % at 4 °C. 97

CHAPTER 6

Figure 6.1 - Caco-2 cell viability in contact to β-Lg/riboflavin micro- and nano-structures A) and β-Lg/quercetin micro-structures B) after 24h incubation (bars represent standard deviation). [a,b,c,d] Values with different letter superscripts for the same compound concentration were statistically different ($p \leq 0.05$). The asterisk (*) indicates significant difference ($p \leq 0.05$) relative to the control. 113

Figure 6.2 - Hydrolysis degree (%) of β-micro and nanostructures with (or without) bioactive riboflavin (rib.) and quercetin (quer.) model compounds during *in vitro* digestion. [a,b,c] Small superscript letters in each column indicate statistical difference between means ($p \leq 0.05$) for the same β-Lg structure. 119

Figure 6.3 - Native-PAGE of *in vitro* digestion samples: control A); β-Lg microstructures B); β-Lg microstructures with riboflavin C); β-Lg microstructures with quercetin D); β-Lg nanostructures E); and β-Lg nanostructures with riboflavin F). The lanes represent: commercial molecular weight marker M) intestinal phase of *in vitro* digestion without sample 1); pancreatin from porcine pancreas 2); pepsin from porcine gastric mucous a 3); initial β-Lg structures (before *in vitro* digestion) 4); oral phase 5); gastric phase 6) and intestinal phase 7). 121

Figure 6.4 - Intact (%) free riboflavin, β-Lg/riboflavin micro- and nanostructures A) and free quercetin and β-Lg/quercetin microstructures B) in oral, gastric and intestinal phases during *in vitro* digestion. Results were present as mean ± standard deviation. [a,b,c] Different small letter superscripts in the same *in vitro* digestion phase correspond to statistically significantly differences ($p \leq 0.05$). ND means that the concentration of quercentin was Not Detected. 124

Figure 6.5 - Bioaccessibility, stability and bioavailability of β-Lg/riboflavin micro- and nanostructures A) and β-Lg/quercetin microstructures B). [a,b,c] Samples in the same parameter designated with different letters superscripts are significantly different ($p \leq 0.05$). ND means that the concentration of quercetin was Not Detected. 127

SUPPLEMETARY MATERIAL

Figure S.1 - β-Lg/riboflavin microstructures into food simulants composed by 50 % ethanol at 25 °C A) and 10 % ethanol at 25 °C B), 50 % ethanol at 4 °C C) and 10 % ethanol at 4 °C D). .. 148

Figure S.2 - β-Lg/riboflavin nanostructures into food simulants composed by 50 % ethanol at 25 °C A) and 10 % ethanol at 25 °C B), 50 % ethanol at 4 °C C) and 10 % ethanol at 4 °C D). .. 149

Figure S.3 - β-Lg/quercetin microstructures into food simulants composed by 50 % ethanol at 25 °C A) and 10 % ethanol at 25 °C B), 50 % ethanol at 4 °C C). 150

LIST OF TABLES

CHAPTER 2

Table 2.1 - Examples of bio-based materials used for developing micro- and nanodelivery systems for encapsulation of riboflavin and quercetin as model hydrophilic and hydrophobic, respectively bioactive compounds. 15

Table 2.2 - List of food simulants and potential applications (Adapted from European Parliament and Council). 21

CHAPTER 3

Table 3.1 - Independent variables and their levels in Box-Behnken experimental design for pH values 3, 4, 6 and 7 37

Table 3.2 - Composition of simulated salivary fluid (SSF), simulated gastric fluid (SGF) and simulated intestinal fluid (SIF) stock solutions. 51

CHAPTER 4

Table 4.1 - Experimental responses of particle size distribution, polydispersity index (PDI), intrinsic fluorescence (IF) and extrinsic fluorescence (EF) intensities for the Box-Behnken design. 67

CHAPTER 5

Table 5.1- Association efficiency (AE), loading capacity (LC), particle size, polydispersity index (PDI) and surface charge (S) of β-Lg micro- and nanostructures for riboflavin concentrations (RC) ranging from 0 to 0.105 mg mL^{-1}. 83

Table 5.2 - Association efficiency (AE), loading capacity (LC), particle size, polydispersity index (PDI) and surface charge (S) of β-Lg micro- and nanostructures for quercetin concentrations (QC) ranging from 0 to 0.08 mg mL^{-1} 84

Table 5.3 - Linear superimposition model (LSM) fitting of riboflavin and quercetin release data from β-Lg micro- and nanostructures. The parameters *RMSE* and $R2$ were used to evaluate the quality of the regression. 99

Table 5.4 - Particle size, polydispersity index (PDI) and surface charge (S) of β-Lg micro- and nanostructures before and after the release of riboflavin and quercetin into food simulants at various temperature (4 and 25 °C), and the bioactive compounds final concentration present in β-Lg structures. 101

CHAPTER 6

Table 6.1 - Apparent permeability coefficient (P_{app}) of riboflavin in free form and when associated to micro- and nanostructures in apical compartment and after cell lysis. 115

Table 6.2 - Particle size, polydispersity index (PDI) and surface charge (S) of β-Lg micro- and nanostructures in eac*h in vitro* digestion phase. 117

SUPPLEMETARY MATERIAL

Table S.1 - Effect of distinct pH values on particle size, polydispersity index (PDI) and surface charge (S) of β-Lg microstructures with the riboflavin (rib.) and quercetin (quer.) associated... 140

Table S.2 - Effect of distinct pH values on particle size, polydispersity index (PDI) and surface charge (S) of β-Lg nanostructures with the riboflavin (rib.) and quercetin (quer.) associated.... 141

Table S.3 - Effect of ionic strength on particle size and polydispersity index (PDI) of β-Lg microstructures with the riboflavin (rib.) and quercetin (quer.) bioactive associated. 142

Table S.4 - Effect of ionic strength on particle size and polydispersity index (PDI) of β-Lg nanostructures with the riboflavin (rib.) and quercetin (quer.) associated. 143

Table S.5 - Thermal effect on particle size, polydispersity index (PDI) and surface charge (S) of β-Lg microstructures with the riboflavin (rib.) and quercetin (quer.) associated. 144

Table S.6 - Thermal effect on particle size, polydispersity index (PDI) and surface charge (S) of β-Lg nanostructures with the riboflavin (rib.) and quercetin (quer.) associated. 145

Table S.7 - Particle size, polydispersity index (PDI) and surface charge (S) of β-Lg microstructures with and without the riboflavin (rib.) and quercetin (quer.) associated under storage at 4 °C and 25 °C..... 146

Table S.8 - Particle size, polydispersity index (PDI) and surface charge (S) of β-Lg microstructures with and without the riboflavin (rib.) and quercetin (quer.) associated under storage at 4 °C and 25 °C..... 147

LIST OF GENERAL NOMENCLATURE

Abbreviations

AE – Association efficiency

CD – Circular dichroism

DLS – Dynamic light scattering

FPLC – Fast protein liquid chromatography

FTIR – Fourier transform infrared spectroscopy

GI – Gastrointestinal

HD – Hydrolysis degree

HDS – Human digestive system

HPLC – High performance liquid chromatography

LC – Loading capacity

LSM – Linear superimposition model

M_w – Molecular weight

pI – Isoelectric point

PDI – Polydispersity index

S – Surface charge

TEER – Transepithelial electrical resistance

TEM – Transmission electronic microscopy

Trp – Tryptophan

β-Lg – β-lactoglobulin

Symbols

k_F – Fickian diffusion rate constant

k_R – Relaxation rate constant

M_∞ – Mass released at equilibrium

$M_{\infty,F}$ – Mass released by Fick diffusion at equilibrium

$M_{\infty,R}$ – Mass released due to relaxation process at equilibrium

M_t – Total mass released

$M_{t,F}$ – Mass released by Fick diffusion at time t

$M_{t,R}$ – Mass released due to relaxation process at time t

P_{app} – Apparent permeability coefficient

T – Temperature (°C)

X – Fraction of bioactive compounds model released by Fickian transport

λ_{max} – Maximum fluorescence intensity

ζ – Zeta potential

LIST OF PUBLICATIONS

The research work performed during this thesis resulted in the following publications:

PAPERS IN PEER REVIEWED JOURNALS

Simões, Lívia S.; Madalena, Daniel A.; Pinheiro, Ana Cristina; Teixeira, José A.; Vicente, António A.; Ramos, Oscar L. Micro- and nano bio-based delivery systems for food applications: *In vitro* behavior. Advances in Colloid and Interface Science, 243, 23-45, 2017. (DOI: 10.1016/j.cis.2017.02.010).

PAPERS TO BE PUBLISHED IN PEER REVIEWED JOURNALS

Simões, Lívia S.; Araújo, João M.; Vicente, António A.; Ramos, Oscar L. Design of β-lactoglobulin micro- and nanostructures by controlling gelation through physical variables. Food Hydrocolloids. Resubmitted in July 29, 2019.

Simões, Lívia S.; Arunhosa, Luis; Vicente, António A.; Ramos, Oscar L. Suitability of β-lactoglobulin micro- and nanostructures for loading and release profile of bioactive model compounds. Journal of Controlled Release. Submitted in August 2, 2019.

Simões, Lívia S.; Martins, Joana T.; Pinheiro, Ana C.; Vicente, António A.; Ramos, Oscar L. β-lactoglobulin micro- and nanostructures as bioactive model compounds vehicle: *In vitro* studies. Food Research International. Submitted in August 10, 2019.

Araújo, João F.; Bourbon Ana I.; **Simões, Lívia S**.; Vicente, António A.; Coutinho, Paulo J.; Ramos, Oscar L. Physicochemical characterization and release behaviour of curcumin-loaded LF nanohydrogels into food simulants. Food Research International. Submitted in June 19, 2019.

BOOK CHAPTER

Ramos, Oscar L.; Pereira, Ricardo N.; **Simões, Lívia S**.; Madalena, Daniel A.; Martins, Rui R.; Teixeira, José A.; Vicente, Antonio A. Functional whey protein-based nanostructures. In: Jafari, S.

(ed) Biopolymer Nanostructures for Food Encapsulation Purposes. pp. 69-100, 2019. (DOI: 10.1016/B978-0-12-815663-6.00003-3).

POSTER PRESENTATION

Simões, Lívia S.; Rodrigues, Rui M.; Ramos, Oscar L.; Pereira, Ricardo N.; Pinheiro, Ana Cristina; Teixeira, José A.; Malcata, F. Xavier; Vicente, António A. Characterization of micro- and nanostructures from β-lactoglobulin formed upon heat treatment and under selected environmental conditions. IFT 2016 Annual Meeting and Food Expo, Chicago, USA, July 16th-19th, 2016.

Simões, Lívia S.; Vicente, António A.; Ramos, Oscar L. Design of micro- and nanostructures from β-lactoglobulin under selected environmental conditions. The 19th Gums & Stabilisers for the Food Industry Conference: Hydrocolloid Multifunctionality, Berlin, Germany, June 27th - 30th, (45), 2017.

Ramos, Oscar L.; **Simões, Lívia S**.; Pereira, Ricardo N.; Vicente, António A. Structural characterization of heat-induced β-lactoglobulin nanohydrogels under the effects of selected physical conditions. The 19th Gums & Stabilisers for the Food Industry Conference: Hydrocolloid Multifunctionality, Berlin, Germany, June 27th - 30th, (51), 2017.

Simões, Lívia S.; Rodrigues, Rui; Vicente, António A.; Ramos, Oscar L. Stability of β-Lactoglobulin micro- and nanostructures under various environmental conditions. The 20th Gums & Stabilisers for the Food Industry, San Sebastian, Spain, June 11th -14th, 2019.

Simões, Lívia S.; Vicente, António A.; Ramos, Oscar L. β-Lg nano delivery systems: Sustained release of riboflavin into food simulants under various temperatures. 8th International Symposium on "Delivery of Functionality in Complex Food Systems", Porto, Portugal, July 7th- 10th, 2019.

Araújo, João F.; Bourbon, Ana A.; **Simões, Lívia S.**; Vicente, Vicente, António A.; Coutinho, Paulo J.; Ramos, Oscar L. Incorporation of curcumin-loaded lactoferrin nanohydrogels into a model gelatine: release kinetics and characterization. 8th International Symposium on "Delivery of Functionality in Complex Food Systems", Porto, Portugal, July 7th - 10th, 2019.

ORAL PRESENTATION

Pereira, Ricardo N.; Rodrigues, Rui M.; **Simões, Lívia S**.; Ramos, Oscar L.; Malcata, F. Xavier; Teixeira, José A.; Vicente, António A. Influence of ohmic heating on production of whey protein aggregates. BIOIBEROAMÉRICA 2016 - Book of Abstracts, Salamanca, Spain, June 5th - 8th, (205), 2016.

Simões, Lívia S.; Abrunhosa, Luís; Vicente, António A.; Ramos, Oscar L. Suitability of β-lactoglobulin micro- and nanostructures for quercetin-loading. FSD 2018 - 3rd Food Structure & Design Conference, Debrecen, Hungary, September, 21th- 22th, 2018

Section I

INTRODUCTION

CHAPTER 1.

MOTIVATION AND OUTLINE

1.1. Research background and motivation 3

1.2. Research aims 5

1.3. Thesis outline 5

1.4. References 6

1.1. Research background and motivation

The daily consumption of bioactive ingredients has been proven to benefit human health, performance, and wellbeing. These benefits enhance consumers' interest for functional foods, so that consumers press the food industry to improve or develop new sustainable and healthier products (Wijaya et al., 2019). In this sense, nanotechnology has become one of the most promising approaches to develop functional foods, once allows the manipulation of bioactive compounds more effectively, thus allowing overcome several technological limitations that has a negative impact on the development of functional foods and their efficient delivery (Aklakur et al., 2016; Singh, 2016). Therefore, the incorporation of bioactive compounds (e.g. antioxidants, antimicrobials, vitamins, probiotics, and prebiotics) into micro- and nanostructures is an emerging tool that holds the potential to act as a delivery system in the food industry (Cerqueira et al., 2017). The European Commission (EC) published a "Recommendation on the definition of nanomaterial" where the term "nanomaterial" is applied for materials with particle size ranging from 1 to 100 nm in excess of 50% of their size distribution by number (Comission, 2011). Moreover, several literature reviews and researches have proposed as diameter of 100 nm as the maximum size for nanostructures (Joye & McClements, 2014; Mcclements, 2017; Singh, 2016). In general, bio-based structures used at micro- and nanoscales exhibit a large surface area-to-volume ratio and their physical and chemical interactions influence their overall properties, in particular the incorporation of bioactive compounds. For instance, a change in their pharmacokinetics and biodistribution contributes to the improvement of bioactive compounds' solubility and bioavailability, thus preventing undesirable chemical reactions and maintaining its activity until its release (Ezhilarasi et al., 2013; Kwak, 2013; Patel & Bhandari, 2012).

Innovative delivery structures for the food industry can be developed from a wide variety of food-grade materials (e.g., proteins, polysaccharides, lipids, among others). Nonetheless, the selection of the appropriate bio-based material requires an understanding of the bioactive compound properties, as well as of the nature of the food matrix, in which such compounds will be incorporated (Vos et al., 2010). Bio-based delivery structures must be able to maintain the activity and stability of bioactive compounds until their release, in a controlled way, and only activate them at the target site (i.e., some compounds lose their activity when they are mixed with food components, due to their early release) (Devi et al., 2017). They should also protect bioactive compounds from adverse environmental conditions inherent to food processing and storage (e.g., variation of pH, temperature, ionic strength and enzymatic activity), thus improving their

bioavailability (Series, 2017). Moreover, delivery systems should not affect the physicochemical and sensory properties of the final food products (Joye et al., 2014).

The development of innovative bio-based structures with improved or novel functionalities for encapsulation, protection and controlled release of bioactive compounds intended their use in diverse food industry applications constitutes the main motivation for developing this thesis, which is schematic represented in Figure 1.1.

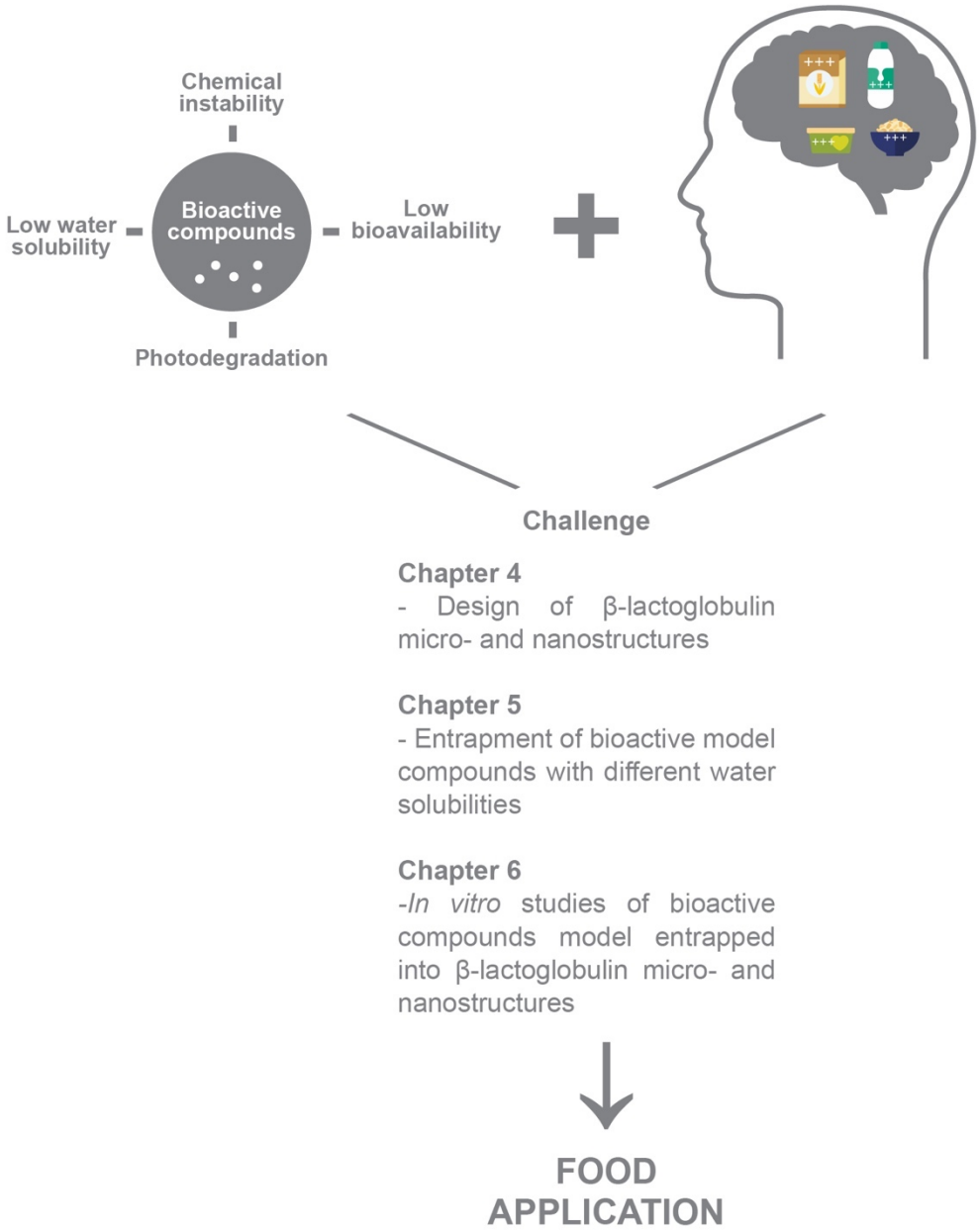


Figure 1.1 - Schematic representation of the motivation for the work presented in this thesis

1.2. Research aims

The main objectives of this thesis is to improve the knowledge about the development of bio-based micro- and nanostructure systems made from whey proteins for release of riboflavin and quercetin used as hydrophilic and hydrophobic bioactive model compounds; assess the release profile of both bioactive model compounds from micro- and nanostructure systems upon food simulants; and evaluate the behaviour of throughout an *in vitro* GI model system, aiming at their potential application in the food products.

The specific aims of this work were:

- Development of micro- and nanostructures from commercial whey proteins (i.e., whey protein isolate) and their physicochemical characterization;
- Evaluation of micro- and nanostructures stability upon various environmental conditions e.g., pH, temperature, ionic strength and storage temperature;
- Entrapment of hydrophilic (i.e., riboflavin) and hydrophobic (i.e., quercetin) bioactive model compounds with different water solubilities into micro- and nanostructures and their characterization including association efficiency and loading capacity;
- Application of such micro- and nanostructures into food simulants (i.e., 10 % of ethanol simulating hydrophilic matrices and 50 % of ethanol simulating hydrophobic matrices) and evaluation of release kinetics of riboflavin and quercetin model compounds from such structures over time;
- Assessment of cytotoxicity, permeability, and rate of absorption of riboflavin and quercetin model compounds through *in vitro* Caco-2 cells lines;
- Evaluation of release kinetics of bioactive model compounds during *in vitro* digestion.

1.3. Thesis outline

Based on its main purpose and subsequent research aims, this thesis was dived in four sections, being the Introduction the Section I, the Materials and methods the Section II, the Results and discussion the Section III and the Final conclusions the Section IV. The sections were dived in chapters, in a total of seven, with three of them reporting experimental results and their discussion (Chapters 4 – 6).

Section I (containing Chapters 1 and 2) comprises an overview of the state-of-the-art of bio-based materials as encapsulating matrices, their properties and applications. A description of bioactive compounds description regarding their health benefits and limitations is provided together with the

main concepts on the *in vitro* studies. The methodologies applied during this work are described in Section II, Chapter 3.

The results obtained in this thesis are presented in Section III, which is dived in three chapters. Chapter 4 comprises the development of β-Lg structures, using as base material β-Lg purified from a commercial whey protein isolate. The purified β-Lg, with a purity level similar to that of commercial protein obtained from Sigma Aldrich, was used to develop innovative β-Lg micro- and nanostructures through specific environmental conditions. In chapter 5 evaluates the ability of β-Lg micro- and nanostructures to associate bioactive model compounds with different water solubilities. The stability of such structures when subjected to various environmental conditions, as well the release profile of bioactive model compounds, when added into food simulants were also assessed. Chapter 6 comprises the bioactive model compounds cytotoxicity, permeability, and rate of absorption through *in vitro* Caco-2 cell line. In this Chapter the behaviour of β-Lg micro- and nanostructures during an *in vitro* gastrointestinal process and the impact on protein structural properties and bioactive model compounds were also determined. In the last section (Section IV), Chapter 7 provides the most relevant conclusion obtained during the course of this work, as well the future perspectives.

1.4. References

Aklakur, M., Rather, M. A., & Kumar, N. (2016). Nano Delivery: An Emerging Avenue for Nutraceuticals and Drug Delivery. Critical Reviews in Food Science and Nutrition, 54, 2317–2361. https://doi.org/10.1080/10408398.2013.839543

Cerqueira, M. Â., Pinheiro, A. C., Ramos, O. L., Silva, H., Bourbon, A. I., & Vicente, A. A. (2017). Advances in Food Nanotechnology. Emerging Nanotechnologies in Food Science. Elsevier Inc. https://doi.org/10.1016/B978-0-323-42980-1.00002-9

Comission, E. (2011). Commission recommendation of 18 October 2011 on the definition of nanomaterial (2011/696/EU). Official Journal of the European Union, L275(June 2010), 38–40. https://doi.org/10.2777/13162

Devi, N., Sarmah, M., Khatun, B., & Maji, T. K. (2017). Encapsulation of active ingredients in polysaccharide–protein complex coacervates. Advances in Colloid and Interface Science, 239, 136–145. https://doi.org/10.1016/j.cis.2016.05.009

Ezhilarasi, P. N., Karthik, P., Chhanwal, N., & Anandharamakrishnan, C. (2013). Nanoencapsulation Techniques for Food Bioactive Components: A Review. Food and Bioprocess Technology, 6(3), 628–647. https://doi.org/10.1007/s11947-012-0944-0

Joye, Iris J., Davidov-Pardo, G., & McClements, D. J. (2014). Nanotechnology for increased micronutrient bioavailability. Trends in Food Science & Technology, 40(2), 168–182. https://doi.org/10.1016/j.tifs.2014.08.006

Joye, Iris Julie, & McClements, D. J. (2014). Biopolymer-based nanoparticles and microparticles: Fabrication, characterization, and application. Current Opinion in Colloid and Interface Science, 19(5), 417–427. https://doi.org/10.1016/j.cocis.2014.07.002

Kwak, H.-S. (2013). Overview of Nano- and Microencapsulation for Foods. In H.-S. Kwak (Ed.), Nano- and Microencapsulation for Foods (First Edit, pp. 1–14). John Wiley& Sons.

Mcclements, D. J. (2017). The future of food colloids : Next-generation nanoparticle delivery systems. Current Opinion in Colloid & Interface Science, 28, 7–14. https://doi.org/10.1016/j.cocis.2016.12.002

Patel, A. R., & Bhandari, B. (2012). Nano- and Microencapsulation of Vitamins. In H.-S. Kwak (Ed.), Nano-and Microencapsulation for Foods (First Edit, pp. 223–248). JohnWiley& Sons. https://doi.org/10.1002/9781118292327.fmatter

Series, F. E. (2017). Engineering Foods for Bioactives Stability and Delivery. https://doi.org/10.1007/978-1-4939-6595-3

Singh, H. (2016). Nanotechnology Applications in Functional Foods ; Opportunities and Challenges. Prev.Nutr.Food Sci., 21(February), 1–8. https://doi.org/10.3746/pnf.2016.21.1.1

Vos, P., Faas, M. M. M., Spasojevic, M., & Sikkema, J. (2010). Encapsulation for preservation of functionality and targeted delivery of bioactive food components. International Dairy Journal, 20(4), 292–302. https://doi.org/10.1016/j.idairyj.2009.11.008

Wijaya, W., Harfieyanto, R. C., Dewettinck, K., Patel, A. R., & Van der Meeren, P. (2019). Whey protein isolate–low methoxyl pectin nanocomplexes improve physicochemical and stability properties of quercetin in a model fat-free beverage. Food & Function, 1–11. https://doi.org/10.1039/c8fo02350f

CHAPTER 2.

LITERATURE REVIEW

2.1. Food nanotechnology 9

2.2. Bio-based materials as ingredients for the encapsulating matrix 9

2.3. Bioactive compounds 14

2.4. Development of protein structures through thermal gelation process 17

2.5. Protein structures characterization techniques 18

2.6. Food simulants 20

2.7. Caco-2 cell models 21

2.8. *In vitro* digestion model 21

2.9. Protein structures considerations in the food industry 23

2.10. Safety and regulatory considerations 24

2.11. References 25

This Chapter was adapted from:

Simões, Lívia S.; Madalena, Daniel A.; Pinheiro, Ana Cristina; Teixeira, José A.; Vicente, António A.; Ramos, Oscar L. Micro- and nano bio-based delivery systems for food applications: *In vitro* behavior. Advances in Colloid and Interface Science, 243, 23-45, 2017. (DOI: 10.1016/j.cis.2017.02.010).

2.1. Food nanotechnology

The world´s population is increasing every year and, consequently, challenges regarding the production, preservation, safety and sustainability of food products have emerged. Therefore, offering the consumer high quality foods with the required level of bioavailable nutrients and dietetic supplements is a current challenge. The application of micro- and nanotechnology in food industry may represent a solution for the potential bioavailability issues, providing new solutions and opportunities to address these challenges (Cerqueira et al., 2017; Jafari, 2019; Mcclements, 2017).

Materials at micro- and nanoscale exhibit different physical, chemical and biological properties, which may enhance the properties of such materials or even exhibit novel material functionalities and applications, when compared with those at the macroscale (Durán & Marcato, 2013; McClements, 2015). Due to their reduced size, micro- and nanosystems can improve solubility, bioavailability and sensorial characteristics (e.g., mask unpleasant flavours), prevent undesirable physical and chemical reactions, as well as protect bioactive compounds from degradation. This behaviour can be related to the large surface area-to-volume ratio, but also to the effect of physical and chemical interactions between materials, found at lower sized structures (i.e., at micro- and nanoscale), which have a significant effect on the overall properties of those systems (Cerqueira et al., 2014). Among these, the incorporation of bioactive compounds in food and the assurance of their stability during processing, storage and digestion, until they reach the appropriate delivery point and timing, are the main concerns regarding the controlled release of bioactive compounds (Balassa et al., 2014). On the other hand, size reduction promotes a great improvement in bioadhesive properties that may include a significant increase in adhesive forces, prolonging gastrointestinal (GI) transit time, thus leading to a higher bioavailability, when compared with larger particles (Acosta, 2009).

One of the major challenges regarding the use of micro- and nanostructures for food applications is the replacement of non-food-grade materials by bio-based, biodegradable and generally recognized as safe (GRAS) alternatives (Kwak, 2013). Other challenges include the design and application of efficient delivery systems for bioactive compounds release.

2.2. Bio-based materials as ingredients for the encapsulating matrix

Encapsulation is a technique in which small substances (i.e., bioactive compounds) are entrapped by a surrounding material to form capsules, at micro- (microencapsulation) or nano-

(nanoencapsulation) scale. This structure can sometimes be an effective protection barrier against environmental agents such as oxygen, light and free radicals. Moreover, micro- and nanoencapsulation have the ability to increase the bioavailability, enhance controlled release and targeting precision of bioactive compounds (Ezhilarasi et al., 2013; Kwak, 2013; Patel & Bhandari, 2012). The release rate of bioactive compounds from micro- and nanostructures is linearly dependent with the surface area of such structures, which is inversely proportional to particle size. Therefore, a decrease in particle size results in an increase of the surface area, and consequently in the release rate of bioactive compounds (Tiwari & Takhistov, 2012).

The encapsulating materials used as delivery systems can be chosen from natural biomaterials as long as they are safe and with Generally Recognized As Safe (GRAS) designation (Augustin & Hemar, 2009).

Bio-based micro- and nanostructures for food industry can be produced from a wide variety of food-grade materials, including proteins, polysaccharides and lipids, isolated or associated to form complex delivery systems. However, the selection of the appropriate bio-based material requires an understanding of the bioactive compound properties, as well as of the nature of the food matrix, in which such compounds will be incorporated (Joye et al., 2014; Vos et al., 2010).

2.2.1. Proteins

Proteins are biological polymers formed by a sequence of amino acids linked by peptide bonds. There are 20 different amino acids categorized according to the properties of their side groups as aliphatic, aromatic, charged (positive or negative), or polar. The proteins that are frequently used in the food industry are obtained from plant (e.g., soy and zein) and animal (e.g., casein, egg and whey protein) sources, or hydrolysates of these proteins (Augustin & Hemar, 2009; Belitz,et al., 2009; Damodaran et al., 2008).

The characterization of protein molecules is of utmost importance since the knowledge of their characteristics (i.e., denaturation temperature, isoelectric point and chemical degradation reactions) is crucial for optimizing the necessary production conditions for the development of protein-based delivery systems (Matalanis et al., 2011). Protein molecules interact with each other or with other molecules in their vicinity through electrostatic, covalent, van der Waals, steric, hydrogen, hydrophobic and disulphide bonds (Ramos et al., 2015). Protein secondary structure (i.e., α-helices and β-sheets) can be organized in adjacent amino acids on protein chains, which may play an important role in the formation, stability and functionality of the resulting structures.

The exposure of protein side groups to the environmental conditions is determined by the conformation of the aminoacid chain, which affects protein stability and reactivity (Davidov-Pardo et al., 2015).

Regarding protein electrical characteristics, they can be described according to their surface charge profile, which varies with pH. Their electrical charge changes from positive (below their isoelectric point - pI), neutral (at their pI) and negative (above their pI) according with the pH value. However, when the protein structure is at its pI, the protein has both positive and negative charged groups on its surface, which enable the formation of attractive and/or repulsive electrostatic interactions (Balassa et al., 2014). Proteins have a high nutritional value and considerable functional properties such as emulsification, gelation, foaming and water binding capacity. Due to their structural versatility, many structures can be produced (i.e., films, particles, fibers, tubules and hydrogels), offering the possibility of delivering both hydrophobic and hydrophilic bioactive compounds (Chen et al., 2006; Wan et al., 2015).

2.2.2. Polysaccharides

Polysaccharides are polymeric carbohydrate molecules composed by several monosaccharide units, bound together by glycosidic linkages. The chemical differences in the polymeric chain regarding the type, number, sequence and linkage of monosaccharides influences the molecular properties of these structures, such as water retention capacity, solubility, digestibility, as well as gelation and emulsification capability (Belitz et al., 2009; Sirisha & Campus, 2015).

Polysaccharides are widely found in Nature and can be obtained from natural sources or from by-products of food industry, mostly through low-cost processing techniques. These polymers present important properties such as good stability, non-toxicity, biodegradability and bioadhesivity that allow their use as delivery systems (Ramos et al., 2014).

Usually polysaccharide-based delivery systems are organized according to their biological origin: plant (e.g., pectin, guar gum, starch and cellulose), animal (e.g., chitosan), algae (e.g., alginate and carrageenan) and microbial (e.g., dextran and xanthan gum) (Akhavan et al., 2016; Patel & Bhandari, 2012).

Polysaccharide-based delivery systems have the ability to interact with bioactive compounds (i.e., through interactions between functional groups), which makes them versatile carriers to bind and entrap a variety of hydrophilic and hydrophobic functional compounds. Due to their thermal stability, they are suitable protective carriers for labile compounds during food processes that

require high temperatures, acting as a suitable alternative to lipid and protein-based delivery systems that melt and denature, respectively (Fathi et al., 2014).

The selection of an appropriate polysaccharide- based material to produce micro- and nano-delivery systems is highly dependent of surrounding environmental conditions, once they may associate to other compounds and form different structures. Therefore, the knowledge about their physical and electrical properties, and susceptibility to chemical and enzymatic reactions is of utmost importance (Matalanis et al., 2011).

Polysaccharides can also produce micro- and nanosystems by assembling mechanisms through electrostatic interactions based on their intrinsic charge that, depending on the base materials, can be classified as neutral (i.e., amylose, amylopectin, cellulose and guar gum), anionic (i.e., alginates, carrageenans, gellan, and arabic and xanthan gums) and cationic (i.e., chitosan) (Thakur & Thakur, 2016). The relation between pH and pKa of the charge groups is of extreme importance to establish the electrical charge level on ionic polysaccharides; for instance, anionic polysaccharides tend to be neutral at pH values considerably below its pKa value, but they acquire a negative charge at pH values above its pKa value. On the other hand, cationic polysaccharides tend to be neutral at pH values above its pKa value, while they acquire a positive charge at pH values below its pKa value (Matalanis et al., 2011).

2.2.3. Lipids

Lipids are generally referred to as fats (in solid form) or oils (in liquid form) depending on their physical state at room temperature. These compounds are classified as nonpolar (e.g., triacylglycerol and cholesterol) or polar (e.g., phospholipids) lipids, causing significant differences in their solubility and functional properties (Belitz et al., 2009; Damodaran et al., 2008).

The physicochemical properties of lipids control their microstructural characteristics, colloidal stability, as well as rheological and moisture barrier properties. A decrease in the length of their hydrocarbon chain attached to the glycerol backbone, or an increase in the degree of unsaturation of the fatty acid chains, lowers their melting point and decreases their moisture barrier properties (Augustin & Hemar, 2009).

Lipid-based delivery systems confer a series of advantages such as the ability to retain materials with different solubilities, in particular those with high hydrophobicity, thus protecting a bioactive compound from biological and chemical degradation, while providing stability during storage.

Moreover, they may enhance the encapsulation efficiency of hydrophobic bioactive compounds, thus increasing its bioavailability and reducing its potential toxicity (Anandharamakrishnan, 2014). Phospholipids are a class of lipids that are essential for human health and the main constituents of cellular membranes. They are biocompatible materials and have amphiphilic nature, which permits self-assembly, emulsifying and wetting properties. Hence, such compounds have demonstrated potential to encapsulate hydrophobic and hydrophilic bioactive compounds (Secolin et al., 2016).

2.2.4. Different combinations of bio-based materials

Some applications may require the properties of different materials and, thus, the combination of different bio-based materials can be performed in order to take advantage of a multi-functional system. The appropriate combination of bio-based materials (e.g., proteins, polysaccharides, lipids and other materials) can improve the properties of micro- and nanodelivery systems in terms of mechanical, thermal and barrier resistance, encapsulation efficiency, stability and bioavailability of bioactive compounds, when compared with those obtained by using a single material (Devi et al., 2017; Fang & Bhandari, 2011).

Proteins have interesting nutritional properties, high capacity to form gels and they are easily hydrolysed by digestive proteases, while polysaccharides (e.g., alginate, pectin, dextran and chitosan) possess high stability under harsh gastric conditions (i.e., are resistant to digestive enzymes) and display a high adhesiveness to the intestinal mucosal surface (Mizrahy & Peer, 2012).

Moreover, the opposite electrical charges between proteins and polysaccharides affected by environmental conditions, contribute to associative interactions between both biopolymers through electrostatic attraction. For instance, a polymeric system composed by a mixture of an anionic polysaccharide and a globular protein (at different specific pH values) can be formed; when the pH of the protein solution is above its pI, there are repulsive electrostatic forces between protein and the anionic groups of the polysaccharide structure. However, if the pH of protein solution is below its pI, the cationic regions of the protein surface can interact with the anionic groups of the polysaccharide chain, thus leading to weak electrostatic interactions and to the formation of soluble complexes. At lower pH values, the content of cationic groups on the proteins surface increases, which leads to greater electrostatic attraction between protein and anionic polysaccharides, thus resulting in charge neutralization and protein–polysaccharide complex formation. At pH values

below the pKa of the anionic groups on the polysaccharide chain, the attractive interactions between the protein and polysaccharide molecules may weaker, which may result in complex dissociation (Gao et al., 1997; Hu & Huang, 2013).

2.3. Bioactive compounds

The development of modern biology, chemistry, molecular biology and biochemistry enabled the isolation of bioactive compounds, as well as the study of their interactions with the human body. Bioactive compounds are molecules that provide several benefits to human health by preventing or retarding the appearance of diseases through e.g., antioxidant, anti-inflammatory or anticancer activities. Therefore, the properties of bioactive compounds should be preserved until the exact moment and specific site where they will be used (Ezhilarasi et al., 2013; Hu & Huang, 2013).

Bioactive compounds such as antioxidants, antimicrobials, vitamins, probiotics, prebiotics, minerals, nutrients and polyphenols are not added in their pure state to food matrices, due to their susceptibility to physical, chemical and enzymatic degradation (and in some cases, due to their low water solubility), during processing, transportation and storage. The performance of these substances can be highly affected by light, heat, water and oxygen exposure, which may compromise its activity and shelf life. Moreover, the degradation of such compounds can cause off-flavour, off-colours or even carcinogenic residues; for instance some micronutrients, such as iron (Dubey & Windhab, 2013) and zinc (Gülseren et al., 2012) can react with other components in a way that their bioactivity and stability is compromised. Therefore, their encapsulation is of utmost importance to allow their incorporation in high water content food products, while preserving their bioavailability and preventing the aforementioned undesired effects (Dordevic et al., 2014; Joye et al., 2014).

The addition of encapsulated compounds (i.e., in a protected form) to food products can overcome some nutritional losses that frequently occur during food processing and storage; thus conferring protection and allowing its better absorption in the small intestine until they reach the bloodstream (Anandharamakrishnan, 2014; Garti & McClements, 2012; Joye et al., 2014). Table 2.1 provides examples of various bio-based materials used for developing delivery systems to incorporated riboflavin and quercetin as model hydrophilic and hydrophobic, respectively, bioactive compounds.

Table 2.1 - Examples of bio-based materials used for developing micro- and nanodelivery systems for encapsulation of riboflavin and quercetin as model hydrophilic and hydrophobic, respectively bioactive compounds.

Bioactive compound	Encapsulating material	Size (nm)	Reference
Riboflavin	WPI	209 – 3674	(Ye et. al, 2019)
	β-Lg	248	(Madalena et al., 2016)
	Liquid oil (hydrogenated canola oil)	104	(Couto et al., 2017)
	Phenylalanine ethyl ester – alginate conjugate	226 – 425	(Zhang et al., 2016)
Quercetin	BSA	15	(Fang et al., 2011)
	Zein	130 – 161	(Patel et al., 2012)
	Lipid oil (medium chain triglyceride)	103 – 127	(Aditya et al., 2014)
	Lipid oil (castor oil)	19.3	(Pangeni et al., 2017)
	Zein protein-soy bean polysaccharide	200	(Li et al., 2019)
	Chitosan – β-Lg	150 – 300 nm	(Ha et al., 2013)

NOTE: WPI - Whey protein isolate; β-Lg - β-lactoglobulin; BSA - Bovine serum albumin

2.3.1. Vitamins

Vitamins are bioactive compounds whose consumption is essential for growth, development and normal maintenance of the human body. These compounds cannot be naturally produced by the human body (except vitamin D and B_3) and, consequently, they must be obtained from external sources (Patel & Bhandari, 2012). The nutritional deficiencies in vitamin uptake can be caused by inadequate ingestion or utilization, poor absorption, increased excretion or destruction in the body, or even due to increased needs, which can lead to the development of certain diseases (e.g., cancer, and cardiovascular and eye degenerative diseases) (Amin et al., 2019; Ball, 2004). Vitamins are susceptible to degradation during processing, storage and until the moment of their

absorption in the GI tract, due to a variety of factors (e.g., exposure to inadequate light, oxygen, temperature, pH or enzymatic conditions). Therefore, vitamin stability is an important parameter that should be considered when these compounds are added to food products.

2.3.1.1. Riboflavin

Riboflavin, also known as vitamin B_2, is a water soluble vitamin found in both animal and plant derived foods (Beztsinna et al., 2016). Microorganisms and plants have capacity to produce riboflavin through the endogenous way, however, humans cannot synthesize it, so it must be supplied by foods and dietary supplements (Kato & Park, 2012).

This vitamin is the central component of the cofactors flavin adenine dinucleotide (FAD) and flavin mononucleotide (FMN), participate in a wide of redox reactions, some of which are absolutely key to the function of aerobic cells (Couto et al., 2017). Moreover, it contributes to normal energy-bioengineered riboflavin in nanotechnology yielding metabolism, functioning of the nervous system and to the maintenance of normal red blood cells (Gironés-Vilaplana et al., 2017).

Riboflavin has heat stability, but the exposure to light results in substantial losses due to its photosensitivity. The vitamin photodegradation can be enhanced by adding sodium bicarbonate, which is used to preserve vegetable colours (Combs Jr, 2013).

The recommended riboflavin daily intake is between 0.3 and 0.4 mg for infants, between 0.5 and 0.9 mg for children and 1.2 mg for adults (Ashoori & Saedisomeolia, 2014; Madalena et al., 2016). Riboflavin deficiency is endemic in populations who have daily diets lacking dairy products and meat (e.g., vegan and vegetarian diets), which may led to oral-buccal cavity lesions, monocystic anemia, seborrheic dermatitis and cheilosis (Beztsinna et al., 2016; Udhayabanu et al., 2017).

2.3.2. Antioxidants

Free radical and nitrogen species can be produced in the human body by various endogenous systems, through the exposure to different physiochemical conditions or through some pathological states. These species are considered one of the major causes of many current diseases, including diabetes and cardiovascular diseases.

Antioxidants can be obtained from natural sources such as vegetables, fruits, leaves, oilseeds, cereal crops and herbs and play an imperative role in providing protection against free radical and nitrogen species (Kumari et al., 2010; Quirós-Sauceda et al., 2014).

Phytochemicals are a large group of plant-derived compounds, including polyphenols, flavonoids, isoflavones, resveratrol and carotenoids that have high antioxidant and anti-inflammatory activity, thus providing several health benefits (Wadood et al., 2013). In many cases, phytochemicals need to be encapsulated in order to prevent undesired sensory properties (e.g., off-flavours and odours) and avoid rapid degradation in food products, thus permitting their use at higher concentrations without causing adverse effects to consumers (Garti & McClements, 2012).

2.3.2.1. Quercetin

Quercetin is a natural flavonoid found in fruits and vegetables (e.g., cranberry, plums, kale, and red onions) (Li et al., 2019), that has attracted increasing attention due to several bio-functional properties such as antioxidant, anti- cancer and antiviral activities (Weiyou Wang et al., 2016). The recommended quercetin daily intake is of 0.015 mg mL^{-1} (Wijaya et al., 2019).

Its exploitation by food and pharmaceutical industries has been limited by its low water solubility and bioavailability, chemical instability and short biological half-life (Sedaghat Doost et al., 2018). Quercetin is a hydrophobic compound with low solubility in water, ca. 0.01 mg mL^{-1} (25 °C), moderate solubility in ethanol, ca. 4 mg mL^{-1} (37 °C), and high solubility in dimethyl sulfoxide ca. 150 mg mL^{-1} (25 °C) (Wang et al., 2016). Dimethyl sulfoxide is not a food grade compound, which compromises the incorporation of needed amounts of quercetin in aqueous matrix to have a final product with the recommended daily dose. Nonetheless, quercetin demonstrate an affinity for proteins and tend to form stable systems, which may either be soluble or precipitate out of solution depending on the strength of the chemical interactions (Wijaya et al., 2019). So, the development of micro- or nanosystems using proteins as encapsulating material may represents a suitable mean to protect and improve the quercetin' solubility and bioavailability, thus overcoming said issues.

2.4. Development of protein structures through thermal gelation process

Gelation typically encompasses two stages: partial unfolding (denaturation) of the native globular structure followed by intermolecular aggregation. Denaturation of the native structure of proteins can be induced by several factors, e.g., addition of chemicals or electrolytes, change in net charge, increase in hydrostatic pressure, partial enzymatic hydrolysis and electrical fields – but mainly by temperature. Each of these processes may induce partial (or total) denaturation of native proteins, which may results in protein aggregation and gel formation (Ramos et al., 2014).

When globular proteins are heated until reaching their denaturation temperature, they start to unfold (i.e., the nonpolar groups, normally buried within the protein structure, are exposed), and may interact with other protein structures, forming different types of aggregates (e.g., fibrillar or particulate aggregates) with diverse mechanical and microstructural properties. Moreover, proteins can maintain their individual structure by balancing attractive and repulsive interactions between them (Matalanis et al., 2011). The extent of aggregation largely depends on extrinsic factors (e.g., temperature, ionic strength and pH) arising from environmental and processing conditions. Aggregation is a prerequisite for the formation of protein micro- and nanostructures; when properly controlled and engineered, that may result in materials with novel functionalities (Davidov-Pardo et al., 2015; Ramos et al., 2012).

2.5. Protein structures characterization techniques

This section summarizes the techniques that are commonly used to study and characterize protein structures. The different approaches, based on their different features, were subdivided into two main sets: physicochemical and imaging techniques.

2.5.1. Dynamic light scattering

Dynamic light scattering (DLS) is an important experimental technique in science and industry for a rapid determination of size distribution of particles in suspension (Stetefeld et al., 2016). DLS measures the Brownian motion (i.e., small molecules move faster than large ones) and relates this to hydrodynamic particle size through Stokes-Einstein equation (Mehalebi et al., 2008). In addition, DLS provides the standard deviation of the particle size distribution through the polydispersity index (PDI) (Lorber et al., 2012).

2.5.2. ζ-potential

ζ-potential is a scientific term for electrokinetic potential in colloidal systems and is used to predict the surface charge of structures in solution by measurement of electrophoretic mobility of the charged particles when submitted to an electric field (Silva et .al, 2012). The ζ-potential magnitude indicates the degree of repulsion between close, similarly charged particles in a dispersion. ζ-potential values above 30 mV (positive or negative) usually means highly charged particles (Das & Chaudhury, 2011). Commonly, high ζ-potential values prevents aggregation of the particles due to electric repulsion, being the colloidal system considered stable (Lin et al., 2014).

2.5.3.Fourier transform infrared spectroscopy

Fourier transform infrared spectroscopy (FTIR) is based on an infrared radiation that passes through the sample, being part of it absorbed by the sample and other part transmitted. The spectrum obtained is constituted by the radiation which results from molecular absorption and transmission, creating a molecular fingerprint of the sample (Silva et al., 2012). Since each sample possesses a unique combination of atoms, it is virtually impossible that two different samples display the same spectrum result (Barth, 2007). For these reasons FTIR is an extremely accurate and reproducible technique for compounds' identification (Nicolet, 2001).

2.5.4. Circular dichroism

Circular dichroism (CD) spectroscopy is a powerful tool for elucidating the proteins' structure because of its high conformational sensitivity (Woody, 2012). Proteins are composed by amino acids, mainly chiral amino acids, liked via peptide bonds (Kobayashi et al., 2012). Physical and chemical interactions are the main forces involved in the stability of protein structure. In far-UV region, the chromophores responsible for the chiral absorption phenomenon are the peptide bonds (amide chromophore), which CD bands provide information on ligand–protein interactions; and allow monitor the protein folding and unfolding and predict different types of protein secondary structure (e.g., α-helix, β-sheet or random coil) (Miles & Wallace, 2016).

2.5.5. Fluorescence spectroscopy

Fluorescence is the result of samples containing fluorophores or fluorescent dyes that absorb light energy at one wavelength and re-emits nearly instantaneously in another, usually at longer wavelengths (Turner Designs, 2015).

This technique is useful to evaluate the structure and dynamics of protein molecules in solution. The intrinsic fluorescence of amino acid residues is sensitive to their microenvironment, and provide information about protein folding and protein conformational changes (Stănciuc et al., 2012). Moreover, the addition of fluorescent dyes (e.g., ANS) in protein solution is a convenient and sensitive tool, which allows investigating the protein hydrophobic regions and potential binding regions (Collini et al., 2009).

2.5.6. Fast protein liquid chromatography

Fast protein liquid chromatography (FPLC) is a high-resolution protein separation technique, based on particle' average diameter size. FPLC is very demanding and sensitive once proteins cannot stand high temperatures, high pressures, or the solvents usually used in HPLC. Thus, it allows to a good differentiation between native and aggregated proteins (O'Sullivan & Sheehan, 2011; Ramos et al., 2012).

2.5.7. Transmission electron microscopy

Transmission electron microscopy (TEM) is a useful technique to determine the shape, morphology, particle size and size distribution of protein structures (Das & Chaudhury, 2011). TEM utilizes a high energy beam of electrons that passes through the sample and the interactions between the electrons and the atoms can be used to observe features of the sample. The resolution attainable for TEM images is the order of 0.2 nm, revealing the finest details of samples internal structure. However, the samples for TEM analysis often require preparation before viewing, which may include dehydration, sputter coating for non-conductive materials, cryofixation, sectioning, and staining (Bourbon et a., 2016; Lin et al., 2014; Wang, 2002).

2.6. Food simulants

The incorporation of delivery systems into food products has brought several advantages to the food industry. However, the behaviour of such systems must be evaluated in food products prior to their commercialization, in order to understand the impact of food conditions on delivery systems properties, functionalities and structural stability (Livney, 2015; Nualkaekul et al., 2013; Wilde et al., 2016), and on bioactive compounds bioavailability (Madalena et al., 2016). The addition of delivery systems to food products should not interfere with the sensory properties of the final product. At micro-, but particularly, at nanoscale, the delivery systems are imperceptible in the mouth and do not impact the food products sensory properties, thus increasing the public acceptance (Livney, 2015).

Food simulants represent, in fact, a good approach to evaluate the impact of food conditions on the controlled delivery systems stability. In this sense, the Commission Regulation (EU) No 10/2011 of 14 January 2011, on plastic materials and articles intended to come into contact with food, listed several food simulants (Table 2.2) that are regulated to study the impact of food environmental conditions on food systems (Comission, 2011a).

Table 2.2 - List of food simulants and potential applications (Adapted from Comission, 2011a).

Food simulant	Composition	Application
A	Ethanol 10 % (v/v)	Hydrophilic products
B	Acetic acid 3 % (v/v)	Hydrophilic and acidic products (pH < 4.5)
C	Ethanol 20 % (v/v)	Hydrophilic and alcoholic products (> 20 % alcohol)
D1	Ethanol 50 % (v/v)	Hydrophobic, alcoholic (> 20 % alcohol) food products and oil-in-water emulsions
D2	Vegetable oil	Hydrophobic food products and superficial fats
E	Poly(2,6-diphenyl-p-phenylene oxide), particle size of 60–80 mesh, pore size 200 nm	Dry food products

2.7. Caco-2 cell models

The use and optimization of cellular models with the purpose of evaluating the bioavailability of bioactive compounds has been increasing over the last years (Gonzales et al., 2016; Jiang et al., 2019; Sedaghat Doost et al., 2019). These models try to mimic the conditions within the human small intestine allowing the determination of several conditions, namely, the bioaccumulation and toxicity level, the adhesion to or the absorption rate through intestinal epithelial cells (Fernandez-Avila et al., 2016; Gonzales et al., 2015; Kamiloglu et al., 2015). Caco-2 cells are a human epithelial cell model, derived from colon carcinoma, with a heterogeneous cell population (i.e., they have different transport rates) that can rapidly differentiate into a monolayer of cells with the morphology and maturity of enterocytes.

2.8. *In vitro* digestion model

The human digestive system (HDS) is a complex, multi-phase (i.e., oral, stomach, small intestine and large intestine compartments) biologic process in which food products undergo a series of processes that transform them into smaller and more basic components, in order to be absorbed

(mostly in the small intestine) and reach the bloodstream. The summary of the main physicochemical conditions is shown in Figure 2.1.

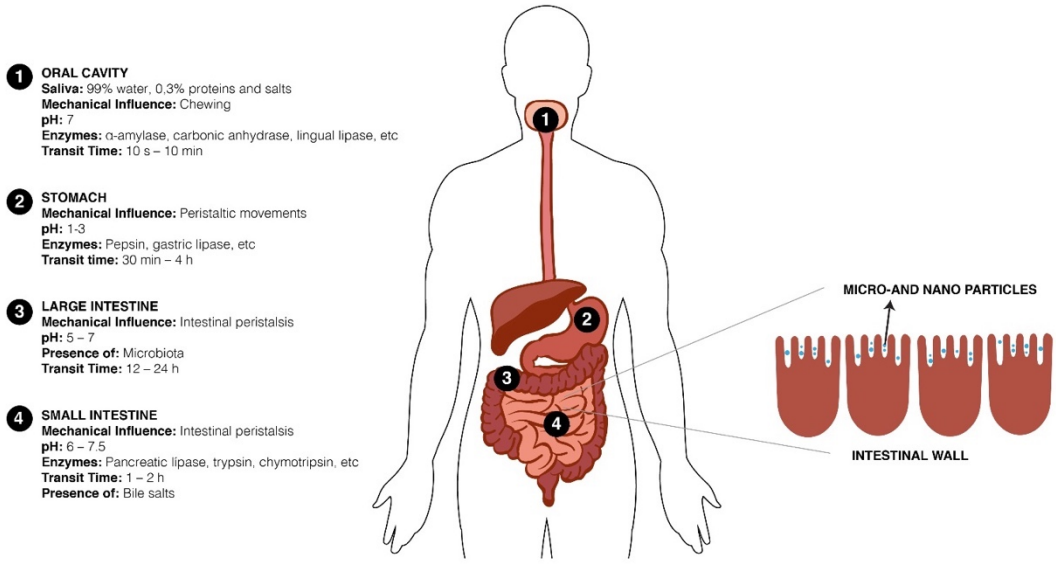


Figure 2.1 - Schematic diagram representing the main physiological conditions present in the human digestive system. Adapted from Simões et al., (2017)

In the oral cavity, food products are submitted to a neutral environment (i.e., pH 7), mechanical stress (i.e., chewing) and to saliva (where they are dissolved), which contains some important enzymes (e.g., α-amylase) and proteins (e.g., mucins). Subsequently, food passes to the gastric compartment, where it is submitted to mechanical agitation (peristaltic movements) and an acidic environment (i.e., pH ranges from 1 to 3), due to HCl secretion. Furthermore, important enzymes (e.g., pepsin and gastric lipase) interact with food products in order to break them down into their basic constituents, so that they can be absorbed in the small intestine. The duodenum is the main absorption site in the small intestine. At this stage, food suffers an increase in the environmental pH (from 6 to 7.5) so that gastric enzymatic activity is interrupted. In this compartment, foods interact with inorganic salts, bile salts and other enzymes (e.g., pancreatic lipase, trypsin, chymotrypsin, among others) to further break down food into smaller constituents. Here, the nutrients can be absorbed once enzymatic digestion is finished (Mao & Miao, 2015; Pinheiro, 2013; Singh & Sarkar, 2011). The non-absorbed digestion products pass to the large intestine, in which water content, electrolytes and bile salts are absorbed. At this compartment, polysaccharides and proteins suffer a fermentation process by the colonic microbiota and the resulting waste products are then excreted from the human body (Guergolett et al., 2016; Guerra et al., 2012).

In vitro models are used to provide some insight regarding the digestibility of controlled release systems and bioavailability of bioactive compounds (Alminger et al., 2014). Static *in vitro* models are practical models that allow the assessment of multiple samples and mimics the physiological digestion conditions (temperature, pH, ionic strength and time). *In vitro* experiments allow obtaining reproductive (without biological variations) and faster results in a more economical way. Moreover they require less manpower, are easy to perform, do not involve ethical issues and allow sampling at any time of digestion process, when compared with *in vivo* experiments (Alminger et al., 2014; Li et al., 2013).

2.9. Protein structures considerations in the food industry

The developments and applications of micro- and nanostructures are successfully marketed by the pharmaceutical and cosmetic industries (Desai & Jin Park, 2005). In the food industry, the investments to scale up this technology to a large variety of processes and products is expected to increase in upcoming years.

One of the emerging fields of micro- and nanotechnology applied to the food industry is the use of proteins with gelation properties to form micro- and nanostructures intended to incorporate a wide variety of bioactive compounds. These features, besides their biodegradability, provide an advantage to act as a delivery systems in food products (Tarhini et al., 2017). Commonly, protein structures are formed using simple preparation procedures that do not need any chemical crosslinking agents, thus representing an advantage for their applicability in the food industry (Chen et al., 2006; Joye et al., 2014). In this sense, the inclination towards the use of protein structures allows the reformulation of food products correspondent to the new consumer's expectations in term of wellbeing and new consumption habits (Guyomarc´h et al., 2014). Protein structures can also be designed to extent the food shelf life, improve food quality and safety, for Instance through the development and use of protein-based biosensors and packagings for food products (Ranjan et al., 2014).

Oral delivery systems-based proteins have a great potential to incorporate, protect, and release bioactive compounds in a food matrix, improving their bioavailability and absorption rates in target site in the gastrointestinal tract (Singh, 2016). The advanced functionalities may came from the responsiveness properties of proteins in relation to external stimuli for instance, pH, temperature, ionic strength that may allow a wide variety of new opportunities for food industry applications (Scholten et al., 2014).

The development and application of protein structures in the food industry is rather long and poses challenges that need to be addressed, which requires multidisciplinary cooperation (Vos et al., 2010). Moreover, the use of these protein structures has to be a viable, cost-effective process, simple to use and alternative to the standard methodologies.

2.10. Safety and regulatory considerations

Particles at nanoscale display new properties and functionalities, which may improve the performance of traditional products. These innovative characteristics have an unpredictable impact in the human organism, animals or environment, due to potential toxic effects. Materials at this scale can penetrate and accumulate much deeper within the human body, breaching the cellular and sub-cellular boundaries, which may cause undesired and uncharacterized effects (Bumbudsanpharoke & Ko, 2015; Coles & Frewer, 2013). Moreover, long term effects regarding the application of nanotechnology to the food industry are still unknown (Handford et al., 2015).

Therefore, the use of nanotechnology for human consumption must be meticulously evaluated and regulated and consumer's acceptance studies should be performed in order to assess the consumer trends and to understand if what has been done is sufficient towards its acceptance and use in the food industry.

Regarding the regulatory measures for nanotechnology/nanomaterials in food sector, a recent overview shows that still exists a lack of information exchange consistency among different countries, which may put in risk the human health and the environment, as well as restrict the commercialization of novel beneficial products at global level (Amenta et al., 2015). The European Union (EU) is, so far, the unique group of countries that have a clear regulatory definition of nanomaterials (and their intended use) in current food legislation. In countries outside the EU this regulation takes place in an implicit form that works only as a guide for the industry (Amenta et al., 2015).

The European Commission (EC) published a definition of nanomaterial through regulation N° 1169/2011 – "'engineered nanomaterial' means any intentionally produced material that has one or more dimensions of the order of 100 nm or less, or that is composed of discrete functional parts, either internally or at the surface, many of which have one or more dimensions in the order of 100 nm or less, including structures, agglomerates or aggregates, which may have a size above the order of 100 nm but retain properties that are characteristic of the nanoscale" (Comission, 2011b). This definition intends to inform the consumers and act as a reference in different regulatory sectors. An alternative to overcome the regulatory issues can be related with the use of

material with a size slightly higher (i.e., at microscale with diameter > 100 nm), but maintaining the physical, chemical and biological properties associated with materials at nanoscale (with diameter < 100 nm) (Cerqueira et al., 2014).

In terms of public acceptance or consumer attitudes, Handford et al., (2015) performed a study involving 102 agri-food stakeholders (i.e., 14 interviews and 88 online questionnaires) to understand the current awareness regarding nanotechnology and its applications in the agri-food industry. The authors observed that the awareness regarding the application of nanotechnology to the agri-food industry is still on its preliminary stage. Although, some opportunities were identified, since the interviewed are more receptive when nanotechnology is used for human health benefit as "functional ingredients" or "more nutritional foods". Moreover, some risks were clearly identified regarding the "unknown effects to the human body and within the ecosystem" as well as "the lack of public knowledge regarding this subject, which may create doubt in the consumer". Therefore, toxicological studies must be made in order to reduce the dubious nature of this subject, regarding the use of nano delivery systems in food products (Bruge et al., 2015).

2.11.References

Acosta, E. (2009). Bioavailability of nanoparticles in nutrient and nutraceutical delivery. Current Opinion in Colloid and Interface Science, 14(1), 3–15. https://doi.org/10.1016/j.cocis.2008.01.002

Aditya, N. P., Macedo, A. S., Doktorovova, S., Souto, E. B., Kim, S., Chang, P. S., & Ko, S. (2014). Development and evaluation of lipid nanocarriers for quercetin delivery: A comparative study of solid lipid nanoparticles (SLN), nanostructured lipid carriers (NLC), and lipid nanoemulsions (LNE). LWT - Food Science and Technology, 59(1), 115–121. https://doi.org/10.1016/j.lwt.2014.04.058

Akhavan Mahdavi, S., Jafari, S. M., Assadpoor, E., & Dehnad, D. (2016). Microencapsulation optimization of natural anthocyanins with maltodextrin, gum Arabic and gelatin. International Journal of Biological Macromolecules, 85, 379–385. https://doi.org/10.1016/j.ijbiomac.2016.01.011

Alminger, M., Aura, A. M., Bohn, T., Dufour, C., El, S. N., Gomes, A., ... Santos, C. N. (2014). *In vitro* models for studying secondary plant metabolite digestion and bioaccessibility. Comprehensive Reviews in Food Science and Food Safety, 13(4), 413–436. https://doi.org/10.1111/1541-4337.12081

Amenta, V., Aschberger, K., Arena, M., Bouwmeester, H., Botelho Moniz, F., Brandhoff, P., ... Peters, R. J. (2015). Regulatory aspects of nanotechnology in the agri/feed/food sector in EU and non-EU countries. Regulatory Toxicology and Pharmacology, 73(1), 463–476. https://doi.org/10.1016/j.yrtph.2015.06.016

Amin, F., Khan, W., & Bano, B. (2019). Oxidation of cystatin imparted by riboflavin generated free radicals: Spectral analysis. International Journal of Biological Macromolecules, 124, 1281–1291. https://doi.org/10.1016/j.ijbiomac.2018.12.021

Anandharamakrishnan, C. (2014). Techniques for Nanoencapsulation of Food Ingredients. (R. W. Hartel, Ed.). New York: Springer. https://doi.org/10.1007/978-1-4614-9387-7

Ashoori, M., & Saedisomeolia, A. (2014). Riboflavin (vitamin B2) and oxidative stress: a review. British Journal of Nutrition, 111(11), 1985–1991. https://doi.org/10.1017/S0007114514000178

Augustin, M. A., & Hemar, Y. (2009). Nano- and micro-structured assemblies for encapsulation of food ingredients. Chemical Society Reviews, 38(4), 902–912. https://doi.org/10.1039/b801739p

Balassa, L. L., Fanger, G. O., Wurzburg, O. B., Balassa, L. L., Fanger, G. O., Wurzburg, O. B., … Corp, B. (2014). Microencapsulation in the food industry - A Practical Implementation Guide. (A. G. Gaonkar, N. Vasisht, A. R. Khare, & R. Sobel, Eds.) (First Edit). Elsevier. https://doi.org/10.1080/10408397109527123

Ball, G. F. M. (2004). Vitamins : their role in the human body.

Barth, A. (2007). Infrared spectroscopy of proteins. Biochimica et Biophysica Acta - Bioenergetics, 1767(9), 1073–1101. https://doi.org/10.1016/j.bbabio.2007.06.004

Belitz, H. D., Grosch, W., & Schieberle, P. (2009). Food Chemistry. (H. D. Belitz, W. Grosch, & P. Schieberle, Eds.) (4th revise). Springer. https://doi.org/10.1007/978-3-540-69934-7

Beztsinna, N., Solé, M., Taib, N., & Bestel, I. (2016). Bioengineered riboflavin in nanotechnology. Biomaterials, 80, 121–133. https://doi.org/10.1016/j.biomaterials.2015.11.050

Bourbon, A. I., Pinheiro, A. C., Cerqueira, M. A., & Vicente, A. A. (2016). Influence of chitosan coating on protein-based nanohydrogels properties and *in vitro* gastric digestibility. Food Hydrocolloids, 60, 109–118. https://doi.org/10.1016/j.foodhyd.2016.03.002

Bruge, F., Damiani, E., Marcheggiani, F., Offerta, A., Puglia, C., & Tiano, L. (2015). A comparative study on the possible cytotoxic effects of different nanostructured lipid carrier (NLC) compositions in human dermal fibroblasts. International Journal of Pharmaceutics, 495(2), 879–885. https://doi.org/10.1016/j.ijpharm.2015.09.033

Bumbudsanpharoke, N., & Ko, S. (2015). Nano-Food Packaging: An Overview of Market, Migration Research, and Safety Regulations. Journal of Food Science, 80(5), R910–R923. https://doi.org/10.1111/1750-3841.12861

Cerqueira, M. Â., Pinheiro, A. C., Ramos, O. L., Silva, H., Bourbon, A. I., & Vicente, A. A. (2017). Advances in Food Nanotechnology. Emerging Nanotechnologies in Food Science. Elsevier Inc. https://doi.org/10.1016/B978-0-323-42980-1.00002-9

Cerqueira, M. A., Pinheiro, A. C., Silva, H. D., Ramos, P. E., Azevedo, M. A., Flores-López, M. L., … Vicente, A. A. (2014). Design of Bio-nanosystems for Oral Delivery of Functional Compounds. Food Engineering Reviews, 6(1–2), 1–19. https://doi.org/10.1007/s12393-013-9074-3

Chen, L., Remondetto, G. E., & Subirade, M. (2006). Food protein-based materials as nutraceutical delivery systems. Trends in Food Science and Technology, 17(5), 272–283. https://doi.org/10.1016/j.tifs.2005.12.011

Coles, D., & Frewer, L. J. (2013). Nanotechnology applied to European food production - A review of ethical and regulatory issues. Trends in Food Science and Technology, 34(1), 32–43. https://doi.org/10.1016/j.tifs.2013.08.006

Collini, M., D'Alfonso, L., & Baldini, G. (2009). New insight on β-lactoglobulin binding sites by 1-anilinonaphthalene-8-sulfonate fluorescence decay. Protein Science, 9(10), 1968–1974. https://doi.org/10.1110/ps.9.10.1968

Combs Jr, G. F. (2013). The Vitamins - Fundamental Aspects in Nutrition and Health. (G. F. Combs Jr, Ed.) (Third Edit). Academic Press Ltd./Elsevier Science Ltd. https://doi.org/10.1017/CBO9781107415324.004

Comission (2011a). Regulation (EU) No 10/2011 of the European Parliament and of the Council of 14 January 2011 on on plastic materials and articles intended to come into contact with food. Off. J. Eur. Union.

Comission (2011b). Regulation (EU) No 1169/2011 of the European Parliament and of the Council of 25 October 2011 on the provision of food information to consumers. Off. J. Eur. Union.

Couto, R., Alvarez, V., & Temelli, F. (2017). Encapsulation of Vitamin B2 in solid lipid nanoparticles using supercritical CO2. The Journal of Supercritical Fluids, 120, 432–442. https://doi.org/10.1016/j.supflu.2016.05.036

Damodaran, S., Parkin, K. L., & Fennema, O. R. (2008). Fennema's Food Chemistry. (S. Damadaram, K. L. Parkin, & O. R. Fennema, Eds.) (Fourth Edi). CRC Press. https://doi.org/10.1080/01932691.2011.584482

Das, S., & Chaudhury, A. (2011). Recent advances in lipid nanoparticle formulations with solid matrix for oral drug delivery. AAPS PharmSciTech, 12(1), 62–76. https://doi.org/10.1208/s12249-010-9563-0

Davidov-Pardo, G., Joye, I. J., & McClements, D. J. (2015). Food-Grade Protein-Based Nanoparticles and Microparticles for Bioactive Delivery. In R. Donev (Ed.), Advances in Protein Chemistry and Structural Biology (First Edit, Vol. 98, pp. 293–325). Elsevier. https://doi.org/10.1016/bs.apcsb.2014.11.004

Desai, K. G. H., & Jin Park, H. (2005). Recent Developments in Microencapsulation of Food Ingredients. Drying Technology (Vol. 23). https://doi.org/10.1081/DRT-200063478

Devi, N., Sarmah, M., Khatun, B., & Maji, T. K. (2017). Encapsulation of active ingredients in polysaccharide–protein complex coacervates. Advances in Colloid and Interface Science, 239, 136–145. https://doi.org/10.1016/j.cis.2016.05.009

Dodero, V. I., Quirolo, Z. B., & Sequeira, M. A. (2011). Biomolecular studies by circular dichroism. Frontiers in Bioscience, 16(Landmark Ed.), 61–73. https://doi.org/10.2741/3676

Dordevic, V., Balanc, B., Belscak-Cvitanovic, A., Levic, S., Trifkovic, K., Kalusevic, A., … Nedovic, V. (2014). Trends in Encapsulation Technologies for Delivery of Food Bioactive Compounds. Food Engineering Reviews, 7(4), 452–490. https://doi.org/10.1007/s12393-014-9106-7

Dubey, B. N., & Windhab, E. J. (2013). Iron encapsulated microstructured emulsion-particle formation by prilling process and its release kinetics. Journal of Food Engineering, 115(2), 198–206. https://doi.org/10.1016/j.jfoodeng.2012.10.013

Durán, N., & Marcato, P. D. (2013). Nanobiotechnology perspectives. Role of nanotechnology in the food industry: A review. International Journal of Food Science and Technology, 48(6), 1127–1134. https://doi.org/10.1111/ijfs.12027

Ezhilarasi, P. N., Karthik, P., Chhanwal, N., & Anandharamakrishnan, C. (2013). Nanoencapsulation Techniques for Food Bioactive Components: A Review. Food and Bioprocess Technology, 6(3), 628–647. https://doi.org/10.1007/s11947-012-0944-0

Fang, R., Hao, R., Wu, X., Li, Q., Leng, X., & Jing, H. (2011). Bovine serum albumin nanoparticle promotes the stability of quercetin in simulated intestinal fluid. Journal of Agricultural and Food Chemistry, 59(11), 6292–6298. https://doi.org/10.1021/jf200718j

Fang, Z., & Bhandari, B. (2011). Effect of spray drying and storage on the stability of bayberry polyphenols. Food Chemistry, 129(3), 1139–1147. https://doi.org/10.1016/j.foodchem.2011.05.093

Fathi, M., Mozafari, M. R., & Mohebbi, M. (2014). Nanoencapsulation of food ingredients using carbohydrate based delivery systems. Trends in Food Science and Technology, 23(1), 13–27. https://doi.org/10.1016/j.tifs.2011.08.003

Fernandez-Avila, C., Arranz, E., Guri, A., Trujillo, A. J., & Corredig, M. (2016). Vegetable protein isolate-stabilized emulsions for enhanced delivery of conjugated linoleic acid in Caco-2 cells. Food Hydrocolloids, 55, 144–154. https://doi.org/10.1016/j.foodhyd.2015.10.015

Gao, J. Y., Dubin, P. L., & Muhoberac, B. B. (1997). Measurement of the binding of proteins to polyelectrolytes by frontal analysis continuous capillary electrophoresis. Analytical Chemistry, 69(15), 2945–2951. https://doi.org/10.1021/ac970026h

Garti, N., & McClements, J. (2012). Encapsulation technologies and delivery systems for food ingredients and nutraceuticals. (N. Garti & J. Mcclements, Eds.) (First Edit). Woodhead Publishing Limited.

Gironés-Vilaplana, A., Villaño, D., Marhuenda, J., Moreno, D. A., & García-Viguera, C. (2017). Vitamins. In C. Galanakis (Ed.), Nutraceutical and Functional Food Components (First Edit, pp. 159–201). Elsevier. https://doi.org/10.1016/B978-0-12-805257-0.00006-5

Gonzales, G. B., Smagghe, G., Vissenaekens, H., Grootaert, C., Rajkovic, A., Van de Wiele, T., … Van Camp, J. (2016). Quercetin mitigates valinomycin-induced cellular stress via stress-induced metabolism and cell uptake. Molecular Nutrition and Food Research, 60(5), 972–980. https://doi.org/10.1002/mnfr.201500999

Gonzales, G. B., Van Camp, J., Vissenaekens, H., Raes, K., Smagghe, G., & Grootaert, C. (2015). Review on the Use of Cell Cultures to Study Metabolism, Transport, and Accumulation of Flavonoids: From Mono-Cultures to Co-Culture Systems. Comprehensive Reviews in Food Science and Food Safety, 14(6), 741–754. https://doi.org/10.1111/1541-4337.12158

Guergoletto, K. B., Costabile, A., Flores, G., Garcia, S., & Gibson, G. R. (2016). *In vitro* fermentation of juçara pulp (Euterpe edulis) by human colonic microbiota. Food Chemistry, 196, 251–258. https://doi.org/10.1016/j.foodchem.2015.09.048

Guerra, A., Etienne-Mesmin, L., Livrelli, V., Denis, S., Blanquet-Diot, S., & Alric, M. (2012). Relevance and challenges in modeling human gastric and small intestinal digestion. Trends in Biotechnology, 30(11), 591–600. https://doi.org/10.1016/j.tibtech.2012.08.001

Gülseren, I., Fang, Y., & Corredig, M. (2012). Zinc incorporation capacity of whey protein nanoparticles prepared with desolvation with ethanol. Food Chemistry, 135(2), 770–774. https://doi.org/10.1016/j.foodchem.2012.04.146

Guyomarc´h, F., Famelart, M.-H., Henry, G., Gulzar, M., Leonil, J., Hamon, P., … Croguennec, T. (2014). Current ways to modify the structure of whey proteins for specific functionalities - a review. Dairy Science and Technology, 95(6), 795–814. https://doi.org/10.1007/s13594-014-0190-5

Ha, H. K., Kim, J. W., Lee, M. R., & Lee, W. J. (2013). Formation and characterization of quercetin-loaded chitosan oligosaccharide/β-lactoglobulin nanoparticle. Food Research International, 52(1), 82–90. https://doi.org/10.1016/j.foodres.2013.02.021

Handford, C. E., Dean, M., Spence, M., Henchion, M., Elliott, C. T., & Campbell, K. (2015). Awareness and attitudes towards the emerging use of nanotechnology in the agri-food sector. Food Control, 57, 24–34. https://doi.org/10.1016/j.foodcont.2015.03.033

Hu, B., & Huang, Q. R. (2013). Biopolymer based nano-delivery systems for enhancing bioavailability of nutraceuticals. Chinese Journal of Polymer Science, 31(9), 1190–1203. https://doi.org/10.1007/s10118-013-1331-7

Jafari, S. M. (2019). Biopolymer Nanostructures for Food Encapsulations Purposes. (S. M. Jafari, Ed.) (Volume 1). Academic Press Ltd./Elsevier Science Ltd.

Jiang, L., Li, Z., Xie, Y., Liu, L., & Cao, Y. (2019). Cyanidin chloride modestly protects Caco-2 cells from ZnO nanoparticle exposure probably through the induction of autophagy. Food and Chemical Toxicology, 127(February), 251–259. https://doi.org/10.1016/j.fct.2019.03.047

Joye, I. J., Davidov-Pardo, G., & McClements, D. J. (2014). Nanotechnology for increased micronutrient bioavailability. Trends in Food Science & Technology, 40(2), 168–182. https://doi.org/10.1016/j.tifs.2014.08.006

Kamiloglu, S., Capanoglu, E., Grootaert, C., & van Camp, J. (2015). Anthocyanin absorption and metabolism by human intestinal Caco-2 cells - A review. International Journal of Molecular Sciences, 16(9), 21555–21574. https://doi.org/10.3390/ijms160921555

Kato, T., & Park, E. Y. (2012). Riboflavin production by Ashbya gossypii. Biotechnology Letters, 34(4), 611–618. https://doi.org/10.1007/s10529-011-0833-z

Kobayashi, N., Muranaka, A., & Mack, J. (2012). Circular Dichroism and Magnetic Circular Dichroism Spectroscopy for Organic Chemists. Royal Society of Chemistry. https://doi.org/10.1039/9781849732932

Kumari, A., Yadav, S. K., Pakade, Y. B., Singh, B., & Yadav, S. C. (2010). Development of biodegradable nanoparticles for delivery of quercetin. Colloids and Surfaces B: Biointerfaces, 80(2), 184–192. https://doi.org/10.1016/j.colsurfb.2010.06.002

Kwak, H.-S. (2013a). Nano- and Microencapsulation for Foods. (H.-S. Kwak, Ed.), Nano- and Microencapsulation for Foods (First Ed.). Wiley Blackwell.

Kwak, H.-S. (2013b). Overview of Nano- and Microencapsulation for Foods. In H.-S. Kwak (Ed.), Nano- and Microencapsulation for Foods (First Edit, pp. 1–14). John Wiley& Sons.

Li, H., Wang, D., Liu, C., Zhu, J., Fan, M., Sun, X., ... Cao, Y. (2019). Fabrication of stable zein nanoparticles coated with soluble soybean polysaccharide for encapsulation of quercetin. Food Hydrocolloids, 87(May 2018), 342–351. https://doi.org/10.1016/j.foodhyd.2018.08.002

Li, J., Ye, A., Lee, S. J., & Singh, H. (2013). Physicochemical behaviour of WPI-stabilized emulsions in *in vitro* gastric and intestinal conditions. Colloids and Surfaces B: Biointerfaces, 111, 80–87. https://doi.org/10.1016/j.colsurfb.2013.05.034

Lin, P.-C., Lin, S., Wang, P. C., & Sridhar, R. (2014). Techniques for physicochemical characterization of nanomaterial. Biotechnol Adv., 32(4), 711–726. https://doi.org/10.1038/mp.2011.182.doi

Livney, Y. D. (2015). Nanostructured delivery systems in food: latest developments and potential future directions. Current Opinion in Food Science, 3, 125–135. https://doi.org/10.1016/j.cofs.2015.06.010

Lorber, B., Fischer, F., Bailly, M., Roy, H., & Kern, D. (2012). Protein analysis by dynamic light scattering: methods and techniques for students. Biochemistry and Molecular Biology Education : A Bimonthly Publication of the International Union of Biochemistry and Molecular Biology, 40(6), 372–382. https://doi.org/10.1002/bmb.20644

Madalena, D. A., Ramos, Ó. L., Pereira, R. N., Bourbon, A. I., Pinheiro, A. C., Malcata, F. X., ... Vicente, A. A. (2016). *In vitro* digestion and stability assessment of β-lactoglobulin/riboflavin nanostructures. Food Hydrocolloids, 58, 89–97. https://doi.org/10.1016/j.foodhyd.2016.02.015

Mao, L., & Miao, S. (2015). Structuring Food Emulsions to Improve Nutrient Delivery During Digestion. Food Engineering Reviews, 7(4), 439–451. https://doi.org/10.1007/s12393-015-9108-0

Matalanis, A., Jones, O. G., & McClements, D. J. (2011). Structured biopolymer-based delivery systems for encapsulation, protection, and release of lipophilic compounds. Food Hydrocolloids, 25(8), 1865–1880. https://doi.org/10.1016/j.foodhyd.2011.04.014

Mcclements, D. J. (2017). The future of food colloids : Next-generation nanoparticle delivery systems. Current Opinion in Colloid & Interface Science, 28, 7–14. https://doi.org/10.1016/j.cocis.2016.12.002

McClements, D. J. (2015). Nanoparticle- and Microparticle-Based Delivery Systems - Encapsulation, Protection and Release of Active Compounds. (D. J. McClements, Ed.) (First Edit). CRC Press. https://doi.org/10.1201/b17280

Mehalebi, S., Nicolai, T., & Durand, D. (2008). Light scattering study of heat-denatured globular protein aggregates. International Journal of Biological Macromolecules, 43(2), 129–135. https://doi.org/10.1016/j.ijbiomac.2008.04.002

Miles, A. J., & Wallace, B. A. (2016). Circular dichroism spectroscopy of membrane proteins. Chem. Soc. Rev. https://doi.org/10.1039/C5CS00084J

Mizrahy, S., & Peer, D. (2012). Polysaccharides as building blocks for nanotherapeutics. Chemical Society Reviews, 41(7), 2623–2640. https://doi.org/10.1039/c1cs15239d

Nicolet, T. (2001). Introduction to Fourier Transform Infrared Spetrometry, 199(1), 1–8.

Nualkaekul, S., Cook, M. T., Khutoryanskiy, V. V., & Charalampopoulos, D. (2013). Influence of encapsulation and coating materials on the survival of Lactobacillus plantarum and Bifidobacterium longum in fruit juices. Food Research International, 53(1), 304–311. https://doi.org/10.1016/j.foodres.2013.04.019

O'Sullivan, S., & Sheehan, D. (2011). Fast protein liquid chromatography. In P. Cutler (Ed.), Methods in molecular biology (Clifton, N.J.) (Vol. 681, pp. 253–258). https://doi.org/10.1007/978-1-60761-913-0_25

Pangeni, R., Kang, S. W., Oak, M., Park, E. Y., & Park, J. W. (2017). Oral delivery of quercetin in oil-in-water nanoemulsion: *In vitro* characterization and *in vivo* anti-obesity efficacy in mice. Journal of Functional Foods, 38, 571–581. https://doi.org/10.1016/j.jff.2017.09.059

Patel, A. R., & Bhandari, B. (2012). Nano- and Microencapsulation of Vitamins. In H.-S. Kwak (Ed.), Nano-and Microencapsulation for Foods (First Edit, pp. 223–248). JohnWiley& Sons. https://doi.org/10.1002/9781118292327.fmatter

Patel, A. R., Heussen, P. C. M., Hazekamp, J., Drost, E., & Velikov, K. P. (2012). Quercetin loaded biopolymeric colloidal particles prepared by simultaneous precipitation of quercetin with hydrophobic protein in aqueous medium. In Food Chemistry (Vol. 133, pp. 423–429). Elsevier Ltd. https://doi.org/10.1016/j.foodchem.2012.01.054

Pinheiro, A. C. B. (2013). Development of nanostructures for application in food technology – evaluation of their *in vitro* behavior. Minho University. Retrieved from http://hdl.handle.net/1822/27378

Quirós-Sauceda, A. E., Ayala-Zavala, J. F., Olivas, G. I., & González-Aguilar, G. A. (2014). Edible coatings as encapsulating matrices for bioactive compounds: a review. Journal of Food Science and Technology, 51(9), 1674–1685. https://doi.org/10.1007/s13197-013-1246-x

Ramos, O. L., Pereira, J. O., Silva, S. I., Amorim, M. M., Fernandes, J. C., Lopes-da-Silva, J. A., ... Malcata, F. X. (2012). Effect of composition of commercial whey protein preparations upon gelation at various pH values. Food Research International, 48(2), 681–689. https://doi.org/10.1016/j.foodres.2012.06.004

Ramos, O. L., Pereira, R., Martins, A., Rodrigues, R., Fuciños, C., Teixeira, J. a., ... Vicente, A. a. (2015). Design of Whey Protein Nanostructures for Incorporation and Release of Nutraceutical Compounds in Food. Critical Reviews in Food Science and Nutrition, 8398(July), 00–00. https://doi.org/10.1080/10408398.2014.993749

Ramos, O., Pereira, R. N., Rodrigues, R., Teixeira, J. A., Vicente, A. A., & Xavier Malcata, F. (2014). Physical effects upon whey protein aggregation for nano-coating production. Food Research International, 66, 344–355. https://doi.org/10.1016/j.foodres.2014.09.036

Ranjan, S., Dasgupta, N., Chakraborty, A. R., Melvin Samuel, S., Ramalingam, C., Shanker, R., & Kumar, A. (2014). Nanoscience and nanotechnologies in food industries: Opportunities and

research trends. Journal of Nanoparticle Research, 16(6). https://doi.org/10.1007/s11051-014-2464-5

Scholten, E., Moschakis, T., & Biliaderis, C. G. (2014). Biopolymer composites for engineering food structures to control product functionality. Food Structure, 1(1), 39–54. https://doi.org/10.1016/j.foostr.2013.11.001

Secolin, V. A., Souza, C. R. F., & Oliveira, W. P. (2016). Spray drying of lipid-based systems loaded with Camellia sinensis polyphenols. Journal of Liposome Research, 2104(February), 1–10. https://doi.org/10.3109/08982104.2016.1140183

Sedaghat Doost, A., Kassozi, V., Grootaert, C., Claeys, M., Dewettinck, K., Van Camp, J., & Van der Meeren, P. (2019). Self-assembly, functionality, and in-vitro properties of quercetin loaded nanoparticles based on shellac-almond gum biological macromolecules. International Journal of Biological Macromolecules, 129, 1024–1033. https://doi.org/10.1016/j.ijbiomac.2019.02.071

Sedaghat Doost, A., Muhammad, D. R. A., Stevens, C. V., Dewettinck, K., & Van der Meeren, P. (2018). Fabrication and characterization of quercetin loaded almond gum-shellac nanoparticles prepared by antisolvent precipitation. Food Hydrocolloids, 83, 190–201. https://doi.org/10.1016/j.foodhyd.2018.04.050

Silva, H. D., Cerqueira, M. Â., & Vicente, A. A. (2012). Nanoemulsions for Food Applications: Development and Characterization. Food and Bioprocess Technology, 5(3), 854–867. https://doi.org/10.1007/s11947-011-0683-7

Simões, L. S., Madalena, D. A., Pinheiro, A. C., Teixeira, J. A., Vicente, A. A., & Ramos, Ó. L. (2017). Micro- and nano bio-based delivery systems for food applications*: In vitro* behavior. Advances in Colloid and Interface Science, 243, 23–45. https://doi.org/10.1016/j.cis.2017.02.010

Singh, H. (2016). Nanotechnology Applications in Functional Foods ; Opportunities and Challenges. Prev.Nutr.Food Sci., 21(February), 1–8. https://doi.org/10.3746/pnf.2016.21.1.1

Singh, H., & Sarkar, A. (2011). Behaviour of protein-stabilised emulsions under various physiological conditions. Advances in Colloid and Interface Science, 165(1), 47–57. https://doi.org/10.1016/j.cis.2011.02.001

Sirisha, V. L., & Campus, K. (2015). Polysaccharide nanoparticles: Preparation and their potential application as drug delivery systems. International Journal of Research in Applied, Natural and Social Sciences (IMPACT: IJRANSS), 3(5), 69–94.

Stănciuc, N., Aprodu, I., Râpeanu, G., & Bahrim, G. (2012). Fluorescence spectroscopy and molecular modeling investigations on the thermally induced structural changes of bovine β-lactoglobulin. Innovative Food Science and Emerging Technologies, 15, 50–56. https://doi.org/10.1016/j.ifset.2012.03.001

Stetefeld, J., McKenna, S. A., & Patel, T. R. (2016). Dynamic light scattering: a practical guide and applications in biomedical sciences. Biophysical Reviews, 8(4), 409–427. https://doi.org/10.1007/s12551-016-0218-6

Tarhini, M., Greige-Gerges, H., & Elaissari, A. (2017). Protein-based nanoparticles: From preparation to encapsulation of active molecules. International Journal of Pharmaceutics, 522(1–2), 172–197. https://doi.org/10.1016/j.ijpharm.2017.01.067

Thakur, V. K., & Thakur, M. K. (2016). Handbook of Sustainable Polymers. (V. K. Thakur & M. K. Thakur, Eds.). CRC Press Web.

Tiwari, R., & Takhistov, P. (2012). Nanotechnology – enabled delivery systems for food functionalization and fortification Introduction : functional foods. In G. W. Padua & Q. Wang

(Eds.), Nanotechnology Research Methods for Foods and Bioproducts (First Edit, pp. 55–101). John Wiley & Sons.

Turner Designs. (2015). An Introduction to Fluorescence Measurements. Turner Designs, 1–15. Retrieved from http://www.turnerdesigns.com/customer-care/fluorometer-technical-notes

Udhayabanu, T., Karthi, S., Mahesh, A., Varalakshmi, P., Manole, A., Houlden, H., & Ashokkumar, B. (2017). Adaptive regulation of riboflavin transport in heart: effect of dietary riboflavin deficiency in cardiovascular pathogenesis. Molecular and Cellular Biochemistry. https://doi.org/10.1007/s11010-017-3163-1

Vos, P., Faas, M. M. M., Spasojevic, M., & Sikkema, J. (2010). Encapsulation for preservation of functionality and targeted delivery of bioactive food components. International Dairy Journal, 20(4), 292–302. https://doi.org/10.1016/j.idairyj.2009.11.008

Wadood, A., Ghufran, M., Jamal, S. B., Naeem, M., Khan, A., & Ghaffar, R. (2013). Phytochemical Analysis of Medicinal Plants Occurring in Local Area of Mardan. Biochemistry & Analytical Biochemistry, 2(4), 2–5. https://doi.org/10.4172/2161-1009.1000144

Wan, Z.-L., Guo, J., & Yang, X.-Q. (2015). Plant protein-based delivery systems for bioactive ingredients in foods. Food Function, 6(9), 2876–2889. https://doi.org/10.1039/C5FO00050E

Wang, W., Sun, C., Mao, L., Ma, P., Liu, F., Yang, J., & Gao, Y. (2016). The biological activities, chemical stability, metabolism and delivery systems of quercetin: A review. Trends in Food Science and Technology, 56, 21–38. https://doi.org/10.1016/j.tifs.2016.07.004

Wang, Z. L. (2002). Transmission Electron Microscopy of Shape-Controlled Nanocrystals and Their Assemblies. The Journal of Physical Chemistry B, 104(6), 1153–1175. https://doi.org/10.1021/jp993593c

Wijaya, W., Harfieyanto, R. C., Dewettinck, K., Patel, A. R., & Van der Meeren, P. (2019). Whey protein isolate–low methoxyl pectin nanocomplexes improve physicochemical and stability properties of quercetin in a model fat-free beverage. Food & Function, 1–11. https://doi.org/10.1039/c8fo02350f

Wilde, S. C., Keppler, J. K., Palani, K., & Schwarz, K. (2016). β-Lactoglobulin as nanotransporter for allicin: Sensory properties and applicability in food. Food Chemistry, 199, 667–674. https://doi.org/10.1016/j.foodchem.2015.12.055

Woody, R. W. (2012). Eletronic Circular Dichroism of Proteins. In N. Berova, P. L. Polavarapu, K. Nakanishi, & R. W. Woody (Eds.), Comprehensive Chiroptical Spectroscopy, Volume 2: Applications in Stereochemical Analysis of Synthetic Compounds, Natural Products, and Biomolecules. (First Edit, pp. 475–497). John Wiley & Sons, Inc.

Ye, Q., Woo, M. W., & Selomulya, C. (2019). Modification of molecular conformation of spray-dried whey protein microparticles improving digestibility and release characteristics. Food Chemistry, 280(December 2018), 255–261. https://doi.org/10.1016/j.foodchem.2018.12.074

Zhang, P., Zhao, S. R., Li, J. X., Hong, L., Raja, M. A., Yu, L. J., & Liu, C. G. (2016). Nanoparticles based on phenylalanine ethyl ester-alginate conjugate as Vitamin B2 delivery system. Journal of Biomaterials Applications, 31(1), 13–22. https://doi.org/10.1177/0885328216630497

Section II

MATERIAL AND METHODS

CHAPTER 3.

MATERIAL AND METHODS

3.1. Development of β-Lg structures 35

3.2. Characterization of β-Lg micro- and nanostructures 38

3.3. Association of bioactive model compounds to β-Lg micro- and nanostructures 41

3.4. Stability under various environmental conditions 43

3.5. *In vitro* release profile of bioactive model compounds from β-Lg micro- and nanostructures 44

3.6. Caco-2 cells studies and gastrointestinal (GI) model and 46

3.7. References 54

3.1. Development of β-Lg structures

3.1.1. Feedstocks and chemicals

Whey Protein Isolate (WPI) powder (Lacprodan DI-9212), kindly supplied by Arla Foods Ingredients (Viby, Denmark), has in a total protein content of 91 % (in dry weight), moisture content of ca. 6 % and vestiges of lactose (max. 0.5 %) and fat (max. 0.2 %), according to the information provided by the supplier. β-Lg was obtained as a commercial lyophilized powder from bovine milk (Sigma L0130), containing variants A and B (36.0 kDa) with a purity of 90 % (L0130). Tris(hydroxymethyl)aminomethane, ammonium persulfate (APS), Coomassie Brilliant Blue (R-250), bromophenol blue and tetramethylethylenediamine were purchased from Sigma Aldrich (St. Louis MO, USA). Sodium hydroxide, phosphoric and acetic acids were obtained from Merck (Merck KGaA, Darmstadt, Germany). Hydrochloric acid, glycine and monosodium phosphate were purchased from Panreac (Barcelona, Spain), whereas sodium phosphate dibasic and methanol were obtained from Chem-Lab (Zedelgem, Belgium). Acrylamide was purchased from Bio-Rad (California, USA) and glycerol was obtained from Himedia (Mumbai, India). All other chemicals used in this study were reagent-grade or higher and were used without further purification.

3.1.2. β-Lg purification method

Purified β-Lg was obtained from WPI by using the salting out method as described by Maté & Krochta (1994) with modifications according with Konrad, Lieske, & Faber (2000). WPI powder (15% w/w) was dispersed in distilled water and the pH of the solution was adjusted to 2.0 with HCl 2 mol L^{-1}. Subsequently, 7% (w/w) NaCl was added in order to promote the separation of most of β-Lg from the other proteins in the precipitate. The precipitation process was held for 20 min at room temperature (i.e. 25 °C). The solution was centrifuged (Sigma 4K15, Germany) at 13 000 *g*, at 4 °C for 15 min. After separating phases, the sediment was discarded. The ultrafiltration with diafiltration of supernatant was performed in order to separate the β-Lg from salt. The process was carried out using Pelicon® ultrafiltration cassettes with membrane cut- off M_w = 10 kDa, which the retentate (β-Lg, salt and water) was recycled to the feed tank and make-up water was added; the permeate (salt and water) was eliminated. The ultrafiltration process was repeated until the feed tank electrical conductivity reached 0.9 mS cm^{-1}. This value ensures the lower amount of salt in the resulting solution. β-Lg was freeze dried to obtain a lyophilized powder. The purity and conformational properties of purified β-Lg were compared with commercial β-Lg lyophilized powder from Sigma. For this purpose, both protein solutions were prepared by dispersing 10 mg mL^{-1} of

β-Lg powder (Dombrowski et al., 2016; Donato et al., 2009; Kosters et al., Gruppen, 2011; Schmitt et al., 2009) in 25 mmol L^{-1} sodium phosphate buffer at pH 6. The pH of solutions was adjusted with 0.5 mol L^{-1} of H_3PO_4 or 1 mol L^{-1} of NaOH, as necessary. The solutions were then stirred continuously with a rotation speed of 400 rpm, for 2 h at room temperature (ca. 25 °C). Afterward, β-Lg solutions were stored at refrigeration temperature (5 °C) overnight to ensure the full rehydration of protein. The β-Lg solutions were then filtered through a 0.2 μm membrane filter (VWR International, USA) to remove any protein aggregates or impurities. Subsequently, β-Lg morphology, purity, secondary structure and conformational state properties were evaluated for both commercial and purified β-Lg, through dynamic light scattering, SDS-PAGE, turbidity, circular dichroism, intrinsic and extrinsic fluorescence analyses and then comparisons were drawn.

3.1.3. Experimental design to optimize the development of β-Lg micro- and nanostructures

Box-Behnken statistical experimental design was used to evaluate the effect of heating temperature (X_1), β-Lg concentration (X_2) and holding time (X_3) (independent variables), upon particle size (Y_1), polydispersity index (Y_2), intrinsic fluorescence (Y_3) and extrinsic fluorescence (Y_4) intensities (dependent variables), on the development of optimized β-Lg micro- and nanostructures at pH 3, 4, 6 and 7. A 3-factor, 3-level design was used because it was the most appropriated for exploring quadratic response surfaces and constructing second order polynomial models for optimization, thus allowing the use of less experiments. The experimental design encompasses the repetition of center points and the set of points lying at the midpoints of each edge of the multidimensional cube that defines the region of interest. The pH values were selected based on the isoelectric point (pI) of β-Lg (Teng et al., 2015). As shown in Table 3.1, the independent variables and levels (i.e. low, medium and high) were selected based in previous results from screening experiments. The design matrix was performed in 15 trials flowing the procedure adopted by Monteiro et al. (2016).

Table 3.1 - Independent variables and their levels in Box-Behnken experimental design for pH values 3, 4, 6 and 7.

Independent variables	Levels		
	Low	Medium	High
X_1 (Heating temperature, °C)	-1 (60)	0 (70)	+1 (80)
X_2 (β-Lg concentration, mg mL^{-1})	-1 (5)	0 (10)	+1 (15)
X_3 (Holding time, min)	-1 (5)	0 (15)	+1 (25)

3.1.4. Development of β-Lg micro- and nanostructures

In order to study the effects of β-Lg concentration, temperature and time of heating upon the formation of protein micro- and nanostructures at different pH values, the solution pH was adjusted to 3, 4, 6 and 7 with 0.5 mol L^{-1} of H_3PO_4 or 1 mol L^{-1} of NaOH, as appropriate. Micro- and nanostructures were formed by dispersing 5, 10 and 15 mg mL^{-1} of β-Lg purified powder in 25 mmol L^{-1} sodium phosphate buffer at pH 3, 4, 6 and 7. The solutions were then stirred continuously with a rotation speed of 400 rpm, for 2 h at room temperature (ca. 25 °C). Afterwards, β-Lg solutions were stored at refrigeration temperature (5 °C) overnight to ensure the full rehydration of protein. The β-Lg solutions (5 mL) were then filtered through a 0.2 μm membrane filter to remove any protein aggregates or impurities and were placed into cylindrical screw-capped glass tubes (100 mm total length and diameter of 20 mm). Heat treatments at different temperatures (i.e., 60, 70, 80 °C) and times (i.e. 5, 15,25 min) were applied through a temperature controlled water bath (MR Hei-Tec + Pt 1000, Heidolph, Germany) with samples continuously stirred with magnetic agitation at a rotation speed of 400 rpm. After the heat treatment, the resulting solutions were cooled in ice for 10 min. β-Lg structures were characterized using the techniques described before. Unheated and native β-Lg suspensions were used as control samples (Fig. 3.1).

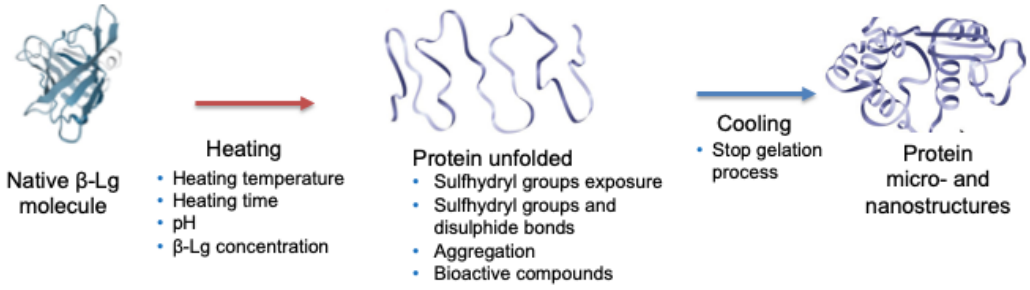


Figure 3.1 - Schematic representation of development β-Lg micro- and nanostructures by gelation process.

3.2. Characterization of β-Lg micro- and nanostructures

3.2.1. Particle size, polydispersity index, and surface charge

Samples of β-Lg were characterized in terms of particle size, polydispersity index (PDI) and surface charge by Dynamic Light Scattering (DLS) apparatus (Zetasizer Nano ZS, Malvern Instruments, UK) equipped with He-Ne laser at a wavelength of 633 nm, at 25 °C (Bourbon et al., 2016). Particle size was determined by the method of cumulants fit and was translated into average particle diameters (*Z*-value) using the Stokes-Einstein relationship (Rodrigues et al., 2015). PDI emerged from cumulants analysis of the measurements and describes the width or the relative variance of the particle diameter distribution. The ζ-potential determines the charge at the surface of the structure and was performed with an angle of 17° (Madalena et al., 2016). Samples (1.5 mL) were poured into disposable sizing cuvettes with a path length of 10 mm for particle size and PDI analyses, and into a folded capillary cell for ζ-potential measurements. All measurements were carried out at 25 °C and the results reported as the average ± standard deviation of at least three replicates.

3.2.2. Turbidity

The turbidity of β-Lg solutions (4 mL) prepared at 10 mg mL^{-1} was evaluated using a double-beam UV/visible spectrophotometer at 500 nm (V-560, Jasco Inc., Tokyo, Japan). The measurements were made at room temperature (ca. 25 °C) according with the procedure reported by Pereira et al., (2015) resorting to a 10 mm path length cuvette, and with 25 mmol L^{-1} sodium phosphate sodium buffer as blank. The measurements were performed in triplicate and experimental values are presented as the average ± standard deviation.

3.2.3. Fluorescence measurements

3.2.3.1. Intrinsic fluorescence

In order to assess the effect of thermal gelation on β-Lg micro- and nanostructures, the intrinsic fluorescence was evaluated. The measurements of β-Lg dispersions from 5 – 15 mg mL^{-1} were obtained at ambient temperature (ca. 25 °C) resorting to a spectrofluorimeter (Jasco FP6200, Tokyo, Japan) equipped with a standard thermostated cell holder and a 10 mm path length quartz cuvette (Hellma Analytics, Germany). The excitation wavelength was set at 295 nm to quenching tryptophan (Trp) fluorescence (Madadlou, Floury, Pezennec, & Dupont, 2018) and the emission spectra were recorded between 300 and 405 nm, and fluorescence intensities were recorded every

2.25 nm. Spectra were baseline-corrected by subtracting blank spectra (i.e., 25 mmol L^{-1} sodium phosphate buffer) according the procedure adopted by Monteiro et al. (2016) and normalized with unheated β-Lg. The maximum intrinsic fluorescence intensity was given as the average of nine successive measurements.

3.2.3.2. Extrinsic fluorescence

In order to assess the hydrophobic sites of β-Lg micro- and nanostructures, the extrinsic fluorescence was assessed. The extrinsic fluorescence of β-Lg dispersions from 5 – 15 mg mL^{-1} was determined by fluorescence spectroscopy (Jasco FP6200, Tokyo, Japan) using 8-anilinonaphtalene-1-sulfonic acid ammonium salt (ANS) (Sigma-Aldrich, St. Louis, EUA) as the hydrophobic probe, according to the methodology adopted by Wang, Zhong, & Hu (2013) with a few modifications. An aliquot of ANS solution (at 1.36 mmol L-1 in methanol) were added in β-Lg solutions and incubated at 25 °C for 10 min in the dark before the analysis. The resulting solution was excited at 370 nm and emission was collected between 400 and 600 nm at room temperature (ca. 25 °C), using a 10 mm path length quartz cuvette. Spectra were baseline-corrected by subtracting blank spectra (i.e., 25 mmol L^{-1} sodium phosphate buffer and ANS solution). Micro- and nanostructures maximum fluorescence intensity values were normalized by the lowest value corresponding to the unheated β-Lg. The maximum ANS binding fluorescence intensity was given as the average of nine successive measurements.

3.2.4. Circular dichroism

The secondary structure content of β-Lg and the effect of heat treatment were evaluated by circular dichroism (CD). CD spectra were obtained resorting to a Jasco J-1500 spectropolarimeter (Jasco International Co, Japan). For far-UV experiments, samples in appropriate dilution and spectra were recorded at 25 °C, under constant nitrogen flush, using a quartz cuvette with an optical path length of 1.0 mm (Hellma Analytics, Germany), from 190 nm to 260 nm wavelength range with data pitch of 1.0 nm and accumulation of 3 scan, following the procedure used by Bourbon et al., (2016). The CD baseline scan was recorded using a standard solution of 25 mmol L^{-1} sodium phosphate buffer and then subtracted to scans from β-Lg solutions.

3.2.5. Native polyacrylamide gel electrophoresis (Native-PAGE)

In order to compare the integrated intensities of β-Lg bands, samples were analysed using Native-PAGE or "nondenaturing" gel electrophoresis. Native-PAGE analyses were carried out using the Mini-Protean II dual slab cell system equipped with a PAC 300 power supply (Bio-Rad Laboratories, Hercules, CA, USA) (Bourbon, Pinheiro, et al., 2016). The resolving and stacking gel contained 12.5 and 3.5 % of polyacrylamide, respectively. Non-reducing loading buffer of tris(hydroxymethyl)aminomethane, 0.5 mol L^{-1} at pH 6.8, 50 % of glycerol and 0.02 % of bromophenol blue was mixed with β-Lg samples. The gels were stained with Coomassie Brilliant Blue (R-250) solution, maintained overnight in 50 % and 10 % of methanol and acetic acid solutions, respectively. Then, gels were destained with 30 % and 7 % of methanol and acetic acid solutions, respectively (Rodrigues et al., 2015). Standard marker protein PageRuler Unstained Broad Range Protein Ladder (Thermo Scientific) was employed to identify samples by their molecular weight.

3.2.6. Fast protein liquid chromatography

β-Lg protein solutions were resolved and quantified by gel filtration chromatography using a Superdex™ 200 10/300 GL column, connected to a fast protein liquid chromatography (FPLC) AKTA-purifier system (GE). β-Lg lyophilized solutions (from Sigma) with concentrations ranging from 5 – 15 mg mL^{-1} were used to prepare a calibration curve, then 10 mg mL^{-1} of β-Lg purified samples were analysed.

The protein samples were then centrifuged at 20,000 *g* for 1 h at 25 °C, using a Sorvall centrifuge (Thermo Scientific, USA), and 5 mL of the clarified liquid was carefully collected and filtered through 0.22 μm filters prior to separation. The eluent was also filtered (0.22 μm) and degassed under vacuum for 1 h before testing. Samples (100 μL) were injected into the column and eluted using 0.05 mol L^{-1} of sodium phosphate buffer (pH 7) containing 0.2 g L^{-1} of sodium azide, as preservative, at a flow rate of 0.5 ml ml^{-1} under a pressure of 1.5 – 2.0 MPa. Identification (through similarity of retention times – RT) and quantification (by integration of peak area of chromatograms) of the β-Lg present in the eluate was monitored at 280 nm following the procedure previously described by Ramos et al., (2012). All measurements were performed at least in duplicate.

3.2.7. Fourier-transform infrared spectroscopy

The binding of bioactive model compounds to β-Lg micro- and nanostructures was evaluated by Fourier-transform infrared (FTIR) spectra (model ABB FTLA2000, Canada), according to the

procedure adopted by Martins et al., (2016) with a few modifications. Samples (2 mg) were prior lyophilized, and then compressed into thin potassium bromide (KBr) (200 mg) pellets and finally analysed in a wavenumber range of 4000 to 500 cm^{-1}. Each spectrum was performed by averaging 16 scans with a spectral resolution of 8 cm^{-1}. Data analysis was performed using ORIGIN 9 software.

3.2.8. Transmission electron microscopy

Transmission electron microscopy (TEM) imaging of β-Lg micro- and nanostructures was conducted on a Zeiss EM 902A (Thornwood, N.Y., USA) microscope at accelerating voltages of 50 and 80 kV. A drop of sample dispersion was deposited onto a carbon support film mounted on a TEM copper grid (Quantifoil, Germany).

The excess of solution was removed after 2 min using a filter paper and the grid let for air-drying. The samples were then negatively stained with uranyl acetate (2 % w/w) (Merck, Germany) for 15 s. The grid was finally air dried at room temperature before introducing it in the electron microscope. These conditions were used based in procedures usually adopted by our research group (Monteiro et al., 2016; Bourbon et al., 2015; Pinheiro et al., 2015).

3.3. Association of bioactive model compounds to β-Lg micro- and nanostructures

After β-Lg solutions thermal treatment, a given volume of each bioactive compound stock solution was added to the resulting β-Lg solutions, and then were cooled in ice for 10 min to form β-Lg micro- and nanostructures.

3.3.1. Feedstocks and chemicals

The following chemicals were purchased from Sigma-Aldrich (St. Louis, MO, USA): quercetin (≥ 95%, HPLC), riboflavin (≥ 98%). Acetonitrile (HPLC grade) and methanol were obtained from Chem-Lab (Zedelgem, Belgium). Dimethyl sulfoxide was obtained from Fisher Scientific Chemical Company (Pittsburgh, PA), while ethanol was purchased from JMGS (Portugal).

3.3.2. Hydrophilic model compound – Riboflavin

Riboflavin, as a hydrophilic bioactive model compound, was dissolved in 0.1 mol L^{-1} Na_3PO_4, being the resulting solutions protected from light with aluminium foil (Zhang et al., 2016) to obtain β-Lg solutions with final concentrations of riboflavin ranging from 0.007 to 0.105 mg mL^{-1}.

In order to separate the free riboflavin in supernatant, 0.5 mL of β-Lg/riboflavin micro- and nanostructure solutions were placed into Amicon® Ultra-0.5 centrifugal filter units with molecular weight cut-off 3 kDa (Merck Millipore, Ireland) and centrifuged (Model 5415 R, Eppendorf) at 16,000 g during 20 min at 4 °C. The filtrate with unbound riboflavin was determined spectrophotometrically at 437 nm (Azevedo et. al, 2014) using the calibration curve $y = 7.9841x + 0.056$ with R^2 = 0.99 (being y and x the absorbance and riboflavin concentration, respectively). These results were used to calculate the association efficiency (*AE*) according to the Equation (1). The concentrate with the β-Lg/riboflavin micro- and nanostructure retained in Amicon® was dried at 55 °C during 24 h in a ventilated oven and the loading capacity (*LC*) was determined by mass difference according to the Equation (2).

$$AE\ (\%) = \frac{C_{Bioactive\ compound\ total} - C_{Bioactive\ compound\ free}}{C_{Bioactive\ compound\ total}} \times\ 100 \qquad \text{Equation (1)}$$

$$LC\ (\%) = \frac{C_{Bioactive\ compound\ total} - C_{Bioactive\ compound\ free}}{W_{structure}} \times\ 100 \qquad \text{Equation (2)}$$

where, $C_{Bioactive\ compound\ total}$ is the concentration of bioactive compound in solution; $C_{Bioactive\ compound\ free}$ is the concentration of free bioactive compound separated from β-Lg structures; and $W_{structure}$ is the β-Lg structure weight.

3.3.3. Hydrophobic model compound – Quercetin

The addition of quercetin to an ethanol solution (used as solvent) was limited due to the protein sensitivity to ethanol (Pace et al., 2004). Distinct quercetin concentrations were previously dissolved in ethanol in order to achieve quercetin concentrations ranging from 0.01 to 0.08 mg mL^{-1}. β-Lg/quercetin micro- and nanostructures (2 mL) were placed into tube samples and subsequently centrifuged (Model 5415 R, Eppendorf) at 14,000 g for 10 min at 4 °C, to separate the unbound quercetin (Madalena et al., 2016). The free quercetin in the supernatant was evaluated by high-performance liquid chromatography (HPLC) with fluorescence detection. The HPLC system used consisted of a Varian Prostar 210 pump, a Varian Prostar 410 autosampler, and a Jasco FP-920 detector. The column was a C18 reversed-phase YMC-Pack ODS (4.6 × 250 mm i.d; 5 μm particle size). The mobile phase was composed of acetonitrile and distilled water (40:60, v/v), and was pumped at a flow rate of 1.0 mL min^{-1}. The wavelengths used for quercetin

detection were excitation = 355 nm and emission = 525 nm (Komori, Inoue, Fujita, Kasajima, & Horii, 2007). The quantification was performed using a calibration curve prepared with standards at concentrations between 0.01 to 0.1 mg mL^{-1}. These results were used to assess the *AE* by Equation (1). The β-Lg/quercetin micro- and nanostructures were dried at 55 °C during 24 h in a ventilated oven and the *LC* was determined using the Equation (2).

3.3.3.1.High performance liquid chromatography

The high performance liquid chromatography (HPLC) system used consisted of a Varian Prostar 210 pump, a Varian Prostar 410 autosampler, and a Jasco FP-920 detector. The column was a C18 reversed-phase YMC-Pack ODS (4.6 × 250 mm i.d; 5 μm particle size). The mobile phase was composed of acetonitrile and distilled water (40:60, v/v), and was pumped at a flow rate of 1.0 mL min^{-1}. The wavelengths used for quercetin detection were excitation = 355 nm and emission = 525 nm (Komori et al., 2007). The quantification was performed using a calibration curve prepared with standards at concentrations between 0.01 to 0.1 mg mL^{-1}.

3.4. Stability under various environmental conditions

The stability of β-Lg micro- and nanostructures in the absence and presence of bioactive model compounds under various environmental conditions (i.e., pH, ionic strength, thermal processing and storage temperature) was evaluated in terms of their particle size, polydispersity index (PDI) and surface charge (S) by dynamic light scattering (DLS) instrument.

3.4.1. pH stability

The effect of pH was assessed by ranging pH between 2 and 10 using 0.1 mol L^{-1} NaOH and/or 0.1 mol L^{-1} H_3PO_4, as necessary.

3.4.2. Ionic strength stability

The influence of ionic strength was evaluated on β-Lg micro- and nanostructures in the absence and presence of bioactive model compounds by adding distinct NaCl concentrations (0 – 200 mmol L^{-1}) (Bourbon et al., 2015; Tokle et al., 2013).

3.4.3. Temperature stability

Thermal stability was assessed by DLS, using the temperature range from 20 to 80 °C, with increments of 5 °C, with 60 s of equilibration before each measurement (Martins et al., 2016).

3.4.4. Storage temperature stability

Samples were stored at temperatures of 4 °C (to simulate refrigeration conditions) and 25 °C (to simulate room temperature conditions) over 90 days, and at an appropriate interval of time, particle size, PDI and S were measured (Monteiro et al., 2016).

3.5. *In vitro* release profile of bioactive model compounds from β-Lg micro- and nanostructures

3.5.1. Material

Dialysis membrane with cut-off 10 kDa (Spectra/Por) was obtained from Spectrum Laboratories, USA.

3.5.2. Release kinetics profile

The *in vitro* release profiles of bioactive model compounds were evaluated by dialysis over 72 h (Azevedo et al., 2014; Bourbon et al., 2016) (Figure 3.2).

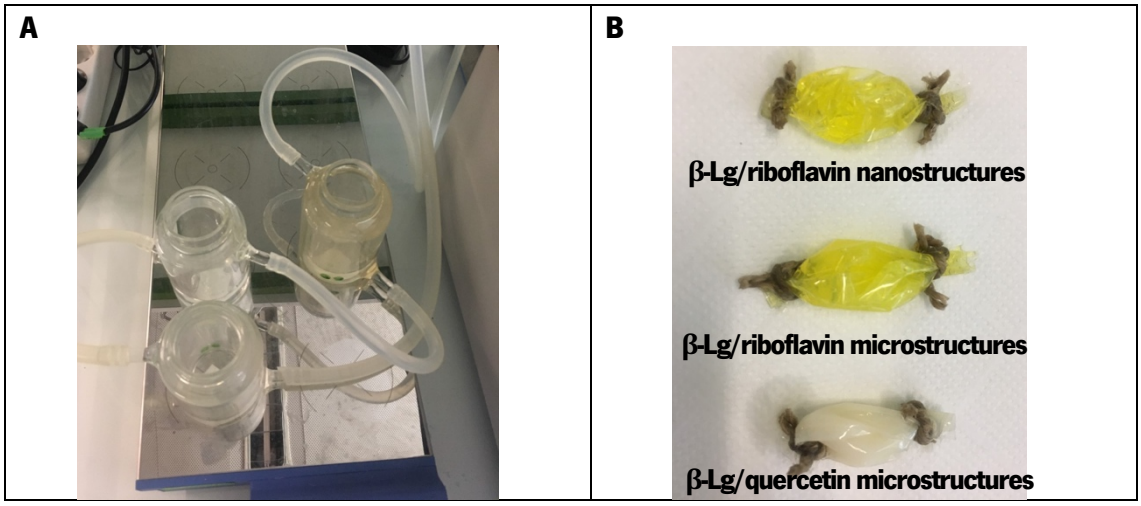


Figure 3.2 - *In vitro* release system: jacketed reactors for controlling temperature A) and samples into dialysis membrane B).

These experiments used two food simulant solutions, composed by 10 and 50 % of ethanol to simulate hydrophilic and hydrophobic food matrices, respectively, according with the Commission

Regulation (EU) No 10/2011 of 14 January 2011, and were conducted at 4 °C (to mimic refrigerated temperatures) and at 25 °C (to mimic room temperature).

Samples (5 mL) were placed inside of a dialysis membrane with cut-off 10 kDa (Spectra/Por, Spectrum Laboratories, USA) and then placed into a reactor with 50 mL of food simulant solutions under continuous magnetic stirring at 200 rpm. At appropriate time intervals, 0.3 mL of supernatant was taken and replaced by the same quantity of fresh food simulant solution to maintain the volume constant. The quantity of riboflavin and quercetin released from β-Lg micro- and nanostructures were evaluated by spectrophotometry for riboflavin and by HPLC for quercetin. These experiments were performed at least in triplicate.

3.5.3. Mathematical modelling

The release mechanisms of bioactive model compounds from β-Lg micro- and nanostructures were assessed by the kinetic model proposed by Berens and Hopfenberg (1978), which considers both Fickian and Case II transport effects as evidenced in Equation (3):

$$M_t = M_{t,F} + M_{t,R} \quad \text{Equation (3)}$$

where, M_t is the total mass released from polymeric β-Lg micro- and nanostructures at time t; $M_{t,F}$ and $M_{t,R}$ are the contributions of the Fickian and biopolymer relaxation effects, respectively. The Fickian transport is described by Equation (4), as follows:

$$M_{t,F} = M_{\infty,F}\left[1 - \frac{6}{\pi^2}\sum_{n=1}^{\infty}\frac{1}{n^2}\exp\left(-n^2 k_F t\right)\right] \quad \text{Equation (4)}$$

where, $M_{\infty,F}$ is the bioactive compound released at equilibrium and k_F is the Fickian diffusion rate constant. Equation (4) can be simplified by applying the first term of the Taylor series (Pinheiro et al., 2012), as presented in Equation (5):

$$M_{\infty,F} = M_F\left[1 - \frac{6}{\pi^2}\exp\left(k_F t\right)\right] \quad \text{Equation (5)}$$

Regarding biopolymer relaxation, it is driven by biopolymer swelling capacity and then associated to the dissipation of stress induced by the penetrant entrance. This behaviour can be characterized as a distribution of relaxation times, each assuming a first order-type kinetic equation (Berens & Hopfenberg, 1978), as follows Equation (6):

$$M_{t,R} = \sum_i M_{\infty,Ri}[1 - \exp(-k_{Ri}t)\,] \quad \text{Equation (6)}$$

where, $M_{\infty,Ri}$ is the contribution of the relaxation processes for bioactive compound release and k_{Ri} is the relaxation i^{th} rate constant. Commonly, only one main biopolymer relaxation influences the relaxation transport (i.e., $i = 1$) (Bourbon et al., 2016).

Thereby, the linear superimposition model (LSM) for bioactive model compounds released from β-Lg micro- and nanostructures can be described by Equation (7):

$$\frac{M_t}{M_\infty} = X\left[1 - \frac{6}{\pi^2}\exp\left(-k_F t\right)\right] + (1 - X)[1 - \exp\left(-k_R t\right)] \quad \text{Equation (7)}$$

where X is the fraction of bioactive compounds released by Fickian transport.

Experimental data were fitted with Equation (7) (LSM) to evaluate the transport mechanism involved in riboflavin and quercetin release from β-Lg micro- and nanostructures at hydrophilic and hydrophobic food simulants at 4 and 25 °C.

3.5.4. Statistical analysis

Equations (4) and (7) were fitted to experimental data using a non-linear regression. The least square function minimization was done by the Leveberg-Marquardt algorithm. The quality of regression curves was assessed by the determination coefficient (R^2) and the squared root mean square error (*RMSE*).

3.6. Caco-2 cells studies and gastrointestinal (GI) model and

3.6.1. Feedstocks and chemicals

The following chemicals were purchased from Sigma-Aldrich (St. Louis, MO, USA): sodium dodecyl sulfate (SDS), tris(hydroxymethyl)aminomethane, ammonium persulfate (APS), Coomassie Brilliant Blue (R-250), bromophenol blue, etramethylethylenediamine, pancreatin from porcine pancreas, pepsin from porcine gastric mucosa, bile extract porcine, Pefabloc® SC, 4-(2-aminoetyl) benenesulfonyl fluoride, sodium and ammonium carbonate, potassium phosphate dibasic, magnesium chloride, penicillin-streptomycin, trypsin-EDTA solution (0.25%), methylthiazolyldiphenyl-tetrazolium (MTT) and celLytic™ MT cell lysis reagent. Acrylamide was purchased from Bio-Rad (California, USA) and glycerol was obtained from Himedia (Mumbai, India). Acetic and phosphoric acids and sodium hydroxide were purchased from Merck (Merck KGaA, Darmstadt, Germany). Potassium and calcium chloride, hydrochloric acid, monosodium phosphate, sodium chloride and glycine were obtained from Panreac (Barcelona, Spain). Methanol and phosphate dibasic were purchased from Chem-Lab (Zedelgem, Belgium) whereas dimethyl sulfoxide was obtained from Fisher Scientific (New Hampshire, USA). Serine was purchased from Acros Organics (Belgium) whereas TNBSA (2,4,6-Trinitrobenzene Sulfonic Acid) was obtained from Thermo Fisher Scientific (Bremen, Germany). Caco-2 cell line, obtained from human colon carcinoma, was kindly supplied by Department of Biology of University of Minho (Braga, Portugal).

Dulbecco's Modified Eagle Medium (DMEM) with L-glutamine, fetal bovine serum, and non-essential amino acids were purchased from Lonza (Basel, Switzerland). Hanks' Balanced Salt solution (HBSS) was purchased from Biochrom GmbH (Berlin, Germany) and others cell culture reagents were purchased from Biowest (Nuaillé, France). All other chemicals used in this study were reagent grade, and were used without further purification.

3.6.2. β–Lg micro- and nanostructures effect on Caco-2 cells

The *in vitro* cellular model based on human colon carcinoma Caco-2 cells was applied to mimic intestinal epithelial cells and to assess β-Lg structures cytotoxicity and bioactive compounds' permeability through the cells.

3.6.2.1. Cell culture

Human colon carcinoma Caco-2 cell line was grown in DMEM supplemented with 10 % heat-inactivated foetal bovine serum, 1 % penicillin-streptomycin, 1 % L-glutamine and 1 % non-essential amino acids. Stocks cells were maintained in culture flasks incubated at 37 °C with 5 % CO_2 humidified atmosphere. Upon reaching approximately 90 % of confluence, cells were harvested from culture flasks using trypsin-EDTA (0.25 %). Viable cell number in suspension was carried out by counting in a Neubauer chamber with an optical microscope (Tibolla et al., 2018).

3.6.2.2. Cytotoxicity assay

Samples cytotoxicity on Caco-2 cells were performed by MTT conversion assay, according to Tibolla et al. (2019) procedure (Figure 3.3).

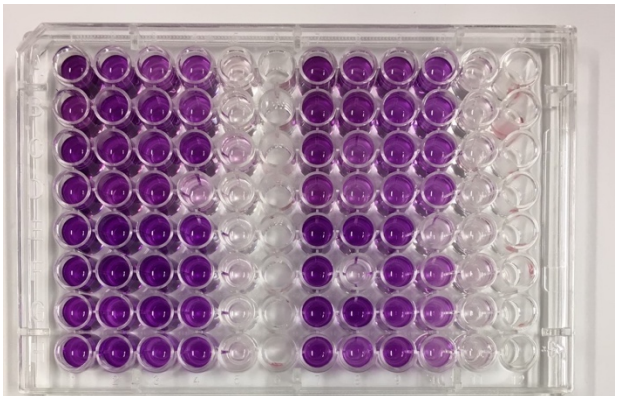


Figure 3.3 - Cytotoxicity assay using Caco-2 cell seeded at a cell density of 4×10^4 cells/well in 96-well plate.

Briefly, β-Lg microstructures (24 x 10^{-3} to 13.5 mg mL^{-1}), nanostructures (1 to 4.5 mg mL^{-1}), β-Lg micro- and nanostructures associated to riboflavin (21.0 x 10^{-3} to 94.5 x 10^{-3} mg mL^{-1} riboflavin), β-Lg micro- and nanostructures associated to quercetin (0.128 x 10^{-3} to 40.0 x 10^{-3} mg mL^{-1} quercetin), free bioactive model compounds and ethanol (in equivalent quercetin concentrations) were diluted in supplemented DMEM medium and homogenized. Caco-2 cells suspension in supplemented DMEM medium were seeded at a cell density of 4×10^4 cells/well in 96-well plate and incubated at 37 °C in 5 % CO_2 atmosphere during 24 h. Cells only with DMEM were used as control. Subsequently, DMEM medium was replaced by β-Lg samples, free bioactive compounds and ethanol, and maintained at 37 °C in 5 % CO_2 during 24 h. After incubation, the supernatant was removed and washed with PBS. Then, 100 μL MTT solution (0.5 mg mL^{-1} in supplemented DMEM) were added into each well and the plate was incubated at 37 °C for 4 h, in order to form soluble purple formazan crystals. The crystals' solubilization was performed by adding 200 μL of DMSO to each well, followed shaking in an orbital shaker (100 rpm) during 30 min. The purple formazan was quantified by measurement of the absorbance at 570 nm and 690 nm (used for background subtraction) in Synergy™ HT Multi-mode Microplate Reader (Biotek Instruments, Winooski, VT, USA). The percentage of cell viability for all samples was assessed by Equation (12).

$$Cell\ viability\ (\%) = \frac{A_{sample}}{A_{control}} \times 100 \qquad \text{Equation (12)}$$

where, A_{sample} is the absorbance value of sample with cell culture and $A_{control}$ is the absorbance value of DMEM with cell culture.

3.6.2.3. Caco-2 cell culture permeability

Caco-2 cell culture permeability assay was performed according to the procedure adopted by Antunes et al., (2013) and Silva et al., (2018) (Figure 3.4).

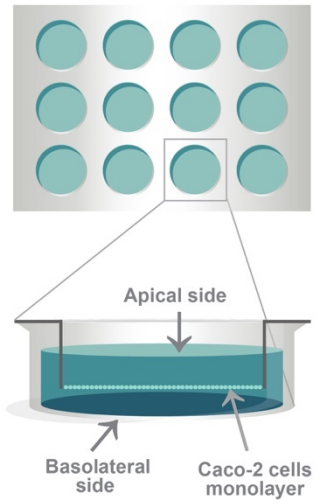


Figure 3.4 - Schematic representation of Caco-2 cells seeded on polycarbonate membrane u for permeability measurements.

Caco-2 cells were seeded at 1×10^5 cells/well density on polycarbonate membrane with a 0.4 μm pore size in 12-well plates (Transwell®, Corning Costar Corp). The apical (mucosal) and basolateral (serosal) compartments contained 0.5 and 1.5 mL of culture medium, respectively. During 21 days, Caco-2 cells were grown and differentiated to confluent by changing the medium (RPMI 1640 supplemented with 10 % of fetal bovine serum and 1 % of penicillin-streptomycin) three times a week. Since the transepithelial electrical resistance (TEER) measurements determines the passive ion transport across the cell and in the cell junctions, it can be used as a criterion to evaluate the tightness of the cell monolayer in order to establish its integrity. Therefore, TEER measurement was carried out to monitoring cells growth in the 21 days, as per the following Equation (13):

$$TEER = \left(R_{monolayer} - R_{control}\right) \times SA \qquad \text{Equation (13)}$$

where, $R_{monolayer}$ is the cell monolayer resistance with the filter membrane, $R_{control}$ is the resistance of filter membrane and SA is the surface area of membrane (ca. 1.12 cm^2 in each well plates). Monolayers cells with TEER value higher than 500 $\Omega.cm^2$ followed to permeability assays.

Before starting the experiment, the cell medium was replaced by Hanks' Balanced Salt solution (HBSS) with a pH value of 7.4, and incubated at 37 °C during 1 h with 5 % CO_2.

In permeability studies, β-Lg micro- and nanostructures with riboflavin and quercetin, and free bioactive model compound samples were diluted in HBSS, to achieve the desired concentration without cytotoxicity. Subsequently, samples (500 μL) were put in the apical compartment and 1.5 mL of HBSS were added in the basolateral side. Transepithelial transport across the Caco-2 cell

monolayer was performed from the apical to the basolateral direction, and in determined periods of time (0 to 240 min) basolateral samples (200 µL) were collected, and then replaced by fresh HBSS to maintain a constant volume. After 2 h, the apical samples were taken and analysed in terms of bioactive model compounds concentration. Riboflavin and quercetin quantifications were determined according to the methodology described in Section 3.3.2 and 3.3.3, respectively. Thus, these results were used to calculated the apparent permeability coefficient (P_{app}) according to Equation (14):

$$P_{app} = \frac{\frac{dQ}{dt}}{C_o \times SA} \quad \text{Equation (14)}$$

where, dQ/dt is the cumulative transport rate (mg min^{-1}) defined as the slope obtained by linear regression of cumulative transported quantity as a function of time (min), C_o is the initial bioactive model compound concentration, and SA the surface area of membrane (ca. 1.12 cm^2 in each well plates).

3.6.2.4. Cellular uptake assay

The cellular uptakes of riboflavin and quercetin were performed using the Caco-2 cells from the permeability assays. For this purpose, final monolayers samples were washed with 100 µL HBSS, in order to remove β-Lg structures with bioactive model compounds associated to the apical side. Subsequently, 100 µL of CelLytic™ MT Cell Lysis Reagent (composed by 1 % Protease Inhibitor Cocktail) were added, and the cells were incubated at 37 °C during 5 min with orbital shaking. The cells were lysed and the amounts of both bioactive compounds were quantified.

3.6.3. *In vitro* digestion

The *in vitro* digestion experiment was carried out using the harmonized INFOGEST *in vitro* digestion model to mimic mouth, stomach, and small intestine conditions as described by Minekus et al., (2014) (Figure 3.5).

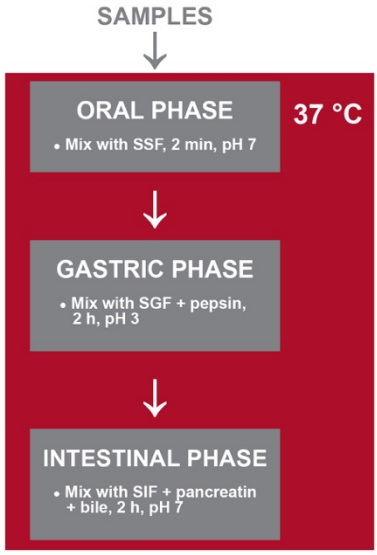


Figure 3.5 - Schematic representation of a simulated in vitro digestion method. (Adapted from Minekus et. al, 2014).

NOTE: SSF: simulated salivary fluid; SGF: simulated gastric fluid; SIF: simulated intestinal fluid

Simulated salivary fluid (SSF), simulated gastric fluid (SGF) and simulated intestinal fluid (SIF) were the electrolyte stock solutions (ca. 1.25 x concentrated) used during *in vitro* digestion (Table 3.2).

Table 3.2 - Composition of simulated salivary fluid (SSF), simulated gastric fluid (SGF) and simulated intestinal fluid (SIF) stock solutions.

	SSF (mmol L^{-1})	**SGF (mmol L^{-1})**	**SIF (mmol L^{-1})**
KCl	15.10	6.90	6.80
KH_2PO_4	3.70	0.90	0.80
$NaHCO_3$	13.60	25.00	85.00
$MgCl_2(H_2O)_6$	0.15	0.12	0.33
$(NH_4)_2CO_3$	0.06	0.50	-
NaCl	-	47.20	38.40
HCl	-	15.60	8.40

NOTE: $CaCl_2(H_2O)_2$ was added to the final of each fluid mixture of digestion to avoid precipitation

Before the *in vitro* digestion procedure, electrolyte stock solutions and β-Lg micro- and nanostructures samples (5 mL) were inserted in a shaking water bath set to 37 °C.

Initially, samples were exposed to simulated mouth conditions (SSF solution) and $CaCl_2(H_2O)_2$) (to achieve the concentration of 1.5 mmol L^{-1} in fluid). Then, the final oral phase volume was adjusted with milli-Q water and samples were returned to shaking water bath and incubated at 37 °C for 2 min. Note that α-amylase was not used since the samples do not contained starch. After oral phase, sample were taken and cooling in ice.

Subsequently, the passage through to stomach was mimicked by adding porcine pepsin solution (with an activity of 2000 U/mL in the final mixture), SGF solution and $CaCl_2(H_2O)_2$ (to achieved 0.15 mmol L^{-1} in the fluid). The pH value was adjusted to 3.0 with 1 mol L^{-1} HCl, when necessary, and the gastric phase volume was completed with milli-Q water. Samples were incubated at 37 °C during 2 h. After gastric phase, samples were taken and cooling in ice.

After 2 h, intestinal phase secretion composed by SIF solution, $CaCl_2(H_2O)_2$ (to achieved 0.6 mmol L^{-1} in the fluid,) pancreatin (with an activity of 100 U/mL in the final mixture) and bile solutions (in order to reach the concentration of 10 mmol L^{-1} in the final mixture) (both prepared in SIF) were added to the gastric phase volume. The pH value was adjusted to 7 with 1 mol L^{-1} NaOH, when necessary. The final intestinal phase volume was adjusted with milli-Q water and then, incubated under the same conditions as before for 2 h. In the end of intestinal phase, the reaction was stopped by adding 1 mmol L^{-1} of enzyme inhibitor Pefabloc® SC.

During *in vitro* digestion, samples were collected after each phase (i.e., oral, gastric and intestinal) and cooled in ice before measurements. Samples were tested in the *in vitro* digestion model at least in triplicate.

3.6.3.1. Bioactive model compounds bioavailability

Riboflavin and quercetin bioavailable fractions were assessed using the method described by Pinheiro et al. (2013) with some modifications. Briefly, intestinal phase samples of the β-Lg structures (10 mL) were centrifuged (Allegra 64R, Beckman Coulter, USA) at 18,000 x *g* during 30 min at 25 °C. Afterwards, samples were separated in two distinct phases, being at bottom an opaque sediment phase and at the top a clear micelle phase. The concentrations of model bioactive compounds in the clear micelle phase provide a measure of the amount of the bioaccessible fraction, which was available to be absorbed and metabolically processed (Silva et al., 2018; Zou et al., 2015). Then, aliquots (5 mL) of the micelle phase (supernatant) were collected and used to quantify the amount of bioactive compound released after *in vitro* digestion. Riboflavin concentration was determined by fluorescence spectroscopy according to the methodology

described in Section 3.3.2 fluorescence intensity was corrected by blank fluorescence subtraction (i.e., *in vitro* digestion without β-Lg/riboflavin micro- and nanostructures). Quercetin quantification was determined by high performance liquid chromatography with fluorescence detection (HPLC-FL). Briefly, quercetin samples were diluted in DMSO and centrifuged (Mikro 120, Andreas Hettich GmbH & Co.KG, Tuttlingen, Germany) at 13,000 x *g* during 10 min at 25 °C. The supernatant was dissolved in methanol to precipitate the protein and centrifuged again at same conditions. Then, resulting sample was filtered through a 0.22 μm nylon filter before analysis (Section 3.3.3). Riboflavin and quercetin bioaccessibility Equation (8), stability Equation (9) and bioavailability Equation (10) were determined as reported by Liu et al., (2018) using the following equations:

$$Bioaccessibility\ (\%) = \frac{C_{Micelle\ Phase}}{C_{Intestinal\ Phase}} \times 100 \qquad \text{Equation (8)}$$

$$Stability\ (\%) = \frac{C_{Intestinal\ Phase}}{C_{Initial}} \times 100 \qquad \text{Equation (9)}$$

$$Bioavailability\ (\%) = \frac{C_{Micelle\ Phase}}{C_{Initial}} \times 100 \qquad \text{Equation (10)}$$

where, $C_{Micelle\ Phase}$ is the concentration of bioactive model compounds in the micelle phase, $C_{Intestinal\ Phase}$ is the concentration of bioactive model compounds after *in vitro* digestion, and $C_{Initial}$ was the initial model bioactive compounds concentration added into the β-Lg structures.

3.6.3.2. Monitoring protein hydrolysis degree during *in vitro* digestion

In order to evaluate β-Lg micro- and nanostructures hydrolysis degree (*HD*) during *in vitro* digestion, TNBSA assay was performed according to Castillo et al., (2006). A sample (0.5 mL) of each *in vitro* digestion phase was diluted directly in 0.1 mol L^{-1} bicarbonate buffer at pH 8.5 to achieve final protein concentration between 0.05 and 0.2 mg mL^{-1}. Subsequently, 0.25 mL of 0.1 % TBNSA was added to the resulting solution (0.5 mL) and incubated at 37 °C during 2 h. Then, 0.25 mL of 10 % SDS and 1 mol L^{-1} HCl was added to each sample and homogenized. Considering the potential interference of the pepsin from the gastric juice and pancreatin from intestinal phase, *in vitro* digestion without sample was used as blank. Sample absorbance measurements were carried out at 335 nm in Synergy™ HT Multi-mode Microplate Reader (Biotek Instruments, Winooski, VT, USA). All samples were analysed in triplicate and the amino group content was performed by reference

serine standard curve ($y = 0.0207\,x + 0.0236;\ \ R^2 = 0.99$; being y and x the absorbance and concentration of serine, respectively). The *HD* was referred according to the percentage of peptide bond cleaved in the total number of peptide bonds (Luo et al., 2015), as shown in Equation (11).

$$HD\ (\%) = \left(\frac{h_{sample}}{h_{total}}\right) \times\ 100 \qquad \text{Equation (11)}$$

where, h_{sample} is the number of peptide bonds cleaved in sample and h_{total} is the total number of peptide bond.

3.7. References

Antunes, F., Andrade, F., Araújo, F., Ferreira, D., & Sarmento, B. (2013). Establishment of a triple co-culture *in vitro* cell models to study intestinal absorption of peptide drugs. European Journal of Pharmaceutics and Biopharmaceutics, 83(3), 427–435. https://doi.org/10.1016/j.ejpb.2012.10.003

Azevedo, M. A., Bourbon, A. I., Vicente, A. A., & Cerqueira, M. A. (2014). Alginate/chitosan nanoparticles for encapsulation and controlled release of vitamin B2. International Journal of Biological Macromolecules, 71, 141–146. https://doi.org/10.1016/j.ijbiomac.2014.05.036

Berens, A. R., & Hopfenberg, H. B. (1978). Diffusion and relaxation in glassy polymer powders: 2. Separation of diffusion and relaxation parameters. Polymer, 19(5), 489–496. https://doi.org/10.1016/0032-3861(78)90269-0

Bourbon, A. I., Cerqueira, M. A., & Vicente, A. A. (2016). Encapsulation and controlled release of bioactive compounds in lactoferrin-glycomacropeptide nanohydrogels : Curcumin and caffeine as model compounds. Journal of Food Engineering, 180, 110–119. https://doi.org/10.1016/j.jfoodeng.2016.02.016

Bourbon, A. I., Pinheiro, A. C., Carneiro-da-Cunha, M. G., Pereira, R. N., Cerqueira, M. a., & Vicente, A. a. (2015). Development and characterization of lactoferrin-GMP nanohydrogels: Evaluation of pH, ionic strength and temperature effect. Food Hydrocolloids, 48, 292–300. https://doi.org/10.1016/j.foodhyd.2015.02.026

Bourbon, A. I., Pinheiro, A. C., Cerqueira, M. A., & Vicente, A. A. (2016). Influence of chitosan coating on protein-based nanohydrogels properties and *in vitro* gastric digestibility. Food Hydrocolloids, 60, 109–118. https://doi.org/10.1016/j.foodhyd.2016.03.002

Castillo, B., Mendez, J., Al-Azzam, W., Barletta, G., & Griebenow, K. (2006). On the relationship between the activity and structure of PEG-α-chymotrypsion conjugates in organic solvents. Biotech Bioeng, 94(3), 565–574. https://doi.org/10.1002/bit

Dombrowski, J., Johler, F., Warncke, M., & Kulozik, U. (2016). Correlation between bulk characteristics of aggregated β-lactoglobulin and its surface and foaming properties. Food Hydrocolloids, 61, 318–328. https://doi.org/10.1016/j.foodhyd.2016.05.027

Donato, L., Schmitt, C., Bovetto, L., & Rouvet, M. (2009). Mechanism of formation of stable heat-induced β-lactoglobulin microgels. International Dairy Journal, 19(5), 295–306. https://doi.org/10.1016/j.idairyj.2008.11.005

Komori, A., Inoue, N., Fujita, K., Kasajima, S., & Horii, A. (2007). Measurement of Rutin and Quercetin in Tartary Buckwheat Flour by Ultraviolet-Induced Fluorescence. Proceedings of the l0th .... Retrieved from http://citeseerx.ist.psu.edu/viewdoc/download?doi=10.1.1.578.2253&rep=rep1&type=pdf

Konrad, G., Lieske, B., & Faber, W. (2000). A large-scale isolation of native β-lactoglobulin: Characterization of physicochemical properties and comparison with other methods. International Dairy Journal, 10(10), 713–721. https://doi.org/10.1016/S0958-6946(00)00099-6

Kosters, H. A., Wierenga, P. A., De Vries, R., & Gruppen, H. (2011). Characteristics and effects of specific peptides on heat-induced aggregation of β-lactoglobulin. Biomacromolecules, 12(6), 2159–2170. https://doi.org/10.1021/bm2002285

Liu, W., Wang, J., McClements, D. J., & Zou, L. (2018). Encapsulation of β-carotene-loaded oil droplets in caseinate/alginate microparticles: Enhancement of carotenoid stability and bioaccessibility. Journal of Functional Foods, 40(December 2017), 527–535. https://doi.org/10.1016/j.jff.2017.11.046

Luo, Q., Boom, R. M., & Janssen, A. E. M. (2015). Digestion of protein and protein gels in simulated gastric environment. LWT - Food Science and Technology, 63(1), 161–168. https://doi.org/10.1016/j.lwt.2015.03.087

Madadlou, A., Floury, J., Pezennec, S., & Dupont, D. (2018). Encapsulation of β-lactoglobulin within calcium carbonate microparticles and subsequent in situ fabrication of protein microparticles. Food Hydrocolloids, 84(March), 38–46. https://doi.org/10.1016/j.foodhyd.2018.05.054

Madalena, D. A., Ramos, Ó. L., Pereira, R. N., Bourbon, A. I., Pinheiro, A. C., Malcata, F. X., ... Vicente, A. A. (2016). *In vitro* digestion and stability assessment of β-lactoglobulin/riboflavin nanostructures. Food Hydrocolloids, 58, 89–97. https://doi.org/10.1016/j.foodhyd.2016.02.015

Martins, J. T., Santos, S. F., Bourbon, A. I., Pinheiro, A. C., González-Fernández, Á., Pastrana, L. M., ... Vicente, A. A. (2016). Lactoferrin-based nanoparticles as a vehicle for iron in food applications - Development and release profile. Food Research International, 90, 16–24. https://doi.org/10.1016/j.foodres.2016.10.027

Maté, J. I., & Krochta, J. M. (1994). β-Lactoglobulin Separation from Whey Protein Isolate on a Large Scale. Journal of Food Science, 59(5), 111–114.

Minekus, M., Alminger, M., Alvito, P., Ballance, S., Bohn, T., Bourlieu, C., ... Brodkorb, A. (2014). A standardised static *in vitro* digestion method suitable for food-an international consensus. Food and Function, 5(6), 1113–1124. https://doi.org/10.1039/c3fo60702j

Monteiro, A. A., Monteiro, M. R., Pereira, R. N., Diniz, R., Costa, A. R., Malcata, F. X., ... Ramos, Ó. L. (2016). Design of bio-based supramolecular structures through self-assembly of α-lactalbumin and lysozyme. Food Hydrocolloids, 58, 60–74. https://doi.org/10.1016/j.foodhyd.2016.02.009

Nobre, C., Sousa, S. C., Silva, S. P., Pinheiro, A. C., Coelho, E., Vicente, A. A., ... Rodrigues, L. R. (2018). *In vitro* digestibility and fermentability of fructo-oligosaccharides produced by Aspergillus ibericus. Journal of Functional Foods, 46(February), 278–287. https://doi.org/10.1016/j.jff.2018.05.004

Pace, C. N., Treviño, S., Prabhakaran, E., Scholtz, J. M., Franks, F., Wilson, K., ... Purkiss, A. (2004). Protein structure, stability and solubility in water and other solvents. Philosophical Transactions of the Royal Society B: Biological Sciences, 359(1448), 1225–1235. https://doi.org/10.1098/rstb.2004.1500

Pereira, R. N., Rodrigues, R. M., Ramos, Ó. L., Xavier Malcata, F., Teixeira, J. A., & Vicente, A. A. (2015). Production of Whey Protein-Based Aggregates Under Ohmic Heating. Food and Bioprocess Technology, 1–12. https://doi.org/10.1007/s11947-015-1651-4

Pinheiro, A. C., Bourbon, A. I., Quintas, M. A. C., Coimbra, M. A., & Vicente, A. A. (2012). K-Carrageenan/Chitosan Nanolayered Coating for Controlled Release of a Model Bioactive Compound. Innovative Food Science and Emerging Technologies, 16, 227–232. https://doi.org/10.1016/j.ifset.2012.06.004

Pinheiro, A. C., Lad, M., Silva, H. D., Coimbra, M. A., Boland, M., & Vicente, A. A. (2013). Unravelling the behaviour of curcumin nanoemulsions during *in vitro* digestion: effect of the surface charge. Soft Matter, 9(11), 3147. https://doi.org/10.1039/c3sm27527b

Ramos, O. L., Pereira, J. O., Silva, S. I., Amorim, M. M., Fernandes, J. C., Lopes-da-Silva, J. A., ... Malcata, F. X. (2012). Effect of composition of commercial whey protein preparations upon gelation at various pH values. Food Research International, 48(2), 681–689. https://doi.org/10.1016/j.foodres.2012.06.004

Rodrigues, R. M., Martins, A. J., Ramos, O. L., Malcata, F. X., Teixeira, J. A., Vicente, A. A., & Pereira, R. N. (2015). Influence of moderate electric fields on gelation of whey protein isolate. Food Hydrocolloids, 43, 329–339. https://doi.org/10.1016/j.foodhyd.2014.06.002

Schmitt, C., Bovay, C., Vuilliomenet, A.-M., Rouvet, M., Bovetto, L., Barbar, R., & Sanchez, C. (2009). Multiscale Characterization of Individualized β-Lactoglobulin Microgels Formed upon Heat Treatment under Narrow pH Range Conditions. Langmuir, 25(14), 7899–7909. https://doi.org/10.1021/la900501n

Silva, H. D., Beldíková, E., Poejo, J., Abrunhosa, L., Cerqueira, M. A., Serra, A. T., ... Vicente, A. A. (2018). Evaluating the effect of chitosan layer on bioaccessibility and cellular uptake of curcumin nanoemulsions. Journal of Food Engineering, 243(September 2018), 89–100. https://doi.org/10.1016/j.jfoodeng.2018.09.007

Silva, H. D., Poejo, J., Pinheiro, A. C., Donsì, F., Teresa, A., Duarte, C. M. M., ... Vicente, A. A. (2018). Evaluating the behaviour of curcumin nanoemulsions and multilayer nanoemulsions during dynamic *in vitro* digestion. Journal of Functional Foods, 48(April), 605–613. https://doi.org/10.1016/j.jff.2018.08.002

Teng, Z., Xu, R., & Wang, Q. (2015). Beta-lactoglobulin-based encapsulating systems as emerging bioavailability enhancers for nutraceuticals: a review. RSC Adv., 5(44), 35138–35154. https://doi.org/10.1039/C5RA01814E

Tibolla, H., Pelissari, F. M., Martins, J. T., Lanzoni, E. M., Vicente, A. A., Menegalli, F. C., & Cunha, R. L. (2019). Banana starch nanocomposite with cellulose nanofibers isolated from banana peel by enzymatic treatment: *In vitro* cytotoxicity assessment. Carbohydrate Polymers, 207(November 2018), 169–179. https://doi.org/10.1016/j.carbpol.2018.11.079

Tibolla, H., Pelissari, F. M., Martins, J. T., Vicente, A. A., & Menegalli, F. C. (2018). Cellulose nanofibers produced from banana peel by chemical and mechanical treatments: Characterization and cytotoxicity assessment. Food Hydrocolloids, 75, 192–201. https://doi.org/10.1016/j.foodhyd.2017.08.027

Tokle, T., Mao, Y., & McClements, D. J. (2013). Potential biological fate of emulsion-based delivery systems: Lipid particles nanolaminated with lactoferrin and β-lactoglobulin coatings. Pharmaceutical Research, 30(12), 3200–3213. https://doi.org/10.1007/s11095-013-1003-x

Wang, W., Zhong, Q., & Hu, Z. (2013). Nanoscale understanding of thermal aggregation of whey protein pretreated by transglutaminase. Journal of Agricultural and Food Chemistry, 61(2), 435–446. https://doi.org/10.1021/jf304506n

Zhang, P., Zhao, S. R., Li, J. X., Hong, L., Raja, M. A., Yu, L. J., & Liu, C. G. (2016). Nanoparticles based on phenylalanine ethyl ester-alginate conjugate as Vitamin B2 delivery system. Journal of Biomaterials Applications, 31(1), 13–22. https://doi.org/10.1177/0885328216630497

Zou, L., Liu, W., Liu, C., Xiao, H., & McClements, D. J. (2015). Designing excipient emulsions to increase nutraceutical bioavailability: Emulsifier type influences curcumin stability and bioaccessibility by altering gastrointestinal fate. Food and Function, 6(8), 2475–2486. https://doi.org/10.1039/c5fo00606f

Section III

RESULTS AND DISCUSSION

CHAPTER 4.

Design of β-lactoglobulin micro- and nanostructures by controlling gelation through physical variables

4.1. Introduction 60

4.2. Results and discussion 62

4.3. Conclusions 74

4.4. References 75

This Chapter was adapted from:

Simões, Lívia S.; Araújo, João M.; Vicente, António A.; Ramos, Oscar L. Design of β-lactoglobulin micro- and nanostructures by controlling gelation through physical variables. Food Hydrocolloids. Resubmitted in July 29, 201

4.1.Introduction

Bovine β-lactoglobulin (β-Lg) is a globular protein obtained from milk and constitutes the main fraction of whey proteins (ca. 50 % of its protein content), widely used as functional and nutritional ingredient in food, cosmetic and pharmaceutical industries (Pereira et al., 2015; Rodrigues et al., 2015). Whey proteins are obtained from whey, which is a by-product of cheese production, relatively inexpensive and classified as a GRAS (generally regarded as safe) material (Madalena et al., 2016).

The interest in β-Lg from both the scientific community and food and pharmaceutical industries is essentially due to its high nutritional value as a consequence of the rich level of amino acids, resistance to proteolytic degradation in the stomach, biological (e.g., digestibility, sensory characteristics and high biological value) properties, and gelation capacity – which is particularly important since it allows the formation of structures with different properties and morphologies (Ramos et al., 2012). However, β-Lg at high purity levels, is commercially available only at high cost, therefore obtaining it from cheaper commercial protein solutions is a more feasible alternative to allow a full understanding of the mechanisms behind the protein gelation that lead to structural conformational changes and thus to the formation of different structures, while guaranteeing the economical sustainability of the eventual system derived therefrom (Ramos et al., 2015; Ramos et al., 2014).

Thermally-induced gelation usually consists in the unfolding of polypeptide chains of protein in native state with concomitant exposure of initially buried hydrophobic amino acid residues, and subsequent self-aggregation of protein molecules through physical (electrostatic and hydrophobic) and chemical (disulphide) interactions (Delahaije et al., 2015; Teng et al., 2015). The extent and behaviour of protein aggregation depends on the environmental conditions (e.g., heating temperature, time of heating, pH, protein concentration and ionic strength) (Ramos et al., 2015), and can result in different structures with various sizes, shapes, morphologies and charge.

Several researchers have focused their work on understanding the structural gelation of β-Lg, but only under limited physical and environmental conditions. For instance, Dombrowski et al., (2017) showed the formation of soluble β-Lg aggregates with a diameter of 50 nm and displaying an increased surface hydrophobicity for β-Lg at 1.0 % and pH 6.8, when treated at 80 °C for 90 min, as compared to native β-Lg. Perez et al. (2014) studied the development β-Lg aggregates as carriers systems, for protein at 1.0 % and pH values ranging from 6.5 to 7.5, upon heat treatment at 85 °C for distinct heating times from 0 to 60 min. The authors reported that β-Lg aggregates

were formed at pH 6.5 with increased surface hydrophobicity, thus suggesting a binding ability, being their behaviour dependent of production conditions (pH, heating time and/or a combination of those). Despite these studies on β-Lg structures formation and discussions about the structural modifications over distinct conditions, there are limited data about how these conditions affect β-Lg morphology and are related with protein denaturation and aggregation phenomena. In another study, Delahaije et al., (2015) evaluated the kinetics of β-Lg heat-induced aggregation under various conditions (pH, ionic strength, concentration, and temperature), but tested separately. They concluded that electrostatic repulsion between proteins was a crucial factor for β-Lg aggregates' formation and that particle size or aggregates structure was not strongly affected by protein concentration and temperature. Nonetheless, these findings did not consider the effect of various environmental conditions combined, neither their relationship with the formation of micro- and nanostructures.

In this context, due to a large amount of β-Lg required to develop micro- and nanostructures and a high cost of available commercial β-Lg, a feasible whey protein purification process was employed to obtain a β-Lg fraction from commercial WPI, with a purity level, similar to that of a commercial β-Lg protein. The purification process allows obtaining a protein fraction from the alternative and low-cost method, consequently, may enable the scale up the β-Lg micro- and nanostructures. Additionally, the purification process intended to reinforce the importance of dairy by-product valorisation and is the great interest to recognises the importance of the system of the circular economy.

The β-Lg purified during this study was extensively characterized and the protein structural (conformational) changes were assessed upon thermal gelation, under combined physical and environmental conditions (i.e., various β-Lg concentrations, heating temperatures and times were tested) at distinct pH values (3 to 7), to design food-grade micro- (with size between 200 and 300 nm) and nanostructures (with sizes ≤ 100 nm). The small size of micro- and nanostructures can impart significant changes to physicochemical properties, among them a high surface/volume ratio, smaller pore size and increase in the solubility when compared with macroscale structures formed from the same proteins (Aklakur et al., 2016; Monteiro et al., 2016). In this regard, the effects of several conditions on β-Lg structures were evaluated through a complementary set of characterization techniques in order to provide detailed information about the specific conditions that can lead to the formation of β-Lg structures at micro- and nanoscale, which hold potential to be used as delivery systems for bioactive compounds.

4.2. Results and discussion

4.2.1. β-Lg purification

In order to evaluate the purification process efficacy using a well-established and reported method, purified β-Lg was extensively characterized in terms of physicochemical properties and the results obtained were compared with the commercial β-Lg at the same conditions. Particle size distribution results of both β-Lg (purified and commercial) are presented in Figure 4.1, showing a polymodal distribution of unheated β-Lg for both purified and commercial protein with two predominant peaks: peak 1 with maximum between 2 and 10 nm, which is attributed to non-aggregated proteins, and peak 2 associated to native β-Lg aggregates. It is also possible to observe a third peak, but only for purified β-Lg, which can be attributed to strands and clumps of small globular aggregates as result of the purification process. This behaviour was somehow expected and has been previously reported elsewhere (Rodrigues et al., 2015).

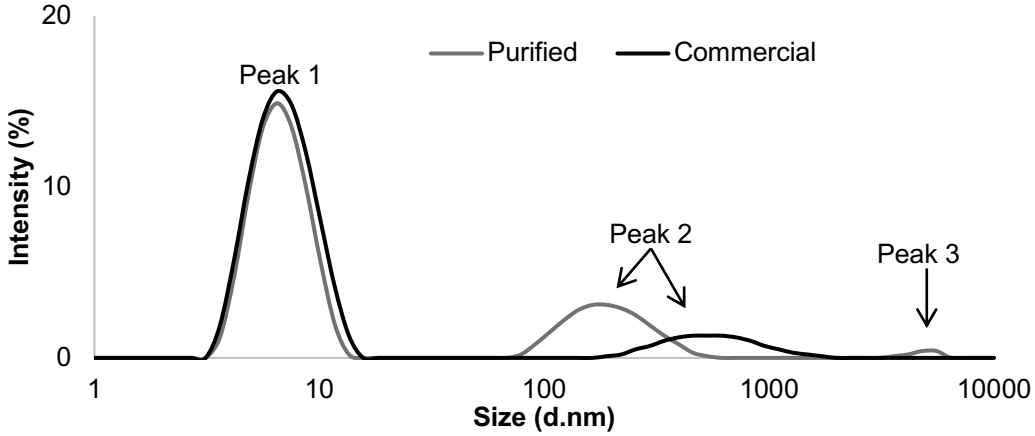


Figure 4.1 - Typical particle size distribution curve (by intensity) obtained for purified and commercial unheated β-Lg, prepared at 10 mg mL^{-1} and pH 6.

In particular for peak 1, measurements revealed a particle size and PDI values of 8.89 ± 0.06 nm and of 0.363 ± 0.004, respectively, for purified β-Lg, and of 6.83 ± 0.16 nm and 0.169 ± 0.031, respectively, for commercial β-Lg. Statistically significant differences ($p \leq 0.05$) were obtained between purified and commercial β-Lg for both parameters. These differences may be due to distinct intensities of intrinsic forces (i.e., electrostatic interactions, hydrogen and disulphide bonds, hydration and hydrophobic effects) involved on the stability of the tertiary folds (Ramos et al., 2014). On the other hand, regarding protein turbidity, purified and commercial β-Lg displayed statistically similar values ($p > 0.05$) – 0.0023 ± 0.0003 and 0.0028 ± 0.0002, respectively –

suggesting that both proteins are in identical "native" state, i.e., the content of aggregated proteins is very small.

In order to evaluate the protein stability promoted by electrostatic interactions, ζ-potential values were determined. Purified and commercial β-Lg solutions showed a statistically similar ($p > 0.05$) ζ-potential of -9.34 ± 0.71 mV and -7.93 ± 0.99 mV, respectively. These values suggest that β-Lg, in its native state, is a relatively unstable system under the measured conditions. According to Ghalandari et al., (2015) and von Staszewski et al. (2012), a colloidal system is considered stable when displaying ζ-potential values above 30 mV or below -30 mV, thus meaning that the charge between particles (i.e., repulsion) is enough to prevent aggregation. The protein conformational changes through intrinsic tryptophan fluorescence measurements was also performed to investigate if there is any change in protein structure and dynamics between both β-Lg proteins. The main responsible for β-Lg fluorescence are two tryptophan (Trp) residues (i.e., Trp-19 and Trp-61), being the intrinsic fluorescence of the protein mostly attributed to Trp-19, since it is found in the hydrophobic calyx of β-Lg, while Trp-61 is located in an external loop, close to protein surface (Simion et al., 2015). Figure 4.2A presents the intrinsic fluorescence intensity results of purified and commercial β-Lg solutions exhibiting both a maximum intensity peak at 333 nm. Typically, β-Lg has a maximum intrinsic fluorescence emission around 335 nm (Diarrassouba et al., 2013), so this result corresponds to a blue shift behaviour, thus suggesting that chromophoric groups of both samples are more buried in the interior of protein, i.e., hydrophobic groups were protected from the aqueous environment (Perez et al., 2014).

The extrinsic fluorescence, by means of the ANS fluorescent probe that binds to hydrophobic sites of proteins, provide information about changes of protein-probe interactions and on variation of the accessible hydrophobic areas (Stănciuc et al., 2012). Figure 4.2B shows a higher intensity ($p \leq 0.05$) in the peak emission of commercial β-Lg than that of purified β-Lg, thus suggesting that the latter β-Lg was less prone to bind to ANS than commercial ones. Probably, the purification process, which has resulted in a significant higher particle size of β-Lg as showed before, led for one hand, to a lower surface-area-to-volume ratio to react with ANS, and for other hand to less change at the conformational level, thus making these hydrophobic groups less exposed and consequently less accessible to ANS (Perez et al., 2014; Simion et al., 2015). Circular dichroism (CD) spectroscopy provides information on the main secondary structural elements (i.e., α-helix, β-sheet and coil) of proteins, through measurement of polarized light absorbed by peptide bonds (Monteiro et al., 2016). The α-helix structure is characterized by displaying an intense and positive band at 190 nm

and negative peaks at 208 and 220 nm, the β-sheet structure typically presents a negative peak with a minimum in the 215 nm region, while random coil structures display a positive peak close to 215 nm and a negative one near to 200 nm (Furtado et al., 2018). The values recorded from 190 to 260 nm for purified and commercial β-Lg in native state is depicted in Figure 4.2C and shows similar spectra in terms of CD intensity and shape. Moreover, the average scans exhibited a negative dichroic peak with a minimum at 217 nm (i.e., in the 215 nm region), indicating that the secondary structure of both purified and commercial β-Lg is rich in β-sheet (Estévez et al., 2017; Fan et al., 2017; Yi et al., 2014).

Electrophoresis analysis from Figure 4.2D shows two sets of results, composed by three lanes, where it is possible to observe an identical profile for purified and commercial β-Lg. Given that unbound dye is removed by long washing gel process, the amount of bound dye is proportional to the protein concentration in the sample (Rodrigues et al., 2015). Both purified and commercial β-Lg samples were characterized by the presence of two high molecular weight bands. The higher molecular weight band has a molecular mass between 30 and 40 kDa, which indicates that β-Lg is present in dimer form, whereas the lower molecular weight band has a molecular mass between 15 and 20 kDa, which suggests that β-Lg is present in monomer form (Halder et al., 2012; Madalena et al., 2016).

Fast Protein Liquid Chromatography (FPLC) is the preferential methodology employed for separation and quantification of proteins, essentially due to the good resolution and low variability associated to this technique (Ramos et al., 2012). In this regard, FPLC was used to compare both purified and commercial β-Lg in terms of protein content. For this purpose, an appropriate calibration curve ($y = 120.1x + 2.8$) was obtained with R^2 = 0.999 using several concentrations of commercial β-Lg, where y is the protein content and x is the β-Lg concentration. Peak area integration showed statistically similar ($p > 0.05$) concentration values of 123.10 ± 1.90 and 120.70 ± 0.80 AU mL^{-1} for purified and commercial β-Lg samples, respectively, prepared at 10 mg mL^{-1}.

The extensive characterization for comparison of both purified and commercial β-Lg proteins revealed similarity in terms of properties tested, indicating a successful purification process. In this sense, purified β-Lg was used to further studies of developing the micro- and nanostructures.

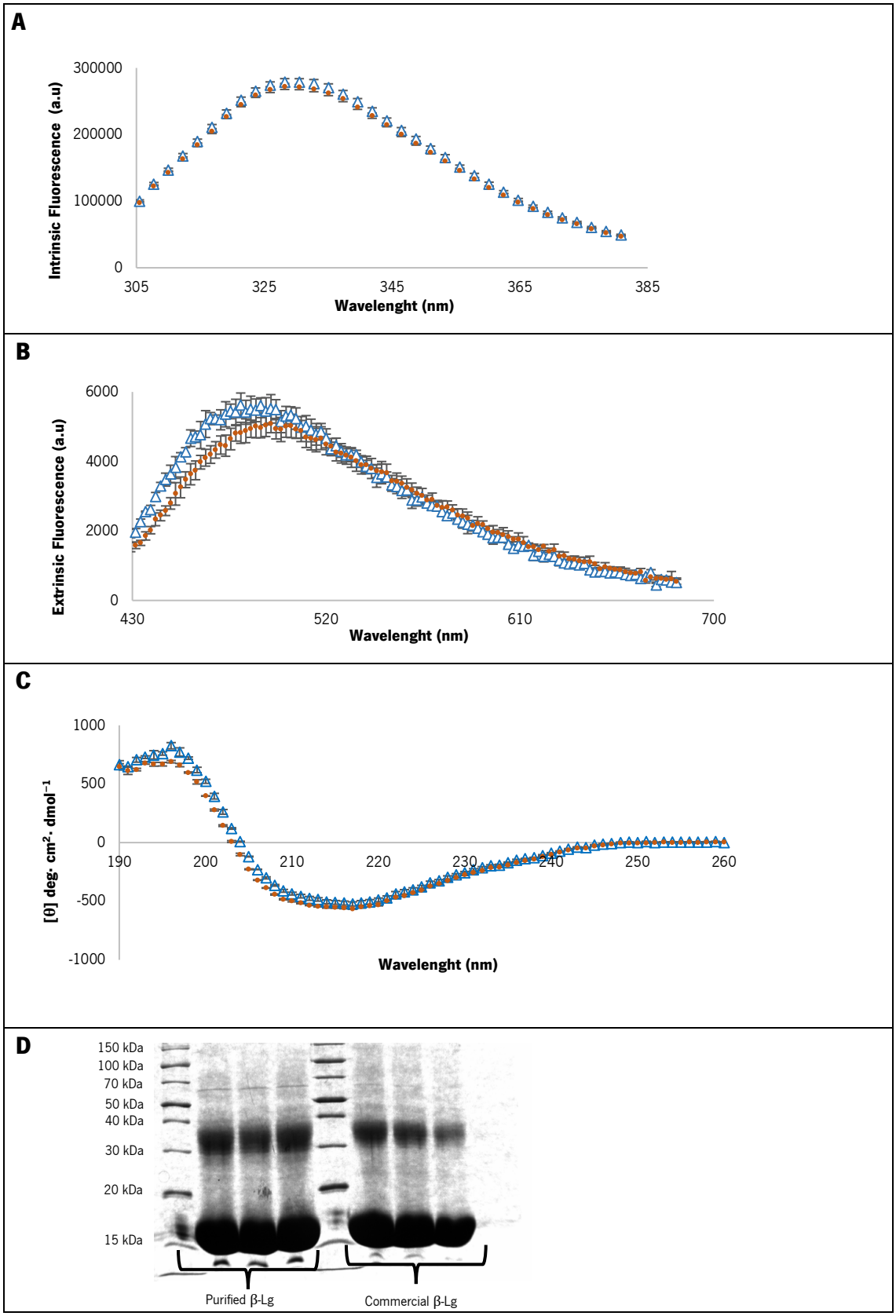


Figure 4.2 - Comparison between (•) purified β-Lg and (Δ) commercial β-Lg solutions. (A) Intrinsic fluorescence emission spectra at 295 nm; (B) extrinsic fluorescence emission spectra at 370 nm; (C) Far-UV CD spectra; (D) Native-PAGE. Standard deviation is represented by error bars.

4.2.2. Development of β-Lg micro- and nanostructure

In order to understand the influence of β-Lg concentration and thermal treatment on the formation of micro- and nanostructures, various combined effects (including different concentrations of β-Lg, heating temperatures and times) were carried out to induce protein aggregation. An experimental design, shown in Table 4.1, was used to evaluate the combined effect of three β-Lg concentrations (5, 10 and 15 mg mL^{-1}), three temperatures (60, 70 and 80 °C), and three holding times (5, 15 and 25 min) on the particle size distribution, polydispersity index, and intrinsic and extrinsic fluorescence intensity of β-Lg solutions prepared at four different pH values (3, 4, 6 and 7).

These results show that performing the β-Lg gelation process in different combinations of environmental conditions allows obtaining β-Lg structures at nanoscale (i.e., with particle sizes below 50 nm), by changing pH to 3 and 7, independently of the protein concentration (5 – 15 mg mL^{-1}), heating temperature (60 – 80 °C) and holding time (5 – 25 min) used. This could be related to the fact that bovine β-Lg at pH values ≤ 3 and ≥ 7 exists as a monomer due to the intermolecular electrostatic repulsions that govern protein interactions at those pH values, thus leading to the formation of low particle size structures under those conditions (Diarrassouba et al., 2013; Ramos et al., 2015). Based on this, we believe that β-Lg structures with small particle sizes (i.e., ≤ 50 nm) can be obtained at pH values far from β-Lg's pI (i.e., 4.6) (Schmitt et al., 2009), since at these conditions the protein is governed by electrostatic repulsions that hamper the aggregation process (Dombrowski et al., 2017).

Regarding fluorescence intensity, at pH 3 for all tested conditions and at pH 7 for heating temperatures of 60 °C and 70 °C, β-Lg structures were characterized by relatively low intrinsic and extrinsic fluorescence intensities with maxima of 1.96 and 2.22 (Table 4.1), respectively. Concerning the structural conformation, the low intrinsic fluorescence intensity obtained suggests that either β-Lg was not completely unfold or the tryptophan residue was not sufficiently exposed, being buried within the native protein structure (Ramos et al., 2015). Regarding extrinsic fluorescence intensity, determined by means of ANS fluorescence probe, it was possible to verify a low accessibility of ANS to hydrophobic areas of β-Lg, translated by a low extrinsic fluorescence intensity emitted (Schmitt et al., 2009). This result corroborates the intrinsic fluorescence observations, thus showing that at these conditions, β-Lg is slightly unfolded, therefore either the tryptophan residues or the hydrophobic groups of β-Lg were less exposed, thus limiting the aggregation process

Table 4.1 - Experimental responses of particle size distribution, polydispersity index (PDI), intrinsic fluorescence (IF) and extrinsic fluorescence (EF) intensities for the Box-Behnken design.

pH	X_1 (Heating temperature, °C)	X_2 (β-Lg concentration, mg mL^{-1})	X_3 (Holding time, min)	Size (nm)	PDI	Normalized IF (a.u)	Normalized EF (a.u)
3	60	10	5	12.1	0.55	1.04	1.15
		15	15	12.6	0.58	1.02	1.92
		5	15	12.3	0.55	0.93	0.80
		10	25	13.1	0.59	0.88	0.96
	70	5	5	15.2	0.68	0.82	1.25
		15	5	13.5	0.62	1.00	1.04
		10	15	12.7	0.58	0.98	1.05
		10	15	12.6	0.58	0.95	0.79
		10	15	13.5	0.62	0.97	1.08
		5	25	17.0	0.75	0.84	0.87
		15	25	13.7	0.63	0.99	0.89
	80	10	5	16.2	0.73	0.95	1.24
		15	15	17.0	0.76	0.97	1.47
		5	15	22.3	0.99	0.81	1.14
		10	25	21.3	0.92	0.94	1.99
4	60	10	5	40.7	0.76	1.05	0.96
		15	15	44.1	0.98	1.02	1.81
		5	15	48.4	0.85	1.02	0.68
		10	25	45.0	0.93	1.00	1.75
	70	5	5	1914.3	0.51	1.01	1.12
		15	5	3790.1	0.66	0.98	3.91
		10	15	2444.5	0.40	1.04	3.18
		10	15	3158.5	0.98	1.04	2.79
		10	15	3622.5	0.76	1.00	2.67
		5	25	1426.0	0.53	0.98	2.09
		15	25	2031.6	0.43	1.05	4.41
	80	10	5	>6000	1.00	1.91	8.32
		15	15	>6000	1.00	2.80	15.00
		5	15	>6000	1.00	2.39	5.64
		10	25	>6000	1.00	0.79	9.49
6	60	10	5	8.6	0.36	1.07	0.89
		15	15	8.9	0.36	1.38	1.13
		5	15	9.8	0.43	1.05	0.67
		10	25	8.7	0.36	1.12	0.90
	70	5	5	10.1	0,44	0.97	0.56
		15	5	10.1	0.42	1.51	1.21
		10	15	11.3	0.48	1.06	1.32
		10	15	13.2	0.56	1.09	1.06
		10	15	12.9	0.55	1.07	1.07
		5	25	13.2	0.58	1.01	0.67
		15	25	14.6	0.57	1.53	1.38
	80	10	5	84.8	0.34	4.67	13.72
		15	15	131.5	0.20	6.73	16.91
		5	15	78.1	0.25	4.42	8.28
		10	25	126.9	0.18	4.90	13.74
7	60	10	5	8.9	0.39	1.05	0.83
		15	15	12.2	0.53	1.05	0.78
		5	15	10.1	0.46	1.04	0.93
		10	25	13.3	0.56	1.00	0.84
	70	5	5	10.6	0.48	1.96	0.94
		15	5	13.3	0.56	0.99	0.79
		10	15	16.0	0.58	1.12	1.04
		10	15	16.5	0.59	1.08	1.04
		10	15	14.9	0.55	1.13	1.14
		5	25	16.9	0.64	1.07	1.28
		15	25	26.5	0.27	1.19	2.22
	80	10	5	33.1	0.38	1.27	2.27
		15	15	34.5	0.16	3.66	9.35
		5	15	21.6	0.59	1.20	1.75
		10	25	35.3	0.14	3.91	10.95

Regarding fluorescence intensity, at pH 3 for all tested conditions and at pH 7 for heating temperatures of 60 °C and 70 °C, β-Lg structures were characterized by relatively low intrinsic and extrinsic fluorescence intensities with maxima of 1.96 and 2.22 (Table 4.1), respectively. Concerning the structural conformation, the low intrinsic fluorescence intensity obtained suggests that either β-Lg was not completely unfold or the tryptophan residue was not sufficiently exposed, being buried within the native protein structure (Ramos et al., 2015). Regarding extrinsic fluorescence intensity, determined by means of ANS fluorescence probe, it was possible to verify a low accessibility of ANS to hydrophobic areas of β-Lg, translated by a low extrinsic fluorescence intensity emitted (Schmitt et al., 2009). This result corroborates the intrinsic fluorescence observations, thus showing that at these conditions, β-Lg is slightly unfolded, therefore either the tryptophan residues or the hydrophobic groups of β-Lg were less exposed, thus limiting the aggregation process.

Within heating treatments at pH 4, it was possible to obtain structures at macroscale (i.e., particles size ≥ 1 μm) for heating temperatures of 70 and 80 °C, independently of the β-Lg concentration used (Table 4.1). Under some combined conditions at 80 °C particles formed a sediment, which indicates that the protein at these conditions is completely unfolded, giving rise to the formation of aggregates. This can be also inferred by the high PDI value (i.e., PDI = 1), and the relatively high extrinsic fluorescence (i.e., ranging from 5.64 to 15.00) (Table 4.1) obtained, suggesting more hydrophobic sites available for ANS binding are exposed at these conditions (Schmitt et al., 2009). A similar behaviour was also observed for intrinsic fluorescence with relatively higher intensity values recorded at this pH for 80 °C, in particular for 15 min holding time (Table 4.1); thus implying that tryptophan residues, originally buried in the interior of protein chain, are more exposed and so more likely to interact with bioactive molecules (He et al., 2015).

At pH 4, which is relatively close to the pI of β-Lg, the net charge of protein is close to zero, and so the repulsive electrostatic forces weaken and the protein tends to aggregate, thus resulting in higher particle size values (Salgin et al., 2012). These observations agree with those reported by Leeb et al., (2015), which showed that β-Lg at 5 mg mL^{-1} prepared at pH 5.1 formed structures with particle sizes of 1332.1 ± 56.3 nm during thermal heating at 80 °C. In another study, Schmitt et al. (2009) obtained large aggregates with sizes above 1 μm for β-Lg at 1 mg mL^{-1} prepared at pH 4 and treated at 80 °C for 15 min.

At pH 6, when the temperature is taken to 80 °C, which is above the β-Lg denaturation temperature – i.e., 76 °C, β-Lg is in a structural transition phase and so it is possible to obtain structures with

particle size below and above 100 nm with relatively low PDI values – Table 4.1. In order to be able to draw accurate conclusions at this transition phase, a full experiment was performed at pH 6 for a heating temperature of 80 °C, and the combined effects of β-Lg concentration and holding time (Figure 4.3) were evaluated to verify if these conditions were able to produce β-Lg structures with desired properties – i.e., particle sizes within micro- (between 200 and 300 nm) and nano- (≤ 100 nm) scales and with relatively low PDI values (i.e., ≤ 0.25).

In terms of particle size (Figure 4.3A), β-Lg structures ranged from 65 nm to 267 nm with relatively constant surface charge (between -15.6 and -18.0 mV) ($p > 0.05$) (Figure 4.3C), as β-Lg concentration or holding time increased. Results showed that β-Lg nanostructures (particles size ≤ 100 nm) can be obtained at 5 mg mL^{-1} for a heating time of up to 25 min, at 10 mg mL^{-1} for a heating time of up to 15 min and at 15 mg mL^{-1} for a holding time of 5 min, without statistically significant differences ($p \leq 0.05$) being found between particles size values. Results also show that large size particles (i.e., microstructures with sizes between 200 and 300 nm) can be obtained at 15 mg mL^{-1} for heating times ≥ 15 min. In fact, the effect of protein concentration and heating time on particles size has been already reported elsewhere (Bourbon et al., 2015; Hu et al., 2007) for other proteins, which pointed to an increase in particles diameter with increased biopolymer concentration and heating time. Furthermore, it is possible to observe that β-Lg solutions present the best PDI values (≤ 0.25) when heated for time periods ≥ 15 min, independently of the β-Lg concentration used (Figure 4.3B), thus suggesting that the aggregation process originated a relatively monodisperse particle size distribution (Schmitt et al., 2009).

According with previously published results, as pH moves away from the protein pI (i.e., between pH 5.2 and 7), β-Lg exhibits an increasing net charge on each molecule and it results in the presence of more dimers (with a molecular weight of approximately 36 700 Da, than monomers (with a molecular weight of 18 277 Da), thus favouring the association and formation of structures with larger particle size (Png et al., 2009). This may be the reason for the higher particle size values observed for β-Lg at pH 6 than at pH 3 and 7, when heated at 80 °C – Table 4.1. This result agrees with a study conducted by Zúñiga et. al (2010), which showed the production of spherical aggregates with an average diameter of 96 nm at pH 6 and linear aggregates with an average diameter of 42 nm at pH 6.8.

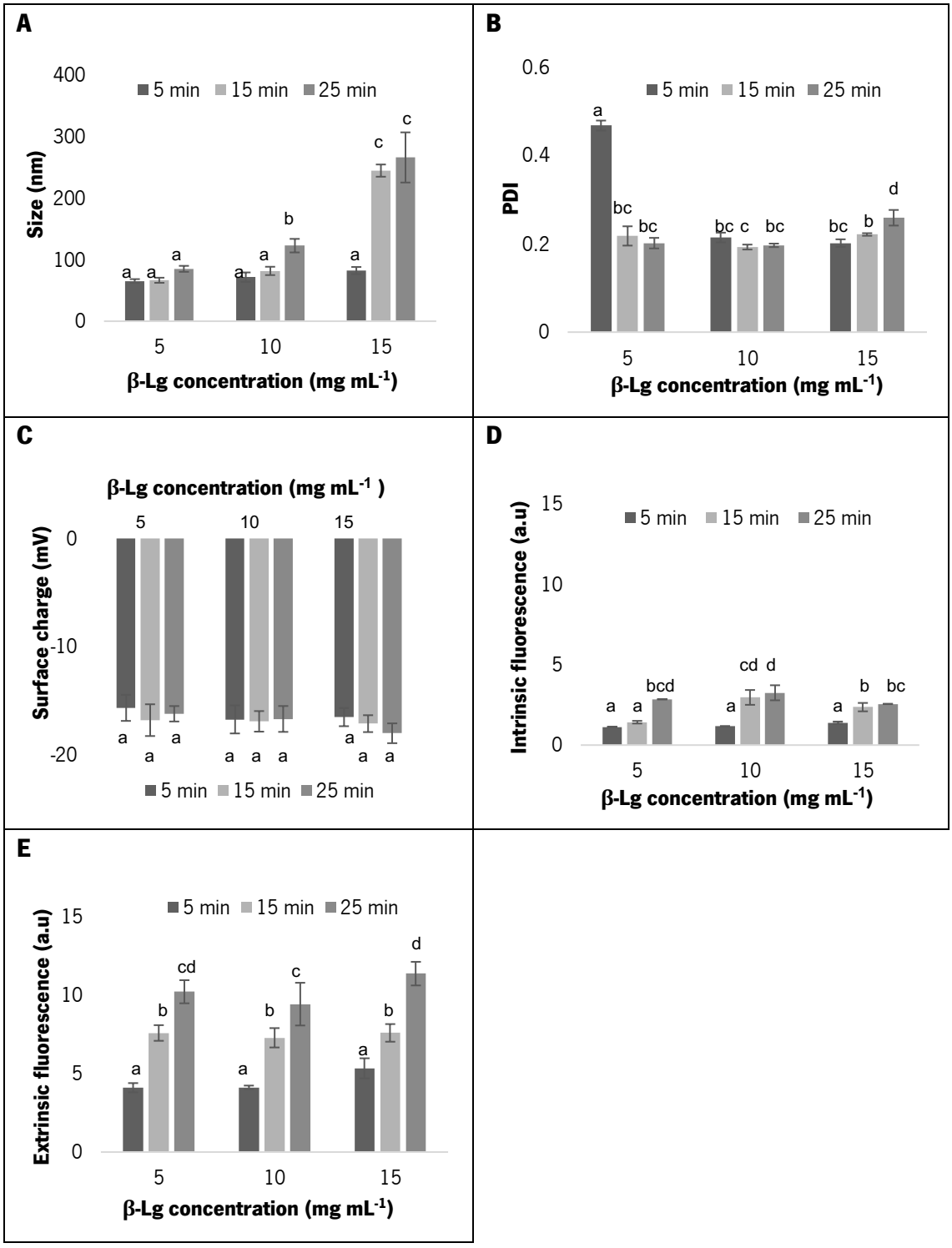


Figure 4.3 - Values of particle size (A), polydispersity (PDI) (B), surface charge (C), normalized maximum peak of intrinsic fluorescence at 295 nm (D) and normalized maximum peak of extrinsic fluorescence intensity at 370 nm (E) of β-Lg structures formed at pH 6 after heating at 80 °C for 5, 10 and 25 min at protein concentrations of 5, 10 and 15 mg mL^{-1}. Each data point is the average of nine successive measurements and the error bars show the standard deviation. ^{a,b,c,d} Means labelled with the same letter do not statistically differ from each other ($p > 0.05$).

The changes in the fluorescence intensity of the maximum intrinsic and extrinsic fluorescence spectra (λ_{max}) were used to follow structural changes of the protein induced by protein concentration and heating time at 80 °C. For intrinsic fluorescence, an increase of fluorescence intensity at λ_{max} was observed as the heating time increased, particularly for periods ≥ 15 min (Figure 4.3D). This difference in fluorescence intensity as a function of heating time may be related to changes in the compactness of the protein molecule due to local molecular unfolding, thus increasing the accessibility of buried tryptophan residues (Royer, 2006). This behaviour has been also observed by Bourbon et al. (2015) for lactoferrin and lactoferrin-GMP nanohydrogels when heated at 80 °C up to 20 min and by Furtado et al. (2018) for lactoferrin solutions when heated at 90 °C up to 30 min. For extrinsic fluorencence (Figure 4.3E) it is possible to see that an increase in heating time (from 5 to 25 min) was accompanied by a significant ($p \leq 0.05$) increase in the intensity of ANS fluorescence, independently of the β-Lg concentration used. This increase in extrinsic fluorescence intensity is in line with intrinsic fluorescence results.

Taking in consideration the best results obtained before, unheated β-Lg at 5, 10 and 15 mg mL^{-1} and heated β-Lg at 5, 10 and 15 mg mL^{-1} at 80 °C for heating times of 15 and 25 min were evaluated by circular dichroism in the far-UV region (from 190 to 260 nm) – Figure 4.4. This technique was used to evaluate the influence of selected conditions of heating time in β-Lg secondary structure content in order to establish the best conditions to form structures at micro- (particle size between 200 – 300 nm) and nano- (particle size ≤ 100 nm) scales (Ghorbani Gorji et al., 2015).

The unheated β-Lg CD scans displayed a negative ellipticity minimum near 216 nm, suggesting that its structure is rich in β-sheet, which is consistent with previously reported results (Dave et al., 2013; Delahaije et al., 2016; Gomaa et al., 2016). Figure 4.4 also shows an increase in the magnitude of ellipticity as β-Lg concentration increased. This technique is only sensitive to proteins that are fully-dissolved in the solution, so the increase in ellipticity intensity could be due to the fact that more protein is soluble with the increase in β-Lg concentration, consequently more amide chromophores of the peptide bonds can be measured by far–UV CD (Miles & Wallace, 2016). This result is in agreement with that reported by Ioannou et. al (2015), which showed an increase in the magnitude of ellipticity as the concentration of β-Lg increased from 1 mg mL^{-1} to 40 mg mL^{-1}.

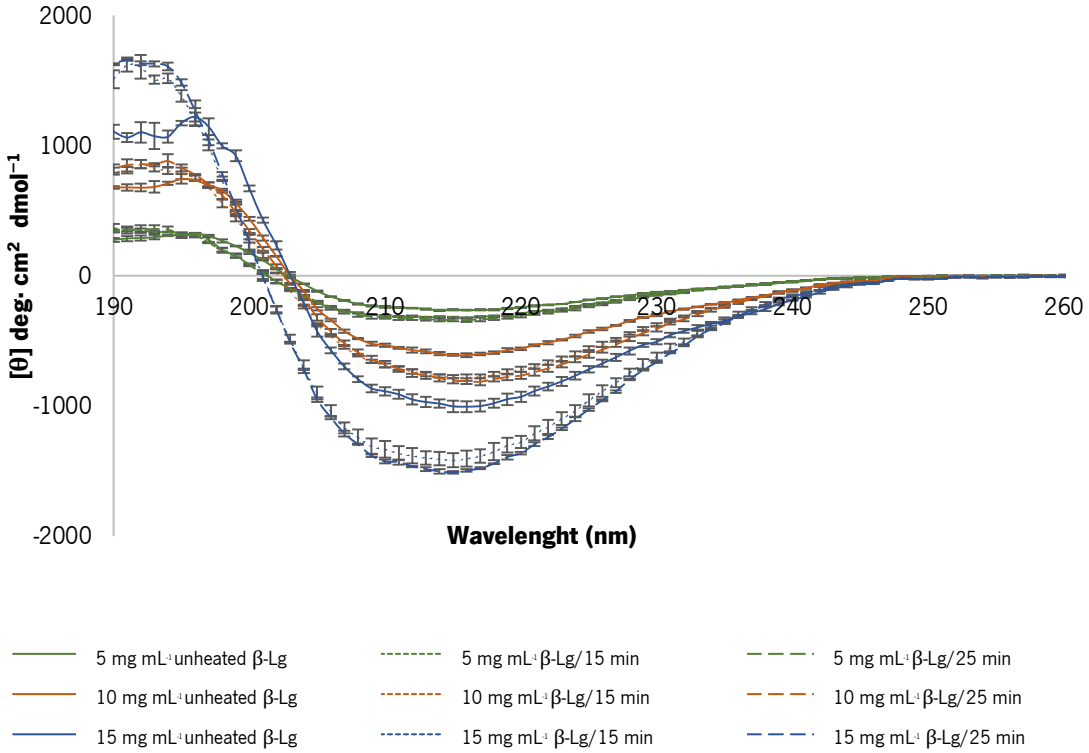


Figure 4.4 - Far-UV circular dichroism spectra of unheated β-Lg at 5, 10 and 15 mg mL^{-1} and heated β-Lg at 80 °C for 15 and 25 min for 5, 10 and 15 mg mL^{-1} at pH 6 (average ± standard deviation represented by error bars).

Regarding the thermal gelation process, a statistically significant difference ($p \leq 0.05$) is observed in the intensity of the negative peak of heated β-Lg in relation to the unheated β-Lg, independently of protein concentration. This can be related with structural changes due to aggregation phenomena (Jia et al., 2017), which is consistent with intrinsic fluorescence data. Native β-Lg is characterized by having most of the hydrophobic amino acid residues buried inside the molecule (Wada et al., 2006), so when the protein is subjected to thermal treatment, hydrophobic interactions responsible for maintaining the stability and conformational structure of β-Lg, may be disrupted, thus affecting β-Lg conformational state, resulting in loss of magnitude of the negative chirality of the CD signal (Ramos et al., 2015).

Simultaneously, β-Lg aggregation was accompanied by statistically significant differences ($p \leq 0.05$) in the red shift of zero-crossing, which suggests the formation of new regular secondary structures during thermal treatment. This result was in agreement with the data reported by Wada et al. (2006), which showed a CD spectra with a decrease of magnitude of the negative ellipticity for β-Lg heated at 80 °C when prepared at 0.5 mg mL^{-1} and at pH 7.5. These authors also observed

a zero-crossing shift to shorter wavelengths, which have been attributed to the increase α-helix structure content in the detriment of β-sheets content.

The results shown in Figure 4.4 4 also indicate that heating time (15 and 25 min) did not significantly affect ($p > 0.05$) the negative signal intensity, independently of the β-Lg concentration used. These results are in accordance with DLS data, in which protein aggregation is shown to form structures without significance differences of particle size ($p > 0.05$), and are also in agreement with the data reported by Delahaije et al. (2016) when β-Lg at 20 mg mL^{-1} and at pH 7.0 was heated at 80 °C up 30 min, and by Dave et al. (2013) when β-Lg at 10 mg mL^{-1} and at pH 2 was heated at 80 °C for up to 30 min. Both authors reported that the far-UV CD spectra of β-Lg heated at 80 °C remained approximately constant during heating time.

The morphology of β-Lg in its native state, and of micro- and nanostructures was observed by TEM and the respective microphotographs are provided as an insert in Figure 4.5. Figure 4.5A indicates that β-Lg in its native state is spherical and heterogeneous, with sizes ranging from 6 to 111.13 nm, which corroborate the high PDI value (> 0.36) obtained by DLS. This figure also shows that aggregates form a black mass as a result of the negative staining procedure (Zúñiga et al., 2010). The particle size of β-Lg microstructures (Figure 4.5B) as measured by TEM is around 140.8 nm, whereas DLS shown size values of 245.0 nm. It has been reported that differences between techniques for particle size measurement can be attributed to a sample drying effect for TEM analysis (Bourbon et al., 2016; Machado et al., 2012). However, β-Lg nanostructures (Figure 4.5C) show a mean particle size of 61.6 nm, which corresponds well with DLS measurements. Micro- and nanostructures are uniform (Figure 4.3A) and homogenous (Figure 4.3B), therefore the low PDI value (≤ 0.22) is well justified by the TEM images. Regarding micro- and nanostructures' shape, images do not reveal a visible and clear limit, but aggregates appear to be spherical and there seem to be clusters present. Clusters can be caused by the negative staining process, in which uranyl ions can be associated to β-Lg (Pinto et al., 2014). These features are consistent with TEM images obtained by Zúñiga et.al (2010) for β-Lg aggregates formed at protein concentration of 5 % w/v at pH 6, heated at 80 °C during 15 min.

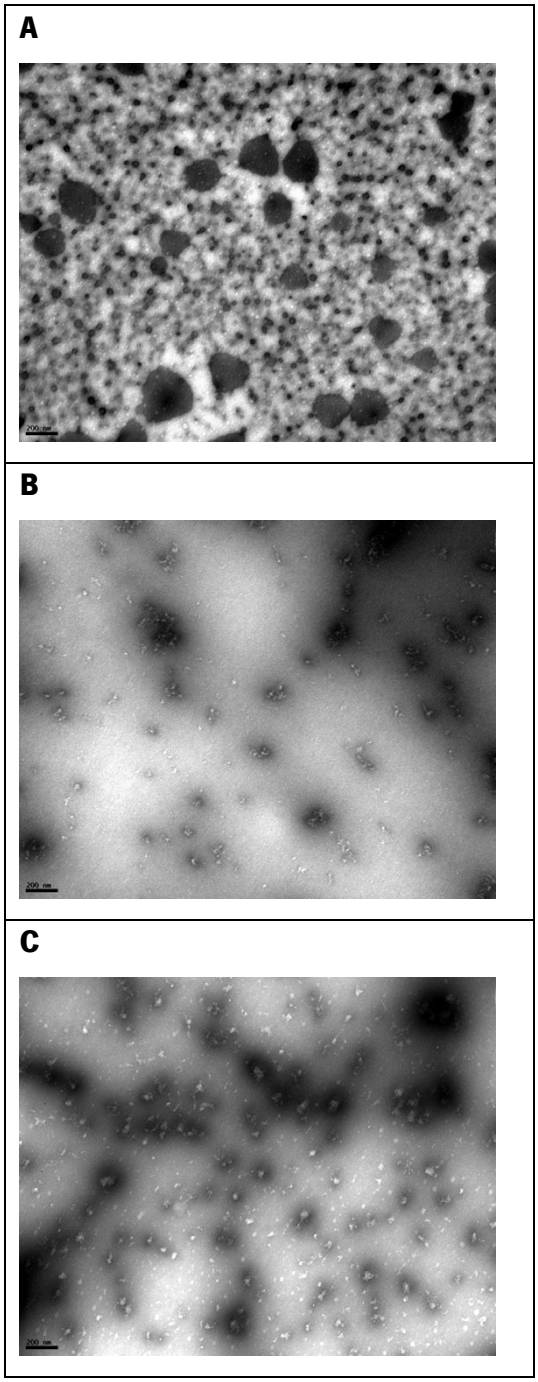


Figure 4.5 - TEM images of β-Lg at native state A), β-Lg microstructures B), and β-Lg nanostructures C) (scale bar = 200 nm, magnification = 50,000 x).

4.3.Conclusions

β-Lg obtained from whey protein isolate was successfully purified and the method used is robust and reproducible. The purified β-Lg displayed identical physicochemical properties when compared with those exhibited by commercial β-Lg, which allows to use the purified β-Lg for the development of micro- and nanostructures. Experimental results at pH 3 and 7, independently of protein

concentration, heating temperature and holding time, show that it is possible to produce structures with a particle size lower than 100 nm. Tryptophan fluorescence and surface hydrophobicity results suggest that the extent of unfolding and aggregation rate at those conditions are reduced due to the increase of electrostatic repulsion. Conversely, at pH 4 unstable structures were obtained, once this pH value is near the protein's pI.

Homogeneous and stable β-Lg micro- and nanostructures are formed at pH 6, after the gelation process takes place at 80 °C (i.e., above β-Lg denaturation temperature) during 15 min: using β-Lg at 5 mg mL^{-1} and 15 mg mL^{-1} it is possible to obtain nano- and microscale structures with particles sizes of 70 nm and 250 nm, respectively. Furthermore, intrinsic and extrinsic fluorescence revealed structural changes and suitable environmental conditions to aggregation. CD spectroscopy showed secondary structure changes with a decrease of β-sheet and increase of α-helix contents, revealing protein folding and the possibility to binding with bioactive compounds.

The results obtained here represent a significant contribution to enrich the knowledge about the impact of several environmental conditions on β-Lg bio-based delivery systems' characteristics, and point at the possibility to tailor such characteristics as a function of the intended final application, e.g., in the food or pharmaceutical industries.

4.4. References

Aklakur, M., Rather, M. A., & Kumar, N. (2016). Nano Delivery: An Emerging Avenue for Nutraceuticals and Drug Delivery. Critical Reviews in Food Science and Nutrition, 54, 2317–2361. https://doi.org/10.1080/10408398.2013.839543

Bourbon, A. I., Pinheiro, A. C., Carneiro-da-Cunha, M. G., Pereira, R. N., Cerqueira, M. a., & Vicente, A. a. (2015). Development and characterization of lactoferrin-GMP nanohydrogels: Evaluation of pH, ionic strength and temperature effect. Food Hydrocolloids, 48, 292–300. https://doi.org/10.1016/j.foodhyd.2015.02.026

Bourbon, A. I., Pinheiro, A. C., Cerqueira, M. A., & Vicente, A. A. (2016). Influence of chitosan coating on protein-based nanohydrogels properties and *in vitro* gastric digestibility. Food Hydrocolloids, 60, 109–118. https://doi.org/10.1016/j.foodhyd.2016.03.002

Dave, A. C., Loveday, S. M., Anema, S. G., Loo, T. S., Norris, G. E., Jameson, G. B., & Singh, H. (2013). β-lactoglobulin self-assembly: Structural changes in early stages and disulfide bonding in fibrils. Journal of Agricultural and Food Chemistry, 61(32), 7817–7828. https://doi.org/10.1021/jf401084f

Delahaije, R. J. B. M., Gruppen, H., Van, E. L., Boxtel, E., Cornacchia, L., & Wierenga, P. A. (2016). Controlling the Ratio between Native-Like, Non-Native-Like, and Aggregated β-Lactoglobulin after Heat Treatment. Journal of Agricultural and Food Chemistry, 64, 4362–4370. https://doi.org/10.1021/acs.jafc.6b00816

Delahaije, R. J. B. M., Wierenga, P. A., Giuseppin, M. L. F., & Gruppen, H. (2015). Comparison of heat-induced aggregation of globular proteins. Journal of Agricultural and Food Chemistry, 63(21), 5257–5265. https://doi.org/10.1021/acs.jafc.5b00927

Diarrassouba, F., Liang, L., Remondetto, G., & Subirade, M. (2013). Nanocomplex formation between riboflavin and β-lactoglobulin: Spectroscopic investigation and biological characterization. Food Research International, 52(2), 557–567. https://doi.org/10.1016/j.foodres.2013.03.025

Dombrowski, J., Gschwendtner, M., & Kulozik, U. (2017). Evaluation of structural characteristics determining surface and foaming properties of β-lactoglobulin aggregates. Colloids and Surfaces A: Physicochemical and Engineering Aspects, 516, 286–295. https://doi.org/10.1016/j.colsurfa.2016.12.045

Estévez, N., Fuciños, P., Bargiela, V., Picó, G., Valetti, N. W., Tovar, C. A., & Rúa, M. L. (2017). Influence of pH on viscoelastic properties of heat-induced gels obtained with a β-Lactoglobulin fraction isolated from bovine milk whey hydrolysates. Food Chemistry, 219, 169–178. https://doi.org/10.1016/j.foodchem.2016.09.137

Fan, Y., Zhang, Y., Yokoyama, W., & Yi, J. (2017). β-Lactoglobulin-chlorogenic acid conjugate-based nanoparticles for delivery of (-)-epigallocatechin-3-gallate. RSC Advances, 7(35), 21366–21374. https://doi.org/10.1039/c6ra28462k

Furtado, G. F., Pereira, R. N. C., Vicente, A. A., & Cunha, R. L. (2018). Cold gel-like emulsions of lactoferrin subjected to ohmic heating. Food Research International, 103(2017), 371–379. https://doi.org/10.1016/j.foodres.2017.10.061

Ghalandari, B., Divsalar, A., Saboury, A. A., & Parivar, K. (2015). β-Lactoglobulin nanoparticle as a chemotherapy agent carrier for oral drug delivery system. Journal of the Iranian Chemical Society, 12(4), 613–619. https://doi.org/10.1007/s13738-014-0519-2

Ghorbani Gorji, E., Rocchi, E., Schleining, G., Bender-Bojalil, D., Furtmuller, P. G., Piazza, L., … Toca-Herrera, J. L. (2015). Characterization of resveratrol-milk protein interaction. Journal of Food Engineering, 167, 217–225. https://doi.org/10.1016/j.jfoodeng.2015.05.032

Gomaa, A. I., Nsonzi, F., Sedman, J., & Ismail, A. A. (2016). Enhanced Unfolding of Bovine β-Lactoglobulin Structure Using Microwave Treatment: a Multi-Spectroscopic Study. Food Biophysics, 11(4), 370–379. https://doi.org/10.1007/s11483-016-9451-6

Halder, U. C., Chakraborty, J., Das, N., & Bose, S. (2012). Tryptophan dynamics in the exploration of micro-conformational changes of refolded β-lactoglobulin after thermal exposure: A steady state and time-resolved fluorescence approach. Journal of Photochemistry and Photobiology B: Biology, 109, 50–57. https://doi.org/10.1016/j.jphotobiol.2012.01.005

He, Z., Chen, J., & Moser, S. E. (2015). Interaction of β-lactoglobulin with (−)-epigallocatechin-3-gallate under different processing conditions of pH and temperature by the fluorescence quenching method. European Food Research and Technology, 241(3), 357–366. https://doi.org/10.1007/s00217-015-2466-2

Hu, J., Yu, S., & Yao, P. (2007). Stable amphoteric nanogels made of ovalbumin and ovotransferrin via self-assembly. Langmuir, 23(11), 6358–6364. https://doi.org/10.1021/la063419x

Ioannou, J. C., Donald, A. M., & Tromp, R. H. (2015). Characterising the secondary structure changes occurring in high density systems of BLG dissolved in aqueous pH 3 buffer. Food Hydrocolloids, 46, 216–225. https://doi.org/10.1016/j.foodhyd.2014.12.027

Jia, J., Gao, X., Hao, M., & Tang, L. (2017). Comparison of binding interaction between β-lactoglobulin and three common polyphenols using multi-spectroscopy and modeling methods. Food Chemistry, 228, 143–151. https://doi.org/10.1016/j.foodchem.2017.01.131

Leeb, E., Gotz, A., Letzel, T., Cheison, S. C., & Kulozik, U. (2015). Influence of denaturation and aggregation of b-lactoglobulin on its tryptic hydrolysis and the release of functional peptides. Food Chemistry, 187, 545–554. https://doi.org/10.1016/j.foodchem.2015.04.034

Machado, A. H. E., Lundberg, D., Ribeiro, A. J., Veiga, F. J., Lindman, B., Miguel, M. G., & Olsson, U. (2012). Preparation of calcium alginate nanoparticles using water-in-oil (W/O) nanoemulsions. Langmuir, 28(9), 4131–4141. https://doi.org/10.1021/la204944j

Madalena, D. A., Ramos, Ó. L., Pereira, R. N., Bourbon, A. I., Pinheiro, A. C., Malcata, F. X., … Vicente, A. A. (2016). *In vitro* digestion and stability assessment of β-lactoglobulin/riboflavin nanostructures. Food Hydrocolloids, 58, 89–97. https://doi.org/10.1016/j.foodhyd.2016.02.015

Miles, A. J., & Wallace, B. A. (2016). Circular dichroism spectroscopy of membrane proteins. Chem. Soc. Rev. https://doi.org/10.1039/C5CS00084J

Monteiro, A. A., Monteiro, M. R., Pereira, R. N., Diniz, R., Costa, A. R., Malcata, F. X., … Ramos, Ó. L. (2016). Design of bio-based supramolecular structures through self-assembly of α-lactalbumin and lysozyme. Food Hydrocolloids, 58, 60–74. https://doi.org/10.1016/j.foodhyd.2016.02.009

Pereira, R. N., Rodrigues, R. M., Ramos, Ó. L., Xavier Malcata, F., Teixeira, J. A., & Vicente, A. A. (2015). Production of Whey Protein-Based Aggregates Under Ohmic Heating. Food and Bioprocess Technology, 1–12. https://doi.org/10.1007/s11947-015-1651-4

Perez, A. A., Andermatten, R. B., Rubiolo, A. C., & Santiago, L. G. (2014). β-Lactoglobulin heat-induced aggregates as carriers of polyunsaturated fatty acids. Food Chemistry, 158, 66–72. https://doi.org/10.1016/j.foodchem.2014.02.073

Pinto, M. S., Léonil, J., Henry, G., Cauty, C., Carvalho, A. F., & Bouhallab, S. (2014). Heating and glycation of β-lactoglobulin and β-casein: Aggregation and *in vitro* digestion. Food Research International, 55, 70–76. https://doi.org/10.1016/j.foodres.2013.10.030

Ramos, O. L., Pereira, R. N., Martins, A., Rodrigues, R., Fuciños, C., Teixeira, J. a., … Vicente, A. a. (2017). Design of Whey Protein Nanostructures for Incorporation and Release of Nutraceutical Compounds in Food. Critical Reviews in Food Science and Nutrition, 57(7), 1377–1393. https://doi.org/10.1080/10408398.2014.993749

Ramos, O. L., Pereira, R. N., Rodrigues, R. M., Teixeira, J. A., Vicente, A. A., & Malcata, F. X. (2015). Whey and Whey Powders: Production and Uses. Encyclopedia of Food and Health (1st ed.). Elsevier Ltd. https://doi.org/10.1016/B978-0-12-384947-2.00747-9

Ramos, Oscar L., Pereira, J. O., Silva, S. I., Amorim, M. M., Fernandes, J. C., Lopes-da-Silva, J. A., … Malcata, F. X. (2012). Effect of composition of commercial whey protein preparations upon gelation at various pH values. Food Research International, 48(2), 681–689. https://doi.org/10.1016/j.foodres.2012.06.004

Ramos, Oscar L., Pereira, R. N., Rodrigues, R., Teixeira, J. A., Vicente, A. A., & Xavier Malcata, F. (2014). Physical effects upon whey protein aggregation for nano-coating production. Food Research International, 66, 344–355. https://doi.org/10.1016/j.foodres.2014.09.036

Rodrigues, R. M., Martins, A. J., Ramos, O. L., Malcata, F. X., Teixeira, J. A., Vicente, A. A., & Pereira, R. N. (2015). Influence of moderate electric fields on gelation of whey protein isolate. Food Hydrocolloids, 43, 329–339. https://doi.org/10.1016/j.foodhyd.2014.06.002

Royer, C. A. (2006). Probing Protein Folding and Conformational Transitions with Fluorescence. Chem. Rev, 106, 1769–1784. https://doi.org/10.1108/SAMPJ-04-2014-0020

Salgin, S., Salgin, U., & Bahadir, S. (2012). Zeta potentials and isoelectric points of biomolecules: The effects of ion types and ionic strengths. International Journal of Electrochemical Science, 7(12), 12404–12414.

Schmitt, C., Bovay, C., Vuilliomenet, A.-M., Rouvet, M., Bovetto, L., Barbar, R., & Sanchez, C. (2009). Multiscale Characterization of Individualized β-Lactoglobulin Microgels Formed upon

Heat Treatment under Narrow pH Range Conditions. Langmuir, 25(14), 7899–7909. https://doi.org/10.1021/la900501n

Simion, A.-M., Aprodu, I., Dumitraşcu, L., Bahrim, G. E., Alexe, P., & Stănciuc, N. (2015). Probing thermal stability of the β-lactoglobulin–oleic acid complex by fluorescence spectroscopy and molecular modeling. Journal of Molecular Structure, 1095, 26–33. https://doi.org/10.1016/j.molstruc.2015.04.019

Stănciuc, N., Aprodu, I., Râpeanu, G., & Bahrim, G. (2012). Fluorescence spectroscopy and molecular modeling investigations on the thermally induced structural changes of bovine β-lactoglobulin. Innovative Food Science and Emerging Technologies, 15, 50–56. https://doi.org/10.1016/j.ifset.2012.03.001

Teng, Z., Xu, R., & Wang, Q. (2015). Beta-lactoglobulin-based encapsulating systems as emerging bioavailability enhancers for nutraceuticals: a review. RSC Adv., 5(44), 35138–35154. https://doi.org/10.1039/C5RA01814E

von Staszewski, M., Jara, F. L., Ruiz, A. L. T. G., Jagus, R. J., Carvalho, J. E., & Pilosof, A. M. R. (2012). Nanocomplex formation between β-lactoglobulin or caseinomacropeptide and green tea polyphenols: Impact on protein gelation and polyphenols antiproliferative activity. Journal of Functional Foods, 4(4), 800–809. https://doi.org/10.1016/j.jff.2012.05.008

Wada, R., Fujita, Y., & Kitabatake, N. (2006). Effects of heating at neutral and acid pH on the structure of β-lactoglobulin A revealed by differential scanning calorimetry and circular dichroism spectroscopy. Biochimica et Biophysica Acta - General Subjects, 1760(6), 841–847. https://doi.org/10.1016/j.bbagen.2005.12.025

Yi, J., Lam, T. I., Yokoyama, W., Cheng, L. W., & Zhong, F. (2014). Controlled Release of β - Carotene in β - Lactoglobulin – Dextran- Conjugated Nanoparticles ' *in vitro* Digestion and Transport with Caco - 2 Monolayers. Journal of Agriculture and Food Chemistry, 62(35), 8900–8907.

Zúñiga, R. N., Tolkach, A., Kulozik, U., & Aguilera, J. M. (2010). Kinetics of formation and physicochemical characterization of thermally-induced β-Lactoglobulin aggregates. Journal of Food Science, 75(5). https://doi.org/10.1111/j.1750-3841.2010.01617.x

CHAPTER 5.

Suitability of β-lactoglobulin micro- and nanostructures for loading and release profile of bioactive model compounds

5.1. Introduction 80

5.2. Results and discussion 82

5.3. Conclusions 102

5.4. References 103

This Chapter was adapted from:

Simões, Lívia S.; Arunhosa, Luis; Vicente, António A.; Ramos, Oscar L. Suitability of β-lactoglobulin micro- and nanostructures for loading and release profile of bioactive model compounds. Journal of Controlled Release. Submitted in August 2, 2019.

5.1. Introduction

The emerging demand for safer, nutritious and high-quality functional foods as a way to address specific human health requirements has gained recently the attention from food industry players and scientific community for developing new sustainable ways to encapsulate, protect and deliver bioactive compounds in food products (Devi et. al 2017; Sedaghat et. al 2018).

β-lactoglobulin (β-Lg), the main protein fraction of whey proteins, is an interesting matrix for designing delivery systems for controlled release of bioactive compounds, due to its bio-based nature, Generally Recognized As Safe (GRAS) designation, high nutritional value, biological and functional (e.g., emulsification) properties, as well as, to its gelation and high binding capacity (Madalena et al., 2016). The conformational state of native β-Lg becomes unfolded when induced by thermal heating, thus resulting in the exposure of initially buried hydrophobic aminoacid residues with subsequent self-aggregation of protein molecules through physical (electrostatic and hydrophobic) and chemical (disulphide) interactions (Delahaije et. al 2015). β-Lg structural characteristics abovementioned allows it to perform well as delivery system for various hydrophilic and hydrophobic bioactive compounds (Aprodu et al., 2017).

Even though previous researches demonstrated that β-Lg has affinity to bind to a wide range of molecules with distinct physiochemical properties (e.g., solubility in water, molecular weight, and structure), its ability to act as delivery system is still limited and there are current challenges related with binding to bioactive compounds that need to be, firstly, well understood, and then overcome. For instance, Berino et al. (2019) investigated the interaction between β-Lg with vitamin D_3 (at several concentrations) and the stability of the complex formed to protect vitamin D_3 from degradation by light, oxygen and pressure. The authors found limitations in the binding of vitamin D_3 to the hydrophobic sites in the calyx and to the hydrophobic surface patches of β-Lg with conformational changes recorded in the protein secondary structure. In another study, Guo et al. (2017) aimed at masking caffeine's bitter taste and unpleasant aftertaste by using β-Lg nanoparticles as delivery systems. The authors obtained low encapsulation efficiencies (i.e., 13.5 %). In fact, the delivery systems should display high encapsulation efficiencies of bioactive compounds and protect them against degradation during production and over storage periods. However, information regarding the best conditions to design and process β-Lg delivery systems, about their performance as encapsulating agents, stability in several environmental conditions (e.g., pH values, ionic strength, temperature) and over time, ability to bind bioactive compounds and behaviour in food matrices is very scarce or inexistent. A few studies are available regarding

the use of other proteins as encapsulating agents for bioactive compounds with emphasis to one conducted by Bourbon et al., (2016). These authors developed lactoferrin-glycomacropeptide nanohydrogels by thermal gelation to encapsulate curcumin (as model lipophilic compound) and caffeine (as model hydrophilic compound). This study showed that such nanohydrogels successfully bound both bioactive compounds, enhanced their antimicrobial activity and promoted their controlled release. Taking into account the limited information available regarding the use of proteins as bio-based delivery systems, and in particular of β-Lg, it is considered of utmost importance to understand how different sizes of β-Lg structures at micro- (with diameters between 200 – 300 nm) and nano (with diameters ≤ 100 nm) scale may affect their physicochemical properties, and thus their performance as potential delivery systems.

In this context, β-Lg micro- and nanostructures were proposed here as potential delivery systems to encapsulate, protect and controlled release of bioactive compounds (i.e., riboflavin and quercetin) with different water solubilities. Riboflavin is a vitamin essential to human growth (Beztsinn et. al 2016), however this compound cannot be naturally synthetized by the human body, thus must be obtained from external sources (Gironés-Vilaplana et. al 2017). Nonetheless, its use in food products is still limited by several issues such as its high degradability when exposed to light and low solubility in water (Ashoori & Saedisomeolia, 2014). For all these reasons riboflavin was studied as hydrophilic model compound. Quercetin attracted the interest of the scientific community due to its anticancer, antioxidant and antiviral activities (Haghi et. al 2017). However, its use in food products is still limited due to its hydrophobic nature (i.e., poor aqueous solubility), low oral bioavailability (i.e., it is highly degraded through the gastrointestinal tract), and stability (Aditya et al., 2014). Therefore, quercetin was investigated as hydrophobic model compound. Hence, this research aims at deepening the understanding of the binding mechanisms of β-Lg micro- and nanostructures to riboflavin (as model hydrophilic compound) and quercetin (as model hydrophobic compound) and assess their potential as encapsulating agents. Also, the impact of various environmental conditions on the physicochemical stability of loaded β-Lg micro- and nanostructures, and the release profile of such model compounds from β-Lg micro- and nanostructures when they are added into food simulants, will be assessed.

5.2. Results and discussion

5.2.1. Bioactive model compounds association

According to the available literature, β-Lg has the capability to associate both hydrophilic and hydrophobic bioactive compounds (Aprodu et al., 2017; Xu et al., 2019; Zagury et al., 2019). The different physicochemical properties of bioactive compounds (e.g., molecular weight, water solubility and chemical structure) can affect the behaviour of β-Lg structures. Therefore, a range of concentrations of each model bioactive compound associated to β-Lg micro- and nanostructures were investigated in terms of association efficiency (*AE*), loading capacity (*LC*), particle size, polydispersity (PDI) and surface charge (S). *AE* provides information about the bioactive compound fraction successfully entrapped within structures (Mirpoor et al., 2017), whereas *LC* is related to the maximum amount of bioactive model compound that can be loaded into a β-Lg structure (Zou et al., 2016).

Table 5.1 shows the results obtained for β-Lg micro- and nanostructures associated to riboflavin, used as hydrophilic model compound.

The *AE* (Table 5.1) of β-Lg/riboflavin microstructures ranged between 31.9 and 64.4 % ($p \leq 0.05$), as riboflavin concentration increased. In turns, β-Lg/riboflavin nanostructures achieved the highest *AE* of 67.9 % at 0.014 mg mL^{-1} of riboflavin ($p > 0.05$). Above this riboflavin concentration, the *AE* did not significantly change, thus suggesting that this is the maximum concentration that such β-Lg nanostructures can associate. In a study conducted by Guo et al., (2017), it was shown that β-Lg nanoparticles were able to bind caffeine (used as hydrophilic bioactive compounds) with an *AE* of 13.54 ± 3.3 % for a caffeine:β-Lg ratio of 50:1. In our work, β-Lg/nanostructures demonstrated a *AE* 4.8 times higher for a lower riboflavin:β-Lg ratio (i.e., 21:1).

On the other hand, the *LC* increased as riboflavin concentration increases, independently of β-Lg structure scale, as depicted in Table 5.1. *LC* values achieved a maximum of 1.80 ± 0.16 % and 1.13 ± 0.03 % ($p \leq 0.05$), for nano- and microstructures, respectively. This result is somehow expected, taking into consideration the higher surface area-to-volume ratio of nanoscale materials, which can bind higher concentrations of bioactive compounds (Jafari & McClements, 2017). Azevedo et al. (2014) reported a similar behaviour for alginate/chitosan nanoparticles, which presented *AE* of 55.9 ± 5.6 % and a *LC* of 2.2 ± 0.6 % for riboflavin. In another study, Shpigelman et al. (2012) developed β-Lg nanosystems by thermal gelation at 70 °C for 20 min at pH 6.8 for encapsulation of (-)-epigallocatechin-3-gallate. These authors obtained nanosystems with particles

sizes lower than 50 nm, which displayed similar *AE* (i.e., 58.5 ± 2.1 %) and *LC* (1.16 ± 0.04 %) values.

Table 5.1- Association efficiency (*AE*), loading capacity (*LC*), particle size, polydispersity index (PDI) and surface charge (S) of β-Lg micro- and nanostructures for riboflavin concentrations (RC) ranging from 0 to 0.105 mg mL^{-1}.

β-Lg structure	RC (mg mL^{-1})	*AE* (%)	*LC* (%)	Size (nm)	PDI	S (mV)
Micro	0	-	-	246.0 ± 10.5^{a}	0.20 ± 0.01^{a}	-20.1 ± 2.1^{a}
	0.007	31.9 ± 1.2^{aA}	0.04 ± 0.01^{aA}	288.4 ± 10.5^{b}	0.24 ± 0.01^{b}	-22.5 ± 1.2^{a}
	0.0105	40.0 ± 1.6^{bA}	0.07 ± 0.01^{aA}	275.6 ± 7.5^{ab}	0.21 ± 0.01^{ac}	-20.4 ± 1.4^{a}
	0.014	43.9 ± 0.6^{cA}	0.09 ± 0.01^{aA}	274.0 ± 9.0^{ab}	0.23 ± 0.01^{bc}	-20.6 ± 1.1^{a}
	0.049	58.7 ± 1.3^{dB}	0.44 ± 0.05^{bA}	306.5 ± 27.9^{b}	0.26 ± 0.01^{d}	-21.6 ± 1.6^{a}
	0.105	64.4 ± 0.8^{eB}	1.13 ± 0.03^{cA}	281.0 ± 26.7^{b}	0.23 ± 0.01^{bc}	-21.1 ± 1.0^{a}
Nano	0	-	-	88.6 ± 4.2^{a}	0.22 ± 0.01^{a}	-18.9 ± 1.2^{abc}
	0.007	44.5 ± 3.6^{aB}	0.09 ± 0.01^{aB}	83.9 ± 3.6^{a}	0.23 ± 0.01^{a}	-16.5 ± 0.3^{a}
	0.0105	54.9 ± 1.6^{bB}	0.15 ± 0.02^{aB}	86.4 ± 6.5^{a}	0.26 ± 0.01^{b}	-17.7 ± 1.1^{abc}
	0.014	67.9 ± 1.4^{cdB}	0.24 ± 0.01^{aB}	88.5 ± 8.1^{a}	0.25 ± 0.01^{b}	-17.4 ± 1.7^{ab}
	0.049	60.2 ± 4.7^{dB}	0.89 ± 0.14^{bB}	91.1 ± 5.5^{a}	0.22 ± 0.01^{a}	-19.5 ± 1.0^{bc}
	0.105	64.4 ± 0.9^{cdB}	1.80 ± 0.16^{cB}	87.8 ± 1.9^{a}	0.22 ± 0.01^{a}	-21.1 ± 1.8^{c}

NOTE: ^{a,b,c,d}Small superscript letters indicate column statistical difference between means ($p \leq 0.05$) for same β-Lg structure. ^{A,B}Capital superscript letters indicate column statistical difference between means ($p \leq 0.05$) for different β-Lg structures.

In terms of particle sizes, it is possible to see (Table 5.1) that β-Lg/riboflavin nanostructures remained constant ($p > 0.05$), thus suggesting that association of riboflavin did not significantly affect ($p > 0.05$) its overall size. On the other hand, for β-Lg/riboflavin microstructures it was observed a statistically significant increase of particles' diameter ($p \leq 0.05$) as the concentration of riboflavin increased. This behaviour may be attributed to structural rearrangement of β-Lg microstructures after riboflavin association. For both β-Lg micro- and nanostructures the PDI values were relatively low (i.e., below 0.26), suggesting a relatively homogenous β-Lg structure and a narrow size distribution. Regarding surface charge (S), β-Lg/riboflavin micro- and nanostructures

displayed relatively constant values ranging from -16.5 to -20.1 mV, thus indicating that electrostatic repulsion forces among the particles are enough to prevent aggregation.

The effect of quercetin concentration on β-Lg micro- and nanostructures was also investigated, and the results are presented in Table 5.2.

Table 5.2 - Association efficiency (*AE*), loading capacity (*LC*), particle size, polydispersity index (PDI) and surface charge (S) of β-Lg micro- and nanostructures for quercetin concentrations (QC) ranging from 0 to 0.08 mg mL^{-1}

β-Lg structure	QC (mg mL^{-1})	*AE* (%)	*LC* (%)	Size (nm)	PDI	S (mV)
Micro	0	-	-	243.3 ± 2.9^{a}	0.19 ± 0.01^{a}	-20.0 ± 1.1^{a}
	0.01	ND	ND	264.4 ± 16.2^{b}	0.16 ± 0.01^{b}	-15.9 ± 2.0^{b}
	0.02	86.5 ± 0.5^{aA}	0.07 ± 0.01^{aA}	283.6 ± 1.9^{bc}	0.19 ± 0.01^{ac}	-16.1 ± 1.2^{bc}
	0.04	93.5 ± 2.8^{bA}	0.14 ± 0.01^{bA}	284.3 ± 6.2^{c}	0.17 ± 0.01^{abc}	-16.4 ± 1.2^{bc}
	0.06	93.2 ± 2.6^{bA}	0.21 ± 0.01^{cA}	277.2 ± 7.3^{bc}	0.17 ± 0.01^{abc}	-16.3 ± 0.7^{bc}
	0.08	96.1 ± 0.1^{bB}	0.29 ± 0.01^{dA}	276.9 ± 3.8^{bc}	0.17 ± 0.01^{bc}	-19.2 ± 0.7^{ac}
Nano	0	-	-	93.6 ± 2.2^{a}	0.21 ± 0.01^{a}	-18.5 ± 1.4^{ab}
	0.01	ND	ND	91.1 ± 4.0^{a}	0.26 ± 0.01^{b}	-16.5 ± 1.6^{a}
	0.02	84.5 ± 3.2^{aA}	0.15 ± 0.02^{aB}	94.2 ± 3.9^{a}	0.26 ± 0.01^{b}	-16.6 ± 1.3^{a}
	0.04	84.8 ± 0.7^{aB}	0.29 ± 0.02^{bB}	97.2 ± 6.2^{a}	0.24 ± 0.01^{b}	-16.4 ± 1.2^{a}
	0.06	88.3 ± 0.6^{aB}	0.44 ± 0.01^{cB}	100.3 ± 6.4^{a}	0.22 ± 0.01^{a}	-15.8 ± 1.1^{a}
	0.08	98.0 ± 0.9^{bB}	0.61 ± 0.05^{dB}	94.7 ± 4.8^{a}	0.21 ± 0.01^{a}	-20.2 ± 2.6^{b}

NOTE: ND: Not detected; ^{a,b,c} Small superscript letters indicate column statistical difference between means ($p \leq 0.05$) for same β-Lg structure. ^{A,B} Capital superscript letters indicate column statistical difference between means ($p \leq 0.05$) for different β-Lg structures.

Concerning the results presented in Table 5.2, the *AE* of β-Lg/quercetin micro- and nanostructures ranged from 84.5 ± 3.2 % to 98.0 ± 0.9 %. These *AE* values agree with those found in the literature. For example, Mirpoor et al. (2017) reported that nanostructures prepared with β-Lg and sodium alginate showed *AE* higher than 93 %; Li et al. (2019) showed that zein particles with soluble soybean polysaccharide coating displayed *AE* of 82.5 %; and Wijaya et al. (2019) showed that whey protein isolate-low methoxyl pectin electrostatic complexes had values of *AE* of 97 %. However,

these structures required both protein and polysaccharide polymers associated to form a stable delivery system.

The *AE* obtained in this study for quercetin is slightly higher than that obtained for riboflavin (Table 5.1 and Table 5.2). This difference can be due to the hydrophobic/hydrophilic amino acids located in a balanced way along the β-Lg polypeptide chains (Ramos et al., 2014). During thermal gelation (thermal treatment at 80 °C for 15 min), the hydrophobic binding sites initially buried inside the β-Lg structure, become exposed and available to bind, thus enhancing the potential to bind to hydrophobic bioactive compounds through hydrophobic interactions. On the other hand, in terms of *LC*, it is possible to observe that both β-Lg micro- and nanostructures displayed a lower capacity to load quercetin (i.e., up 0.61 %) then riboflavin (i.e., up to 1.80 %). This difference could be attributed to the molecular weight, water solubility and chemical structure of the bioactive model compounds employed.

Overall, the β-Lg nanostructures showed higher *LC* values ($p \leq 0.05$) for riboflavin (Table 5.1) and quercetin (Table 5.2) in comparison with β-Lg microstructures. This may be related to the higher surface area-to-volume ratio of nanoscale structures, which may be able to bind higher levels of bioactive compounds (Jafari & McClements, 2017).

In terms of particle sizes, it is possible to observe from Table 5.2 that β-Lg microstructures significantly increased the ($p \leq 0.05$) particle sizes as the quercetin concentration increases. The change in particle size values of β-Lg microstructures as affected by quercetin concentration may be related to two possible phenomena that may be occurring: protein-polyphenol interaction; and/or surface charge-modulated structural changes, for instance, flexibility, specific surface (Mirpoor et al., 2017).

Nonetheless, it was found that the association of both bioactive model compounds did not affect significantly ($p > 0.05$) the β-Lg nanostructures' particle sizes, which have a monomodal distribution with relatively low PDI values (PDI < 0.26). Further, the incorporation of quercetin into β-Lg micro- and nanostructures gradually shifted the surface charge as the concentration of quercetin increased up to 0.06 mg mL^{-1}, thus suggesting conformational rearrangements of β-Lg structures with the quercetin association. However, for quercetin concentration of 0.08 mg mL^{-1}, the values of surface charge for β-Lg/quercetin micro- and nanostructures become similar to those exhibited by β-Lg structures without quercetin. This behaviour may indicate that higher quercetin concentrations (≥ 0.08 mg mL^{-1}) may be able to promote conformational rearrangements on β-Lg

structures with the establishment of stable electrostatic interactions capable of preventing aggregation (Liu et al., 2018).

Based on the best results obtained for the *AE* and *LC* and taking into consideration the physicochemical properties evaluated by DLS and discussed above, and in order to minimize the number of experimental tests to be performed, the concentration of 0.105 mg mL^{-1} of riboflavin and 0.08 mg mL^{-1} of quercetin were selected to associate to β-Lg micro- and nanostructures in the subsequent assays.

5.2.2. Morphology

The shape and size of β-Lg micro- and nanostructures associated with riboflavin and quercetin bioactive compounds are shown in Figure 5.1.

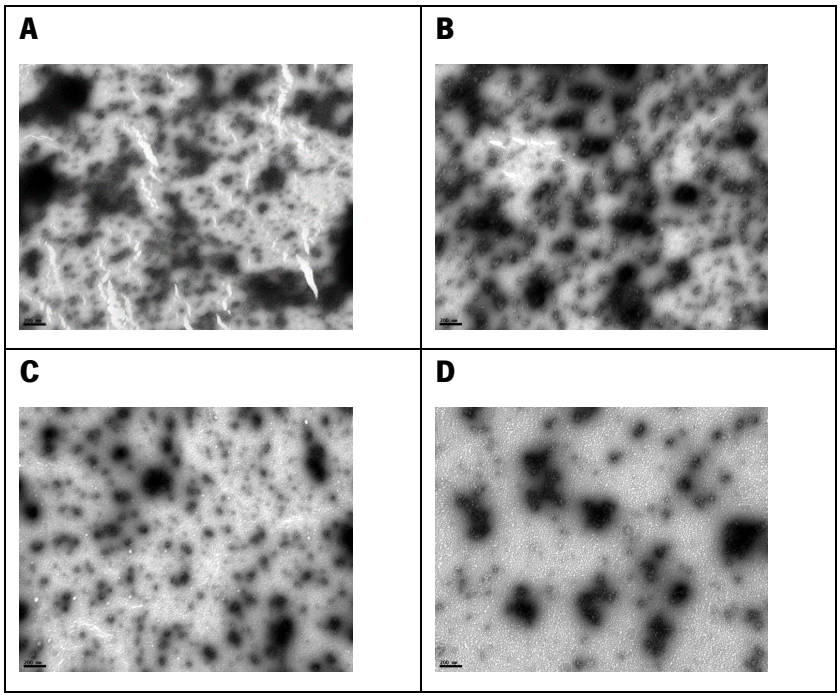


Figure 5.1 - TEM images of β-Lg/riboflavin microstructures A), β-Lg/quercetin microstructures B), β-Lg/riboflavin nanostructures C), β-Lg/quercetin nanostructures D) (scale bar = 200 nm, magnification = 50.000 x).

Figure 5.1 shows images of β-Lg structures with a spherical shape and with a smooth surface. Measurements from images of β-Lg/riboflavin microstructures (Figure 5.1A) and β-Lg/quercetin microstructures (Figure 5.1B) revealed an average particle size of ca. 152.0 and 142.3 nm, respectively. DLS results demonstrated higher particle sizes than those obtained by TEM. This difference between both techniques may be due to a drying effect caused by samples preparation for TEM visualization, which may lead to the reduction of particle size. This phenomenon has been

equally reported by other authors (Bourbon et al., 2016; Zhang et al., 2018). β-Lg/riboflavin nanostructures (Figure 5.1C) and β-Lg/quercetin nanostructures (Figure 5.1D) showed particle sizes around 75.6 and 76.1 nm, respectively, which corroborates the results obtained by DLS. These results are in agreement with those reported by Liu et al. (2018), which showed homogenous β-Lg/astaxanthin nanoparticles characterized by a spherical and uniform shape, with particle sizes below 100 nm (i.e., ca. 40 nm).

5.2.3. Binding properties

5.2.3.1. Extrinsic fluorescence

The accessibility and conformational changes of protein hydrophobic regions were detected through the binding of the fluorescence hydrophobic probe ANS (Singh et al., 2019). According to the literature, β-Lg exhibit two different binding ANS sites, being located internally (i.e., in the hydrophobic protein core), which contain disulphide bridges; and at externally (i.e., close to the hydrophobic patch on the protein surface), being responsible for nonspecific ANS interaction (Aprodu et al., 2017; Collini et al., 2009). The ANS interactions with β-Lg micro- and nanostructures, in the absence or presence of bioactive compounds, are depicted in Figure 5.2.

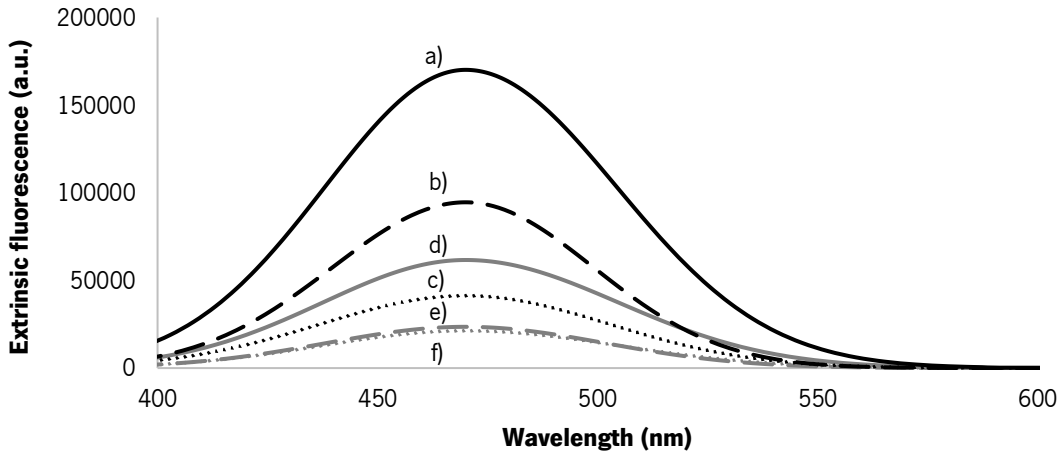


Figure 5.2 - Extrinsic fluorescence emission spectra at 370 nm of microstructures: β-Lg a); β-Lg/riboflavin b); and β-Lg/quercetin c); and of nanostructures: β-Lg d); β-Lg/riboflavin e); β-Lg/quercetin f).

Extrinsic fluorescence spectra (Figure 5.2) showed a maximum peak at a wavelength of 470 nm, which corresponds to β-Lg hydrophobic sites. The binding of riboflavin and quercetin with β-Lg micro- and nanostructures led to a loss of signal intensity, thus suggesting that some interactions

occurred at the protein hydrophobic regions, competing with ANS binding (Zhang et al., 2018). These results are in accordance with the observations reported by Bourbon et al. (2016), which obtained a decrease of peak intensity in lactoferrin-glycomacropeptide nanohydrogels with the encapsulation of curcumin and caffeine.

However, two different behaviours were observed among β-Lg micro- and nanostructures. While at microscale the binding of quercetin promoted a decrease of the peak intensity, when compared with riboflavin, at nanoscale it was observed a similar fluorescence intensity for both bioactive model compounds. This difference may be related with the fact that for β-Lg/riboflavin microstructures the *AE* reached its maximum (64.4 ± 0.8 %) for the highest concentration of riboflavin tested (i.e., 0.105 mg/mL), so most probably there were still sites available for ANS binding, whereas for β-Lg/riboflavin nanostructures the maximum *AE* was attained for a riboflavin concentration of 0.014 mg mL^{-1}, which may suggest that all binding sites were occupied by riboflavin, and thus not available to bind to ANS.

Another possible explanation for this observation is that riboflavin has affinity to bind initially to β-Lg through hydrogen and electrostatic interactions, and consequently enable that some hydrophobic patches are available to binding with ANS (Li et al., 2019). However, besides hydrogen and electrostatic interactions and due to the high surface area-volume ratio, β-Lg/riboflavin nanostructures also have the capability to block hydrophobic patches available on the protein surface. This could also be the explanation for the higher *LC* obtained for β-Lg/riboflavin nanostructures (Table 5.1) when compared with β-Lg/riboflavin microstructures for the same concentration of the hydrophilic bioactive compound.

5.2.3.2. Circular dichroism

A Far-UV CD spectra (190-260 nm) were used to analyse protein structural transitions due to the fact that β-Lg interactions with small ligands may lead to relevant changes in the β-Lg secondary structure (Liang et al., 2008). β-Lg secondary structure have a characteristic CD spectrum according to their major elements, i.e., an α-helix (positive band at 190 nm and negative peaks at 208 and 220 nm), an β-sheet (negative peak in the 215 nm region) and a random coil (positive peak at 215 nm and negative band near 200 nm). Thus, it is crucial to investigate the impact of riboflavin and quercetin on the secondary structures of β-Lg in micro- and nanostructures (Essemine et al., 2011; Gomaa et al., 2016).

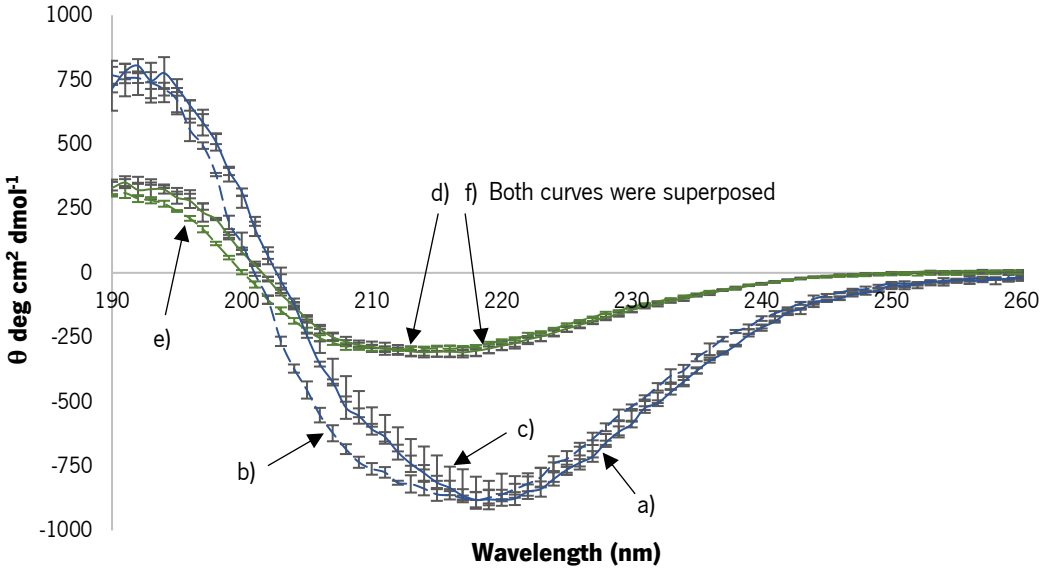


Figure 5.3 - Far-UV CD spectra (190-260 nm) of microstructures: β-Lg a); β-Lg/riboflavin b); and β-Lg/quercetin c); and of nanostructures: β-Lg d); β-Lg/riboflavin e); β-Lg/quercetin f).

Far UV-CD spectra (Figure 5.3) of β-Lg microstructures showed a negative peak with a minimum at 218 nm, which reveals the presence of β-sheet structures (characteristic at 215 nm) and the presence of α-helix conformation due to the band near 220 nm. β-Lg nanostructures displayed a conformational profile with an anti-parallel β-structure with a broad negative minimum at 214 nm. The CD spectra of β-Lg/quercetin micro- and nanostructures were superposed with the corresponding structures of isolated β-Lg. This finding indicates that interaction between quercetin and β-Lg did not cause changes in the protein secondary structure; however, this evidence should be confirmed by other complementary techniques. On the other hand, for far-UV spectra of β-Lg/riboflavin micro- and nanostructures, it was observed a slight red shift (from 202 to 200 nm for micro- and from 201 to 200 nm for nanostructures), thus suggesting that riboflavin chromophoric groups were exposed to the hydrophilic environment.

5.2.3.3. Fourier-transform infrared spectroscopy

The FTIR spectra of β-Lg/riboflavin (Figure 5.4A) and β-Lg/quercetin (Figure 5.4B) micro- and nanostructures were evaluated in terms of their protein secondary structure and main functional groups present.

Protein conformational changes in the secondary structure are related with amide I band ranging between 1700 to 1600 cm^{-1} and amide II band around 1530 cm^{-1} (Xu et al., 2019). As shown in Figure 5.4A (a, d) for the β-Lg microstructures and in Figure 5.4B (a, d) for the β-Lg nanostructures,

both amide I (mainly C=O stretch) and amide II (C–N stretch coupled with N–H bending mode) increased in intensity with the association of riboflavin – Figure 5.4A (b, e) or quercetin – Figure 5.4B (b, e), independently of the structures' scale used. These changes have been reported in the literature as conformational changes in the β-sheet structure, thus suggesting that the association of both bioactive model compounds led to relevant perturbations on the secondary structure of the protein. The association of such bioactive compounds may also cause some disturbances in the tertiary structure of the protein, resulting from rearrangement of hydrophobic interactions, hydrogen and ionic bonds (Ramos et al., 2014).

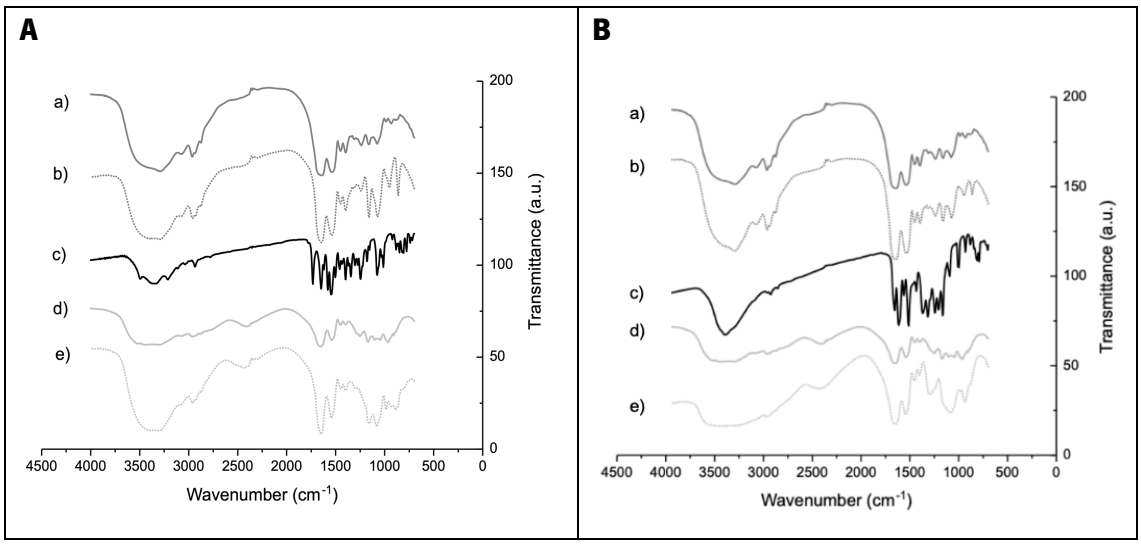


Figure 5.4 - FTIR spectra of β-Lg/riboflavin micro- and nanostructures A) and β-Lg/quercetin micro- and nanostructures B), being a) β-Lg microstructures; b) β-Lg microstructures associated with respective bioactive model compound; c) free bioactive model compound; d) β-Lg nanostructures; and e) β-Lg nanostructures associated with respective bioactive model compound.

FTIR spectra of free riboflavin presented an absorption band between 3571 and 2974 cm^{-1} attributed to -OH stretch, and peaks at 1731 and 1542 cm^{-1} corresponding to the carbonyl stretching vibration of the amide group and to $-CH_3$ stretching, respectively, as depicted in Figure 5.4A (c). Besides, the peak assigned at 848 cm^{-1} can be ascribed as out-of-plane N-H wagging vibration from the pyrimidine ring (Orsuwan et al., 2019; Ye et al., 2019). In addition, C-O stretching appeared in two different absorption bands at 1072 and 1014 cm^{-1} (Mansour et al.,2014).

In Figure 5.4A, comparing β-Lg/microstructures (a) to β-Lg/riboflavin microstructures (b), it is possible to observe a band shift from 1654 to 1643 cm^{-1} (C=O stretching) and from 1527 to 1539 cm^{-1} ($-CH_3$ stretching), promoted by the association of riboflavin. The intensities of C-O stretching

(present at 1161 and 1068 cm^{-1}) and of out-of-plane N-H wagging vibration (present at 864 cm^{-1}), characteristic of β-Lg structure, increased in β-Lg/riboflavin microstructures.

For β-Lg/riboflavin nanostructures (e), it was also observed a shift in stretching vibration of C=O (from 1531 to 1542 cm^{-1}) and in -CH_3 stretching (from 1650 to 1647 cm^{-1}), as well as an increase in the intensity of peaks at 1157 and 1080 cm^{-1} (mainly C-O stretch) and in the region from 3571 to 2974 cm^{-1}, which may be attributed to the establishment of hydrogen bonds. Riboflavin has a hydrophobic extremity (due the presence of an aromatic ring), which enables binding to β-Lg through hydrophobic bonds; and a hydrophilic group (due to the ribitol chain and pyrimidine ring), which allows the interaction to β-Lg by hydrogen and electrostatic bonding (Morrison et al., 2013; Zhang et al., 2016). These findings were consistent with our β-Lg/riboflavin micro- and nanostructure *LC* results.

FTIR spectra of free quercetin – Figure 5.4B (c) exhibited bands in 3394 cm^{-1} region, which is attributed to O-H stretching vibration of hydroxyl group and aromatic groups (Li et al., 2019), C=O stretching (at 1658 cm^{-1}), C=C stretching (at 1515 cm^{-1}), C-O aromatic stretching (at 1315 cm^{-1}) and an aromatic bending and stretching (at 810 cm^{-1}) (Ma et al., 2018; Patel et al., 2012).

As shown in Figure 5.4B (b), FTIR spectra of β-Lg/quercetin microstructures revealed characteristic bands of free quercetin with a peak intensity increase at 1650 cm^{-1} (C=O stretch), 1164 cm^{-1} (aromatic bending and stretching) and at 856 cm^{-1} (aromatic bending and stretching). The peak in free quercetin at 3394 cm^{-1} related to O-H stretching vibration of the hydroxyl group, was shifted from 3278 cm^{-1} in β-Lg microstructures to 3290 cm^{-1} in β-Lg/quercetin microstructures. The broader peak of free quercetin suggests that hydrogen bonding was one of the main interactions involved in the binding to β-Lg microstructure. This evidence is in agreement with Shpigelman et al. (2012) findings that indicate that polyphenols may interact with protein partially by hydrogen bonds.

The differences on the FTIR spectra of β-Lg nanostructures – Figure 5.4B (d) when compared with β-Lg/quercetin nanostructures – Figure 5.4B (e) are mainly due to the progressive increase of peaks at 1647 cm^{-1}, corresponding to C=O stretch, at 1307 cm^{-1} due to C-O aromatic stretching, and at 933 cm^{-1} attributed to aromatic bending and stretching. Moreover, the band in the region of 3394 cm^{-1} associated to the presence of hydroxyl group and aromatic groups was not obtained for β-Lg/quercetin nanostructures, thus suggesting that hydrogen bonding was not the main binding interactions occurring between quercetin and β-Lg structures at the nanoscale.

5.2.4. β-Lg structures stability under various environmental conditions

The effect of several environmental conditions (e.g., pH, temperature, ionic strength, and storage temperature) on β-Lg micro- and nanostructures associated with bioactive compounds was assessed to provide information about the food product characteristics that facilitate their incorporation.

5.2.4.1. pH stability

The effect of pH was evaluated by adjusting aqueous solutions of β-Lg micro- and nanostructures (data were available in the Supplementary Material, Table S.1 and Table S.2, respectively) structures to various pH values in order to assess its impact on their particle size, PDI and surface charge (S). Taking in consideration the β-Lg isoelectric point (pI), which is near pH = 4.8 (Ramos et al., 2012), the zeta potential of aqueous solutions of β-Lg micro- and nanostructures shifted from positive values, at pH 2, towards negative values, at pH 10 (Table S.1 and Table S.2). At pH values near the pI of β-Lg, aggregates with large mean particle sizes (i.e., > 5 μm) and white appearance were obtained, independently of the structures' scale. This result is somehow expected since at pI the electrostatic repulsions become weak and proteins tend to aggregate and/or flocculate, forming structures with larger sizes (Ramos et al., 2012).

Chen et al. (2014) evaluated the pH stability, from 3 to 7, of zein/β-Lg nanoparticles encapsulating tagerentin (i.e., low water solubility compound), showing aggregation phenomena for such nanoparticles complex for pH values between 4.5 and 5.5, and high stability for pH above 5.5 or below 4.5.

The particle diameter of β-Lg micro- and nanostructures with/without bioactive model compounds remained constant ($p > 0.05$) (Table S.1 and Table S.2) with low PDI values (i.e., below 0.25) for pH range between 2 and 3 (Table S.1 and Table S.2). According to the literature, β-Lg structure has stability and remains mostly intact in acid conditions (Liang & Subirade, 2012; Shafaei et al., 2017). For pH conditions between 6 and 10, particle size and PDI are stable, which may be attributed to the formation of strong covalent or hydrophobic bonds among β-Lg molecules and bioactive model compounds during thermal gelation (Bengoechea et al., 2011).

These results suggest that β-Lg micro- and nanostructures may be suitable carriers for riboflavin and quercetin into soft drinks (with pH values ranging from 2 to 3) and into some dairy products (with pH values between 6 to 9), and also effective delivery systems upon oral intake since they resist to the acid environment, which is characteristic of the human stomach.

5.2.4.2. Ionic strength stability

The impact of ionic strength on properties of β-Lg micro- and nanostructures was evaluated in order to estimate their behaviour in aqueous commercial products composed by distinct types and amounts of electrolytes, as well as within the human gastrointestinal tract (Chen et al., 2014).

The ionic strength study was carried out by solubilizing β-Lg micro- and nanostructures in various concentrations of sodium chloride (NaCl), in order to evaluate the ionic strength effect on particle size and PDI (data were present in the Supplementary Material, Table S.3 and Table S.4, respectively). Results demonstrated that β-Lg structures displayed particle sizes in the nanoscale range (i.e., 104.3 ± 5.9 nm) when added to NaCl until 100 mmol L^{-1}, and remained homogenous (i.e., PDI < 0.22) at this scale-range. The association of riboflavin was able to maintain β-Lg structures homogeneous and within the nanoscale at NaCl concentrations up to 200 mmol L^{-1}; PDI values were ranging from 0.21 ± 0.01 to 0.22 ± 0.01 and particles sizes were ranging from 77.4 ± 8.2 nm to 73.9 ± 6.9 nm ($p > 0.05$). On the other hand, the addition of NaCl at concentrations ≤ 25 mmol L^{-1} did not impact the stability of β-Lg nanostructures showing a particle size in the nano range (i.e., 77.9 ± 9.6 nm). However, for progressively higher concentrations of NaCl, the particle sizes of β-Lg/quercetin nanostructures increased significantly ($p \leq 0.05$) above 100 nm, and structures became more heterogeneous. According to Bourbon et al. (2015), the presence of NaCl may impacts the size and PDI of protein structures by two different mechanisms: i) by promoting the establishment of attractive interactions, for instance, van der Waals or hydrophobic, which dominate the repulsive interactions; or ii) by modifying the organization of structural water molecules, which changes the strength of hydrophobic interactions between nonpolar groups.

Regarding the impact of ionic strength, the addition of NaCl at concentrations ≤ 200 mmol L^{-} did not impact the stability (i.e., particle size and PDI) of β-Lg/quercetin microstructures, however higher concentrations of NaCl increased significantly ($p \leq 0.05$) its particle size (383.8 ± 26.6 nm) and PDI (0.28 ± 0.03) values. This result may indicate that at higher (i.e., micro-) scale range the Na^{+} and Cl^{-} ions may have a lower impact on β-Lg microstructures, since as the surface-to-volume ratio is lower than that in nanostructures, β-Lg is less subjected to the action of NaCl, and thus a higher concentration of salt is needed to neutralize β-Lg's charge and to reduce electrostatic repulsion (Hu & McClements, 2014).

These results suggest that β-Lg/riboflavin nanostructures, and β-Lg/riboflavin and β-Lg/quercetin microstructures are suitable delivery systems for a large variety of food systems since they are stable at a relatively broad range of salt concentrations. Additionally, they also should be stable in

the gastrointestinal tract during digestion when considering this parameter, since the normal ionic strength in the stomach is 100 mmol L^{-1} and in the small intestine is 140 mmol L^{-1} (McClements & Li, 2010; Pinheiro et al., 2017).

5.2.4.3. Thermal stability

Heating is a common processing treatment in the food industry, therefore it is crucial to evaluate the thermal stability of delivery systems at a temperature range of at least 20 to 80 °C. Therefore, the effect of temperature on β-Lg micro- and nanostructures (data were available in the Supplementary Material, Table S.5 and Table S.6, respectively) properties was investigated at those conditions. The particle size of β-Lg micro- and nanostructures in the absence and presence of bioactive compounds did not change ($p > 0.05$) for temperatures below 70 °C and slightly increased ($p \leq 0.05$), when subjected to temperatures between 70 and 80 °C. The PDI values of β-Lg structures were below 0.25, independently of temperature, indicating a good homogeneity of such protein structures within a narrow size distribution. This temperature stability may be due to some changes in the conformational state (Bourbon et al., 2015) or reorganization of β-Lg molecules, without compromising its functionality (Hu & McClements, 2014). These results are in the same line of those presented in a previous study conducted by Yi et al. (2016), which showed thermal stability of α-lactalbumin/curcumin nano-complexes for temperatures ranging from 30 to 90 °C, with a slight increase in particle diameter observed for temperatures above 70 °C.

5.2.4.4. Storage

Temperature is an important condition to preserve the effective quality and benefits of bioactive compounds, thus contributing to physiological wellbeing (Kang et al., 2019; Ramos et al., 2017). Therefore, a storage stability study was performed to assess the effect of temperature at 4 °C (to simulate refrigerated conditions) and at 25 °C (to simulate room temperature conditions) over 90 days of storage. β-Lg microstructures (data were present in Supplementary Material, Table S.7) without association of bioactive model compounds maintained their stability in terms of particle size (from 202.5 ± 5.8 nm to 202.0 ± 11.1 nm), PDI (from 0.18 ± 0.02 to 0.17 ± 0.01) and S (from -22.2 ± 1.9 mV to -21.4 ± 1.2 mV) at the beginning and after 90 days of storage, respectively, at 4 °C; while at 25 °C it was possible to observe the formation of precipitates over 50 days of storage, indicating loss of colloidal stability.

β-Lg nanostructures (data were available in Supplementary Material, Table S.8) without the association of bioactive model compounds were able to maintain their properties without significant changes ($p > 0.05$) in terms of particle size, PDI and S over the storage period, independently of the temperature tested, thus suggesting that β-Lg nanostructures were stable and able to retain their structure. These nanostructures displayed higher storage stability when compared with the performance exhibited by α-lactalbumin-lysozyme nanoparticles (with sizes of 61 ± 2.3 nm), tested by Monteiro et al. (2016). In that case, α-lactalbumin-lysozyme nanoparticles were able to maintain their stability over 90 days at 4 °C but only for 30 days at 25 °C. This difference may be related to the different protein characteristics or to the weak intermolecular interactions established between α-lactalbumin-lysozyme.

In terms of stability of β-Lg/quercetin nanostructures, precipitates were formed over 2 days of storage, independently of the storage temperature tested. As mentioned before, quercetin use is limited by its poor water solubility (Ni et al., 2017). When ethanolic solutions (used in the solubilization of quercetin) were added into β-Lg aqueous systems, large precipitates were formed, displaying an atypical needle-like morphology, which is extremely unstable and leads to sedimentation. Despite of this, the precipitates' shape may be controlled by increasing protein concentration, thus leading to a decrease in the appearance of needle-shaped crystals (Patel et al., 2012).

Regarding the stability of β-Lg/riboflavin microstructures (Table S.7), they were stable over the 90 days at both temperatures tested. The association of riboflavin was even able to prevent the formation of precipitates observed in β-Lg microstructures isolated after 50 days of storage. This evidence may be due to possible changes promoted by riboflavin at the β-Lg surface, possibly the establishment of strong interactions that may have prevented the electrostatic attraction between protein molecules. The magnitude of surface charge for β-Lg microstructures with and without bioactive model compounds (Table S.7) association did not change significantly ($p > 0.05$) during the storage time, being around – 20.0 mV.

β-Lg/riboflavin nanostructures (Table S.8) demonstrated a slight change in particle size ranging from 70.8 ± 2.3 nm to 78.0 ± 4.7 nm with PDI value lower than 0.25, over 80 days of storage at 4 °C. However, over 90 days, the particle sizes and PDI increased more pronouncedly, reaching 84.3 ± 8.7 nm and 0.30 ± 0.01, respectively. These results are in line with those reported by Martins et al. (2016), which showed that lactoferrin/iron nanoparticles were stable in terms of particle size and PDI during 76 days at 4 °C.

At 25 °C, the stability of β-Lg/riboflavin nanostructures decreased significantly to 22 days (particles sizes of 67.8 ± 1.9 nm and PDI of 0.25 ± 0.01), when compared with those exhibited over 90 days (particles sizes of 70.5 ± 1.6 nm, but PDI values of 0.40 ± 0.10), which may indicate that dissociation or aggregation phenomena occurred after 22 days. This evidence indicates that refrigeration could improve the storage stability of β-Lg micro- and nanostructures loaded with riboflavin and quercetin.

β-Lg/riboflavin micro- and nanostructures and β-Lg/quercetin microstructures showed the best performance in terms of stability for the tests performed above, and for that reason the behaviour of such structures was evaluated into food simulants.

5.2.5. *In vitro* release kinetics

Release profiles were used to ensure that a delivery system will act according to the designed goal. These profiles are expected to estimate the behaviour of β-Lg micro- and nanostructures into food products. The release profile of riboflavin and quercetin bioactive compounds from β-Lg micro- and nanostructures added into food simulants (i.e., 10 % of ethanol simulating hydrophilic matrices and 50 % of ethanol simulating hydrophobic matrices) were assessed at 4 °C (to simulate refrigerated conditions) and at 25 °C (to simulate room temperatures). The release kinetics of bioactive model compounds from β-Lg micro- and nanostructures were monitored during 72 h. The amount (%) of bioactive compound released as a function of time is plotted in Figure 5.5.

Figure 5.5 shows a typical release profile, where the initial 8 h comprises a burst release stage associated to the faster release of unbound bioactive compounds, followed by a controlled release phase attributed to the behaviour of bioactive compounds bounded to β-Lg micro- and nanostructures or to β-Lg conformational changes under contact with food simulants (Heydari et al., 2018). These release profiles are in agreement with other release studies that use proteins as the main encapsulating agent (Liu et al., 2018; Luo et al., 2011; Wang et al., 2018). O'Neill et al. (2015) reported a release of 42 % of riboflavin from whey protein hydrogels within 2 h in a water matrix at 20 °C. The authors concluded that this delivery system was not suitable for food products with high moisture content stored at room temperature conditions. Kumari et al. (2010) developed poly-D,L-lactide nanoparticles for quercetin delivery and reported a rapid burst, releasing 40-45 % of quercetin within 30 min in 0.1 mol L^{-1} of phosphate-buffered saline (PBS) buffer solution.

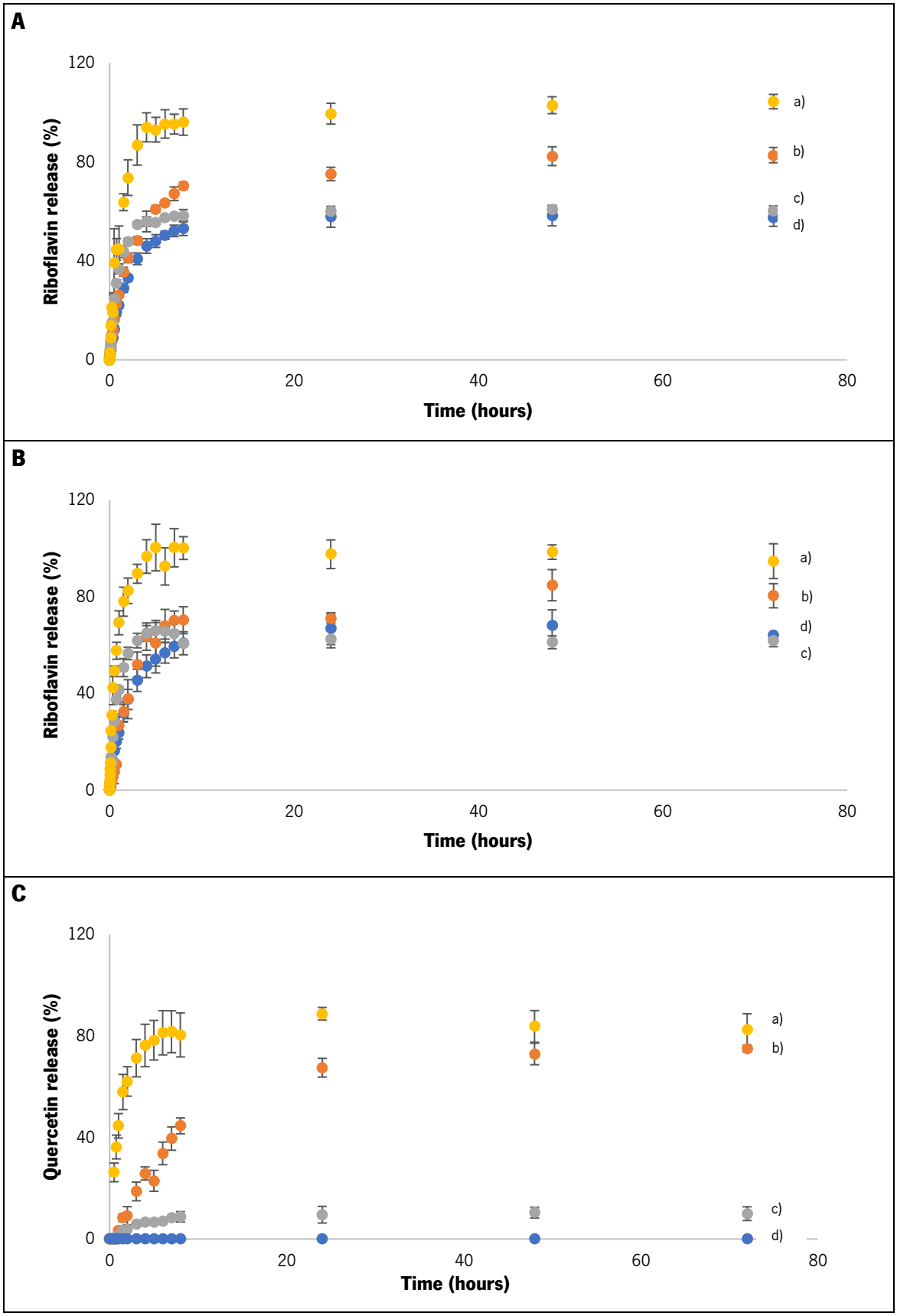


Figure 5.5 - Release profiles of riboflavin from β-Lg micro- A) and β-Lg nanostructures B); and quercetin from β-Lg microstructures C), added into the following food simulants: a) 50 % at 25 °C; b) 50 % at 4 °C; c) 10 % at 25°C and d) 10 % at 4 °C.

In our study, riboflavin and quercetin were rapidly released from β-Lg micro- and nanostructures when added into a hydrophobic (50 % ethanol) food simulant at 25 °C. This result may be related to the fact that ethanol present at high concentrations (i.e., 50 %) in contact with β-Lg may affect the stability of this protein, by promoting irreversible changes in the protein's secondary structure with consequent protein disintegration (Yoshizawa et al., 2014).

β-Lg/riboflavin micro- (Figure 5.5A) and nanostructures (Figure 5.5B) showed a similar release profile when tested in both hydrophilic and hydrophobic food simulants at 4 °C and 25 °C. Commonly, the "responsiveness" is related to the interactions established between bio-based materials used as carriers and the surrounding environment (Musyanovych & Landfester, 2014); however, it is essential to determine the mechanism involved in this process, in order to allow the controlled release of bioactive compounds at the micro- and nanoscale.

As shown in Figure 5.5C, under hydrophilic food simulant conditions, β-Lg microstructures practically did not release quercetin at 4 °C, over 72 h. This could be due to the hydrophobic character of quercetin that did not diffuse to the hydrophilic food simulant; thus, it was not possible to describe the release profile of quercetin in these conditions. These results are in agreement with those published by Bourbon et al. (2016), which showed that curcumin (hydrophobic compound) was not released from lactoferrin-glycomacropeptide nanohydrogels due the low solubility of curcumin at pH 7.3 in phosphate buffer solution, used as food simulant.

The release kinetics results of both bioactive compounds (Figure 5.5) were fitted to a mathematical model – Linear Superimposition Model (LSM) (Equation 7) – to find the most adequate release mechanism model. The plots of β-Lg/riboflavin micro- (data were present in Supplementary Material, Figure S.1), β-Lg/riboflavin nanostructures (data were available in Supplementary Material, Figure S.2) and β-Lg/quercetin microstructures (data were present in Supplementary Material, Figure S.3) fitted well with the LSM. Table 5.3 shows the fitting parameters of LSM to experimental data of riboflavin and quercetin released from β-Lg micro-and nanostructures.

Results from Table 5.3 demonstrate that LSM fitted well to data obtained with a $R^2 > 0.98$, thus indicating that this model was suitable to describe the release mechanisms of riboflavin and quercetin from β-Lg micro- and nanostructures. The model suggests that the transport mechanisms involved can be described by Fick's diffusion and Case II transport (biopolymer relaxation), with one main relaxation of the β-Lg micro- and nanostructures.

Table 5.3 - Linear superimposition model (LSM) fitting of riboflavin and quercetin release data from β-Lg micro- and nanostructures. The parameters *RMSE* and R^2 were used to evaluate the quality of the regression.

Bioactive compound	β-Lg Structure	Food Simulant	T (°C)	*RMSE*	R^2	*X*	K_F (min^{-1})	K_R (min^{-1})
Riboflavin	Micro	10 % ethanol	4	0.02	0.99	0.07	2.95	0.37
			25	0.03	0.99	0.08	6.08	0.80
		50 % ethanol	4	0.10	0.99	0.09	2.92	0.25
			25	0.04	0.99	0.09	0.01	0.63
	Nano	10 % ethanol	4	0.07	0.99	0.06	3.63	0.36
			25	0.02	0.99	0.03	6.29	1.15
		50% ethanol	4	0.06	0.97	0.06	0.01	0.27
			25	0.11	0.99	0.10	8.37	1.10
Quercetin	Micro	10 % ethanol	25	0.04	0.98	0.01	0.03	0.18
		50 % ethanol	4	0.03	0.99	0.06	0.09	0.10
			25	0.02	0.99	0.01	2.74	0.80

NOTE: T: Temperature; *RMSE*: Root Mean Square Error; *X*: Bioactive compound fraction released by Fickian transport; K_F: Fick rate constant; K_R: relaxation rate constant.

Table 5.3 shows that release kinetics of bioactive compounds can be affected by both food simulants (i.e., with hydrophilic and hydrophobic nature) and temperature (i.e., 4 and 25 °C). The relaxation rate constant (K_R) increased with temperature, independently of the food simulant used, which may be attributed to the input of energy into the system that promotes a more relaxed and weaker protein structure, thus increasing the diffusion of the bioactive compound.

In the hydrophilic food simulant (10 % ethanol) the amount of riboflavin released from β-Lg micro- and nanostructures was higher than that obtained for the hydrophobic counterparts. On the contrary, the quercetin release into hydrophobic food simulant at 25 °C was higher than that obtained in the hydrophilic environment. These findings might be due the relaxation rate constant value (K_R) and related with the hydrophilic and hydrophobic nature of riboflavin and quercetin, respectively, and with their affinity to diffuse to hydrophilic and hydrophobic food simulants, respectively.

It was found that β-Lg/bioactive compound micro- and nanostructures exhibited a similar relaxation rate constant for both food simulants at 4 °C. However, in the simulant at room temperature (i.e., 25 °C) the β-Lg nanostructures showed faster release kinetics, confirmed by the high K_F obtained, as compared to that of β-Lg microstructures. This behaviour may be related with the higher exposure area as a result of the higher surface-to-volume ratio, characteristic of nanoscale

materials, which in association with the effect of temperature (25 °C), has enhanced the protein relaxation and thus an increased riboflavin release.

For most conditions tested, the Fickian (K_f) rate constant was higher than the relaxation (K_R) rate constant, which may be indicating that bioactive compounds release was quicker by Fick's diffusion instead of relaxation mechanism (Martins et al., 2016).

The bioactive compound fraction released by Fickian transport (X value), defined as $\frac{M_{\infty F}}{M_t}$, allows determining the governing bioactive compound release mechanism. If $X > 0.5$ the prevailing bioactive compound release mechanism is Fickian diffusion, while if $X < 0.5$ relaxation is the main mechanism of release (Pinheiro et al., 2012). Therefore, this implies that the release of both bioactive model compounds from β-Lg micro- and nanostructures is mainly governed by the relaxation mechanism.

Wichchukit et al. (2013) reported that riboflavin release from whey protein beads in a beverage model food exhibited a transport mechanism governed by Case II, which resulted in slow release rates during product shelf life and until its consumption. Yan et al. (2018) investigated the controlled release of quercetin-loaded chitosan nanoparticle into 50 % ethanol and water-oil (50:50) food simulants at 25 °C and reported an initial burst followed by sustained slow release. These authors described the quercetin release profile as a Fick's curve; however, they did not apply a mathematical model to prove this behaviour.

Table 5.4 shows β-Lg micro- and nanostructure properties (i.e., particle size, PDI and S) analysed before and after bioactive compounds (i.e., riboflavin and quercetin) release, and bioactive compounds final concentrations in β-Lg structures.

Data presented in Table 5.4 show that β-Lg micro- and nanostructures increased their particle size ($p \leq 0.05$) during the release period, for all conditions tested. This behaviour is typical when the release mechanism is governed by biopolymer relaxation and when structures present a swelling behaviour in response to chemical (e.g., pH, solvent and ionic strength) and/or physical (e.g., temperature, light) stimuli (Simões et al., 2017). The swelling capacity of β-Lg micro- and nanostructures may be related with the presence of hydrophilic moieties (e.g., hydroxyl, amino, or carboxyl groups) in their structure (Ramos et al., 2015). This hypothesis is supported by FTIR results, which showed the presence of such hydrophilic groups in β-Lg's structure. Bourbon et al. (2016) also demonstrated that lactoferrin-glycomacropeptide nanohydrogels increased their particle size with the release or curcumin due to the swelling behaviour of nanohydrogels, which is a typical case of release mechanisms dominated by biopolymer relaxation. Nonetheless, the

authors obtained small sized nanohydrogel particles when Fick's diffusion was the main release mechanism.

Table 5.4 - Particle size, polydispersity index (PDI) and surface charge (S) of β-Lg micro- and nanostructures before and after the release of riboflavin and quercetin into food simulants at various temperature (4 and 25 °C), and the bioactive compounds final concentration present in β-Lg structures.

Bioactive compound	β-Lg Structure	Food Simulant	T (°C)		Particle size (nm)	PDI	S (mV)	Final concentration (mg mL^{-1})
Riboflavin	Micro	10 % ethanol	4	**I**	243.9 ± 5.8^{a}	0.25 ± 0.01^{a}	-21.3 ± 1.3^{a}	0.005 ± 0.001
				F	316.1 ± 8.0^{b}	0.25 ± 0.02^{a}	-23.2 ± 0.5^{b}	
			25	**I**	241.8 ± 1.9^{a}	0.19 ± 0.01^{a}	-19.9 ± 1.5^{a}	0.007 ± 0.001
				F	280.9 ± 8.8b	0.18 ± 0.01^{b}	-25.6 ± 0.9^{b}	
		50 % ethanol	4	**I**	258.2 ± 6.5^{a}	0.23 ± 0.02^{a}	-22.0 ± 1.4^{a}	0.005 ± 0.001
				F	670.5 ± 14.5^{b}	0.18 ± 0.03^{b}	-10.7 ± 1.7^{b}	
			25	**I**	249.5 ± 3.6^{a}	0.19 ±0.01^{a}	-21.8 ± 1.3^{a}	0.006 ± 0.002
				F	680.3 ± 10.3^{b}	0.16 ± 0.04^{a}	-11.7 ± 1.2^{b}	
	Nano	10 % ethanol	4	**I**	76.8 ± 5.1^{a}	0.25 ± 0.01^{a}	-20.4 ± 1.4^{a}	0006 ± 0.002
				F	112.9 ± 10.4^{b}	0.28 ± 0.01^{b}	-21.0 ±0.8^{a}	
			25	**I**	93.0 ± 6.2^{a}	0.24 ± 0.02^{a}	-16.1 ± 0.4^{a}	0.007 ± 0.001
				F	132.2 ± 13.4^{b}	0.32 ± 0.05^{b}	-20.2 ± 1.9^{b}	
		50 % ethanol	4	**I**	84.3 ± 4.1^{a}	0.25 ± 0.02^{a}	-21.0 ± 1.5^{a}	0.006 ± 0.001
				F	273.8 ± 4.9^{b}	0.31 ± 0.03^{b}	-12.5 ± 0.7^{b}	
			25	**I**	76.0 ± 1.2^{a}	0.25 ± 0.01^{a}	-18.8 ± 1.6^{a}	0.010 ± 0.001
				F	205.5 ± 26.3^{b}	0.53 ± 0.07^{b}	-10.5 ± 2.3^{b}	
Quercetin	Micro	10 % ethanol	4	**I**	212.6 ± 8.9^{a}	0.25 ± 0.01^{a}	-21.1 ± 1.7^{a}	0.043 ± 0.006
				F	259.2 ± 7.8^{b}	0.23 ± 0.01^{a}	-18.2 ± 2.3^{a}	
			25	**I**	249.3 ± 3.3^{a}	0.18 ± 0.02^{a}	-19.8 ± 0.9^{a}	0.003 ± 0.002
				F	253.5 ± 4.2^{b}	0.17 ± 0.02^{a}	-23.0± 1.3^{b}	
		50 % ethanol	4	**I**	276.6 ± 4.1^{a}	0.20 ± 0.02^{a}	-20.7 ± 1.3^{a}	0.004 ± 0.001
				F	666.9 ± 11.8^{b}	0.20 ± 0.04^{a}	-9.5 ± 0.2^{b}	
			25	**I**	245.9 ± 7.7^{a}	0.18 ± 0.01^{a}	-20.1 ± 1.3^{a}	0.002 ± 0.001
				F	556.0 ± 15.9^{b}	0.18 ± 0.02^{a}	-9.5 ± 0.8^{b}	

NOTE: T: Temperature; I: Initial release; F: Final release; ^{a,b}Small superscript letters within column indicate statistical difference between initial and final means ($p \leq 0.05$) for the same parameter.

In terms of surface charge, it was possible to observe that β-Lg/bioactive compounds maintained their surface charge constant, with zeta potential values of ca. -20 mV, during release in hydrophilic food simulant conditions, which indicates a relatively stable system. For β-Lg/quercetin microstructures, when they were added to a hydrophobic simulant (in this particular case with a higher content of ethanol), β-Lg loses its structural stability, as demonstrated by the decrease of

the surface charge (Table 5.4). This effect can be explained by the fact that ethanol molecules affect the repulsive interactions responsible for β-Lg stability (Yoshizawa et al., 2014).

On the other hand, when β-Lg/quercetin microstructures were added to a hydrophilic food simulant (i.e., 10 % ethanol) at 4 °C it was possible to observe that ca. half of the initial concentration of quercetin was released to the hydrophilic food simulant. Moreover, it was possible to see that temperature had an effect on the release of both bioactive model compounds, as mentioned above. Thus, the hydrophobic characteristics of quercetin and slow release results in hydrophilic food simulants at 25 °C, suggest that the combination of a hydrophilic food simulant with the temperature at 4 °C influences the β-Lg structure relaxation and thus a reduction of quercetin release.

An effective delivery system should be able to release the bioactive compounds associated to it, in a controlled way and for prolonged periods, to the surrounding environment (Wichchukit et al., 2013).. β-Lg micro- and nanostructures were able to keep at least 5 % of the initial concentration of riboflavin, while β-Lg microstructures were able to maintain ca. 2.5 % of the initial concentration of quercetin, both over 72 h, independently of the food simulant and temperature used.

5.3. Conclusions

β-Lg micro- and nanostructures were able to bind bioactive compounds with different physicochemical properties (i.e., water solubility). β-Lg nanostructures maintained their physicochemical properties (i.e., size, PDI and surface charge) independently of the concentrations of both bioactive model compounds added. Furthermore, β-Lg nanostructures showed a higher association efficiency and loading capacity when compared with β-Lg microstructures, for the same concentration of hydrophilic (riboflavin) or hydrophobic (quercetin) bioactive compound used. These structures exhibited stability under acidic (pH 2 to 3) and neutral (pH 6 to 10) pH conditions, at relatively high ionic strength (NaCl concentrations up to 100 mmol L^{-1}) and thermal processing (until 70 °C) conditions. β-Lg/riboflavin micro- and nanostructures showed to be stable over 90 days of storage, while β-Lg/quercetin microstructures were stable during 50 days of storage, being susceptible to aggregation and precipitation after that period. The release for both bioactive model compounds from β-Lg micro- and nanostructures demonstrated that the LSM model was the most suitable to describe the release kinetics, which is mainly governed by a relaxation mechanism. Additionally, the refrigerated temperature of 4 °C allowed a slow release of both bioactive model

compounds, when compared with the results at room temperature (25 °C), independently of the food simulant used.

Our findings improve the knowledge about the potential applicability of β-Lg micro- and nanostructures for delivery and controlled release of hydrophilic and hydrophobic bioactive compounds into food systems with different hydrophilic natures. Nevertheless, further investigations regarding the evaluation of bioaccessibility and bioavailability of these bioactive model compounds upon ingestion are needed before their possible application into real food products.

5.4.References

Aditya, N. P., Macedo, A. S., Doktorovova, S., Souto, E. B., Kim, S., Chang, P. S., & Ko, S. (2014). Development and evaluation of lipid nanocarriers for quercetin delivery: A comparative study of solid lipid nanoparticles (SLN), nanostructured lipid carriers (NLC), and lipid nanoemulsions (LNE). LWT - Food Science and Technology, 59(1), 115–121. https://doi.org/10.1016/j.lwt.2014.04.058

Aprodu, I., Ursache, F. M., Turturica, M., Râpeanu, G., & Stanciuc, N. (2017). Thermal stability of the complex formed between carotenoids from sea buckthorn (Hippophae rhamnoides L.) and bovine β-lactoglobulin. Spectrochimica Acta - Part A: Molecular and Biomolecular Spectroscopy, 173, 562–571. https://doi.org/10.1016/j.saa.2016.10.010

Ashoori, M., & Saedisomeolia, A. (2014). Riboflavin (vitamin B2) and oxidative stress: a review. British Journal of Nutrition, 111(11), 1985–1991. https://doi.org/10.1017/S0007114514000178

Azevedo, M. A., Bourbon, A. I., Vicente, A. A., & Cerqueira, M. A. (2014). Alginate/chitosan nanoparticles for encapsulation and controlled release of vitamin B2. International Journal of Biological Macromolecules, 71, 141–146. https://doi.org/10.1016/j.ijbiomac.2014.05.036

Bengoechea, C., Peinado, I., & McClements, D. J. (2011). Formation of protein nanoparticles by controlled heat treatment of lactoferrin: Factors affecting particle characteristics. Food Hydrocolloids, 25(5), 1354–1360. https://doi.org/10.1016/j.foodhyd.2010.12.014

Berino, R. P., Báez, G. D., Ballerini, G. A., Llopart, E. E., Busti, P. A., Moro, A., & Delorenzi, N. J. (2019). Interaction of vitamin D3 with beta-lactoglobulin at high vitamin/protein ratios: Characterization of size and surface charge of nanoparticles. Food Hydrocolloids, 90(October 2018), 182–188. https://doi.org/10.1016/j.foodhyd.2018.11.027

Beztsinna, N., Solé, M., Taib, N., & Bestel, I. (2016). Bioengineered riboflavin in nanotechnology. Biomaterials, 80, 121–133. https://doi.org/10.1016/j.biomaterials.2015.11.050

Bourbon, A. I., Cerqueira, M. A., & Vicente, A. A. (2016). Encapsulation and controlled release of bioactive compounds in lactoferrin-glycomacropeptide nanohydrogels : Curcumin and caffeine as model compounds. Journal of Food Engineering, 180, 110–119. https://doi.org/10.1016/j.jfoodeng.2016.02.016

Bourbon, A. I., Pinheiro, A. C., Carneiro-da-Cunha, M. G., Pereira, R. N., Cerqueira, M. a., & Vicente, A. a. (2015). Development and characterization of lactoferrin-GMP nanohydrogels: Evaluation of pH, ionic strength and temperature effect. Food Hydrocolloids, 48, 292–300. https://doi.org/10.1016/j.foodhyd.2015.02.026

Bourbon, A. I., Pinheiro, A. C., Cerqueira, M. A., & Vicente, A. A. (2016). Influence of chitosan coating on protein-based nanohydrogels properties and *in vitro* gastric digestibility. Food Hydrocolloids, 60, 109–118. https://doi.org/10.1016/j.foodhyd.2016.03.002

Chen, J., Zheng, J., McClements, D. J., & Xiao, H. (2014). Tangeretin-loaded protein nanoparticles fabricated from zein/β-lactoglobulin: Preparation, characterization, and functional performance. Food Chemistry, 158, 466–472. https://doi.org/10.1016/j.foodchem.2014.03.003

Collini, M., D'Alfonso, L., & Baldini, G. (2009). New insight on β-lactoglobulin binding sites by 1-anilinonaphthalene-8-sulfonate fluorescence decay. Protein Science, 9(10), 1968–1974. https://doi.org/10.1110/ps.9.10.1968

Delahaije, R. J. B. M., Wierenga, P. A., Giuseppin, M. L. F., & Gruppen, H. (2015). Comparison of heat-induced aggregation of globular proteins. Journal of Agricultural and Food Chemistry, 63(21), 5257–5265. https://doi.org/10.1021/acs.jafc.5b00927

Devi, N., Sarmah, M., Khatun, B., & Maji, T. K. (2017). Encapsulation of active ingredients in polysaccharide–protein complex coacervates. Advances in Colloid and Interface Science, 239, 136–145. https://doi.org/10.1016/j.cis.2016.05.009

Essemine, J., Hasni, I., Carpentier, R., Thomas, T. J., & Tajmir-Riahi, H. A. (2011). Binding of biogenic and synthetic polyamines to β-lactoglobulin. International Journal of Biological Macromolecules, 49(2), 201–209. https://doi.org/10.1016/j.ijbiomac.2011.04.016

Gironés-Vilaplana, A., Villaño, D., Marhuenda, J., Moreno, D. A., & García-Viguera, C. (2017). Vitamins. In C. Galanakis (Ed.), Nutraceutical and Functional Food Components (First Edit, pp. 159–201). Elsevier. https://doi.org/10.1016/B978-0-12-805257-0.00006-5

Gomaa, A. I., Nsonzi, F., Sedman, J., & Ismail, A. A. (2016). Enhanced Unfolding of Bovine β-Lactoglobulin Structure Using Microwave Treatment: a Multi-Spectroscopic Study. Food Biophysics, 11(4), 370–379. https://doi.org/10.1007/s11483-016-9451-6

Guo, Y., Harris, P., Kaur, A., Pastrana, L., & Jauregi, P. (2017). Characterisation of β-lactoglobulin nanoparticles and their binding to caffeine. Food Hydrocolloids, 71, 85–93. https://doi.org/10.1016/j.foodhyd.2017.04.027

Haghi, A., Azimi, H., & Rahimi, R. (2017). A Comprehensive Review on Pharmacotherapeutics of Three Phytochemicals, Curcumin, Quercetin, and Allicin, in the Treatment of Gastric Cancer. Journal of Gastrointestinal Cancer, 48(4), 314–320. https://doi.org/10.1007/s12029-017-9997-7

Heydari, A., Mehrabi, F., Shamspur, T., Sheibani, H., & Mostafavi, A. (2018). Encapsulation and Controlled Release of Vitamin B2 Using Peracetyl-β-Cyclodextrin Polymer-Based Electrospun Nanofiber Scaffold. Pharmaceutical Chemistry Journal, 52(1), 19–25. https://doi.org/10.1007/s11094-018-1759-8

Hu, K., & McClements, D. J. (2014). Fabrication of surfactant-stabilized zein nanoparticles: A pH modulated antisolvent precipitation method. Food Research International, 64, 329–335. https://doi.org/10.1016/j.foodres.2014.07.004

Jafari, S. M., & McClements, D. J. (2017). Nanotechnology Approaches for Increasing Nutrient Bioavailability. Advances in Food and Nutrition Research (1st ed., Vol. 81). Elsevier Inc. https://doi.org/10.1016/bs.afnr.2016.12.008

Kang, Y.-R., Lee, Y.-K., Kim, Y. J., & Chang, Y. H. (2019). Characterization and storage stability of chlorophylls microencapsulated in different combination of gum Arabic and maltodextrin. Food Chemistry, 272(March 2018), 337–346. https://doi.org/10.1016/j.foodchem.2018.08.063

Kumari, A., Yadav, S. K., Pakade, Y. B., Singh, B., & Yadav, S. C. (2010). Development of biodegradable nanoparticles for delivery of quercetin. Colloids and Surfaces B: Biointerfaces, 80(2), 184–192. https://doi.org/10.1016/j.colsurfb.2010.06.002

Li, H., Wang, D., Liu, C., Zhu, J., Fan, M., Sun, X., ... Cao, Y. (2019). Fabrication of stable zein nanoparticles coated with soluble soybean polysaccharide for encapsulation of quercetin. Food Hydrocolloids, 87(May 2018), 342–351. https://doi.org/10.1016/j.foodhyd.2018.08.002

Liang, L., & Subirade, M. (2012). Study of the acid and thermal stability of β-lactoglobulin–ligand complexes using fluorescence quenching. Food Chemistry, 132(4), 2023–2029. https://doi.org/10.1016/j.foodchem.2011.12.043

Liang, L., Tajmir-Riahi, H. A., & Subirade, M. (2008). Interaction of β-Lactoglobulin with resveratrol and its biological implications. Biomacromolecules, 9(1), 50–56. https://doi.org/10.1021/bm700728k

Liu, C., Liu, Z., Sun, X., Zhang, S., Wang, S., Feng, F., ... Xu, Y. (2018). Fabrication and Characterization of β-Lactoglobulin-Based Nanocomplexes Composed of Chitosan Oligosaccharides as Vehicles for Delivery of Astaxanthin. Journal of Agricultural and Food Chemistry, 66(26), 6717–6726. research-article. https://doi.org/10.1021/acs.jafc.8b00834

Luo, Y., Zhang, B., Whent, M., Yu, L. L., & Wang, Q. (2011). Preparation and characterization of zein/chitosan complex for encapsulation of alpha-tocopherol, and its *in vitro* controlled release study. Colloids and Surfaces B: Biointerfaces, 85(2), 145–152. https://doi.org/10.1016/j.colsurfb.2011.02.020

Ma, A., Qu, H., Liu, C., Yan, L., Wang, H., Wang, R., ... Sheng, K. (2018). Formulation and characterization of chitosan hydrochloride and carboxymethyl chitosan encapsulated quercetin nanoparticles for controlled applications in foods system and simulated gastrointestinal condition. Food Hydrocolloids, 84(November 2017), 450–457. https://doi.org/10.1016/j.foodhyd.2018.06.025

Madalena, D. A., Ramos, Ó. L., Pereira, R. N., Bourbon, A. I., Pinheiro, A. C., Malcata, F. X., ... Vicente, A. A. (2016). *In vitro* digestion and stability assessment of β-lactoglobulin/riboflavin nanostructures. Food Hydrocolloids, 58, 89–97. https://doi.org/10.1016/j.foodhyd.2016.02.015

Mansour, A., Abdel-Fattah, A. A., & Soliman, Y. S. (2014). Gamma radiation-induced effects on riboflavin EPR investigation and spectroscopic analyses. Journal of Drug Delivery Science and Technology, 24(1), 105–110. https://doi.org/10.1016/S1773-2247(14)50015-9

Martins, J. T., Santos, S. F., Bourbon, A. I., Pinheiro, A. C., González-Fernández, Á., Pastrana, L. M., ... Vicente, A. A. (2016). Lactoferrin-based nanoparticles as a vehicle for iron in food applications - Development and release profile. Food Research International, 90, 16–24. https://doi.org/10.1016/j.foodres.2016.10.027

McClements, D. J., & Li, Y. (2010). Review of *in vitro* digestion models for rapid screening of emulsion-based systems. Food & Function, 1(1), 32–59. https://doi.org/10.1039/c0fo00111b

Mirpoor, S. F., Hosseini, S. M. H., & Nekoei, A.-R. (2017). Efficient delivery of quercetin after binding to beta-lactoglobulin followed by formation soft-condensed core-shell nanostructures. Food Chemistry, 233, 282–289. https://doi.org/10.1016/j.foodchem.2017.04.126

Monteiro, A. A., Monteiro, M. R., Pereira, R. N., Diniz, R., Costa, A. R., Malcata, F. X., ... Ramos, Ó. L. (2016). Design of bio-based supramolecular structures through self-assembly of α-lactalbumin and lysozyme. Food Hydrocolloids, 58, 60–74. https://doi.org/10.1016/j.foodhyd.2016.02.009

Morrison, P. W. J., Connon, C. J., & Khutoryanskiy, V. V. (2013). Cyclodextrin-mediated enhancement of riboflavin solubility and corneal permeability. Molecular Pharmaceutics, 10(2), 756–762. https://doi.org/10.1021/mp3005963

Musyanovych, A., & Landfester, K. (2014). Polymer micro- and nanocapsules as biological carriers with multifunctional properties. Macromolecular Bioscience, 14(4), 458–477. https://doi.org/10.1002/mabi.201300551

Ni, S., Hu, C., Sun, R., Zhao, G., & Xia, Q. (2017). Nanoemulsions-Based Delivery Systems for Encapsulation of Quercetin: Preparation, Characterization, and Cytotoxicity Studies. Journal of Food Process Engineering, 40(2), e12374. https://doi.org/10.1111/jfpe.12374

O'Neill, G. J., Jacquier, J. C., Mukhopadhya, A., Egan, T., O'Sullivan, M., Sweeney, T., & O'Riordan, E. D. (2015). *In vitro* and *in vivo* evaluation of whey protein hydrogels for oral delivery of riboflavin. Journal of Functional Foods, 19, 512–521. https://doi.org/10.1016/j.jff.2015.09.043

Orsuwan, A., Kwon, S., Bumbudsanpharoke, N., & Ko, S. (2019). Novel LDPE-riboflavin composite film with dual function of broad-spectrum light barrier and antimicrobial activity. Food Control, 100(January), 176–182. https://doi.org/10.1016/j.foodcont.2019.01.012

Patel, A. R., Heussen, P. C. M., Hazekamp, J., Drost, E., & Velikov, K. P. (2012). Quercetin loaded biopolymeric colloidal particles prepared by simultaneous precipitation of quercetin with hydrophobic protein in aqueous medium. In Food Chemistry (Vol. 133, pp. 423–429). Elsevier Ltd. https://doi.org/10.1016/j.foodchem.2012.01.054

Pinheiro, A. C., Bourbon, A. I., Quintas, M. A. C., Coimbra, M. A., & Vicente, A. A. (2012). K-Carrageenan/Chitosan Nanolayered Coating for Controlled Release of a Model Bioactive Compound. Innovative Food Science and Emerging Technologies, 16, 227–232. https://doi.org/10.1016/j.ifset.2012.06.004

Pinheiro, A. C., Gonçalves, R. F. S., Madalena, D. A., & Vicente, A. A. (2017). Towards the understanding of the behavior of bio-based nanostructures during *in vitro* digestion. Current Opinion in Food Science. https://doi.org/10.1016/j.cofs.2017.06.005

Ramos, Ó. L., Fernandes, J. C., Silva, S. I., Pintado, M. E., & Malcata, F. X. (2012). Edible Films and Coatings from Whey Proteins: A Review on Formulation, and on Mechanical and Bioactive Properties. Critical Reviews in Food Science and Nutrition, 52(6), 533–552. https://doi.org/10.1080/10408398.2010.500528

Ramos, O. L., Pereira, R. N., Martins, A., Rodrigues, R., Fuciños, C., Teixeira, J. a., … Vicente, A. a. (2017). Design of Whey Protein Nanostructures for Incorporation and Release of Nutraceutical Compounds in Food. Critical Reviews in Food Science and Nutrition, 57(7), 1377–1393. https://doi.org/10.1080/10408398.2014.993749

Ramos, O. L., Pereira, R. N., Rodrigues, R. M., Teixeira, J. A., Vicente, A. A., & Malcata, F. X. (2015). Whey and Whey Powders: Production and Uses. Encyclopedia of Food and Health (1st ed.). Elsevier Ltd. https://doi.org/10.1016/B978-0-12-384947-2.00747-9

Ramos, O., Pereira, R. N., Rodrigues, R., Teixeira, J. A., Vicente, A. A., & Xavier Malcata, F. (2014). Physical effects upon whey protein aggregation for nano-coating production. Food Research International, 66, 344–355. https://doi.org/10.1016/j.foodres.2014.09.036

Sedaghat Doost, A., Muhammad, D. R. A., Stevens, C. V., Dewettinck, K., & Van der Meeren, P. (2018). Fabrication and characterization of quercetin loaded almond gum-shellac nanoparticles prepared by antisolvent precipitation. Food Hydrocolloids, 83, 190–201. https://doi.org/10.1016/j.foodhyd.2018.04.050

Shafaei, Z., Ghalandari, B., Vaseghi, A., Divsalar, A., Haertlé, T., Saboury, A. A., & Sawyer, L. (2017). β-Lactoglobulin: An efficient nanocarrier for advanced delivery systems.

Nanomedicine: Nanotechnology, Biology, and Medicine, 13(5), 1685–1692. https://doi.org/10.1016/j.nano.2017.03.007

Shpigelman, A., Cohen, Y., & Livney, Y. D. (2012). Thermally-induced β-lactoglobulin-EGCG nanovehicles: Loading, stability, sensory and digestive-release study. Food Hydrocolloids, 29(1), 57–67. https://doi.org/10.1016/j.foodhyd.2012.01.016

Simões, L. S., Madalena, D. A., Pinheiro, A. C., Teixeira, J. A., Vicente, A. A., & Ramos, Ó. L. (2017). Micro- and nano bio-based delivery systems for food applications: *In vitro* behavior. Advances in Colloid and Interface Science, 243, 23–45. https://doi.org/10.1016/j.cis.2017.02.010

Singh, K., Hussain, I., Mishra, V., & Akhtar, M. S. (2019). New insight on 8-anilino-1-naphthalene sulfonic acid interaction with TgFNR for hydrophobic exposure analysis. International Journal of Biological Macromolecules, 122, 636–643. https://doi.org/10.1016/j.ijbiomac.2018.10.208

Wang, Q., Ren, Y., Ding, Y., Xu, M., & Chen, B. (2018). The influence of pH and enzyme cross-linking on protein delivery properties of WPI-beet pectin complexes. Food Research International, 105, 678–685. https://doi.org/10.1016/j.foodres.2017.11.076

Wichchukit, S., Oztop, M. H., McCarthy, M. J., & McCarthy, K. L. (2013). Whey protein/alginate beads as carriers of a bioactive component. Food Hydrocolloids, 33(1), 66–73. https://doi.org/10.1016/j.foodhyd.2013.02.013

Wijaya, W., Harfieyanto, R. C., Dewettinck, K., Patel, A. R., & Van der Meeren, P. (2019). Whey protein isolate–low methoxyl pectin nanocomplexes improve physicochemical and stability properties of quercetin in a model fat-free beverage. Food & Function, 1–11. https://doi.org/10.1039/c8fo02350f

Xu, H., Lu, Y., Zhang, T., Liu, K., Liu, L., He, Z., … Wu, X. (2019). Characterization of binding interactions of anthraquinones and bovine β-lactoglobulin. Food Chemistry, 281(2018), 28–35. https://doi.org/10.1016/j.foodchem.2018.12.077

Yan, L., Wang, R., Wang, H., Sheng, K., Liu, C., Qu, H., … Zheng, A. (2018). Formulation and characterization of chitosan hydrochloride and carboxymethyl chitosan encapsulated quercetin nanoparticles for controlled applications in foods system and simulated gastrointestinal condition. Food Hydrocolloids, 84(November 2017), 450–457. https://doi.org/10.1016/j.foodhyd.2018.06.025

Ye, Q., Woo, M. W., & Selomulya, C. (2019). Modification of molecular conformation of spray-dried whey protein microparticles improving digestibility and release characteristics. Food Chemistry, 280(December 2018), 255–261. https://doi.org/10.1016/j.foodchem.2018.12.074

Yi, J., Fan, Y., Zhang, Y., Wen, Z., Zhao, L., & Lu, Y. (2016). Glycosylated α-lactalbumin-based nanocomplex for curcumin: Physicochemical stability and DPPH-scavenging activity. Food Hydrocolloids, 61, 369–377. https://doi.org/10.1016/j.foodhyd.2016.05.036

Yoshizawa, S., Arakawa, T., & Shiraki, K. (2014). Dependence of ethanol effects on protein charges. International Journal of Biological Macromolecules, 68, 169–172. https://doi.org/10.1016/j.ijbiomac.2014.04.041

Zagury, Y., Kazir, M., & Livney, Y. D. (2019). Improved antioxidant activity, bioaccessibility and bioavailability of EGCG by delivery in β-lactoglobulin particles. Journal of Functional Foods, 52(October 2018), 121–130. https://doi.org/10.1016/j.jff.2018.10.025

Zhang, J., Teng, Z., Yuan, Y., Zeng, Q. Z., Lou, Z., Lee, S. H., & Wang, Q. (2018). Development, physicochemical characterization and cytotoxicity of selenium nanoparticles stabilized by beta-lactoglobulin. International Journal of Biological Macromolecules, 107, 1406–1413. https://doi.org/10.1016/j.ijbiomac.2017.09.117

Zhang, P., Zhao, S. R., Li, J. X., Hong, L., Raja, M. A., Yu, L. J., & Liu, C. G. (2016). Nanoparticles based on phenylalanine ethyl ester-alginate conjugate as Vitamin B2 delivery system. Journal of Biomaterials Applications, 31(1), 13–22. https://doi.org/10.1177/0885328216630497

Zou, L., Zheng, B., Zhang, R., Zhang, Z., Liu, W., Liu, C., ... McClements, D. J. (2016). Food-grade nanoparticles for encapsulation, protection and delivery of curcumin: comparison of lipid, protein, and phospholipid nanoparticles under simulated gastrointestinal conditions. RSC Advances, 6(4), 3126–3136. https://doi.org/10.1039/C5RA22834D

CHAPTER 6.

β-lactoglobulin micro- and nanostructures as bioactive model compounds vehicle: *In vitro* studies

6.1. Introduction 110

6.2. Results and discussion 112

6.3. Conclusions 130

6.4. References 130

This Chapter was adapted from:

Simões, Lívia S.; Martins, Joana T.; Pinheiro, Ana C.; Vicente, António A.; Ramos, Oscar L. β-lactoglobulin micro- and nanostructures as bioactive model compounds vehicle: *In vitro* studies. Food Research International. Submitted in August 10, 2019.

6.1. Introduction

The steady interest on the improvement of food quality and human health led to a growing use of bioactive compounds level in food products (Chen et al., 2016). Commonly, challenges regarding to their inclusion in food products are attributed to the poor solubility (e.g., hydrophobic compounds) in food matrices and their instability along the digestion process (Bourbon et al., 2018). Thus, to overcome these factors, designing of an appropriate bio-based system to transport and deliver bioactive compounds to a specific target site is of utmost importance (Gonçalves et al., 2018).

β-lactoglobulin (β-Lg) is one the most abundant whey proteins (ca. 50 – 60 %) present in bovine serum (Samadarsi & Dutta, 2019). This protein has nutritional and functional features (e.g., gelation capacity) which allows the formation of structures with distinct properties and morphologies (Ramos et al., 2012). These characteristics enable its use as an oral vehicle system of bioactive compounds in food products (Singh & Sarkar, 2011). Our previous results demonstrated that β-Lg samples purity level similar to a commercial β-Lg sample obtained from purification of a commercial whey protein isolate was able to form β-Lg micro- (with diameters between 200 – 300 nm) and nano (diameters ≤ 100 nm) structures (Chapter 4). Also, these structures successfully associated hydrophilic (i.e., riboflavin) and hydrophobic (i.e., quercetin) bioactive model compounds. In addition, β-Lg micro- and nanostructures maintained the stability, when subjected to various environmental conditions, and the release properties, in two food simulants with different hydrophobicities under different temperatures (4 °C and 25 °C) (Chapter 5). Despite all these findings, β-Lg micro- and nanostructures need to assure bioactive compounds' bioaccessibility in the gastrointestinal (GI) tract to exert their bioactivity at a specific target tissues (Rein et al., 2012). *In vitro* digestion models have been used as a tool for understanding the influence of complex physicochemical and physiological processes on β-Lg bio-based structures and on the release of bioactive compounds from those structures when they pass through the different regions of the GI tract (Pinheiro et. al 2017; Pinheiro et al. 2013). Caco-2 cells derived from human colon adenocarcinoma have similar properties to the small intestine layer (Tibolla et al., 2018). Thus, these cells gain a prominence in *in vitro* assays because they mimic the absorption of the bioactive compound through the intestinal membrane and they can be used for toxicological assessment (Tibolla et al., 2019).

Few *in vitro* studies were found in the literature regarding β-Lg structures associated with bioactive compounds. Madalena et al. (2016) studied the β-Lg/riboflavin (hydrophilic compound)

nanostructures during static *in vitro* GI digestion to improve the bioactive compound bioavailability. These authors concluded that β-Lg/riboflavin nanostructures act as a vehicle for riboflavin until it reaches the intestine (i.e., target site), where the protein degradation occurs. Moreover, they demonstrated that 12 % of riboflavin recommended daily dose reached the intestine if 100 mL of a food simulant solution was ingested. Le Maux et al. (2013) investigated the potential changes in β-Lg/linoleate (hydrophobic compound) complex after static *in vitro* digestion, as well as the linoleate acid bioaccessibility and their intracellular transport into Caco-2 cells. These authors demonstrated that binding β-Lg to linoleic acid influences the protein susceptibility to digestion. Also, β-Lg was capable to modify linoleic acid transport and metabolism on Caco-2 cells. Although these researches had underlined the importance of the *in vitro* studies, there is limited information available regarding the *in vitro* simulated mouth phase and the use of other bioactive compounds in such structures. Moreover, information is very scarce or inexistent about the potential effect of different β-Lg particle size structures – micro (diameters between 200 – 300 nm) and nano (diameters ≤ 100 nm) – on the bioavailability of bioactive compounds with different solubilities. In this sense, the harmonized INFOGEST *in vitro* digestion model was used, which mimics the main *in vivo* physiological digestion conditions (i.e., temperature, pH, ionic strength and residence time), exhibiting a simple and standard methodology and, that allow the comparison with other researches who use the same procedure. The present work provides information about bioactive compounds' cytotoxicity through Caco-2 cell monolayer. This research also evaluates the behaviour of β-Lg micro- and nanostructures associated with two bioactive model compounds with different solubilities – riboflavin, as hydrophilic model compound, and quercetin as hydrophilic model compound. Bioaccessibility, stability and bioavailability of both bioactive model compounds were assessed and compared with their respective free bioactive compounds form. Additionally, β-Lg micro- and nanostructures hydrolysates during *in vitro* GI tract were evaluated. The final intention is to provide useful information about the impact of β-Lg micro- and nanostructures on the oral bioavailability of bioactive compounds with distinct solubilities.

6.2. Results and discussion

6.2.1. β-Lg micro- and nanostructures effect on cell viability

6.2.1.1. Cell viability

It is important to assess riboflavin and quercetin cytotoxicity once the presence of toxic substances may causes damage to cells and leads to losses in the efficiency of bioactive compounds absorption loss (Sedaghat Doost et al., 2019). However, it was reported that bile salts compounds (i.e., glycine and taurine conjugates of cholic acid or deoxycholic acid sodium salt mixtures) may be toxic to cells, leading to DNA damage (Benedetti et al., 1997; Yi et al., 2015). In this sense, the potential cytotoxicity of initial (i.e., before *in vitro* digestion) of β-Lg micro- and nanostructure samples were evaluated on Caco-2 cells after 24 h of exposure (Figure 6.1).

Figure 6.1A showed the potential adverse effect of β-Lg micro- and nano-structures with or without riboflavin and free riboflavin on Caco-2 cells. Overall, the cell viability decreased as the exposure concentration increased ($p \leq 0.05$*).* According to the literature, β-Lg is a Generally Recognized As Safe (GRAS) bio-based material (Ramos et al., 2017; Tavares et al., 2017) and riboflavin is an essential compound for the human body (Madadlou et al., 2018; Madalena et al., 2016; O'Neill et al., 2015). Thus, the adverse effect of such structures could be related to their concentration. The Caco-2 cell exposure to increased concentration of riboflavin and quercetin presumably indicated an enhance compounds cellular uptake leading to lysosomes saturation, reactive oxygen species (ROS) generation, DNA cells impairment and injured membrane (Tibolla et al., 2018).

β-Lg microstructures without bioactive compounds showed a cell viability between 25.6 and 82.0 %, whereas β-Lg nanostructures' demonstrated a cell viability of ca. 39.5 to 58.5 % ($p \leq 0.05$) (for riboflavin equivalent concentration ranging from 31.5 to 94.5 × 10^{-3} mg mL^{-1}) (Figure 6.1A). Possibly, the particles' size may have an adverse effect on the cellular uptake of β-Lg structures in Caco-2 cells. Structures at nanoscale have a large surface area per unit, which can possibly increase the adherence and interaction with cell membranes, leading to an enhanced cellular uptake of nanostructures (Ha et al., 2015; Quintanilla-Carvajal et al., 2010), and consequently, to a higher cell cytotoxicity.

On the other hand, cytotoxicity results revealed that β-Lg/riboflavin micro- and nanostructures at concentrations ranging from 52.5 to 73.5 × 10^{-3} mg mL^{-1} of riboflavin did not significantly decrease Caco-2 cell viability as compared to the control group (ca. cell viability = 100.0 %) ($p > 0.05$). This behaviour may be attributed to riboflavin protective effect against the possible toxicity caused by β-Lg micro- and nanostructures (Diarrassouba et al., 2013). β-Lg micro- and nanostructures with

riboflavin associated (Figure 6.5A) at concentration of 21 × 10^{-3} mg mL^{-1} showed cell viabilities higher than 90 % for all samples tested. This result (21 × 10^{-3} mg mL^{-1} riboflavin) indicated that β-Lg/riboflavin microstructures (12.8 × 10^{-3} mg mL^{-1} β-Lg microstructures) and β-Lg/riboflavin nanostructures (16.9 × 10^{-3} mg mL^{-1} β-Lg nanostructures) will not cause damage to cells.

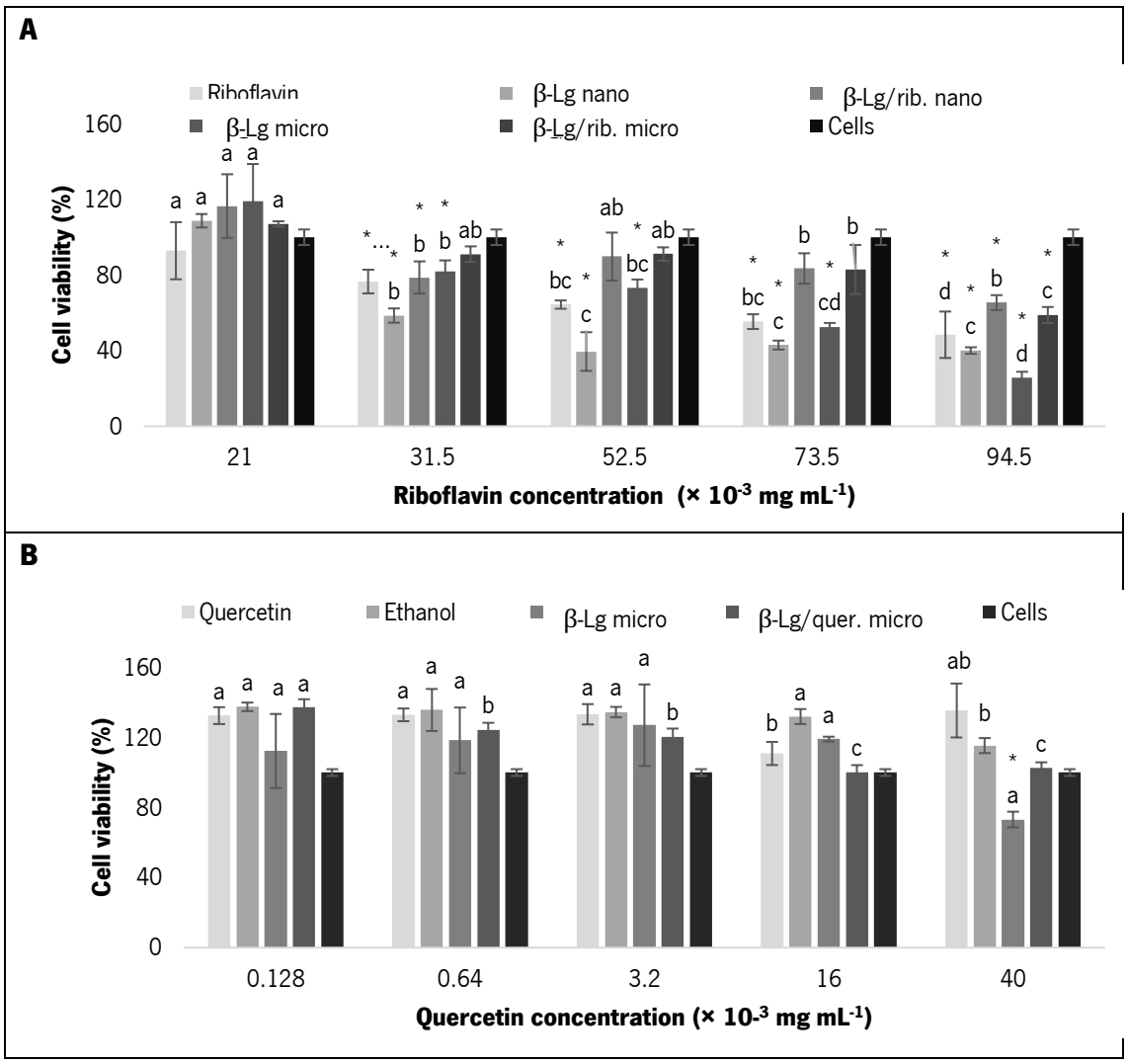


Figure 6.1 - Caco-2 cell viability in contact to β-Lg/riboflavin micro- and nano-structures A) and β-Lg/quercetin micro-structures B) after 24h incubation (bars represent standard deviation). [a,b,c,d] Values with different letter superscripts for the same compound concentration were statistically different ($p \leq 0.05$). The asterisk (*) indicates significant difference ($p \leq 0.05$) relative to the control.

Regarding quercetin cell viability (Figure 6.1B), all samples tested showed 100 % cell viability until 16 × 10^{-3} mg mL^{-1} of quercetin. However, increased concentrations up to 40 × 10^{-3} mg mL^{-1} of β-Lg microstructures, without quercetin, reduced the cell viability to 73.1 %, which demonstrated an adverse effect comparing to the control group ($p \leq 0.05$). Martirosyan et. al. (2016) reported that

silver nanoparticles (particle size < 20 nm) reduced the Caco-2 cell viability, promoting the generation of ROS and reactive nitrogen species (RSN). Nevertheless, 50 μmol L^{-1} of quercetin was able to protect cells against oxidative stress and/or inflammatory activities. Due to quercetin hydrophobic nature, ethanol is often used to dissolve it (Malik et al., 2019). Nonetheless, the organic solvent concentration and cell exposure period may have caused a toxic effect on Caco-2 cell viability (Tseng et al., 2006). Figure 6.1B shows that ethanol at all concentrations tested did not produced cytotoxicity to the cells compared to the control group ($p > 0.05$). From Figure 6.1B, cell viability above 100 % was observed for free quercetin in all concentrations tested. Literature works reported that cytotoxicity is narrowly associated with the oxidative stress in cells (Wang et al., 2014) and as quercetin and its cellular metabolites have antioxidant properties, this compound is able to promote ROS scavenging due to cellular stress (Gonzales et al., 2016). Similar behaviour for other hydrophobic bioactive compound were reported by Le Maux et. al (2012). These authors investigated the *in vitro* cytotoxicity on intestinal epithelial cells of β-Lg as a vehicle of linoleate. They demonstrated an enhanced cell viability compared to the control group at low free bioactive compound concentrations (ranging from 5 to 25 μmol L^{-1}).

Based on Caco-2 cell viability results of β-Lg/quercetin microstructures, the concentration of 16 × 10^{-3} mg mL^{-1} maintained 100 % of cell viability. Therefore, since this structure remained bioavailable at 0.35 × 10^{-3} mg mL^{-1} of quercetin, this is an indication that the β-Lg/quercetin microstructures produced could be used without potential risk to cells.

6.2.1.2. Cell permeability

The bioactive compounds absorption is related to its permeability across Caco-2 cells, which mimic the desired intestinal epithelia tight junctions (Pathak & Raghuvanshi, 2015). Table 6.1 summarized the permeability mechanism of riboflavin (21 × 10^{-3} mg mL^{-1}), as well its concentration in apical compartment and after cell lysis.

The Caco-2 cells model is commonly useful to evaluate the bioactive compounds' absorption across the monolayer, the apparent permeability coefficient and the uptake mechanism, for instance absorption or diffusion (Gonçalves et al., 2018).

Table 6.1 - Apparent permeability coefficient (P_{app}) of riboflavin in free form and when associated to micro- and nanostructures in apical compartment and after cell lysis.

	Riboflavin		
	P_{app} ($\times 10^{-5}$ cm s^{-1})	Apical compartment ($\times 10^{-3}$ mg mL^{-1})	Cell lysis ($\times 10^{-3}$ mg mL^{-1})
Free bioactive compound	5.10 ± 0.03^{a}	18.2 ± 0.8^{a}	4.9 ± 0.8^{a}
β-Lg microstructures	$8.10 \pm 2.40^{a,A}$	$21.7 \pm 0.6^{b,A}$	$5.6 \pm 1.1^{a,A}$
β-Lg nanostructures	$6.60 \pm 0.02^{b,A}$	$21.5 \pm 0.8^{b,A}$	$4.6 \pm 0.5^{a,A}$

NOTE: Data were expressed as mean ± standard deviation (n = 3). ^{a,b}Small letter superscripts in the same column were statistically different from control (free bioactive compound) ($p \leq 0.05$). ^{A,B}Capital letter superscripts in the same column were statistically different between β-Lg structures ($p \leq 0.05$).

According to Table 6.1, the apparent permeability coefficient (P_{app}) of riboflavin through Caco-2 cells was statistically enhanced ($p \leq 0.05$) using β-Lg/riboflavin nanostructures (6.60 ± 0.02) x 10^{-5} cm s^{-1}, when compared to riboflavin in free form (5.10 ± 0.03) x 10^{-5} cm s^{-1}. The higher riboflavin permeability rate may be attributed to small size and large surface area of β-Lg nanostructures. A study conducted by Zielinska-Dawinziak et. al (2009) evaluated the transport of high riboflavin concentrations across Caco-2 intestinal epithelial cells. The authors concluded that at low riboflavin concentrations (at 25 and 42 μmol L^{-1}), the main mechanism was active transport, whereas at high bioactive compound concentrations (at 95 and 114 μmol L^{-1}), the main mechanism was the passive transport. On the other hand, β-Lg/riboflavin microstructures (Table 6.1) revealed a P_{app} of (8.10 ± 2.4) x 10^{-5} cm s^{-1}, but comparing with riboflavin in free form, it was not statistically different ($p > 0.05$). The P_{app} value of β-Lg/riboflavin microstructures shown a high value of the standard deviation, which may be related to the surface area-to-volume ratio of β-Lg/riboflavin microstructures and compromise the riboflavin transport across Caco-2 cell.

Regarding quercetin (results not showed), after 4 h of evaluating the permeability at 80 μg mL^{-1} of quercetin in free form and β-Lg/quercetin microstructures across the Caco-2 cell, the bioactive compound was not detected in the basolateral side, in the apical compartment and after cell lysis. So, Caco-2 cells may have absorbed the quercetin and transformed it in others compounds (Wang

et al., 2016). β-Lg/quercetin microstructures were not capable of transporting the bioactive compounds across the monolayer. Gonzales et al., (2016) reported that when Caco-2 cells where exposed to quercetin during 24 h, the cellular metabolism resulted in its conversion into methyl, glucuronide, and sulfate conjugates, which were mostly secreted into to the culture medium. According to Pangeni et. al (2017), at molecular level, quercetin enhances the barrier function of Caco-2 cells through increasing levels of tight junction proteins, for instance claudin-1, claudin-4, occludin, and zonula occludens-2, thus leading the association of these proteins with the actin cytoskeleton, as well as their assembly at the tight junction. In this sense, further assays of basolateral side with HPLC analysis are required to monitoring the quercetin metabolites across the monolayer and thus confirm the behaviour of quercetin interaction with Caco-2 cells.

6.2.2. Evaluation of β-Lg micro- and nanostructures responsiveness along *in vitro* digestion process

In order to evaluate the structural properties of β-Lg micro- and nanostructures during *in vitro* digestion, initial samples (i.e., before *in vitro* digestion) and samples collected in each digestion phase (i.e., oral, gastric and intestinal) were analysed in terms of particle size, PDI and surface charge by DLS (Table 6.2).

β-Lg microstructures' initial samples exhibited an average particle size ranging from 205.3 ± 3.8 to 235.7 ± 7.8 nm. whereas β-Lg nanostructures initial samples showed average particle sizes between 58.0 ± 1.7 and 79.4 ± 2.2 nm (Table 6.1). PDI values demonstrated that these structures were homogenous with a narrow size distribution (PDI < 0.25). These results were consistent with our previous research (Chapter 5).

After mimicking the mouth digestion phase, β-Lg micro- and nanostructures size and PDI values remained similar to the values of initial samples ($p > 0.05$), indicating that β-Lg structures were stable and maintained the initial characteristics under simulated oral phase with salivary fluids. The surface charge values suggested that electrostatic repulsion among the particles was sufficiently high enough to prevent aggregation. Taking in consideration the β-Lg micro- and nanostructures as a potential oral delivery system, it is crucial to guarantee the protein structural properties until reaching the intestine (McClements, 2015).

Table 6.2 - Particle size, polydispersity index (PDI) and surface charge (S) of β-Lg micro- and nanostructures in each *in vitro* digestion phase.

Structure	*In vitro* digestion phase	Particle size (nm)	PDI	S (mV)
β-Lg micro	Initial	235.7 ± 7.8^{a}	0.14 ± 0.06^{a}	-19.7 ± 2.1^{a}
	Oral	226.0 ± 8.6^{a}	0.20 ± 0.03^{a}	-21.6 ± 0.8^{a}
	Gastric	3853.7 ± 509.7^{b}	0.34 ± 0.14^{ab}	1.0 ± 0.2^{b}
	Intestinal	529.1 ± 44.0^{c}	0.43 ± 0.12^{b}	-24.3 ± 0.6^{c}
β-Lg/riboflavin micro	Initial	205.3 ± 3.8^{a}	0.23 ± 0.03^{a}	-21.8 ± 1.6^{a}
	Oral	193.2 ± 6.6^{a}	0.27 ± 0.06^{a}	-23.8 ± 1.4^{a}
	Gastric	2655.7 ± 362.8^{b}	0.53 ± 0.08^{b}	11.1 ± 0.4^{b}
	Intestinal	547.1 ± 40.7^{c}	0.72 ± 0.11^{c}	-23.2 ± 0.5^{a}
β-Lg/quercetin micro	Initial	224.4 ± 6.4^{a}	0.18 ± 0.03^{a}	-18.5 ± 1.1^{a}
	Oral	210.7 ± 3.2^{a}	0.17 ± 0.03^{a}	-21.0 ± 1.1^{b}
	Gastric	3136.9 ± 220.1^{b}	0.69 ± 0.16^{b}	2.0 ± 0.4^{c}
	Intestinal	538.6 ± 30.8^{c}	0.46 ± 0.15^{c}	-21.4 ± 0.6^{b}
β-Lg nano	Initial	58.0 ± 1.7^{a}	0.24 ± 0.01^{a}	-16.8 ± 1.0^{a}
	Oral	66.6 ± 2.8^{a}	0.37 ± 0.02^{a}	-16.9 ± 2.2^{a}
	Gastric	1291.7 ± 136.1^{b}	0.78 ± 0.09^{b}	-1.5 ± 0.3^{b}
	Intestinal	582.4 ± 39.9^{c}	0.63 ± 0.12^{c}	-22.6 ± 0.9^{c}
β-Lg/riboflavin nano	Initial	79.4 ± 2.2^{a}	0.23 ± 0.01^{a}	-16.5 ± 0.3^{a}
	Oral	79.5 ± 2.7^{a}	0.25 ± 0.01^{a}	-16.2 ± 2.2^{a}
	Gastric	4017.5 ± 497.6^{b}	0.97 ± 0.05^{b}	0.9 ± 0.5^{b}
	Intestinal	600.8 ± 44.8^{c}	0.66 ± 0.06^{c}	-24.3 ± 0.6^{c}

NOTE: ^{a,b,c} Different superscript letters indicate statistical difference in the same column between *in vitro* digestion phase mean values ($p \leq 0.05$) for the same β-Lg structure.

After β-Lg micro- and nano-structures pass from the simulated oral to gastric phase (Table 6.2), an increase of particles' size was observed ($p \leq 0.05$), suggesting that β-Lg structures at simulated gastric phase tend to agglomerate. These changes were accompanied by β-Lg structures instability,

due to surface charge close to 0 mV, and heterogeneity, characterized by high PDI values (> 0.34) (Table 6.1). Indeed, the stomach environment is characterized by high acidity (i.e., pH value ranging from 1 to 3) and ionic strength (values around 100 mmol L^{-1}) (Gonçalves et al., 2018). Considering that β-Lg micro- and nanostructures samples were initially at pH 6 and their isoelectric point (pI) is near pH 4.8, this could explain the results obtained in the gastric phase. The transition to gastric phase might promote changes in the interfacial composition leading to β-Lg micro- and nanostructures aggregation. Some authors reported similar behaviour for β-Lg and other structures. For instance, Madalena et al. (2016) described that β-Lg/riboflavin nanostructures particle size increased (from 232 ± 21 nm to 329 ± 23 nm) after simulated gastric phase. Pinheiro et al. (2013) evaluated oil-in-water nanoemulsions with curcumin in a "human gastric simulator" and described the influence of highly acidic conditions on particle size in the stomach phase. However, the authors reported that it was not possible to determine the precise mechanism involved on the structural changes (Pinheiro et al., 2013).

Results from the intestinal phase showed that surface charge of β-Lg micro- and nanostructures decreased to approximately -22 mV (Table 6.2), which were very similar to surface charge values of the β-Lg structure samples before *in vitro* digestion. This behaviour can be attributed to pH changing to 7 in intestinal phase and/or due adsorption of bile salts and electrolytes on sample surface (Hur et al., 2009; Pinheiro et al., 2013). Comparing to gastric phase digestion, it was observed a decrease of β-Lg micro- and nanostructures' particle sizes ($p \leq 0.05$) in simulated intestinal phase; however, samples remained heterogeneous (PDI > 0.72). These large particles sizes were due to precipitates formed during *in vitro* digestion.

β-Lg micro- and nanostructures with and without a bioactive model compounds associated revealed similar behaviour for particle size, PDI and surface charge. Therefore, the structural properties of β-Lg micro- and nano-structures, during *in vitro* digestion process, were further characterized by native-PAGE and primary amine amino groups quantification.

6.2.3. β-Lg micro- and nanostructures hydrolysis degree during *in vitro* digestion

In order to predict the extent of β-Lg micro- and nanostructures hydrolysis during *in vitro* digestion, the TNBSA assay was performed to determine the number of peptide bonds cleaved (Figure 6.2)

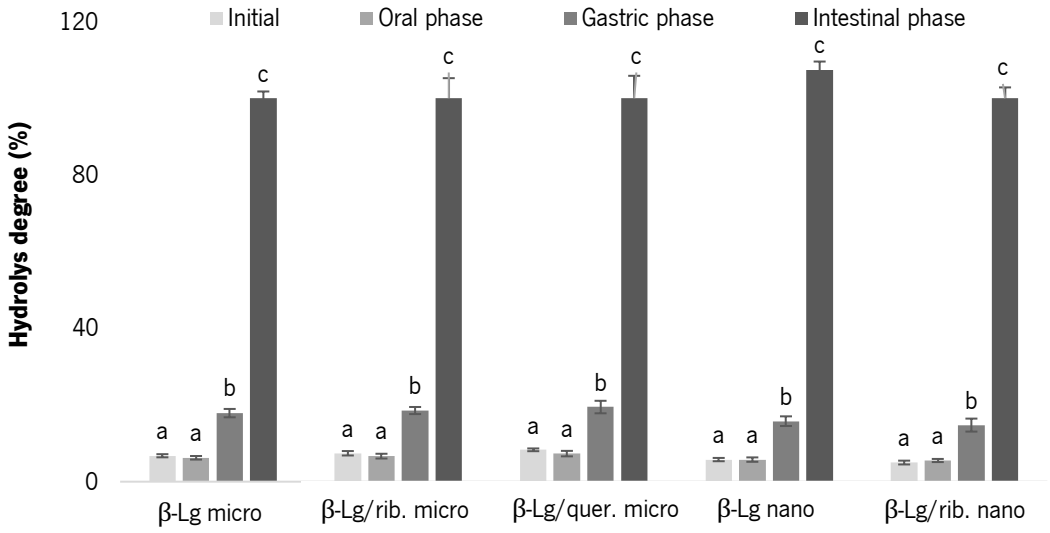


Figure 6.2 - Hydrolysis degree (%) of β-micro and nanostructures with (or without) bioactive riboflavin (rib.) and quercetin (quer.) model compounds during *in vitro* digestion. [a,b,c] Small superscript letters in each column indicate statistical difference between means ($p \leq 0.05$) for the same β-Lg structure.

The TNBSA method determines the amount of primary amine molecules in the system (Spellman et.al, 2003). As the peptide bonds of β-Lg structures were cleaving during *in vitro* digestion, the number of free amino groups increased and consequently, the hydrolysis degree (*HD*) increased. The TNBSA results (Figure 6.2) revealed that *HD* of the initial samples (i.e., before *in vitro* digestion) and of the samples under simulated oral phase were maintained at values lower than 8.3 %. In both conditions, no statically significant differences ($p > 0.05$) were observed, independently of β-Lg structures studied. Additionally, the *HD* profile observed for β-Lg micro- and nanostructures in initial and oral phases was very similar to the ones observed to β-Lg micro- and nanostructures with associated bioactive compounds. This behaviour was consistent with DLS data (Table 6.2), which showed that particle size, PDI and surface charge were maintained in initial and oral phases. Subsequently, after 2 h under gastric phase, it was obtained a slight enhance of β-Lg structures *HD* to a maximum of 19.5 % ($p \leq 0.05$). Generally, food proteins are usually hydrolysed in the stomach environment (Zhang & Vardhanabhuti, 2014). Bourbon et al. (2018) evaluated both lactoferrin (Lf) and glycomacropeptide (GMP) nanohydrogels hydrolysis using an *in vitro* dynamic GI model. These authors observed that at least 45 % of Lf and 70 % of GMP remain undigested after simulated gastric phase. Our results demonstrated that 80.5 % of β-Lg micro- and nanostructures remained almost intact. β-Lg is highly resistant to proteolytic enzymes and pH

conditions of the stomach due to its stable globular tertiary structure at low pH (i.e., pH < 3) (Ramos et al., 2017). Pepsin is the major enzyme present in the gastric fluid and it has been reported that this enzyme has broad specificity with a preference for hydrophobic residues (Luo et al., 2015; Zhang & Vardhanabhuti, 2014). Nonetheless, the highly hydrophobic β-barrel present inside the β-Lg structure hampers pepsin to access target peptide bonds (Bateman et al., 2010). These features are crucial to maintain the protein structure, form and activity until attaining the delivery target (Bourbon et al., 2018).

After β-Lg micro- and nanostructures having been exposed to simulated intestinal conditions, the *HD* reached 100 % (Figure 6.1), indicating a complete hydrolysis of the β-Lg structures. This result can be attributed to the proteolytic action of pancreatin, which digested β-Lg micro- and nanostructures into smaller peptides (Mantovani et al., 2017). These results are in agreement with others authors. Guo et. al (2017) produced β-Lg nanoparticles for caffeine encapsulation and evaluated their behaviour upon *in vitro* digestion. The authors observed that caffeine remained entrapped in β-Lg nanoparticles under the harsh stomach environment. However, a total release of the bioactive compound was achieved in intestinal conditions. Mandalari et al., (2009) proposed a work on a β-Lg *in vitro* digestion under simulated human gastric and duodenal conditions focused on the digestibility of protein. They reported that β-Lg resists to physiological gastric digestion, being susceptible to degradation during duodenal digestion. Another interesting approach based on *in vivo* studies using force-fed rats was assessed by Diarrassouba et al. (2015) to enhance the bioavailability of vitamin D_3 associated with β-Lg nanoparticles. The authors demonstrated that β-Lg nanoparticles were degraded and the bioactive compound released in the rat intestine.

To further explore the β-Lg micro- and nanostructures hydrolysis, a native-PAGE electrophoresis was carried out.

6.2.4. Native polyacrylamide gel electrophoresis (Native-PAGE)

Native-PAGE electrophoresis is a complementary technique used to provide new insights on β-Lg structures hydrolysis during *in vitro* digestion. Figure 6.3 shows Native-PAGE series with sample band patterns, which allowed a better elucidation on the β-Lg structures hydrolysis as function of the different *in vitro* digestion phases.

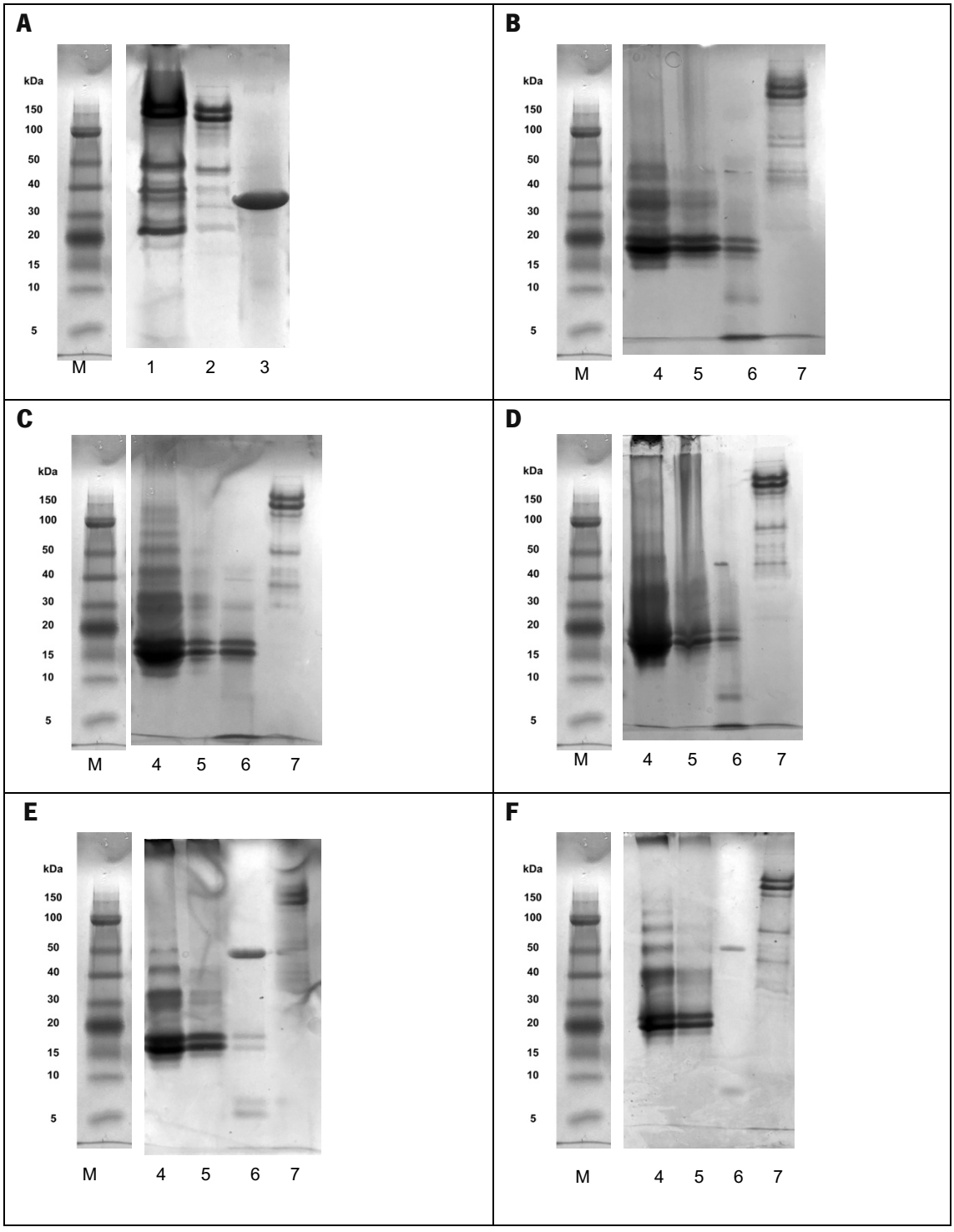


Figure 6.3 - Native-PAGE of *in vitro* digestion samples: control A); β-Lg microstructures B); β-Lg microstructures with riboflavin C); β-Lg microstructures with quercetin D); β-Lg nanostructures E); and β-Lg nanostructures with riboflavin F). The lanes represent: commercial molecular weight marker M) intestinal phase of *in vitro* digestion without sample 1); pancreatin from porcine pancreas 2); pepsin from porcine gastric mucous a 3); initial β-Lg structures (before *in vitro* digestion) 4); oral phase 5); gastric phase 6) and intestinal phase 7).

Gel electrophoresis is a technique for separation and analysis of macromolecules (e.g., proteins) and their fragments according to their molecular weight (M_w) (Arndt et al., 2012). Since pancreatin and pepsin are digestive enzymes (i.e., proteins) (Sullivan et al., 2018) used during *in vitro* digestion it was crucial to identify their M_w, as control samples. Native-PAGE results in Figure 6.3A showed an *in vitro* digestion without samples (lane 1), pancreatin (lane 2) and pepsin (lane 3) profiles. Pancreatin is a mixture of several enzymes, for instance trypsin, amylase and lipase, secreted by the exocrine cells of pigs pancreas (Picariello et al., 2015). Pancreatin sample (lane 2) showed M_w bands corresponding to trypsin (M_w = 20 kDa), amylase (M_w = 45 kDa) and lipase (M_w = 38 kDa) (Shen et al., 2013). Moreover, pepsin (lane 3) was characterized by the presence of a single band with M_w of 30 kDa. These results are in agreement with Peram et. al. (2013) results. These authors evaluated heat-induced β-Lg aggregates upon *in vitro* gastric digestion by native-PAGE electrophoresis and they obtained a M_w = 37 kDa for pepsin. Thus, the bands identified in lanes 2 and 3 were presented in lane 1, which correspond to the final sample taken from the *in vitro* digestion process.

β-Lg structures (with or without bioactive compounds) before *in vitro* digestion revealed similar electrophoretic profiles, showing the major M_w band with values ranging from 15 to 20 kDa (Figures 6.3B - 2F, lane 4). This band was attributed to β-Lg because its M_w is 18.4 kDa (Zagury et al., 2019). It was also observed the presence of a high M_w band which could be related to protein aggregates formed during gelation treatment. These results were consistent with those reported elsewhere (Madalena et al., 2016; Rodrigues et al., 2015).

The electrophoretic profile of β-Lg micro- and nanostructures upon oral phase and gastric phase showed the predominant band with M_w ranging from 15 to 20 kDa (Figures 6.3B – 2E, lanes 5 and 6). These results suggested that β-Lg micro- and nano-structures remained almost intact until the gastric phase – in agreement with the results obtained in TNBSA test. In fact, β-Lg has a highly proteolytic resistant to the gastric conditions (Ramos et al., 2015). Moreover, the band corresponding to the β-Lg (M_w = 18 kDa) was not detected in β-Lg/riboflavin nanostructures' samples after gastric phase (Figure 6.3F, lane 6). Nevertheless, Madalena et al. (2016) studied β-Lg/riboflavin nanostructures throughout digestion, simulating the physiological conditions in the stomach and small intestine using an *in vitro* static GI system. The authors performed a native-PAGE electrophoresis for each *in vitro* digestion phase and obtained a M_w band corresponding to β-Lg after being submitted to gastric conditions. Taking into consideration the results obtained,

including *HD* data of β-Lg/riboflavin nanostructures and their capacity to protect riboflavin (demonstrated by intact bioactive compound results - Figure 6.2), it can be suggested that β-Lg micro- and nanostructures are highly resistant to stomach environment conditions.

Similar electrophoresis profiles were observed comparing β-Lg micro- and nanostructures upon passage by the intestinal phase (Figures 6.3B-2F, lane 7). The band attributed to β-Lg with M_w ranging from 15 to 20 kDa was not observed, suggesting the β-Lg micro- and nanostructures degradation, which is in accordance with protein hydrolysis data of intestinal phase samples (Figure 6.2). Despite the resistance of β-Lg, it was more susceptible to pancreatin degradation (Lassé et al., 2016). β-Lg degradation under intestinal conditions was also reported by Zagury et al., (2019) who conducted a study with β-Lg system to enhance the *in vitro* bioaccesibility of (-)-epigallocatechin-3-gallate. For this purpose, the authors performed a simulated GI digestion of the β-Lg/(-)-epigallocatechin-3-gallate system and obtained β-Lg resistance in simulate gastric conditions and a complete degradation under intestinal environment. Diarrassouba et al., (2013) studied the pH-stability of the β-Lg/vitamin D_3 complex to evaluate the potential impact on the stability of such structures through the GI tract. The authors concluded that β-Lg/D_3 complex remained stable under acidic (pH ranging from 3.0 to 4.0) and alkaline (pH ranging from 6.8 to 8.0) environments, suggesting that this complex could be stable along the digestion process.

6.2.5. Bioactive model compounds behaviour under gastrointestinal environmental conditions

Throughout *in vitro* GI digestion, β-Lg micro- and nanostructures were subjected to several conditions, such as pH changes and enzymatic action. These factors could affect the capacity of such structures to protect bioactive compounds. Therefore, the amounts of intact riboflavin and quercetin in oral, gastric and intestinal phases were assessed (Figure 6.4).

Figure 6.4A shows the intact riboflavin in free form (%) during *in vitro* digestion. Free riboflavin (Figure 6.4A) results showed that only 28.7 ± 0.4 % of their initial concentration (i.e., 0.105 mg mL^{-1}) reached the intestinal phase; thus, it is crucial to use β-Lg structures to protect them from chemical and enzymatic degradation.

On the first phase of digestion (i.e., oral phase with simulated salivary fluid), it was observed a decrease ($p \leq 0.05$) of free riboflavin concentration of ca. 3 % (to 96.6 ± 2.0%) compared with β-Lg/riboflavin micro- (106 ± 5.5 %) and nano (104.9 ± 2.6 %) structures. The harmonized INFOGEST *in vitro* model mimics the oral phase, which is constituted by a neutral environment (i.e., pH 7)

and an electrolyte solution (SSF) (Minekus et al., 2014). Since the presence of ions in the SSF did not affect the β-Lg structure properties (Table 6.2), the observed riboflavin concentration decrease might be attributed to the degradation by light since riboflavin is light sensitive (Beztsinna et al., 2016). Thus, β-Lg micro- and nanostructures might delay the riboflavin degradation in the oral phase.

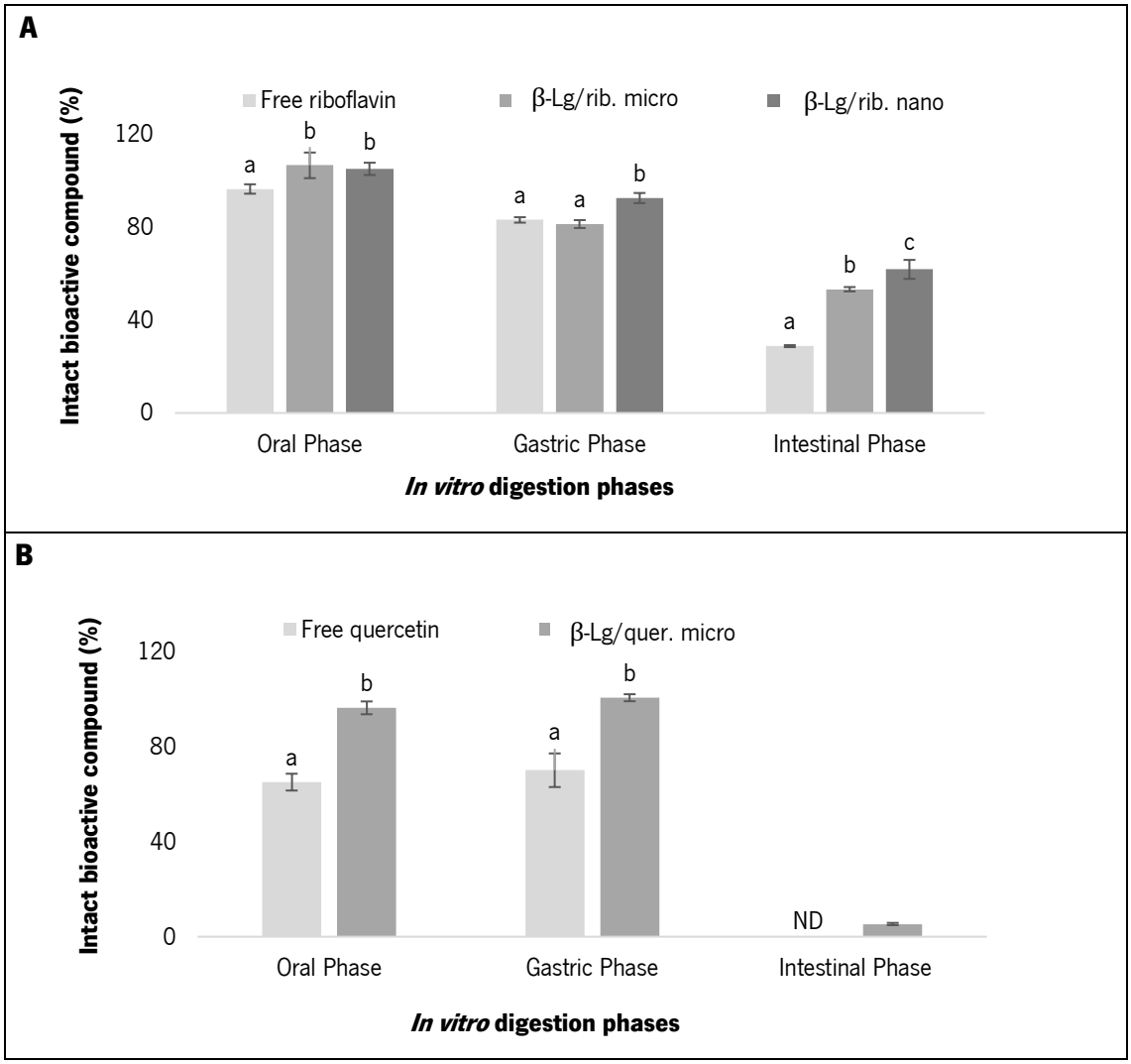


Figure 6.4 - Intact (%) free riboflavin, β-Lg/riboflavin micro- and nanostructures A) and free quercetin and β-Lg/quercetin microstructures B) in oral, gastric and intestinal phases during *in vitro* digestion. Results were present as mean ± standard deviation. [a,b,c] Different small letter superscripts in the same *in vitro* digestion phase correspond to statistically significantly differences ($p \leq 0.05$). ND means that the concentration of quercentin was Not Detected.

In the gastric phase (Figure 6.4A), 81.2 ± 1.7 % of riboflavin from β-Lg/riboflavin microstructure samples were intact. This result was similar ($p > 0.05$) to that obtained for free riboflavin. However,

the percentage of intact riboflavin from β-Lg/riboflavin nanostructures was significantly different ($p \leq 0.05$) from those obtained for riboflavin in free form or for β-Lg/riboflavin microstructures. This behaviour suggests that β-Lg nanostructures were able to better protect riboflavin from degradation at gastric phase than β-Lg microstructures. Intestinal phase results (Figure 6.4A) shown that β-Lg microstructures were able to retain 53.2 ± 0.9 % of intact riboflavin until absorption, whereas β-Lg nanostructures maintained 61.7 ± 4.1% of intact riboflavin ($p \leq 0.05$). The information obtained in this study was consistent with results observed by Maltais et. al (2010). The authors investigated a soy protein filamentous hydrogel for riboflavin release under simulated GI conditions. They observed in simulated gastric fluid with pepsin, that 13 % of total riboflavin was released from hydrogel. It was argued that the low riboflavin release in gastric conditions was due to the soy hydrogel resistance to pepsin. The pepsin resistance was attributed to a low amount of hydrophobic aromatic amino acids available in soy protein hydrogel, which are the preferential cleavage sites of pepsin in proteins. Moreover, the pancreatin in intestinal phase led to the thorough degradation of soy protein filamentous hydrogels and a release of 100 % of the total riboflavin content was observed.

Quercetin content in each *in vitro* digestion phase was also studied (Figure 6.4B). Free quercetin started to be degraded after exposure to simulated oral phase conditions, being the level of intact quercetin of 65.0 ± 3.5 % in relation to the initial quercetin concentration (i.e., 0.8 mg mL^{-1}). The content of free quercetin content was maintained in the gastric phase, being, however, not detected in the intestinal phase (Figure 6.4B). These results demonstrated that quercetin needs to be protected from physiological conditions of the GI tract. Quercetin has poor water solubility (Wang et al., 2014), and requires prior solubilization in an organic solvent, in this case, ethanol. When this ethanolic solution is added in the aqueous system, large precipitates were formed, displaying an atypical needle-like morphology, which is extremely unstable (Patel et al., 2012). Moreover, quercetin also has a low solubility in simulated gastric (5.5 μg mL^{-1}) and intestinal (28.9 μg mL^{-1}) fluids (Gao et al., 2009), which increase the formation of precipitates when quercetin is present in its free form. When quercetin is associated with β-Lg microstructures (Figure 6.4B), it was observed an increase of the content of intact quercetin along the various phases of *in vitro* digestion ($p \leq 0.05$). The content of intact quercetin increased in oral and gastric phases being 96.2 ± 2.5 % and 100.5 ± 1.5 %, respectively, and decreased in the intestinal phase to 5.3 ± 0.5 %. This behaviour may be attributed to the fact that quercetin molecules were protected by the β-Lg microstructures from the surrounding aqueous phase (Chen et al., 2018), avoiding their degradation . Fang et al.,

(2011) developed bovine serum album nanoparticles to encapsulate quercetin and reported that the system could maintain quercetin bioactive properties under both neutral and acidic environments.

6.2.6. Bioactive model compounds bioaccessibility, stability and bioavailability

In the reports found in the literature regarding the food applications, studies about the determination of bioaccessibility, stability, and bioavailability of bioactive compounds are still limited. In this sense, the evaluation of bioaccessibility, stability and bioavailability of riboflavin and quercetin was conducted to fill this gap (Figure 6.5)

Bioaccessibility is related with the fraction of bioactive compound released from the structure and potentially available for absorption (Gonçalves et al., 2018). The riboflavin bioaccessibility results (Figure 6.5A) revealed that 100 % of riboflavin in free form and β-Lg/riboflavin micro- and nanostructures reach the intestinal phase and can be potentially absorbed. This can be due to the water solubility properties of riboflavin that may facilitate a higher passage through the various simulated GI phases. Regarding quercetin bioaccessibility results (Figure 6.5B), this bioactive compound in free form was not capable to reach to intestinal phase and be bioaccessible, which may be attributed to the low solubility of quercetin in simulated intestinal fluid (Chen et al., 2018). The bioaccessibility of quercetin in free form in bulk water was reported to be low (< 5%) when tested at 0.1 and 0.5 mg mL^{-1} (Pool et. al 2013). Nevertheless, β-Lg microstructures enhanced quercetin bioaccessibility (Figure 6.5B) to 47.2 ± 3.9 % ($p \leq 0.05$), which is in agreement with previous studies on protein as a promising vehicle for hydrophobic compounds (Chen et al., 2015). This result may be attributed to the β-Lg microstructures capacity to protect quercetin from the aqueous environment. Also, this suggests that after hydrolysis of β-Lg microstructures under simulated intestinal phase conditions, the presence of digestion products (i.e., mixed micelles) formed by bile salts and bile acids allowed solubilizing free fatty acids, monoacylglycerols and some bioactive compounds (Pinheiro et al., 2016).

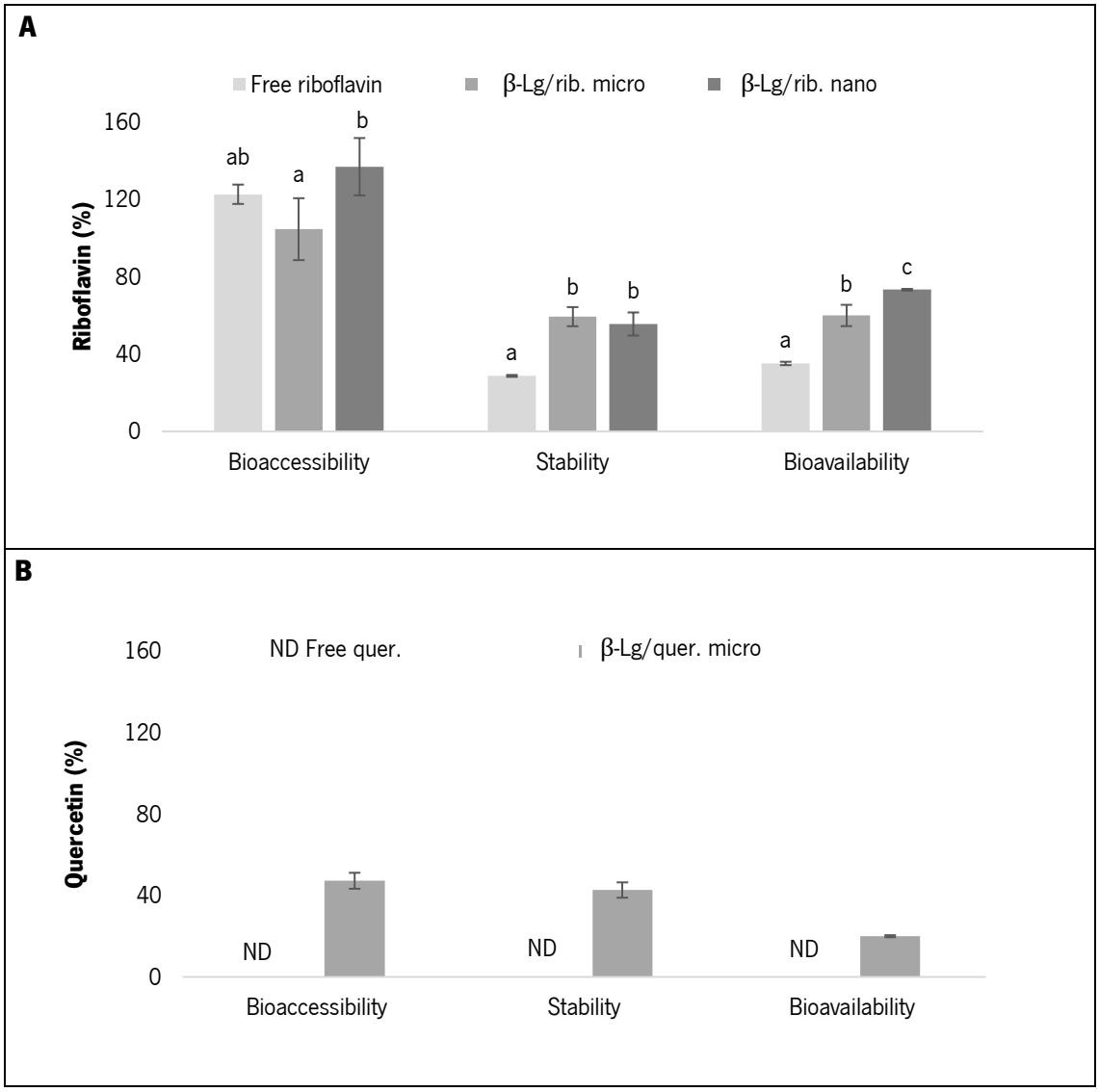


Figure 6.5 - Bioaccessibility, stability and bioavailability of β-Lg/riboflavin micro- and nanostructures A) and β-Lg/quercetin microstructures B). [a,b,c] Samples in the same parameter designated with different letters superscripts are significantly different ($p \leq 0.05$). ND means that the concentration of quercetin was Not Detected.

The susceptibility of β-Lg micro- and nanostructures to the digestion process, may affect the stability of bioactive compounds (Chen et al., 2015), leading to a loss of their bioavailability. The stability of a bioactive compound comprises the fraction which is maintained in a non-transformed state in the intestinal phase after the digestion process (Liu et al., 2018). Based on this consideration, the stability of riboflavin (Figure 6.5A) and quercetin (Figure 6.5B) was assessed. Comparing with riboflavin in free form (Figure 6.5A), β-Lg micro- and nanostructures demonstrated an increase capacity to maintain riboflavin, being 59.3 ± 4.9 % and 55.5 ± 6.0 %, respectively, present in its non-transformed state ($p \leq 0.05$). Moreover, Figure 6.5B showed that β-Lg

microstructures could promote higher stability towards degradation of quercetin 42.7 ± 3.8 % than the quercetin in its free form. These results may indicate that β-Lg micro- and nanostructures are able to preserve such bioactive compounds during an *in vitro* digestion process, preventing their premature degradation and increasing their solubility (in particular for quercetin), and potentially their bioavailability (Ramos et al., 2014).

According to the literature, the term "bioavailability" is related to the amount of the compound ingested, which is absorbed and reaches the systemic circulation to exert its physiological functions (Gonçalves et al., 2018). Comparing with the riboflavin in free form, β-Lg micro- and nanostructures were capable to enhance the bioavailability of riboflavin ($p \leq 0.05$) (Figure 6.5A). Bourbon et al. (2018) observed a similar behaviour when using a dynamic *in vitro* GI model to determine the bioavailable fraction of caffeine (as hydrophilic model compound) using Lf-GMP nanohydrogels with chitosan coating as the encapsulation matrix. The authors obtained a caffeine bioavailability of 63.1 ± 0.2 % when caffeine was associated to nanohydrogels and of 59.2 ± 2.1 % when caffeine is present in its free form. Riboflavin bioavailability (Figure 6.5A) significantly increased ($p \leq 0.05$) when the particle size decreased, being 60.0 ± 5.5 % for β-Lg micro-structures and 73.2 ± 0.4 % for β-Lg nanostructures. Indeed, the reduced size of β-Lg nanostructures may has greater potential in improving the solubility, and bioavailability, in preventing undesirable physical and chemical reactions, as well as in protecting bioactive compounds against degradation (Samadarsi & Dutta, 2019).

As shown in Figure 6.5B, β-Lg/quercetin microstructures demonstrated a prominent enhancement of quercetin absorption, leading to an increase of bioavailability of 20.0 ± 0.5 %, when compared to quercetin in free form. Diarrassouba et al., (2015) evaluated β-Lg-based coagulum matrix as oral delivery system for of vitamin D_3 and obtained an enhanced bioactive compound bioavailability determined by rat plasma analysis.

After assessing the bioaccessible, stable and bioavailable fraction of model bioactive compounds (Figure 6.5), it was possible to determine the effective riboflavin and quercetin concentrations that might be potentially absorbed. First, we considered into account our previous results of association efficiency (*AE*) (Chapter 5), which evaluated the bioactive compound fraction successfully entrapped within structures. The initial riboflavin concentration used was 0.105 mg mL^{-1}, which led to a maximum *AE* of 64.4 % for both β-Lg micro- and nanostructures. In this sense, upon determining the bioaccessibility, stability and bioavailability of riboflavin (Figure 6.5A), β-Lg/riboflavin microstructures were able to maintain 0.013 mg mL^{-1} of riboflavin, while β-

Lg/riboflavin nanostructures were capable to retain 0.017 mg mL^{-1} of riboflavin. Since the recommended daily dose (RDD) for riboflavin is approximately 1.2 mg for adults (Madalena et al., 2016), it will be necessary to incorporate a solution of 93.75 mL of β-Lg/riboflavin microstructures or a solution of 71.00 mL of β-Lg/riboflavin nanostructures into a food product to reach the riboflavin RDD. Regarding quercetin, the initial concentration used was 0.08 mg mL^{-1} and β-Lg/quercetin microstructures revealed 98.0 % of *AE*. Thus, with the results obtained from Figure 6.4B, it was assessed that β-Lg/quercetin micro-structures were able maintain 0.35×10^{-3} mg mL^{-1} of bioavailable quercetin after simulated GI tract. Quercetin, a polyphenolic compound with potentially beneficial effects on human health (e.g., antioxidant, anti-inflammatory and anti-cancer) needs to be consumed at a RDD of 0.015 mg mL^{-1} (Wijaya et al., 2019). Thus, it would be necessary to incorporate a of a solution of 45 mL of β-Lg/quercetin microstructures into a food product to achieve the quercetin RDD. Furthermore, the determination of the quantity of β-Lg/bioactive compound structures solutions does not contemplate possible degradation of the bioactive compounds into complex food matrices; thus, taking this into consideration the final solution quantity to achieve the RDD may be higher.

The solutions of β-Lg structures with bioactive compounds associated intend to incorporate as a food product formulation, for instance, in healthy food products and food supplement system. In these conditions, the final amount ingested of this product by the final consumers to achieve the RDD of bioactive compounds would be inviable. However, assuming that people ingest an amount of riboflavin daily, the purpose is providing an alternative to reach riboflavin RDD. This product may be an option to complement the RDD for people do not have a healthy diet or have a deficiency as a consequence of disease.

Regarding the potential toxicity problem associated with the ingest the bioactive compound amount above the RDD, riboflavin is a hydrophilic compound and is not stored in the human body, consequently the excessive intake results in increased urinary excretion rather than toxicity (Jafari, 2017). Quercetin has a poor water solubility and the excessive intake compromise the urinary excretion, however, the quercetin toxicity is not well understood with a discrepancy in the studies about the potential in case of excessive intake of the bioactive compound (Wang et al., 2016; Chen et al., 2014).

6.3. Conclusions

The cell viability assay revealed that 21 × 10^{-3} mg mL^{-1} riboflavin and 16 × 10^{-3} mg mL^{-1} quercetin, as well as β-Lg micro- and nanostructures in equivalent compounds concentrations were non-toxic to the Caco-2 cells. In addition, the concentration of both bioactive compounds that reached the intestinal phase is lower than these values. Thus, it is not expected that those compounds will not exhibit toxicity towards Caco-2 cells. Therefore, 93.75 mL of a solution of β-Lg/riboflavin microstructures or 71.00 mL of a solution of a solution of β-Lg/riboflavin nanostructures may provide the RDD, while and a 45 mL of a solution of β-Lg/quercetin microstructures may able to ensure the quercetin antioxidant properties. Regarding cell permeability, β-Lg/riboflavin nanostructures were able to enhance the permeability rate in 1.3-fold higher ($p < 0.05$) than the value obtained for the riboflavin free.

In vitro GI digestion results demonstrated that β-Lg micro- and nanostructures were effective in protecting both hydrophilic and hydrophobic bioactive compounds during the gastric phase, thus releasing them in the desirable target site (i.e., intestine), where β-Lg structures were completely hydrolysed. Moreover, the *in vitro* digestion results indicate an improvement of both bioactive compounds fractions bioavailability on β-Lg/riboflavin micro- (60.0 %) and nano (73.2 %) structures, and on β-Lg/quercetin microstructures (20.0 %) when compared to the respective compound in its free form.

Our work results contributed to the improvement of the knowledge regarding the use of β-Lg micro- and nanostructures as an effective oral delivery system strategy to augment the hydrophilic and hydrophobic bioactive compounds' bioavailability. However, further studies will be needed to fully understand the behaviour of β-Lg micro- and nanostructures during digestion for example, using a dynamic GI model that mimics the GI peristaltic movements. Also, it would be important to assess the permeability and absorption rates of both bioactive model compounds across Caco-2/HT-29 cells, once this other system allows simulating the production of mucus on the epithelium, thus mimicking more closely its properties.

6.4. References

Benedetti, A., Alvaro, D., Bassotti, C., Gigliozzi, A., Ferretti, G., La Rosa, T., ... Jezequel, A. M. (1997). Cytotoxicity of bile salts against biliary epithelium: A study in isolated bile ductule fragments and isolated perfused rat liver. Hepatology, 26(1), 9–21. Retrieved from http://ovidsp.ovid.com/ovidweb.cgi?T=JS&PAGE=reference&D=emed7&NEWS=N&AN=27280301

Bourbon, A. I., Pinheiro, A. C., Cerqueira, M. A., & Vicente, A. A. (2018). *In vitro* digestion of lactoferrin-glycomacropeptide nanohydrogels incorporating bioactive compounds: Effect of a chitosan coating. Food Hydrocolloids, 84(February), 267–275. https://doi.org/10.1016/j.foodhyd.2018.06.015.

Chen, R., Lin, J., Hong, J., Han, D., Zhang, A. D., Lan, R., ... Zhang, H. (2014). Potential toxicity of quercetin: The repression of mitochondrial copy number via decreased POLG expression and excessive TFAM expression in irradiated murine bone marrow. Toxicology Reports, 1, 450–458. https://doi.org/10.1016/j.toxrep.2014.07.014

Chen, X., Zou, L., Liu, W., & McClements, D. J. (2016). Potential of Excipient Emulsions for Improving Quercetin Bioaccessibility and Antioxidant Activity: An *in vitro* Study. Journal of Agricultural and Food Chemistry, 64(18), 3653–3660. https://doi.org/10.1021/acs.jafc.6b01056

Diarrassouba, F., Liang, L., Remondetto, G., & Subirade, M. (2013). Nanocomplex formation between riboflavin and β-lactoglobulin: Spectroscopic investigation and biological characterization. Food Research International, 52(2), 557–567. https://doi.org/10.1016/j.foodres.2013.03.025

Gonçalves, R. F. S., Martins, J. T., Duarte, C. M. M., Vicente, A. A., & Pinheiro, A. C. (2018). Advances in nutraceutical delivery systems: From formulation design for bioavailability enhancement to efficacy and safety evaluation. Trends in Food Science and Technology, 78(January), 270–291. https://doi.org/10.1016/j.tifs.2018.06.011

Gonzales, G. B., Smagghe, G., Vissenaekens, H., Grootaert, C., Rajkovic, A., Van de Wiele, T., ... Van Camp, J. (2016). Quercetin mitigates valinomycin-induced cellular stress via stress-induced metabolism and cell uptake. Molecular Nutrition and Food Research, 60(5), 972–980. https://doi.org/10.1002/mnfr.201500999

Ha, H., Kim, J. W., Lee, M., Jun, W., & Lee, W. (2015). Cellular Uptake and Cytotoxicity of β - Lactoglobulin Nanoparticles : The Effects of Particle Size and Surface Charge. Asian Australas. J. Anim. Sci., 28(3), 420–427.

Jafari, S. M. (2017). Nanoencapsulation of Food Bioactive Ingredients - Principles and Applications. (S. M. Jafari, Ed.). Academic Press Ltd./Elsevier Science Ltd.

Le Maux, S., Brodkorb, A., Croguennec, T., Hennessy, A. a, Bouhallab, S., & Giblin, L. (2013). β-Lactoglobulin-linoleate complexes: *In vitro* digestion and the role of protein in fatty acid uptake. Journal of Dairy Science, 96(7), 4258–4268. https://doi.org/10.3168/jds.2013-6682

Le Maux, S., Giblin, L., Croguennec, T., Bouhallab, S., & Brodkorb, A. (2012). β-Lactoglobulin as a molecular carrier of linoleate: Characterization and effects on intestinal epithelial cells *in vitro*. Journal of Agricultural and Food Chemistry, 60(37), 9476–9483. https://doi.org/10.1021/jf3028396

Madadlou, A., Floury, J., Pezennec, S., & Dupont, D. (2018). Encapsulation of β-lactoglobulin within calcium carbonate microparticles and subsequent in situ fabrication of protein microparticles. Food Hydrocolloids, 84(March), 38–46. https://doi.org/10.1016/j.foodhyd.2018.05.054

Madalena, D. A., Ramos, Ó. L., Pereira, R. N., Bourbon, A. I., Pinheiro, A. C., Malcata, F. X., ... Vicente, A. A. (*2016). In vitro* digestion and stability assessment of β-lactoglobulin/riboflavin nanostructures. Food Hydrocolloids, 58, 89–97. https://doi.org/10.1016/j.foodhyd.2016.02.015

Malik, A., Alsenaidy, M. A., Khan, M. I., Khan, R. H., Zamzami, M. A., Husain, F. M., ... Shahzad, S. A. (2019). A quercetin-based flavanoid (rutin) reverses amyloid fibrillation in β-

lactoglobulin at pH 2.0 and 358 K. Spectrochimica Acta Part A: Molecular and Biomolecular Spectroscopy, 214, 40–48. https://doi.org/10.1016/j.saa.2019.02.004

Martirosyan, A., Grintzalis, K., Polet, M., Laloux, L., & Schneider, Y. J. (2016). Tuning the inflammatory response to silver nanoparticles via quercetin in Caco-2 (co-)cultures as model of the human intestinal mucosa. Toxicology Letters, 253, 36–45. https://doi.org/10.1016/j.toxlet.2016.04.018

O'Neill, G. J., Jacquier, J. C., Mukhopadhya, A., Egan, T., O'Sullivan, M., Sweeney, T., & O'Riordan, E. D. (2015). *In vitro* and *in vivo* evaluation of whey protein hydrogels for oral delivery of riboflavin. Journal of Functional Foods, 19, 512–521. https://doi.org/10.1016/j.jff.2015.09.043

Pangeni, R., Kang, S. W., Oak, M., Park, E. Y., & Park, J. W. (2017). Oral delivery of quercetin in oil-in-water nanoemulsion: *In vitro* characterization and *in vivo* anti-obesity efficacy in mice. Journal of Functional Foods, 38, 571–581. https://doi.org/10.1016/j.jff.2017.09.059

Pathak, K., & Raghuvanshi, S. (2015). Oral Bioavailability: Issues and Solutions via Nanoformulations. Clinical Pharmacokinetics, 54(4), 325–357. https://doi.org/10.1007/s40262-015-0242-x

Pinheiro, A. C., Gonçalves, R. F. S., Madalena, D. A., & Vicente, A. A. (2017). Towards the understanding of the behavior of bio-based nanostructures during *in vitro* digestion. Current Opinion in Food Science. https://doi.org/10.1016/j.cofs.2017.06.005

Pinheiro, A. C., Lad, M., Silva, H. D., Coimbra, M. A., Boland, M., & Vicente, A. A. (2013). Unravelling the behaviour of curcumin nanoemulsions during *in vitro* digestion: effect of the surface charge. Soft Matter, 9(11), 3147. https://doi.org/10.1039/c3sm27527b

Quintanilla-Carvajal, M. X., Camacho-Díaz, B. H., Meraz-Torres, L. S., Chanona-Pérez, J. J., Alamilla-Beltrán, L., Jimenéz-Aparicio, A., & Gutiérrez-López, G. F. (2010). Nanoencapsulation: A new trend in food engineering processing. Food Engineering Reviews, 2(1), 39–50. https://doi.org/10.1007/s12393-009-9012-6

Ramos, O. L., Pereira, R. N., Martins, A., Rodrigues, R., Fuciños, C., Teixeira, J. a., … Vicente, A. a. (2017). Design of Whey Protein Nanostructures for Incorporation and Release of Nutraceutical Compounds in Food. Critical Reviews in Food Science and Nutrition, 57(7), 1377–1393. https://doi.org/10.1080/10408398.2014.993749

Ramos, Oscar L., Pereira, J. O., Silva, S. I., Amorim, M. M., Fernandes, J. C., Lopes-da-Silva, J. A., … Malcata, F. X. (2012). Effect of composition of commercial whey protein preparations upon gelation at various pH values. Food Research International, 48(2), 681–689. https://doi.org/10.1016/j.foodres.2012.06.004

Rein, M. J., Renouf, M., Cruz-Hernandez, C., Actis-Goretta, L., Thakkar, S. K., & da Silva Pinto, M. (2012). Bioavailability of bioactive food compounds: A challenging journey to bioefficacy. British Journal of Clinical Pharmacology, 75(3), 588–602. https://doi.org/10.1111/j.1365-2125.2012.04425.x

Samadarsi, R., & Dutta, D. (2019). Design and characterization of mangiferin nanoparticles for oral delivery. Journal of Food Engineering, 247(August 2018), 80–94. https://doi.org/10.1016/j.jfoodeng.2018.11.020

Sedaghat Doost, A., Kassozi, V., Grootaert, C., Claeys, M., Dewettinck, K., Van Camp, J., & Van der Meeren, P. (2019). Self-assembly, functionality, and in-vitro properties of quercetin loaded nanoparticles based on shellac-almond gum biological macromolecules. International Journal of Biological Macromolecules, 129, 1024–1033. https://doi.org/10.1016/j.ijbiomac.2019.02.071

Singh, H., & Sarkar, A. (2011). Behaviour of protein-stabilised emulsions under various physiological conditions. Advances in Colloid and Interface Science, 165(1), 47–57. https://doi.org/10.1016/j.cis.2011.02.001

Tavares, T., Ramos, O. L., & Malcata, F. X. (2017). β-Lactoglobulin microparticles obtained by high intensity ultrasound as a potential delivery system for bioactive peptide concentrate. Journal of Food Science and Technology, 54(13), 4387–4396. https://doi.org/10.1007/s13197-017-2912-1

Tibolla, H., Pelissari, F. M., Martins, J. T., Lanzoni, E. M., Vicente, A. A., Menegalli, F. C., & Cunha, R. L. (2019). Banana starch nanocomposite with cellulose nanofibers isolated from banana peel by enzymatic treatment: *In vitro* cytotoxicity assessment. Carbohydrate Polymers, 207(November 2018), 169–179. https://doi.org/10.1016/j.carbpol.2018.11.079

Tibolla, H., Pelissari, F. M., Martins, J. T., Vicente, A. A., & Menegalli, F. C. (2018). Cellulose nanofibers produced from banana peel by chemical and mechanical treatments: Characterization and cytotoxicity assessment. Food Hydrocolloids, 75, 192–201. https://doi.org/10.1016/j.foodhyd.2017.08.027

Tseng, Y. M., Lin, S. K., Hsiao, J. K., Chen, I. J., Lee, J. H., Wu, S. H., & Tsai, L. Y. (2006). Whey protein concentrate promotes the production of glutathione (GSH) by GSH reductase in the PC12 cell line after acute ethanol exposure. Food and Chemical Toxicology, 44(4), 574–578. https://doi.org/10.1016/j.fct.2005.09.003

Wang, W., Sun, C., Mao, L., Ma, P., Liu, F., Yang, J., & Gao, Y. (2016). The biological activities, chemical stability, metabolism and delivery systems of quercetin: A review. Trends in Food Science and Technology, 56, 21–38. https://doi.org/10.1016/j.tifs.2016.07.004

Wang, Y., Yuan, L., Yao, C., Ding, L., Li, C., Fang, J., ... Wu, M. (2014). A combined toxicity study of zinc oxide nanoparticles and vitamin C in food additives. Nanoscale, 6(24), 15333–15342. https://doi.org/10.1039/c4nr05480f

Yi, J., Zhong, F., Zhang, Y., Yokoyama, W., & Zhao, L. (2015). Effects of Lipids on *in vitro* Release and Cellular Uptake of β-Carotene in Nanoemulsion-Based Delivery Systems. Journal of Agricultural and Food Chemistry, 63(50), 10831–10837. https://doi.org/10.1021/acs.jafc.5b04789

Zielinska-Dawinziak, M., Grajek, K., Olejnik, A., Czaczyk, K., & Grajek, W. (2009). Transport of High Concentration of Thiamin, Riboflavin and Pyridoxine across Intestinal Epithelial Cells Caco-2. Journal of Nutritional Science and Vitaminology, 54(6), 423–429. https://doi.org/10.3177/jnsv.54.423

Section IV

CONCLUSIONS

CHAPTER 7.

General conclusions

7.1. General conclusions 136

7.2. Guidelines for the future works 137

7.1. General conclusions

There is an increasing number of reports and recent research articles showing that micro- and nanostructured delivery systems enriched with bioactive compounds added to food products contribute to prevention of several chronic diseases, thus promoting health benefits to consumers, when part of the daily diet. The development of delivery systems for food industry possess a great number of challenges, including the selection of the adequate type of bioactive compound, functionality, particle size required, food compatibility, costs, rheological and textural impacts. Therefore, the composition and structure of delivery system must be carefully selected in order to promote the adequate functional properties and applications such as improvement of chemical stability and high bioavailability.

In this context, this thesis aimed at evaluating strategies to promote the valorisation and use of β-Lg structures to develop innovative delivery systems. The main contributions of this thesis are summarized below:

- β-Lg purified from commercial whey protein isolate using a simple methodology demonstrated to form micro- and nanostructures under a strict control of the physiological and environment conditions;
- β-Lg nanostructures were formed at pH 3 and 7 (with diameter below 50 nm), whereas at pH 4 it was possible to obtain structures at the macroscale (i.e., ≥ 3 μm). Stable β-Lg micro- (with diameter between 200-300 nm)- and nano (diameter ≤ 100 nm) structures were formed at pH 6 and above the denaturation temperature;
- β-Lg micro- and nanostructures are were able to bind bioactive compounds with different solubilities, wherein β-Lg nanostructures showed a higher association efficiency and loading capacity;
- β-Lg structures revealed stability under acidic and neutral conditions, at high ionic strength and under thermal processing. Moreover, β-Lg/riboflavin micro- and nanostructures and β-Lg/quercetin microstructures were stable for at least 50 days; while β-Lg/quercetin nanostructures exhibited precipitation after 2 days;
- The linear superimposition model was fitted to the results of bioactive model compounds release, which was found to be mainly governed by a relaxation mechanism. In addition, the refrigeration temperature of 4 °C allowed a slower release comparing with room temperature (25 °C);
- The *in vitro* digestion in a static gastrointestinal model revealed that β-Lg micro- and nanostructures were able to protect both hydrophilic and hydrophobic compounds from gastric

conditions, and deliver them to target site (i.e., intestinal phase). Moreover, β-Lg micro- and nanostructures are completely hydrolysed in the intestinal phase;

•β-Lg/riboflavin nanostructures revealed a higher bioaccessibility, stability and bioavailability, when compared to β-Lg/riboflavin microstructures. β-Lg/quercetin microstructures were able to enhance the bioavailability of quercetin in its free form;

• Cytotoxicity results in Caco-2 cells demonstrated that the concentrations of up to 21 μg mL^{-1} of riboflavin and 16 μg mL^{-1} of quercetin in β-Lg micro- and nanostructures can be considered as non-toxic. The concentrations used in β-Lg micro- and nanostructures and that reach the intestinal phase, are below those inducing cell cytotoxicity;

• The permeability across Caco-2 cells demonstrated that β-Lg/riboflavin nanostructures were able to enhance the permeability rate compared to riboflavin in its free form. β-Lg/quercetin microstructures did not reveal a bioactive compound protection function, since they were presumably transformed into distinct compounds;

In conclusion, this work contributed to the understanding of the mechanisms of protein aggregation and intermolecular interaction when designing β-Lg structures with novel functionalities. Our findings showed that β-Lg micro- and nanostructures may have potential for delivering hydrophilic and hydrophobic bioactive compounds into food systems with different hydrophilic natures. However, β-Lg/riboflavin nanostructures upon digestion demonstrated to improve the bioavailability and permeability rate compared to β-Lg/riboflavin microstructures. β-Lg/quercetin microstructures need to be optimized to allow an enhancement of the permeability across Caco-2 cells. In this sense, this work represents a significant contribution to enrich the knowledge about the use of β-Lg as bio-based material to protect and delivery bioactive compounds in foods.

7.2. Guidelines for the future works

Despite this work has improved the knowledge about the new functionalities and possible applications of β-Lg structures in food products, there are some suggested topics that need to be addressed further:

- Assessment of β-Lg/riboflavin nanostructures behaviour in a dynamic gastrointestinal model that mimics the peristaltic movements;
- Further evaluation of β-Lg/riboflavin nanostructures in Caco2/HT-29 co-culture systems;
- Application of β-Lg/riboflavin nanostructures into a food model systems and evaluation of potential interaction effects between the food models and such delivery structures;
- Application of β-Lg/riboflavin nanostructures into real food;
- To evaluate if the application of an extra coating layer (e.g., made from chitosan) on β-Lg/quercetin microstructures provides an improvement of Caco-2 cell permeability;
- Assessment of optimized β-Lg structures in *in vivo* studies.

SUPPLEMENTARY MATERIAL

Table S.1 - Effect of distinct pH values on particle size, polydispersity index (PDI) and surface charge (S) of β-Lg microstructures with the riboflavin (rib.) and quercetin (quer.) associated.

pH	Size (nm)		
	β-Lg micro	**β-Lg /rib. micro**	**β-Lg/quer. micro**
2	246.6 ± 15.4^{a}	207.7 ± 8.5^{a}	210.4 ± 11.2^{a}
3	223.6 ± 12.5^{a}	208.4 ± 12.5^{a}	208.7 ± 8.7^{a}
4	376.6 ± 42.7^{a}	252.6 ± 11.0a	2104.0 ± 81.6^{b}
5	3980.0 ± 15.4^{b}	5122.3 ± 11.3^{b}	5332.6 ± 10.0^{c}
6	208.9 ± 9.8^{a}	207.2 ± 11.1^{a}	209.3 ± 9.0^{a}
7	221.5 ± 11.5^{a}	206.7 ± 15.5^{a}	201.2 ±13.3^{a}
8	228.3 ± 14.7^{a}	223.2 ± 6.4^{a}	236.9 ± 27.5^{a}
9	234. 1 ± 15.1^{a}	209.8 ± 14.5^{a}	210.0 ± 8.7^{a}
10	257.4 ± 22.0^{a}	202.4 ± 12.5^{a}	215.8 ± 9.0^{a}
	PDI		
	β-Lg micro	**β-Lg /rib. micro**	**β-Lg/quer. micro**
2	0.21 ± 0.02^{ad}	0.21 ± 0.01^{a}	0.25 ± 0.20^{ab}
3	0.15 ± 0.02^{b}	0.21 ± 0.01^{a}	0.25 ±0.01^{a}
4	0.28 ± 0.02^{e}	0.23 ± 0.03^{ab}	1.00 ± 0.00^{b}
5	1.00 ± 0.00^{f}	1.00 ± 0.00^{c}	1.00 ± 0.00^{c}
6	0.20 ± 0.03^{acd}	0.22 ± 0.01^{ab}	0.25 ± 0.02^{d}
7	0.16 ± 0.03^{bc}	0.21 ± 0.01^{a}	0.24 ± 0.02^{de}
8	0.17 ± 0.03^{bcd}	0.22 ± 0.01^{ab}	0.28 ± 0.01^{de}
9	0.21 ± 0.03^{a}	0.22 ± 0.01^{ab}	0.25 ± 0.01^{de}
10	0.23 ± 0.02^{a}	0.24 ± 0.01^{b}	0.26 ± 0.01^{e}
	S (mV)		
	β-Lg micro	**β-Lg /rib. micro**	**β-Lg/quer. micro**
2	17.7 ±1.7^{a}	23.2 ± 4.0^{a}	16.2 ± 0.4^{ab}
3	20.0 ± 0.5^{a}	20.8 ± 2.2^{a}	16.7 ± 2.5^{a}
4	12.2 ± 1.0^{b}	12.5 ± 1.2^{ab}	12.1 ± 1.8^{b}
5	-4.0 ± 1.0^{c}	1.0 ± 2.1^{c}	-2.3 ± 1.8^{c}
6	-20.1 ± 2.3^{d}	-18.3 ± 1.0^{ab}	-17.3 ± 1.8^{d}
7	-23.4 ± 1.3^{de}	-22.7 ± 1.5^{a}	-17.4 ± 2.7^{de}
8	-25.0 ± 1.4^{e}	-24.5 ± 1.7^{ab}	-20.2 ± 1.8^{de}
9	-25.3 ± 1.5^{e}	-22.2 ± 2.9^{ab}	-21.1 ± 2.0^{de}
10	-22.8 ± 1.8^{de}	-21.8 ± 2.1^{c}	-22.0 ± 1.5^{e}

NOTE: ^{a,b,c,d,e} Small superscript letters for each parameter in the column indicate statistical difference between means ($p \leq 0.05$).

Table S.2 - Effect of distinct pH values on particle size, polydispersity index (PDI) and surface charge (S) of β-Lg nanostructures with the riboflavin (rib.) and quercetin (quer.) associated.

pH	Size (nm)		
	β-Lg nano	**β-Lg /rib. nano**	**β-Lg/quer. nano**
2	68.1 ± 1.3^{ab}	61.2 ± 4.4^{a}	65.6 ± 8.6^{a}
3	65.4 ± 1.0^{ab}	77.9 ± 7.4^{a}	56.9 ± 8.7^{a}
4	63.8 ± 2.6^{a}	280.7 ± 62.2^{b}	158.5 ±18.0^{b}
5	6000.0 ± 87.1^{d}	6000.0 ± 10.4^{c}	6000.0 ±91.4^{c}
6	62.3 ± 1.2^{a}	69.3 ± 4.6^{a}	66.6 ± 9.0^{a}
7	66.0 ± 1.8^{ab}	68.3 ± 2.8^{a}	63.8 ± 5.8^{a}
8	66.2 ± 1.2^{ab}	65.4 ± 2.7^{a}	64.2 ± 1.8^{a}
9	80.7 ±11.8^{bc}	71.8 ± 12.1^{a}	63.6 ± 1.9^{a}
10	86.5 ± 1.0^{c}	61.2 ± 9.3^{a}	68.6 ± 9.3^{a}
	PDI		
	β-Lg nano	**β-Lg /rib. nano**	**β-Lg/quer. nano**
2	0.23 ± 0.01^{a}	0.23 ± 0.03^{a}	0.21 ± 0.02^{a}
3	0.28 ± 0.03^{a}	0.25 ± 0.02^{a}	0.24 ± 0.03^{a}
4	0.24 ± 0.01^{a}	0.45 ± 0.07^{b}	0.36 ± 0.04^{a}
5	0.98 ± 0.01^{b}	0.99 ± 0.01^{c}	0.85 ± 0.20^{b}
6	0.27 ± 0.03^{a}	0.22 ± 0.02^{a}	0.23 ± 0.01^{a}
7	0.28 ± 0.05^{a}	0.22 ± 0.02^{a}	0.28 ± 0.01^{a}
8	0.27 ±0.04^{a}	0.26 ± 0.02^{a}	0.27 ± 0.01^{a}
9	0.37 ± 0.04^{a}	0.32 ± 0.02^{a}	0.28 ± 0.02^{a}
10	0.39 ± 0.04^{a}	0.35 ± 0.02^{a}	0.31 ± 0.02^{a}
	S (mV)		
	β-Lg nano	**β-Lg /rib. nano**	**β-Lg/quer. nano**
2	19.4 ± 1.1^{a}	16.7 ± 0.7^{a}	12.7 ± 1.0^{a}
3	16.7 ± 2.6^{a}	16.9 ± 1.8^{a}	15.3 ± 2.0^{b}
4	12.8 ± 0.8^{b}	12.6 ± 0.7^{b}	13.4 ± 1.0^{ab}
5	-2.3 ± 2.6^{c}	0.1 ± 0.9^{c}	-1.9 ± 1.0^{c}
6	-16.9 ± 1.0^{d}	-15.9 ± 1.9^{d}	-16.8 ± 0.7^{d}
7	-22.7 ±1.6^{e}	-21.5 ± 1.3^{e}	-18.6 ± 1.4^{d}
8	-17.5 ± 0.8^{d}	-17.5 ± 1.0^{d}	-16.4 ± 1.9^{d}
9	-17.9 ± 1.1^{d}	-17.5 ± 1.0^{d}	-16.4 ± 0.5^{d}
10	-17.6 ± 1.0^{d}	-17.4 ± 0.8^{d}	-17.8 ± 0.3^{d}

NOTE: ^{a,b,c,d}Small superscript letters for each parameter in the column indicate statistical difference between means ($p \leq 0.05$).

Table S.3 - Effect of ionic strength on particle size and polydispersity index (PDI) of β-Lg microstructures with the riboflavin (rib.) and quercetin (quer.) bioactive associated.

mmol L^{-1}	Size (nm)		
	β-Lg micro	**β-Lg /rib. micro**	**β-Lg/quer. micro**
0	239.1 ± 5.2^{a}	259.6 ± 7.4^{a}	222.8 ± 4.8^{a}
25	249.2 ± 4.4^{ab}	257.4 ± 4.4^{a}	227.0 ± 9.0^{a}
50	256.9 ± 8.9^{ab}	263.9 ± 6.6^{a}	238.9 ± 5.5^{ab}
100	264.2 ± 7.6^{b}	252.3 ± 6.9^{a}	261.2 ± 7.4^{b}
150	262.4 ± 20.6^{ab}	257.8 ± 2.2^{a}	292.2 ± 16.5^{c}
200	265.1 ± 10.6^{b}	261.8 ± 17.2^{a}	383.8 ± 26.6^{d}
	PDI		
	β-Lg micro	**β-Lg /rib. micro**	**β-Lg/quer. micro**
0	0.14 ± 0.01^{a}	0.21 ± 0.02^{a}	0.18 ± 0.03^{a}
25	0.17 ± 0.01^{ab}	0.19 ± 0.02^{a}	0.17 ± 0.01^{a}
50	0.16 ± 0.02^{ab}	0.19 ± 0.03^{a}	0.19 ± 0.02^{ab}
100	0.18 ± 0.01^{b}	0.17 ± 0.02^{a}	0.20 ± 0.01^{ab}
150	0.17 ± 0.01^{ab}	0.20 ± 0.03^{a}	0.23 ± 0.01^{b}
200	0.17 ± 0.02^{b}	0.19 ± 0.02^{a}	0.28 ± 0.03^{c}

NOTE: ^{a,b,c,d}Small superscript letters for each parameter in the column indicate statistical difference between means ($p \leq 0.05$).

Table S.4 - Effect of ionic strength on particle size and polydispersity index (PDI) of β-Lg nanostructures with the riboflavin (rib.) and quercetin (quer.) associated.

mmol L^{-1}	Size (nm)		
	β-Lg nano	**β-Lg /rib. nano**	**β-Lg/quer. nano**
0	85.2 ± 4.2^{a}	77.4 ± 8.2^{a}	77.9 ± 9.6^{a}
25	104.9 ± 6.9^{b}	72.0 ± 9.6^{a}	126.4 ± 15.4^{ab}
50	102.1 ± 8.5^{b}	68.6 ± 3.8^{a}	184.7 ± 14.0^{cd}
100	104.3 ± 5.9^{b}	70.4 ± 7.3^{a}	159.3 ± 18.7^{bc}
150	88.9 ± 4.2^{ab}	66.2 ± 3.4^{a}	226.6 ± 32.4^{d}
200	97.5 ± 12.9^{ab}	73.9 ± 6.9^{a}	326.3 ± 34.4^{e}
	PDI		
	β-Lg nano	**β-Lg /rib. nano**	**β-Lg/quer. nano**
0	0.22 ± 0.01^{a}	0.21 ± 0.01^{a}	0.22 ± 0.02^{a}
25	0.22 ± 0.02^{b}	0.25 ± 0.01^{b}	0.29 ± 0.02^{c}
50	0.21 ± 0.01^{a}	0.24 ± 0.01^{bc}	0.26 ± 0.02^{bc}
100	0.22 ± 0.01^{a}	0.24 ± 0.01^{bc}	0.24 ± 0.01^{ab}
150	0.28 ± 0.02^{c}	0.24 ± 0.01^{bc}	0.44 ± 0.03^{d}
200	0.26 ± 0.01^{c}	0.22 ± 0.01^{ac}	0.42 ± 0.01^{d}

NOTE: ^{a,b,c,d}Small superscript letters for each parameter in the column indicate statistical difference between means ($p \leq 0.05$).

Table S.5 - Thermal effect on particle size, polydispersity index (PDI) and surface charge (S) of β-Lg microstructures with the riboflavin (rib.) and quercetin (quer.) associated.

T (°C)	Size (nm)		
	β-Lg micro	**β-Lg /rib. micro**	**β-Lg/quer. micro**
20	231.6 ± 4.9[a]	224.4 ± 8.8[a]	209.1 ± 10.4[a]
25	237.5 ± 7.8[a]	230.5 ± 9.6[ab]	215.7 ± 3.6[a]
30	235.0 ± 5.5[a]	233.8 ± 4.6[ab]	215.8 ± 6.2[a]
35	236.3 ± 5.2[a]	228.0 ± 9.0[ab]	214.2 ± 3.6[a]
40	238.0 ± 7.1[a]	231.9 ± 5.8[ab]	213.4 ± 1.9[a]
45	238.5 ± 3.1[a]	224.7 ± 6.2[a]	215.4 ± 2.5[a]
50	236.5 ± 4.2[a]	228.5 ± 5.9[ab]	212.6 ± 3.6[a]
55	238. 6 ± 3.9[a]	231.4 ± 6.4[ab]	213.0 ± 2.9[a]
60	233.4 ± 5.7[a]	232.6 ± 5.5[ab]	213.1 ± 2.4[a]
65	229.2 ± 8.1[a]	231.0 ± 9.1[ab]	210.6 ± 4.5[a]
70	238.2 ± 5.0[a]	233.4 ± 6.4[ab]	211.2 ± 5.2[a]
75	241.2 ± 3.5[ab]	244.3 ± 4.0[bc]	217.5 ± 3.8[a]
80	253.9 ± 2.0[b]	253.2 ± 8.7[c]	232.5 ± 3.8[b]
	PDI		
	β-Lg micro	**β-Lg /rib. micro**	**β-Lg/quer. micro**
20	0.13 ± 0.01[a]	0.19 ± 0.01[a]	0.19 ± 0.01[a]
25	0.14 ± 0.01[a]	0.20 ± 0.01[ab]	0.19 ± 0.01[a]
30	0.14 ± 0.01[a]	0.13 ± 0.01[bc]	0.19 ± 0.01[a]
35	0.14 ± 0.01[a]	0.20 ± 0.01[abc]	0.18 ± 0.01[a]
40	0.14 ± 0.01[a]	0.20 ± 0.01[ab]	0.18 ± 0.01[a]
45	0.12 ± 0.01[a]	0.20 ± 0.01[ab]	0.18 ± 0.01[a]
50	0.12 ± 0.01[a]	0.20 ± 0.01[ab]	0.18 ± 0.01[a]
55	0.13 ± 0.01[a]	0.20 ± 0.01[abc]	0.19 ± 0.01[a]
60	0.14 ± 0.01[a]	0.21 ± 0.01[bc]	0.19 ± 0.01[a]
65	0.13 ± 0.01[a]	0.21 ± 0.01[abc]	0.19 ± 0.01[a]
70	0.14 ± 0.01[a]	0.22 ± 0.01[bc]	0.18 ± 0.01[a]
75	0.12 ± 0.01[a]	0.22 ± 0.01[bc]	0.19 ± 0.01[a]
80	0.13 ± 0.01[a]	0.23 ± 0.01[c]	0.19 ± 0.01[a]

NOTE: [a,b,c] Small superscript letters for each parameter in the column indicate statistical difference between means ($p \leq 0.05$).

Table S.6 - Thermal effect on particle size, polydispersity index (PDI) and surface charge (S) of β-Lg nanostructures with the riboflavin (rib.) and quercetin (quer.) associated.

T (°C)	Size (nm)		
	β-Lg nano	**β-Lg /rib. nano**	**β-Lg/quer. nano**
20	70.5 ± 2.0[a]	84.1 ± 2.5[a]	101.5 ± 3.2[a]
25	71.1 ± 1.8[a]	85.2 ± 2.3[a]	101.4 ± 3.3[a]
30	71.5 ± 1.8[a]	85.5 ± 2.2[ab]	101.5 ± 3.3[a]
35	71.6 ± 2.0[a]	85.8 ± 2.6[ab]	101.0 ± 3.3[a]
40	71.6 ± 2.0[a]	85.7 ± 2.4[ab]	100.2 ± 3.3[a]
45	71.5 ± 2.2[a]	85.5 ± 2.4[ab]	99.7 ± 3.2[a]
50	71.4 ± 1.9[a]	85.6 ± 2.5[ab]	99.4 ± 3.1[a]
55	71.3 ± 2.2[a]	85.6 ± 2.4[ab]	99.2 ± 2.9[a]
60	71.5 ± 2.0[a]	86.0 ± 2.4[ab]	99.2 ± 3.1[a]
65	72.4 ± 2.1[ab]	86.5 ± 2.3[ab]	100.7 ± 2.9[a]
70	73.6 ± 2.1[ab]	87.3 ± 2.4[ab]	104.7 ± 3.0[a]
75	77.1 ± 2.3[b]	89.0 ± 2.4[ab]	114.0 ± 3.5[b]
80	86.3 ± 3.1[c]	91.3 ± 3.1[b]	141.9 ± 5.7[c]
	PDI		
	β-Lg nano	**β-Lg /rib. nano**	**β-Lg/quer. nano**
20	0.24 ± 0.01[ab]	0.24 ± 0.01[ab]	0.19 ± 0.01[a]
25	0.25 ± 0.02[a]	0.25 ± 0.01[a]	0.18 ± 0.01[a]
30	0.25 ± 0.01[a]	0.24 ± 0.01[ab]	0.18 ± 0.01[a]
35	0.24 ± 0.01[a]	0.24 ± 0.01[ab]	0.19 ± 0.01 a
40	0.25 ± 0.01[a]	0.25 ± 0.01[ab]	0.19 ± 0.01[a]
45	0.24 ± 0.01[a]	0.24 ± 0.01[abc]	0.19 ± 0.01[a]
50	0.24 ±0.01[ab]	0.24 ± 0.01[abc]	0.19 ± 0.01[a]
55	0.24 ±0.01[ab]	0.24 ± 0.01[ab]	0.18 ± 0.01[a]
60	0.23 ± 0.02[ab]	0.24 ± 0.01[abc]	0.19 ± 0.01[ab]
65	0.23 ± 0.01[ab]	0.23 ± 0.01[abc]	0.19 ± 0.01[a]
70	0.22 ± 0.01[ab]	0.23 ± 0.01[abc]	0.18 ± 0.01[a]
75	0.22 ± 0.01[bc]	0.23 ± 0.01[bc]	0.18 ± 0.01[a]
80	0.19 ± 0.01[c]	0.23 ± 0.01[c]	0.20 ± 0.01[b]

NOTE: [a,b] Small superscript letters for each parameter in the column indicate statistical difference between means ($p \leq 0.05$).

Table S.7 - Particle size, polydispersity index (PDI) and surface charge (S) of β-Lg microstructures with and without the riboflavin (rib.) and quercetin (quer.) associated under storage at 4 °C and 25 °C.

			Size (nm)			
Day	**β-Lg micro**		**β-Lg /rib. micro**		**β-Lg/quer. micro**	
	4 °C	**25 °C**	**4 °C**	**25 °C**	**4 °C**	**25 °C**
0	202.5 ± 5.8^{a}	201.3 ± 3.6^{a}	206. 6 ± 8.5^{ab}	202.9 ± 4.6^{ab}	232.2 ± 20.8^{a}	215.6 ± 23.6^{a}
2	194.7 ± 4.9^{a}	192.4 ± 27.6^{a}	184.2 ± 15.4^{a}	204.8 ± 11.6^{ab}	210.8 ± 33.8^{a}	230.5 ± 17.5^{a}
5	209.6 ± 9.8^{a}	187.3 ± 27.0^{a}	180.8 ± 17.8^{a}	219.8 ± 17.2^{ab}	219.6 ± 23.9^{a}	225.4 ± 17.1^{a}
12	199.3 ± 5.0^{a}	182.6 ± 19.2^{a}	198.6 ± 22.9^{ab}	210.2 ± 15.0^{ab}	211.7 ± 28.6^{a}	225.8 ± 20.3^{a}
16	218.6 ± 21.4^{a}	187.9 ± 23.9^{a}	194.5 ± 24.3^{a}	216.8 ± 18.9^{ab}	202.4 ± 30.3^{a}	233.0 ± 25.5^{a}
22	194.8 ± 8.3^{a}	203.9 ± 14.0^{a}	192.0 ± 28.1^{a}	217.3 ± 8.4^{ab}	208.2 ± 28.9^{a}	226.4 ± 17.4^{a}
29	193.2 ± 12.8^{a}	199.0 ± 11.2^{a}	201.4 ± 26.4^{ab}	209.7 ± 14.7^{ab}	213.0 ± 29.4^{a}	215.5 ± 30.6^{a}
36	202.0 ± 10.0^{a}	190.2 ± 20.7^{a}	211.5 ± 26.6^{ab}	204.5 ± 14.8^{ab}	227.5 ± 18.9^{a}	225.3 ± 21.6^{a}
43	205.8 ± 14.3^{a}	183.0 ± 19.9^{a}	211.3 ± 29.3^{ab}	210.0 ± 6.2^{ab}	223.2 ± 22.5^{a}	222.4 ± 17.7^{a}
50	202.5 ± 13.2^{a}	206.8 ± 7.4^{a}	190.8 ± 22.6^{a}	202.2 ± 5.8^{ab}	232.0 ± 22.2^{a}	226.3 ± 19.6^{a}
60	189.9 ± 12.0^{a}	203.5 ± 3.5^{a}	179.5 ± 17.4^{a}	225.5 ± 26.6^{b}	249.4 ± 2.8^{a}	23.36 ± 18.2^{a}
70	196.3 ± 12.1^{a}		194.6 ± 19.6^{a}	206.2 ± 15.1^{ab}		
80	197.8 ± 10.5^{a}		175.2 ± 12.3^{a}	202.3 ± 7.9^{ab}		
90	202.0 ± 11.1^{a}		264.5 ± 53.6^{b}	192.1 ± 15.8^{a}		
			PDI			
	β-Lg micro		**β-Lg /rib. micro**		**β-Lg/quer. micro**	
	4 °C	**25 °C**	**4 °C**	**25 °C**	**4 °C**	**25 °C**
0	0.18 ± 0.02^{abc}	0.23 ± 0.01^{ab}	0.21 ± 0.01^{ab}	0.19 ± 0.01^{ab}	0.16 ± 0.04^{a}	0.14 ± 0.02^{a}
2	0.15 ± 0.02^{a}	0.23 ± 0.01^{ab}	0.20 ± 0.02^{a}	0.18 ± 0.01^{a}	0.16 ± 0.03^{a}	0.16 ± 0.01^{a}
5	0.18 ± 0.01^{abc}	0.20 ± 0.02^{ab}	0.23 ± 0.03^{ab}	0.25 ± 0.01^{b}	0.17 ± 0.02^{a}	0.13 ± 0.03^{a}
12	0.17 ± 0.02^{abc}	0.24 ± 0.01^{a}	0.22 ± 0.02^{ab}	0.19 ± 0.01^{ab}	0.17 ± 0.02^{a}	0.17 ± 0.02^{a}
16	0.21 ± 0.01^{bc}	0.21 ± 0.01^{ab}	0.20 ± 0.01^{a}	0.20 ± 0.02^{ab}	0.14 ± 0.01^{a}	0.14 ± 0.02^{a}
22	0.16 ± 0.02^{ab}	0.24 ± 0.03^{a}	0.22 ± 0.01^{ab}	0.21 ± 0.01^{ab}	0.15 ± 0.02^{a}	0.16 ± 0.03^{a}
29	0.17 ± 0.01^{abc}	0.25 ± 0.03^{a}	0.20 ± 0.01^{b}	0.20 ± 0.02^{ab}	0.18 ± 0.02^{a}	0.13 ± 0.02^{a}
36	0.22 ± 0.01^{c}	0.20 ± 0.02^{ab}	0.24 ±0.01^{ab}	0.20 ± 0.02^{ab}	0.15 ± 0.04^{a}	0.15 ± 0.02^{a}
43	0.21 ± 0.02^{bc}	0.21 ± 0.02^{ab}	0.23 ± 0.01^{ab}	0.18 ± 0.02^{a}	0.16 ± 0.04^{a}	0.14 ± 0.02^{a}
50	0.18 ± 0.01^{abc}	0.19 ± 0.01^{ab}	0.20 ± 0.01^{a}	0.23 ± 0.06^{ab}	0.13 ± 0.02^{a}	0.15 ± 0.01^{a}
60	0.17 ± 0.02^{a}	0.17 ± 0.01^{b}	0.27 ± 0.03^{ab}	0.22 ± 0.03^{ab}	0.13 ± 0.02^{a}	0.13 ± 0.02^{a}
70	0.16 ± 0.01^{ab}		0.20 ± 0.02^{a}	0.20 ± 0.02^{ab}		
80	0.20 ± 0.03^{abc}		0.25 ± 0.02^{ab}	0.18 ± 0.02^{a}		
90	0.17 ± 0.01^{ab}		0.24 ± 0.01^{ab}	0.23 ± 0.04^{ab}		
			S (mV)			
	β-Lg micro		**β-Lg /rib. micro**		**β-Lg/quer. micro**	
	4 °C	**25 °C**	**4 °C**	**25 °C**	**4 °C**	**25 °C**
0	-22.2 ± 1.9^{a}	-21.2 ± 1.8^{a}	-22.5 ± 1.6^{a}	-22.7 ± 1.3^{a}	-19.1 ± 1.6^{a}	-19.3 ± 1.5^{a}
2	-23.6 ± 1.8^{a}	-20.8 ± 1.6^{a}	-24.5 ± 1.5^{a}	-24.2 ± 1.6^{a}	-17.6 ± 1.2^{a}	-18.5 ± 1.6^{a}
5	-23.1 ± 1.7^{a}	-21.2 ± 2.0^{a}	-23.8 ± 1.2^{a}	-22.8 ± 1.8^{a}	-17.5 ± 1.4^{a}	-18.9 ± 1.1^{a}
12	-21.4 ± 1.8^{a}	-20.6 ± 1.6^{a}	-23.5 ± 1.5^{a}	-22.7 ± 1.4^{a}	-19.5 ± 1.7^{a}	-19.4 ± 1.5^{a}
16	-21.6 ± 1.8^{a}	-22.7 ± 2.4^{a}	-21.1 ± 1.2^{a}	-23.6 ± 2.1^{a}	-19.4 ± 1.8^{a}	-19.3 ± 1.8^{a}
22	-21.0 ± 1.7^{a}	-21.1 ± 0.9^{a}	-22.2 ± 1.2^{a}	-23.2 ± 1.2^{a}	-19.4 ± 1.3^{a}	-20.3 ± 1.6^{a}
29	-22.4 ± 2.1^{a}	-21.5 ± 1.9^{a}	-23.7 ± 2.2^{a}	-23.8 ± 1.5^{a}	-19.0 ± 1.5^{a}	-17.6 ± 1.4^{a}
36	-22.8 ± 2.0^{a}	-19.6 ± 0.7^{a}	-24.0 ± 1.5^{a}	-24.6 ± 1.6^{a}	-18.7 ± 1.3^{a}	-17.9 ± 1.6^{a}
43	-22.5 ± 1.6^{a}	-23.5 ± 1.8^{a}	-21.9 ± 1.0^{a}	-22.0 ± 1.6^{a}	-18.0 ± 1.2^{a}	-18.3 ± 1.3^{a}
50	-22.4 ± 1.8^{a}	-21.2 ± 1.7^{a}	-21.2 ± 1.7^{a}	-22.2 ± 1.9^{a}	-16.8 ± 1.1^{a}	-17.6 ± 1.3^{a}
60	-22.2 ± 1.8^{a}	-22.3 ± 2.1^{a}	-22.1 ± 1.5^{a}	-21.2 ± 1.2^{a}	-16.4 ± 0.7^{a}	-17.0 ± 1.2^{a}
70	-22.8 ± 1.6^{a}		-22.6 ± 1.8^{a}	-23.2 ± 1.5^{a}		
80	-24.5 ± 2.0^{a}		-22.6 ± 1.2^{a}	-22.3 ± 2.0^{a}		
90	-21.4 ± 1.2^{a}		-21.5 ± 1.3^{a}	-21.8 ± 2.2^{a}		

NOTE: ^{a,b,c} Small superscript letters for each parameter in the column indicate statistical difference between means ($p \leq 0.05$).

Table S.8 - Particle size, polydispersity index (PDI) and surface charge (S) of β-Lg microstructures with and without the riboflavin (rib.) and quercetin (quer.) associated under storage at 4 °C and 25 °C.

Day	β-Lg nano		β-Lg /rib. nano	
	Size (nm)			
	4 °C	**25 °C**	**4 °C**	**25 °C**
0	61.3 ± 0.7^{a}	62.7 ± 3.2^{ab}	70.8 ± 2.3^{a}	72.4 ± 2.0^{ab}
2	63.3 ± 1.1^{ab}	58.9 ± 1.3^{a}	76.4 ± 4.8^{ab}	73.5 ± 3.5^{ab}
5	64.5 ± 2.1^{ab}	58.8 ± 1.2^{a}	75.3 ± 4.0^{ab}	75.9 ± 4.2^{ab}
12	62.8 ± 0.7^{ab}	59.0 ± 1.2^{a}	76.1 ± 4.3^{ab}	72.2 ± 2.1^{ab}
16	60.4 ± 4.4^{b}	60.8 ± 2.0^{ab}	76.3 ± 4.0^{ab}	68.8 ± 1.6^{a}
22	66.7 ± 4.9^{ab}	61.0 ± 1.7^{ab}	81.4 ± 4.3^{ab}	67.8 ± 1.9^{a}
29	62.9 ± 3.9^{ab}	63.0 ± 1.0^{ab}	78.8 ± 4.9^{ab}	85.5 ± 5.3^{c}
36	64.0 ± 1.8^{ab}	60.6 ± 2.1^{ab}	80.3 ± 3.8^{ab}	71.9 ± 1.5^{a}
43	62.8 ± 2.2^{ab}	63.6 ± 2.9^{ab}	79.3 ± 4.6^{ab}	80.3 ± 5.9^{bc}
50	64.1 ± 4.8^{ab}	61.2 ± 2.8^{b}	76.4 ± 5.2^{ab}	69.0 ± 2.0^{a}
60	64.1 ± 1.5^{ab}	63.0 ± 2.1^{ab}	78.6 ± 4.5^{ab}	76.5 ± 1.5^{abc}
70	62.2 ± 2.9^{ab}	63.0 ± 2.4^{ab}	77.9 ± 4.9^{ab}	71.7 ± 2.3^{a}
80	65.3 ± 1.3^{ab}	60.3 ± 2.4^{ab}	78.0 ± 4.7^{ab}	73.2 ± 2.6^{ab}
90	61.1 ± 3.6^{a}	64.1 ± 2.8^{ab}	84.3 ± 8.7^{b}	70.5 ± 1.6^{a}
	PDI			
	β-Lg nano		**β-Lg /rib. nano**	
	4 °C	**25 °C**	**4 °C**	**25 °C**
0	0.24 ± 0.01^{abc}	0.24 ± 0.01^{ab}	0.25 ± 0.01^{a}	0.24 ± 0.01^{ab}
2	0.24 ± 0.01 ^{abc}	0.24 ± 0.01^{ab}	0.26 ± 0.01^{ab}	0.23 ± 0.01^{a_b}
5	0.26 ± 0.02 ^{abc}	0.24 ± 0.01^{ab}	0.26 ± 0.01^{ab}	0.28 ± 0.02^{a_b}
12	0.24 ± 0.01^{abc}	0.24 ± 0.01^{ab}	0.26 ± 0.01^{a}	0.27 ± 0.02^{a_b}
16	0.29 ± 0.06^{c}	0.23 ± 0.01^{ab}	0.25 ± 0.01^{a}	0.27 ± 0.02^{a_b}
22	0.23 ± 0.01^{abc}	0.23 ± 0.01^{ab}	0.25 ± 0.01^{a}	0.25 ± 0.01^{a}
29	0.24 ± 0.02^{abc}	0.23 ± 0.01^{ab}	0.25 ± 0.01^{a}	0.42 ± 0.09^{b}
36	0.21 ± 0.01^{a}	0.23 ± 0.01^{ab}	0.25 ± 0.01^{a}	0.28 ± 0.02^{a_b}
43	0.21 ± 0.02^{a}	0.24 ± 0.02^{ab}	0.24 ± 0.01^{a}	0.36 ± 0.06^{a_b}
50	0.28 ± 0.04^{bc}	0.27 ± 0.04^{b}	0.27 ± 0.01^{a}	0.32 ± 0.06^{a_b}
60	0.22 ± 0.02^{ab}	0.23 ± 0.01^{ab}	0.26 ± 0.02^{ab}	0.41 ± 0.01^{a_b}
70	0.23 ± 0.02^{abc}	0.23 ± 0.01^{ab}	0.25 ± 0.02^{ab}	0.33 ± 0.06^{a_b}
80	0.24 ± 0.01^{abc}	0.21 ± 0.01^{a}	0.25 ± 0.01^{a}	0.37 ± 0.08^{a_b}
90	0.27 ± 0.04^{abc}	0.23 ± 0.02^{ab}	0.30 ± 0.01^{b}	0.40 ± 0.10^{a_b}
	S (mV)			
	β-Lg nano		**β-Lg /rib. nano**	
	4 °C	**25 °C**	**4 °C**	**25 °C**
0	-18.2 ± 0.9^{a}	-18.5 ± 1.0^{a}	-20.4 ± 1.7^{a}	-19.6 ± 1.8^{a}
2	-18.2 ± 0.8^{a}	-17.1 ± 1.0^{ab}	-19.8 ± 2.1^{ab}	-21.4 ± 1.6^{a}
5	-17.3 ± 1.2^{a}	-17.0 ± 0.6^{ab}	-15.2 ± 1.0^{b}	-21.3 ± 1.7^{a}
12	-17.8 ± 1.2^{a}	-18.0 ± 1.0^{ab}	-20.3 ± 1.6^{a}	-19.7 ± 1.5^{a}
16	-16.8 ± 0.8^{a}	-17.4 ± 0.9^{ab}	-21.3 ± 2.7^{a}	-18.8 ± 2.2^{a}
22	-16.7 ± 1.1^{a}	-17.0 ± 0.9^{ab}	-18.9 ± 2.0^{ab}	-21.0 ± 2.5^{a}
29	-16.3 ± 1.2^{a}	-16.0 ± 1.1^{abc}	-19.9 ± 2.1^{a}	-21.5 ± 1.4^{a}
36	-16.0 ± 1.9^{a}	-13.4 ± 2.2^{c}	-22.7 ± 1.4^{a}	-21.7 ± 1.5^{a}
43	-17.2 ± 0.9^{a}	-16.4 ± 0.9^{abc}	-20.7 ± 2.3^{a}	-16.9 ± 3.2^{a}
50	-16.4 ± 1.0^{a}	-16.4 ± 1.2^{abc}	-20.2 ± 1.0^{a}	-19.7 ± 0.8^{a}
60	-17.3 ± 1.0^{a}	-17.6 ± 1.0^{ab}	-20.9 ± 1.4^{a}	-18.4 ± 3.8^{a}
70	-15.6 ± 0.9^{a}	-15.3 ± 0.9^{bc}	-19.9 ± 2.4^{ab}	-19.2 ± 2.0^{a}
80	-16.3 ± 0.9^{a}	-16.4± 0.8^{abc}	-18.2 ± 1.4^{ab}	-18.4 ± 2.9^{a}
90	-17.2 ± 0.8^{a}	-17.8 ± 2.0^{ab}	-18.0 ± 1.3^{ab}	-17.2 ± 2.6^{a}

NOTE: ^{a,b,c} Small superscript letters for each parameter in the column indicate statistical difference between means ($p \leq 0.05$).

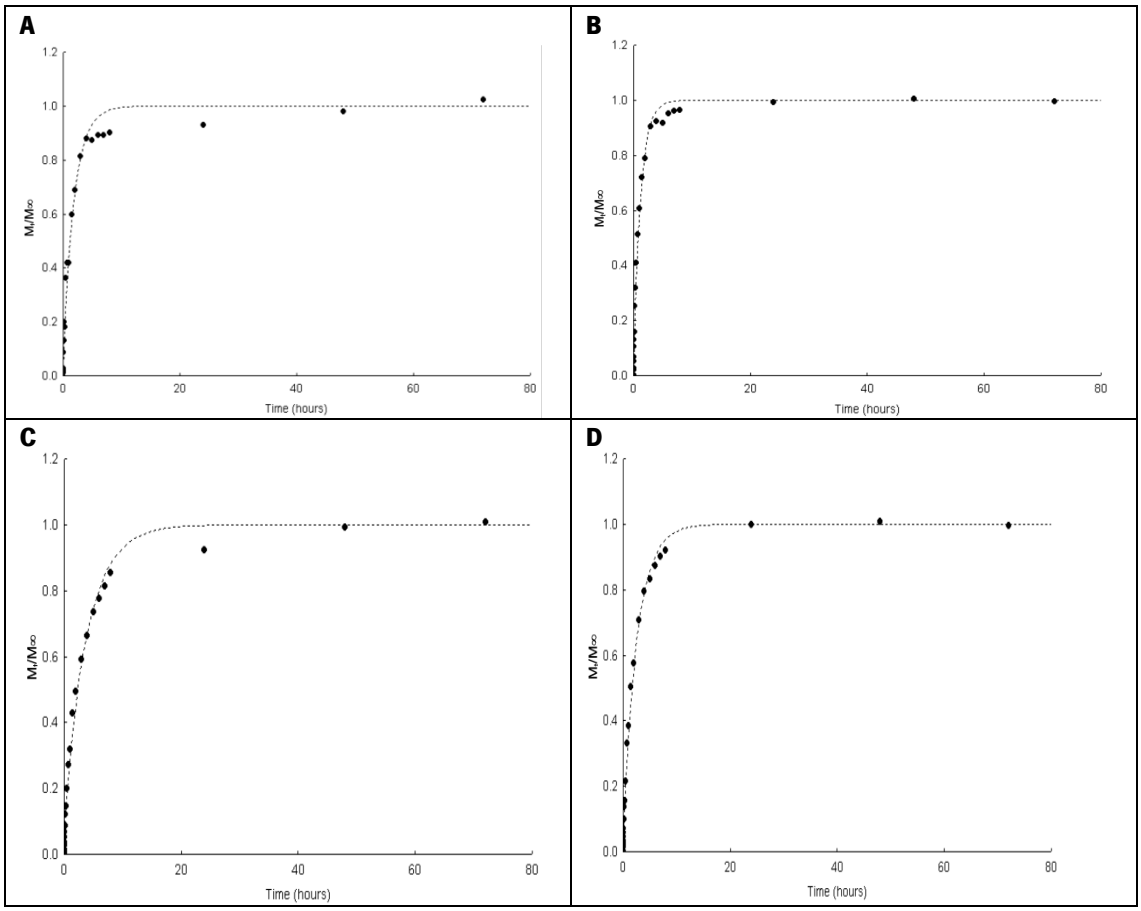


Figure S.1 - β-Lg/riboflavin microstructures into food simulants composed by 50 % ethanol at 25 °C A) and 10 % ethanol at 25 °C B), 50 % ethanol at 4 °C C) and 10 % ethanol at 4 °C D).

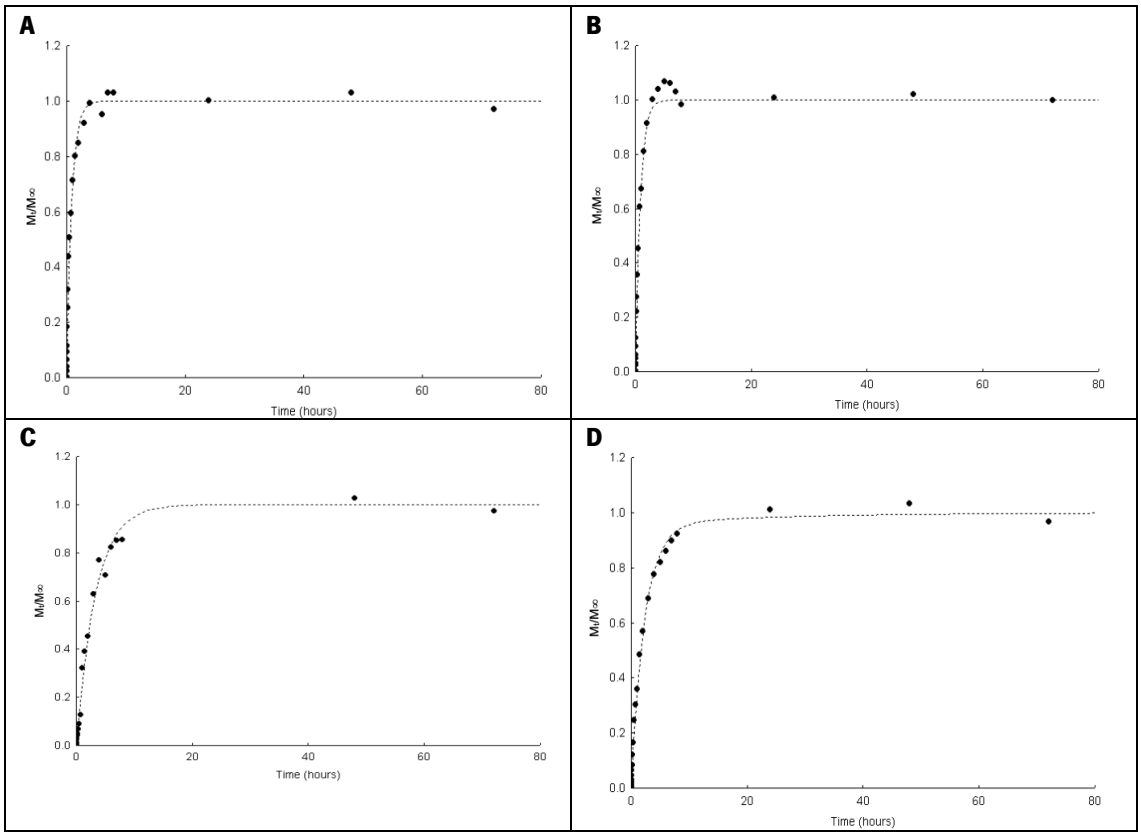


Figure S.2 - β-Lg/riboflavin nanostructures into food simulants composed by 50 % ethanol at 25 °C A) and 10 % ethanol at 25 °C B), 50 % ethanol at 4 °C C) and 10 % ethanol at 4 °C D).

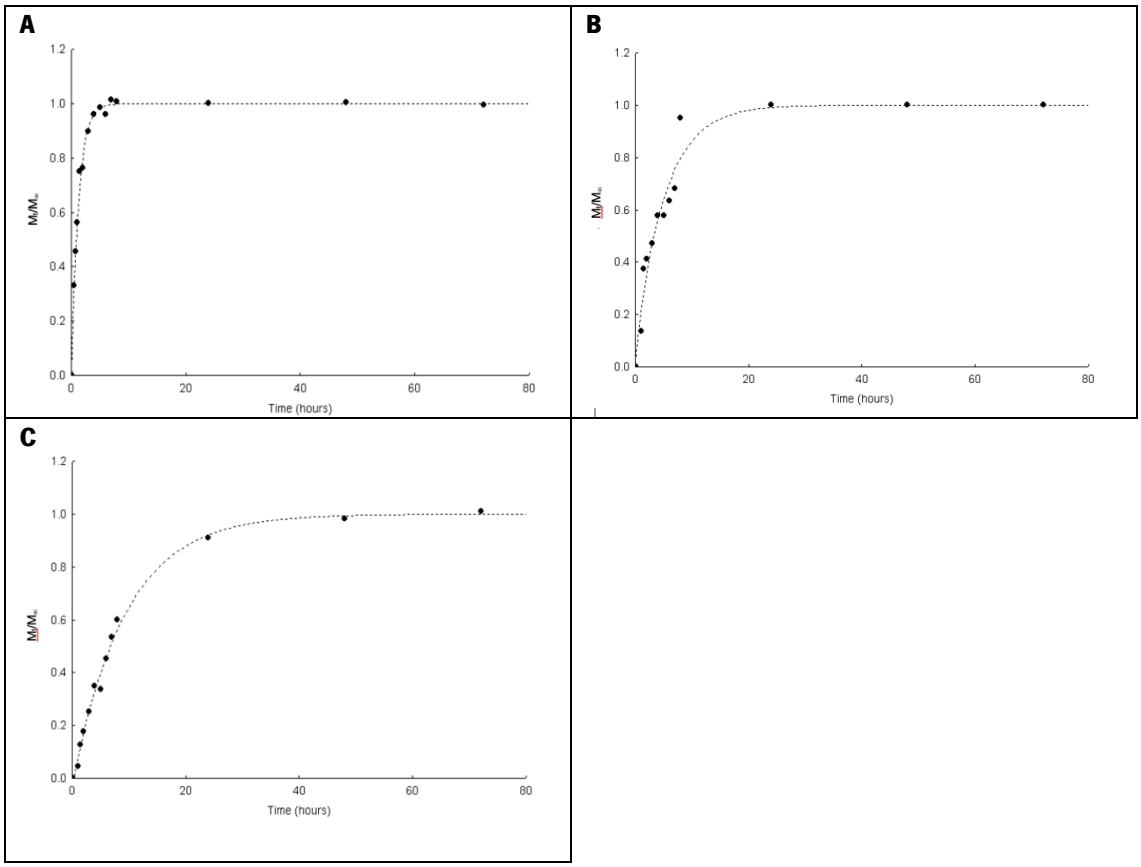


Figure S.3 - β-Lg/quercetin microstructures into food simulants composed by 50 % ethanol at 25 °C A) and 10 % ethanol at 25 °C B), 50 % ethanol at 4 °C C).